MAGNETIZATION DISTRIBUTION AND REVERSAL BEHAVIOUR IN 1D FERROMAGNETIC Co-Pt-BASED NANOSTRUCTURES

Muhammad Shahid Arshad

Doctoral Dissertation
Jožef Stefan International Postgraduate School
Ljubljana, Slovenia, December 2015

Supervisor: Prof. Dr. Spomenka Kobe, IPS and Jožef Stefan Institute, 1000 Ljubljana, Slovenia
Co-Supervisor: Asst. Prof. Dr. Kristina Žužek Rožman, IPS and Jožef Stefan Institute, 1000 Ljubljana, Slovenia

Evaluation Board:
Prof. Dr. Darko Makovec, Chair, IPS and Jožef Stefan Institute, 1000 Ljubljana, Slovenia
Prof. Dr. Zvonko Jagličič, Member, Institute of Mathematics, Physics and Mechanics, 1000 Ljubljana, Slovenia
Asst. Prof. Dr. Matej Komelj, Member, Jožef Stefan Institute, 1000 Ljubljana, Slovenia

MEDNARODNA PODIPLOMSKA ŠOLA JOŽEFA STEFANA
JOŽEF STEFAN INTERNATIONAL POSTGRADUATE SCHOOL



Muhammad Shahid Arshad

MAGNETIZATION DISTRIBUTION AND REVERSAL BEHAVIOUR IN 1D FERROMAGNETIC Co-Pt-BASED NANOSTRUCTURES

Doctoral Dissertation

PORAZDELITEV MAGNETIZACIJE IN PREISKOVANJE PROCESA DEMAGNETIZACIJE V ENODIMENZIONALNIH FEROMAGNETNIH NANOSTRUKTURAH NA OSNOVI SISTEMA Co-Pt

Doktorska Disertacija

Supervisor: Prof. Dr. Spomenka Kobe

Co-Supervisor: Asst. Prof. Dr. Kristina Žužek Rožman

Ljubljana, Slovenia, December 2015

Dedicated to my late mother and father and world peace

Acknowledgments

First and foremost I would like to thank Allah Almighty for making my mother's (late) dream come true. I got accepted for this PhD position on 18th May 2011 and my mother passed away on 03th June 2011, I always had a strong feeling that she gave me this task to finish. She expressed her wish to see me PhD (Dr. Shahid) many times while she was alive.

I would like to express my sincere thanks to Asst. Prof. Kristina Žužek Rožman and Prof. Dr. Spomenka Kobe who together made it possible for me to finish my PhD. I spent these precious four years at the Jožef Stefan Institute, where I learned so much, not just about science but life itself. My special thanks go to Asst. Prof. Kristina Žužek Rožman for her encouragement, guidance, advice, ideas and fruitful discussions. She has been an asset and available when needed. Whenever I entered her office there was a problem and when I left her office it was either solved or I knew how to solve it. She has been being a superb supervisor throughout this PhD process. She helped me to look deeper into my results and analyze each details with a critical point of view. I learned a lot from her. Thanks a lot Tina!

Thanks also go to Prof. Dr. Spomenka Kobe who made me what I am today. Her advices, guidance and future vision showed me the way to success, I will always remember her advices. I feel lucky to be her student. I would specially like to thank her for Thursday meetings, an opportunity to discuss problems and a wonderful way to find the solutions. If I ever become a group leader there will be Thursday meetings for sure. ☺ I would also like to thank her for giving me the opportunity to travel to Dresden for a short period (4 months) to perform research work and learn new techniques.

There were so many people involved who helped me during my PhD work. First of all Thursday meeting senior members (former colleague Asst. Prof. Paul McGuiness, Asst. Prof. Matej Komelj, Asst. Prof. Sašo Šturm and Beno Podmiljšak) and of course junior members (alphabetical order: Božo Skela, Darja Pečko, Jana Ferčič, Kristina Žagar, Luka Kelhar, Marko Soderžnik, Martin Topole, Nina Kostevšek, Petra Jenuš, Tomaž Tomše) for valuable discussion, suggestions and advice every Thursday. They made me think outside the box. Coming from the physics background I did not have deep understanding about electrodeposition, many thanks go to Nina Kostevšek, Špela Trafela and Dr. Darja Pečko for helping me regarding the electrodeposition technique. Many thanks go to Dr. Janez Zavašnik and Asst. Prof. Sašo Šturm for TEM analysis, I learnt a lot from them. Thanks to the K8 lab members (Prof. Dr. Darko Makovec, Petra Jenuš now in K7) for allowing me to use their VSM device. Thanks also go to Dr. Jana Ferčič, Edi Kranjc, Prof. Dr. Aleksander Rečnik, and Dr. Nina Daneu for XRD measurements and their interpretation. Thanks to Bojan Ambrožič for FIB measurements. Thanks to Dr. Goran Dražič (former

colleague, K7), Maja Koblar and Dr. Zoran Samardžija for his help related to the SEM analysis. Thanks again to Asst. Prof. Paul McGuiness (former colleague) for English proof readings.

In order to thoroughly investigate Co-Pt nanowires, an interdisciplinary approach was used. For that reason international group from all over the world were involved, I would particularly like to thank Prof. Dr. Juan Escrig (Chile), Dr. Mariana P Proenca (Portugal), Prof. Dr. Manuel Vazquez (Spain), Alvaro P. Espejo (Chile), Asst. Prof. Volker Neu (Germany), Dr. Ulrike Wolff (Germany), Sven Stienen (Germany) for their help with different characterizations related to my project.

I would like to thank Prof. Dr. Rudolf Schaefer from Leibniz-Institut für Festkörper und Werkstoffforschung in Dresden, Germany, for providing me the opportunity to work for 4 months in his group. Thanks to Dr. Volker Neu and Dr. Ulrike Wolff for teaching me the quantitative MFM technique and micromagnetic simulations.

Thanks to my colleagues at the Department for Nanostructured Materials for their immense support, good energy and wonderful moments during the past four years. I only see my real family once a year, also thank you for being my family away from home. Thanks to Sanja Fidler (secretary, K7) for her smiles and help especially with English translations of official documents. My lunch, party, picnic and fun group, I feel lucky to know you guys (in alphabetical order: Mateja, Martina, Milivoj, Nadežda) and would like to thank you for every moment we spent together. You have been wonderful support throughout. I also want to thank all the people I have met during my stay at Department for Nanostructured Materials, K7.
Out of work-space I would like to thank my cricket club (Loka kriket www.lokakriket.si) friends, we won and we lost together. It was an amazing experience to hang out with you guys. Thanks!

Nina Makovec, you have been amazing company and I feel lucky to have you around. Your encouragement, trust and optimism help me fly high. The thesis writing process would not be that easy and enjoyable without your help. It is hard to return what you gave me with thanks or appreciation, you deserve everything I possess, do not change, stay like this forever. Thanks for worrying about me so I can worry about work. Thanks to Nina's parents for their kindness. No less thanks to *govani* (you knows who I am talking about)!

I am so grateful to my father and my late mother who always showed great trust in my abilities. Their trust was a driving force which makes me move forward. They are lucky stars for me, one in the sky and the other one on earth, and they will always shine on me. My siblings! Oh they are so lovely, always, as if we were younger. I do not have enough words to describe your contributions, thanks Fouzia, Sobia, Ali, Sonia, Hina and Zahid for your immense support and trust over the years.

Abstract

Ferromagnetic nanostructures (nanowires-NWs and nanotubes-NTs) have attracted considerable interest due to their unique properties and potential applications, ranging from the magnetic storage and recording devices, sensors and logic application. The fundamental understanding about the magnetic domain structure and magnetization reversal mechanism in a nanostructure is key to utilize them in possible applications. The main parameter that influences these magnetic properties of nanostructures is the effective anisotropy which further consists of a shape and a magnetocrystalline anisotropy (MCA) for most of the nanomaterials. Therefore, fine tuning of the effective anisotropy requires a control over involved anisotropies, thus providing the ability to tailor the magnetic properties for specific applications. For instance hcp, Co-Pt nanostructures with high MCA can be building blocks for racetrack memory (or domain-wall memory) devices due to their ability to contain a large number of domains, whereas, Fe-Pd NWs with a high shape anisotropy can be useful for logic devices.

In this thesis, we synthesized and characterized Co-rich Co-Pt nanostructures by potentiostatiostatic electrodeposition technique, into nanoporous of anodic aluminum oxide (AAO) as well as polycarbonate (PC) membranes with diameter ranges from 15-200 nm.

First we focused on the synthesis of relatively new complex magnetic structures with a tube-wire segments. The current transient (I-t curve) monitored during the deposition procedure allowed us to distinguish between the NT and NW formation during the electrodeposition synthesis, thus we present ground breaking results to fabricate Co-Pt nanostructures with a tube-wire morphology. For the first time we studied the magnetization reversal mechanisms in these complex Co-Pt nanostructures. We found that the tube segment always reverses its magnetization first, through nucleation and propagation of a vortex domain wall, whereas the wire segment magnetization follows via nucleation and propagation of a transverse domain wall. In order to further explain the results, micromagnetic simulations were performed that confirmed our experimental results. Such nanostructures are attractive from the application point of view due to their ability to control the motion of the magnetic domain wall. **(See Chapter 3)**

According to the phase diagram, Co-rich Co-Pt can crystalize in a hcp crystal structure, known to be highly anisotropic, with its magnetic response being dependent on the hcp c-axis orientation, which is the magnetization easy axis in this system.

The results showed that the crystal structure of the Co-Pt NWs depends on Co content and it was found that with Co content higher than 80 at% only hcp, 60-80 at% intermixed hcp and fcc and below 60 at% only fcc crystal structure was observed. The crystallographic orientation (texturing) analysis showed that c-axis [001] of hcp phase and the [111] of fcc phase are pointing almost perpendicular to the NW long axis. These observations allowed

us to understand the perpendicular easy magnetization axis of the Co-Pt NW arrays. **(See Chapter 4, 5, and 6)**

In order to determine the effective anisotropy in the Co-Pt NW system, we performed analytical calculations and compared them with the experimental measurements of the angular dependence of the coercivity (ADC) for Co-Pt NWs. From the good agreement between the two, we were able to determine the effective anisotropy constant (K_{eff}=2.6 $\times 10^4$ J/m^3) for Co-Pt NWs (diameter~200 nm) which further helped us to explain the magnetic properties of such NWs.

It is known that the in-plane magnetostatic interactions between the Co-Pt NWs in an array can be responsible for perpendicular easy axis. To determine the parameter influencing the perpendicular easy axis orientation, we performed first-order reversal curves (FORCs). We found that there are weak magnetostatic interactions between the Co-Pt NWs, thus, perpendicular magnetization easy axis is due to hcp crystal structure with strong texturing of c-axis perpendicular to NW long axis. The complex FORC diagrams were obtained for Co-Pt arrays in AAO membranes which is related to the variation of the hcp crystal orientation. The ferromagnetic resonance (FMR) results confirmed our hypothesis, where we obtained large linewidth connected to the inhomogeneity in hcp c-axis orientation in Co-Pt NWs arrays in AAO membranes. The information about hcp c-axis orientation is crucial for application point of view as it significantly influences switching-field distribution and the magnetic domain structure of such NWs. On the basis of these information we proposed the "oblivious growth" of Co-Pt NWs, related to small fluctuation in pore diameter and pore shape first time. From the FMR measurements we were able to estimate the effective anisotropy constant (K_{eff}=4$\times 10^4$ J/m^3) which was found to be very close to the observed values from ADC for Co-Pt NWs, confirmed the validity of both methods. **(See Chapter 5)**

The results obtained from interacting Co-Pt NWs array accentuate that the characterization of an individual NW can be washed out, thus it is important to gain magnetic information on an individual NW structure. Thus, we separated Co-Pt NWs from their membranes and studied their magnetic domain structure with magnetic force microscopy (MFM). In hcp Co-Pt NWs (daimeter~200 nm) with c-axis pointing perpendicular to NW long axis a rapid alternation of pairs of diametrically opposed dark-and-bright contrasts along the lengths of the NWs was observed. Such contrast can be originated by a competition between the shape and MCA and can be interpreted as transverse (TS) and/or longitudinal stripe (LS) domain structures in NWs. It is important to stress out that such magnetic domain structures in high perpendicular anisotropic NWs are under intense research and conflicting in some cases. We have found that both domain structures (TS and LS) have the lowest energy state when the strong MCA is acting perpendicular to NWs long axis. In case of acute angle of hcp c-axis w.r.t to NW along axis the vortex domain structure became favorable. Our conclusion is based on a large number of MFM experimental results compared with micromagnetic simulation (NMAG). **(See Chapter 5 and 6)**

For the comparative purpose the magnetic response of ferromagnetic Fe-Pd NW arrays and individual Fe-Pd NWs are presented. Unlike Co-Pt NWs we observed that equiatomic Fe-Pd NWs show a single domain behaviour with the magnetization easy axis along the long axis. Square hysteresis loop was obtained for a single Fe-Pd NW, however strong magnetostatic interactions was observed to be responsible for sheered hysteresis loop in arrays, information obtained is critical for such applications. **(See Chapter 7)**

This study shows that the magnetization distribution and magnetization reversal in Co-rich Co-Pt NWs is driven by the MCA and it is tuned by the crystal structure. On the other hand in low MCA materials like *fcc* Fe-Pd the shape anisotropy is the governing factor. Moreover, a complete control over these anisotropies (including hcp c-axis) is paramount to tune the magnetic properties of such NWs for possible applications such as racetrack memory devices or as structural components in micro- and nano-electronic devices.

Povzetek

Feromagnetne nanostrukture v eni razsežnosti (nanožice) so pritegnile precej pozornosti, predvsem zaradi njihovih edinstvenih lastnosti v potencialno zanimivih aplikacijah, kot so; magnetne pomnilne in zapisovalne naprave, senzorji in druge digitalno-logične aplikacije. Ključno, pri integraciji teh materialov v možne aplikacije, je bazično razumevanje porazdelitve magnetizacije v magnetnih domenskih strukturah ter razumevanje mehanizma obračanja magnetizacije pod vplivom zunanjega magnetnega polja. Glavni parameter, ki vpliva na magnetne lastnosti nanostruktur, je efektivna anizotropija. Ta je za večino materialov vsota dveh prispevkov, ki sta morfološka ali oblikovna in magnetno-kristalna anizotropija. Da bi prilagodili magnetne lastnosti odgovarjajoči aplikaciji, je potrebno natančno kontrolirati vključujoče anizotropije, ki posledično spreminjajo efektivno anizotropijo ter s tem uporabne magnetne lastnosti. Na primer, nanožice Co-Pt z veliko magnetokristalno anizotropijo so lahko gradniki pomnilnih naprav, kot so novi magnetni spominski mediji na osnovi domenskih sten. Ti mediji, kot bo prikazano v disertaciji, vsebujejo veliko domenskih sten. Za primerjavo nanožice, na osnovi sistema Fe-Pd, odlikuje monodomenska struktura, zaradi prevladujoče oblikovne anizotropije in se lahko uporabljajo za druge aplikacije kot na primer elemente v logičnih vezjih.
V tej doktorski disertaciji smo sintetizirali in analizirali nanožice Co-Pt, bogate s kobaltom. Sintetizirali smo jih z metodo elektro nananšanja pri konstantnih potencialih. Za pripravo nanožic smo uporabili dve vrsti membran, nano-porozni aluminijev oksid in polikarbonatne membrane. Premer por v membranah je bil med 15 in 200 nm.

Najprej smo se osredotočili na sintezo relativno novih kompleksnih magnetnih nanostruktur z zloženima segmentoma, cevke in žice. S tem predstavljamo prelomne rezultate pri sintetiziranju tovrstnih Co-Pt kompleksnih materialov. Kot prvi smo tudi študirali mehanizem obračanja magnetizacije v teh nanostrukturah. Ugotovili smo, da magnetizacijo vedno prvi obrne cevni segment, in to tako, da nukleira in propagira magnetno vrtinčasto domensko steno. Magnetizacija v žičnem segmentu pa se spremeni z nukleacijo in translacijo transverzalne domenske stene. Da bi bolje razumeli in razložili te pojave smo izvedli tudi mikromagnetne simulacije. Pokazali smo, da so take nanostrukture aplikativno zanimive, saj imamo možnost, da nadzorujemo premikanje magnetnih domenskih sten. (*glej* Poglavje 3)

Glede na ravnotežni fazni diagram sistema Co-Pt, faza Co-Pt, ki je bogata na kobaltu, kristalizira v strukturo heksagonalnega najgostejšega sklada (hexagonal close packed - *hcp*), ki izkazuje visoko magnetokristalno anizotropijo. Magnetni odziv sistema je tako odvisen od orientacije osi c, ki je v tem sistemu tudi lahka os/smer magnetizacije.

Rezultati kažejo, da je kristalna struktura Co-Pt nanožic odvisna od vsebnosti kobalta. Če je slednjega več kot 80 at. %, struktura zavzame *hcp* ureditev. Kadar je Co med 60 in 80 at. %, sta prisotni dve kristalni strukturi. Poleg že omenjene, nastopi tudi kubični najgostejši sklad oz. ploskovno centrirana kubična struktura (*face centered cubic - fcc*). Fcc pa je edina kristalna faza zastopana v nanožicah, ko je vsebnost Co pod 60 at.%. Kristalografska karakterizacija je pokazala, da je orientacija *hcp* (001) ravnin in (111) ravnin v strukturi *fcc* skoraj pravokotna na daljšo os v analizirani žici. Posledično smo na račun teh ugotovitev lahko razložili pravokotno usmeritev lahke smeri magnetizacije v nizih nanožic Co-Pt, izmerjenih z magnetometrom s tresočim vzorcem. (*glej* Poglavje 4, 5 in 6)
Da bi določili efektivno anizotropijo sistema nanožic Co-Pt, smo napravili tudi analitične izračune in jih primerjali z eksperimentalnimi meritvami kotne odvisnosti koercitivnosti v nanožicah Co-Pt. Iz dobljenih dobro ujemajočih se rezultatov smo lahko določili efektivno konstanto anizotropije ($K_{eff} = 2.6 \times 10^{4}$ J/m^3) za nanožice Co-Pt (s premerom ~200 nm), kar je dodatno pripomoglo k razumevanju magnetnih lastnosti takšnih nanožic.

Znano je, da so lahko dipolne medsebojne interakcije med nanožicami Co-Pt vzrok za pravokotno usmeritev lahke smeri magnetizacije. Da bi določili parametre, ki določajo trend, smo izmerili povratne histerezne krivulje prvega reda (FORCs). Ugotovili smo, da je magnetna dipolna interakcija med nanožicami Co-Pt le šibka. Zato lahko sklepamo, da je pravokotna usmeritev lahke smeri magnetizacije posledica kristalne strukture *hcp,* z visoko orientiranostjo c-osi pravokotno na dolžino nanožic. Rezultati feromagnetnih resonančnih merjenj (FRM) so potrdili hipotezo o manjših odstopanjih od visoke orientiranosti. Take informacije o orientacijah c-osi v *hcp* so ključne za aplikacije, saj te pomembno vplivajo na porazdelitev polj, pri katerih se magnetizacija obrne, ter tudi na strukturo magnetnih domen. Na podlagi teh informacij smo predlagali posebni mehanizem rasti nanožic Co-Pt, kot posledico majhnih fluktuacij v radiju in obliki por. Iz rezultatov FORC smo lahko določili konstanto efektivne anizotropije ($K_{eff} = 4 \times 10^{4}$ J/m^3), ki je bila zelo podobna tisti, ki smo jo določili iz meritve kotne odvisnosti koercitivnosti. Podobni rezultati obeh meritev na Co-Pt nanožicah potrjujejo ustreznost obeh meritev. (*glej* Poglavje 5)
Ker je magnetni doprinos posamezne nanožice v nizu zaradi medsebojnih vplivov zabrisan, smo posamezne nanožice ločili od membran in sosednjih nanožic. Domenske strukture smo nato preučevali na eni nanožici s pomočjo mikroskopa na magnetno silo (MFM). V nanožicah Co-Pt *hcp* (premera ~ 200 nm) in z lahko osjo magnetizacije orientirano pravokotno na daljšo os nanožice, smo opazili hitro se menjajoča diametralna temna in svetla področja vzdolž dolžine nanožic. Tak kontrast lahko nastane kot posledica vzajemnega delovanja oblikovne in magnetokristalne anizotropije in ga lahko interpretiramo s transverzalno in/ali longitudinalno pasovno domensko strukturo. Pomembno je dodati, da je taka magnetna domenska struktura na splošno, in predvsem v zadnjem času, intenzivno raziskovana, interpretacije pa so si nasprotujoče. Ugotovili smo, da imata obe domenski strukturi, tako longitudinalna kot transverzalna pasovna, najnižjo energijo, ko intenzivna lahka os deluje pravokotno na daljšo os nanožice. Pri žicah s c-osjo *hcp* odmaknjeno od pravokotne smeri glede na dolžino žice, pa smo opazili, da obstajajo tudi druga domenska stanja, kot je vrtinčasta domenska struktura. Naši zaključki temeljijo

na velikem številu rezultatov eksperimentalnih meritev z MFM in njihovimi korelacijami z mikromagnetnimi simulacijami (NMAG). (*glej* Poglavje 5 in 6)

Za primerjalne namene smo predstavili magnetni odziv feromagnetnih nizov nanožic Fe-Pd in odzive na posamezni nanožici Fe-Pd. Za razliko od nanožic Co-Pt smo opazili, da imajo nanožice Fe-Pd monodomensko strukturo, z usmeritvijo lahke smeri magnetizacije vzdolž žice, kar je posledica nizke magnetokristalne anizotropije kubične kristalne faze Fe-Pd. Posledica take usmeritve magnetizacije je kvadratna histerezna zanka, ki pa se zoži, ko obravnavamo nize takih nanožic, ki so v medsebojnem magnetnem vplivu. (*glej* Poglavje 7)

Raziskave opravljene tekom te disertacije kažejo, da je porazdelitev magnetizacije in njeno obračanje v nanožicah Co- Pt bogatih s kobaltom, posledica magnetokristalne anizotropije, ki jo lahko krojimo s spreminjanjem usmeritve kristalne strukture v žici. Po drugi strani pa je porazdelitev magnetizacije v strukturah z nizko magnetokristalno anizotropijo, kot so žice Fe-Pd, ki kristalizirajo v kubični kristalni strukturi, pogojena z obliko oz. velikostjo in posledično oblikovno anizotropijo. Popolno razumevanje in kontrola teh anizotropij (vključno s c-osjo v *hcp*) je najpomembnejše za nadaljnjo integracijo teh materialov v možne aplikacije, kot so; novi magnetni spominski mediji na osnovi domenskih sten, ali strukturne komponente v mikro in nano- elektronskih napravah.

Contents

List of Figures **xix**

List of Tables **xxi**

Abbreviations **xxiii**

1 Introduction **1**
1.1 Why Study Nanomagnets? ... 1
1.2 Basics of Nanomagnetism ... 2
1.2.1 Magnetic Anisotropies ... 2
1.2.1.1 Shape anisotropy ... 2
1.2.1.2 Magnetocrystalline anisotropy ... 3
1.3 1D Nanostructures ... 4
1.3.1 Nanowires and nanotubes ... 4
1.3.1.1 Nanowires as potential candidate for racetrack memory devices 5
1.3.2 Nanostructures with tube-wire Morphology ... 6
1.3.3 High anisotropy hcp Co-Pt based NWs ... 6
1.4 Magnetic Properties of 1D Nanostructures ... 7
1.4.1 Magnetic domains configurations in NWs ... 7
1.4.2 Magnetization reversal modes in nanowire and nanotubes ... 8
1.5 Characterization of Nanomagnets ... 11
1.5.1 Magnetic force microscopy ... 11
1.5.2 First-order reversal curves (FORCs) measurements ... 13
1.5.3 Ferromagnetic resonance (FMR) measurements ... 15
1.5.4 Micromagnetic simulation ... 17
1.6 Fabrication of Nanomagnets ... 18
1.6.1 Template-assisted electrodeposition ... 18

2 Aims and Hypothesis **21**
2.1 Description of the Problem ... 21
2.2 Purpose and Goals of the Thesis ... 22

3 Angular Dependence of the Coercivity in Electrodeposited Co-Pt Nanostructures with a Tube-Wire Morphology **27**

4 Effect of Magnetocrystalline Anisotropy on the Magnetic Properties of Electrodeposited Co-Pt Nanowires **33**

5 An Oblivious Growth Mechanism for High-Magnetic-Anisotropy hcp Co-Pt Nanowire Arrays: The Role of the Crystal Orientation in the Switching-Field Distribution and the Magnetic-Domain Configuration **53**

6 Microstructure and Magnetic Properties of Electrodeposited Co-Pt Nanowires (NWs) with Diameters below 100 nm 75

7 Magnetization-Switching Study of fcc Fe-Pd Nanowire and Nanowire Arrays Studied by In-Field Magnetic Force Microscopy 81

8 Miscellaneous Results 87
8.1 Current Induced Domain-Wall Movement in Cylindrical Co-Pt Nanowires: Theoretical Approach 87
8.1.1 Current induced domain wall motion in periodic magnetic domains in Co-Pt nanowires 88
8.2 A Domain-Wall-Pinning Mechanism in Notched Cylindrical Electrodeposited Co-Pt Nanowires 90
8.3 Magnetization Switching Behaviour of Individual Single Domain Co-Pt Nanowire 93

9 Summary and Conclusions 95
9.1 Future Directions 98

10 Appendix 99
10.1 Journal Papers Submitted and Published: 99
10.2 Conference Papers/Presentations Accepted and Published: 100
10.3 Research Poster Presentations 101

11 References 103

List of Figures

Figure 1.1: Illustration of the different type of materials by their dimension and size; 0D (zero dimensional) nanoparticles; 1D NWs/NTs; 2D thinfilms (adapted from [5]). 1
Figure 1.2: Characteristic length scales in magnetism. Adapted from [5]. 2
Figure 1.3: Schematic of Racetrack memory devices showing working principle of device. Adapted from [29]. 5
Figure 1.4: Geometrical characterization of a wire-tube nanostructure. Adapted from [36]. 6
Figure 1.6: Different MR modes: Coherent (C), Transverse (T) and Vortex (V) modes. w_T and w_V represent the domain wall widths of a transverse and vortex domain wall, respectively. Adapted from [2]. 9
Figure 1.7: a magnetic tip interacts with the magnetic stray field of the sample. The changes in the status of the cantilever are measured by the deflection sensor, and recorded to generate the image. Adapted from [63]. 12
Figure 1.8: Tapping/lift mode (dual), first tapping scan is used to obtain the sample's topography, which in the lift scan magnetostatic interactions are recorded. 13
Figure 1.9: Mathematical hysteron from the classical Preisach model [67]. 14
Figure 1.10: FORC measurements (insets) and FORC diagrams of the Co-Pt NWs arrays when the applied field is (a) parallel to the Co-Pt NW's long axis for PC membrane. 14
Figure 1.11: (a) Motion of M under constant H (b) Torque component exerted on the magnetization M by rotational field H. Adapted from [70]. 16
Figure 1.12: (a) and (c) Schematic image of the AAO and PC membrane, respectively. (b) and (c) schematic of NWs fabricated after electrodeposition into AAO and PC membranes, respectively. 19
Figure 1.13: Schematic of the electrochemical cell for the electrodeposition of Co-Pt NWs. 20
Figure 3.1: (a) geometrical characterization of a wire-tube nanostructure. (b) Micromagnetic simulation results of nanostructure with tube-wire morphology showing domain pinning at the interface between tube and wire. (c) Hysteresis curve for a Co-Pt wire-tube nanostructure when a magnetic field is applied along its axis. The central snapshot shows the vortex domain wall that appears between the two segments of the nanostructure. 28
Figure 8.1: Schematic diagram of a racetrack memory operation (a) selecting, (b) writing and (c) reading a memory bit. By applying a negative (or positive) current pulse to the NW, the magnetic domain walls move to the left (right) in the diagram, controlling in this way the access to the data stored along the wire. Adopted from [99]. 87
Figure. 8.2: (a)-(c) and (e)-(h) The experimental MFM images of individual Co-Pt NWs with a diameter of ~250 nm. Upper row shows dark-and-bright contrast along the length of the NW, while in the lower row the contrast is along the short axis of the NW. (a1) and (d1) NMAG simulation images of the magnetization profile in a small segment of the NW at two different angles (90°). (d) and (i) TS and LS configuration, respectively. 89

Figure 8.3: Micromagnetic simulation results for spin polarized current induced domain wall motion in Co-Pt NWs..... 90
Figure 8.5: (a) SEM image of the Co-Pt nanowire (length~2 μm and diameter~50 nm) with a notch in the middle, (inset) close-up image of the notch area. (b) AFM image (c) MFM image. (d) micromagnetic simulation on cylindrical Co-Pt NW with same dimension as in experiment with notch half the size of the wire diameter. (e) and (f) simulation showing formation of the transverse domain wall at the notch site as evident by the arrows pointing outward. 92
Figure 8.6: (a) The SEM image of the Co-Pt NW with length ~1μm and diameter 200 nm with non-magnetic part of membrane is attached to the top end of the nanowire (BSE image). (b) AFM picture showing the topology of an individual Co-Pt nanowire (height image). (c) MFM picture of Co-Pt NW under no external field showing uniform dark contrast (phase image). (d) and (e) MFM images under negative and positive external magnetic field (±15 mT) respectively. 93
Figure 9.1: Visual summary of the thesis. 95

List of Tables

Table 1: AAO and PC membranes with different diameters used in this thesis.....19

Abbreviations

1D	...	One-dimensional
2D	...	Two-dimensional
A	...	Exchange stiffness constant
AAO	...	Anodic Aluminum Oxide
ADC	...	Angular dependence of the coercivity
AFM	...	Atomic force microscopy
A_w	...	Atomic weight
BSE	...	Backscattered electron
d, D	...	diameter
d_c	...	Pore separation
d_{in}	...	Internal diameter of nanotube
d_o	...	Outer radius of nanotube
d_p	...	Pore diameter
e	...	Charge of an electron
E	...	Energy
ED	...	Electrodeposition
EDX	...	Energy-dispersive x-ray spectroscopy
E_{ex}	...	Exchange energy
F	...	Faraday constant
fcc	...	Face centered cubic
fct	...	Face centered tetragonal
FEG-SEM	...	Field emission gun scanning electron microscopy
FIB	...	Focused ion beam
FMR	...	Ferromagnetic resonance
FORC	...	First-order reversal curve
G	...	Gilbert damping constant
h	...	Plank constant
H_c	...	Coercivity
hcp	...	Hexagonal close packed
H_d	...	demagnetizing field
HDD	...	Hard disk drive
H_{eff}	...	Effective anisotropy field
$H_{eff,o}$	...	Overall effective anisotropy field
H_{MCA}	...	Magnetocrystalline anisotropy field
H_{ms}	...	Magnetostatic interaction field
H_u	...	Magnetostatic interaction
I	...	Current
J_p	...	Bessel function of first kind with order p

K	...	Crystal anisotropy constant
K_{eff}	...	Effective anisotropy constant
K_{mca}	...	Magnetocrystalline anisotropy constant
K_{sh}	...	Shape anisotropy constant
L	...	Length
LLG	...	Landau Lifshitz Gilbert
LS	...	Longitudinal stripe
L_{ex}	...	Exchange length
m	...	Mass
M	...	Magnetization
MCA	...	Magnetocrystalline anisotropy
MEMS	...	Magneto-electromechanical system
MFM	...	Magnetic force microscopy
M_r	...	Remanent magnetization
MR	...	Magnetization reversal
M_s	...	Saturation magnetization
n	...	Number of electrons
N_d	...	Demagnetizing factor
$N_{x,y,z}$	...	Demagnetizing factor along x, y and z-axis
NT	...	Nanotube
NW	...	Nanowire
Q	...	Charge
SCE	...	Saturated calomel electrode
SEM	...	Scanning electron microscope
T mode	...	Transvers mode
TEM	...	Transmission electron microscope
TS	...	Transverse stripe
V mode	...	Vortex mode
VSM	...	Vibrating sample magnetometry
w_T,w_V	...	Transverse and vortex domain wall width
XRD	...	X-ray diffraction
Y_p	...	Bessel function of second kind with order p
α	...	Gilbert damping constant
α_i	...	Direction cosines
μ, μ_o	...	Permeability, Permeability of free space
γ	...	Gyromagnetic ratio
η	...	Geometrical parameter
σ	...	Standard deviation
σ_{int}	...	Local magnetostatic interactions
κ	...	Mean magnetostatic interactions
ω	...	Microwave frequency

Chapter 1

Introduction

1.1 Why Study Nanomagnets?

This Chapter provides a brief introduction of the magnetic nanostructures, an investigation of their magnetic properties and a presentation of their potential applications. Recent progress in advanced electronics, magnetic sensors, actuators and data storage devices has motivated a large research effort to scale down the size of the components and to investigate different novel ferromagnetic materials such as thinfilms (2D), nanowires (NWs)/nanotubes (NTs) (1D) and nanoparticles (0D) as shown in Figure 1.1. In particular, special attention has been focused on 1D ferromagnetic nanostructures (NWs and NTs) to address not only fundamental physical questions, e.g. magnetic domain configurations [1] and magnetization reversal processes [2], but also for technological reasons, owing to their potential applications in biosensors [3] and magnetic memory devices [4].

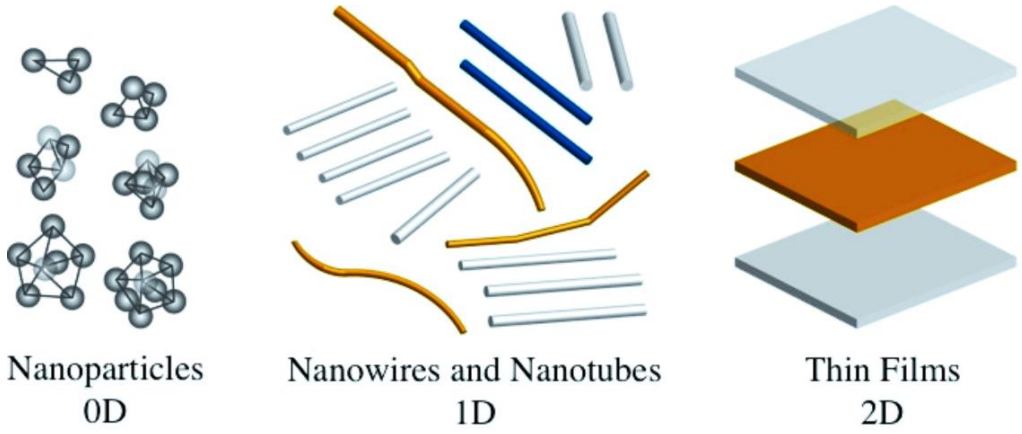


Figure 1.1: Illustration of the different type of materials by their dimension and size; 0D (zero dimensional) nanoparticles; 1D NWs/NTs; 2D thinfilms (adapted from [5]).

A fundamental aspect to take into account when reducing the dimension of a material, is the size of the critical length scales which triggers different physical phenomena as shown in Figure 1.2. When a sample or one of its dimensions is reduced to a specific size, e.g. ≈100 nm, its dimensions become comparable to the exchange length $L_{ex} = \sqrt{\frac{2A}{\mu_0 M_s^2}}$, where A is the magnetic stiffness constant, $\mu_0 = 4\pi \times 10^{-7}\mathrm{NA}^{-2}$ is the vacuum magnetic permeability and M_s is the saturation magnetization of the magnetic materials. The

exchange length characterizes the competition between exchange and the dipolar energies in a material. It is in the length range of 2-15 nm for most of the ferromagnetic materials, and is a measure of the shortest scale on which the magnetization can be twisted in order to minimize the dipolar interaction. Other important length scales are domains and domain wall width (transition region between two different magnetic domains e.g. Bloch domain wall, $\delta_w \approx \pi\sqrt{\frac{A}{K_u}} \approx 20 - 130$ nm), where K_u is the uniaxial anisotropy constant; and the coherent radius (maximum size of the uniformly magnetized particle where magnetization reversal takes place by coherent rotation; $R_{coh} = 3(A)^{1/2}/M_s$~10-50 nm). The combination of the high surface area and the unique properties exhibited by the materials reduced to the nanoscale, are of great interest to the scientists and engineers making research in nanotechnology. It is worth mentioning that the research in the field of nanotechnology also stimulates the understanding of the physics of different phenomenon and processes as shown in Figure 1.2, impelling the development of new modelling and experimental tools, generating new device principles and manufacturing methods [5].

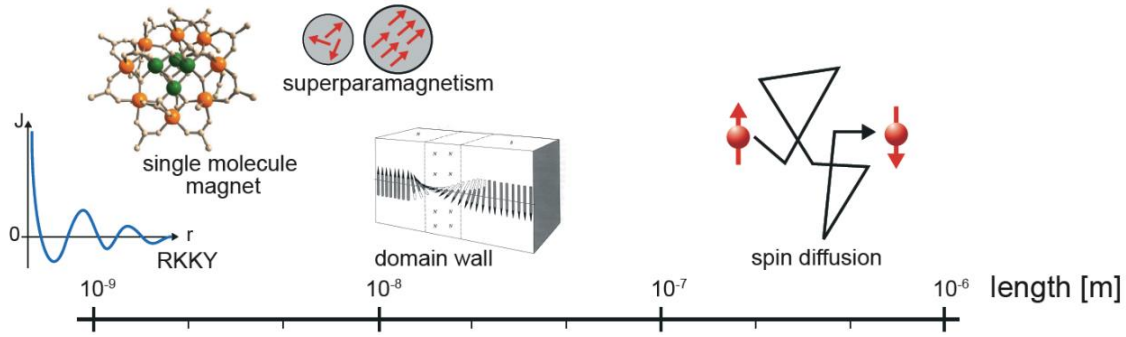


Figure 1.2: Characteristic length scales in magnetism. Adapted from [5].

1.2 Basics of Nanomagnetism

1.2.1 Magnetic Anisotropies

Magnetic materials have one most significant feature to align their magnetization in a certain preferential direction. This corresponds to the energetically most favorable direction of the spontaneous magnetization and is usually called the easy-axis of the magnetization. The dependence of the magnetic properties of a material on the direction is determined by the magnetic anisotropies of such material. Without these anisotropies magnetic order could hardly be observed, the reason for this is the short range character of the exchange interaction. The effective magnetic anisotropy is mainly caused by different contributions made up of shape, and magnetocrystalline anisotropy. These anisotropies are further explained in the next Section.

1.2.1.1 Shape anisotropy

As 1D nanostructures such as NWs are non-spherical objects, the demagnetizing field will not be equal in all directions, creating easy axis along the length of the NWs. Therefore, it is easier to magnetize a NW along its long axis than along its short axis. When a NW is

magnetized along its long axis, a demagnetizing field H_d acts in the opposite direction from the magnetization M which creates it, and is proportional to it,

$$H_d = -N_d M_s \tag{1.1}$$

Where N_d is the demagnetizing factor and is dependent on the shape of the body, it can be exactly calculated for a uniformly magnetized ellipsoid. Material with weak magnetocrystalline anisotropy energy show strong shape anisotropy for instance Ni, Fe Fe-Pd and Ni-Fe etc. [6-8]. For an array of such NWs the overall effective anisotropy H_{eff} can be calculated by considering only the contribution of the shape anisotropy and the dipolar interactions between the NWs [7, 9, 10]. This coupling depends on the distance between the wires and is proportional to the wire packing P.

$$H_{eff} = 2\pi Ms(1 - 3P) \tag{1.2}$$

where P ($= \frac{\pi}{2\sqrt{3}}\left(\frac{D_p}{D_c}\right)^2$) [11], is the membrane-packing factor. D_p and D_c are pore diameter and pore separation of the membrane, respectively. This Eq 1.2 is known as mean field model and it yields a demagnetizing factor parallel to the axis of the wire equal to the packing factor (P) of the membrane and a factor equal to $\frac{1-P}{2}$ in the perpendicular direction [10, 12] when the hysteresis loop of the arrays of NWs is measured.

1.2.1.2 Magnetocrystalline anisotropy

The magnetocrystalline anisotropy (MCA) results due to the spin-orbit coupling in a magnetic material. The crystallographic structure of a highly anisotropic material, such as hexagonal close packed (hcp) Co-Pt, face centered tetragonal (fct) Fe-Pt will strongly influence its magnetic response, as some of the crystallographic directions are preferential for the magnetization alignment e.g. c-axis of the hcp crystal structure. Co-Pt in the hcp structure is a well-known magnetic material with high MCA (K_u=1x10^6 J/m^3), comparable to or even stronger than the shape anisotropy ($\pi\mu_o Ms^2$=4x10^5 J/m^3) in magnetic NWs [13, 14]. It is well-known that in hcp Co-Pt NWs c-axis favors to align perpendicular to NW long axis. Thus, it is possible that the MCA and shape anisotropy competes with each other and triggers interesting physical phenomena such as periodic domain structure in NWs. It is important to note that the MCA of the polycrystalline NWs depends on the preferred orientation of the enclosed crystallites (c-axis). There are two boundary cases: (1) if all crystallites have the same orientation, the anisotropy of the polycrystalline NWs exactly equals that of the single crystal NWs [15, 16], (2) for the case of the isotropic system in which all the orientations occur with the same probabilities, the behaviour of the polycrystalline NWs is isotropic and MCA in many cases is negligible. Forster *et al.* [17] and Ivanov *et al.* [18] investigated the magnetization reversal of hcp Co NWs made up of grains with different orientations w.r.t. wires long axis, using the finite-element method; their results showed that the granular structure and orientation of crystallites greatly influence the magnetization reversal of such nanowires and should be taken into account. Ivanov *et al.* [18] simulated that when the angle of the MCA easy axis with the NW axis is larger than 70^o the MCA competes with shape anisotropy. There are some experimental reports about hcp Co NWs where the orientation of the c-axis plays an important role in the magnetization and magnetization reversal process [19, 20]. Therefore, it is possible to

tune the magnetization and magnetization reversal of high anisotropic materials such as hcp Co-Pt NWs by controlling the crystal orientation (c-axis) [19].

In a case the MCA plays a significant role one has to modify the expression for effective anisotropy field (Eq. 1.2) for arrays of NWs [17]. Thus, the effective anisotropy field H_{eff} in this case can be summed up as [7, 21],

$$H_{eff} = H_{ms} - H_{MCA} = 2\pi Ms(1-3P) - \tfrac{1}{2} < H_{MCA} > \qquad (1.3)$$

Where H_{MCA} is the MCA term. The first part of the Eq. 1.3 is the mean field model and the second part is a contribution from MCA. The question is how can we estimate the contribution of MCA in effective anisotropy field? Currently, an understanding of the MCA can be obtained from the ab initio band structure calculations [22], e.g. by using density function theory. Nevertheless, from an experimental point of view a universal and fast description of the situation is needed. Hence, phenomenological approach for the free energy density is used for decades. It is based on a power series expansion of the component of the magnetization and by taking into account the symmetry as [23].

$$E = E_o + \sum_i b_i \alpha_i + \sum_{ij} b_{ij}\alpha_i\alpha_j + \sum_{ijk} b_{ijk}\alpha_i\alpha_j\alpha_k + \sum_{ijkl} b_{ijkl}\alpha_i\alpha_j\alpha_k\alpha_l + \ldots\ldots \quad (1.4)$$

Where α_i= (α_1=sinθcosφ, α_2=sinθsinφ, α_3=cosθ) are the direction cosines and satisfy the condition $\alpha_1^2 + \alpha_2^2 + \alpha_3^2 = 1$. For a hexagonal system, the energy density can be expressed as [23]

$$E = K_1 sin^2\theta + K_2 \sin^4\theta + K_3 \, sin^6\,\theta + \cdots \quad (1.5)$$

where θ and φ are polar angles of the magnetic moment in the crystal axis frame and K's are the crystal anisotropy constants. And for cubic system, the energy density can be written as [23]

$$E = K_o + K_1(\alpha_1^2\alpha_2^2 + \alpha_1^2\alpha_3^2 + \alpha_2^2\alpha_3^2) + K_2\alpha_1^2\alpha_2^2\alpha_3^2 + K_3(\alpha_1^2\alpha_2^2 + \alpha_1^2\alpha_3^2 + \alpha_2^2\alpha_3^2 + \cdots \quad (1.6)$$

1.3 1D Nanostructures

1.3.1 Nanowires and nanotubes

Several lithography techniques have been employed to fabricate 1D nanostructures (NWs and NTs), which are usually expensive and time-consuming [21, 24]. An alternative bottom-up route to synthesize ordered and high aspect-ratio NWs and NTs is a template-assisted electrodeposition [25-27]. Most widely used templates/membranes are anodic aluminum oxide (AAO) and polycarbonate (PC). This method stands out because, it is a low cost and very versatile in fabricating ordered arrays of magnetic NWs, NTs and other nanostructures. We will discuss in more detail about template-assisted electrodeposition in the next Section **(1.6.1 Template-assisted electrodeposition)**.

1.3.1.1 Nanowires as potential candidate for racetrack memory devices

With the growing need for miniaturization of devices, the use of nanowires (NWs) for magnetic recording media has gained attention in the last couple of years. The racetrack memories are revolutioning the research and technology developments on magnetic storage devices [28]. The racetrack memory device is a ferromagnetic NW where the information is stored along the length of the wire, as a sequence of magnetic domains as shown in Figure 1.3.

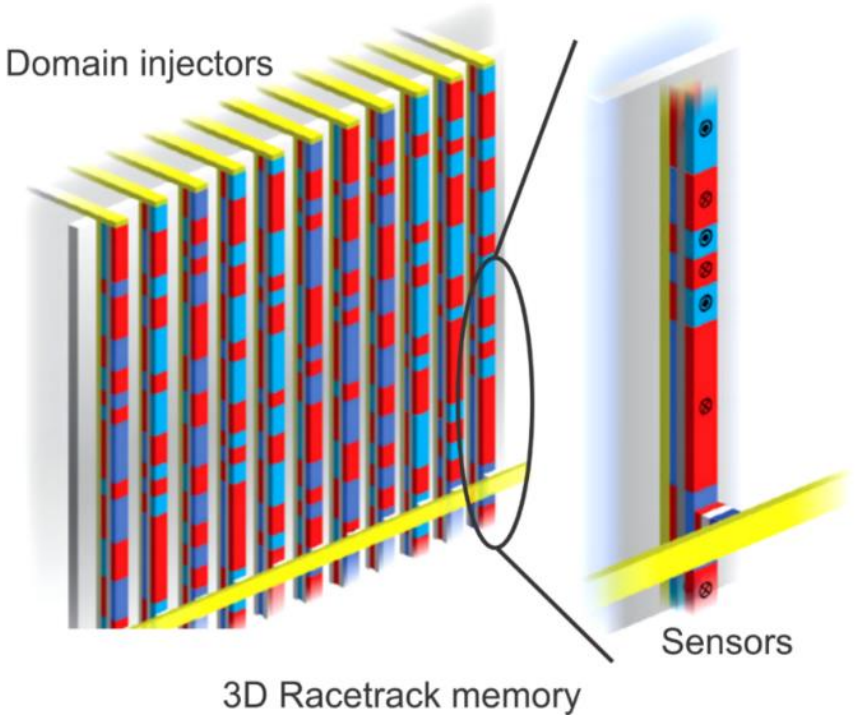


Figure 1.3: Schematic of Racetrack memory devices showing working principle of device. Adapted from [29].

By applying short pulses of a spin polarized current, one can move magnetic domain walls along the length of the NWs, reaching the sensors as shown in Figure 1.3. The precise control of the movement of magnetic domain walls along the NW is under an intense investigation, as its accurate understanding is paramount for the device application. Recently a huge research has been focused on soft magnetic NWs such as permalloy ($Ni_{80}Fe_{20}$) and some promising results have been obtained [30, 31]. However, there are some limitations of the permalloy which prevent the improvement of the racetrack memory density. The limitations are due to the soft magnetic nature of the permalloy e.g. (1) fewer domain walls can be created and (2) domain wall expansion due to the spin polarized current [32]. According to the roadmap for racetrack memory devices such limitations can be improved with implementation of the high anisotropic materials [28]. The possible candidates are cobalt-based alloys e.g. hcp Co-Pt, hcp Co-Ni, and hcp Co-Fe etc.

1.3.2 Nanostructures with tube-wire Morphology

A new type of nanostructures with tube-wire morphology (see Figure 1.4) is also proposed for possible applications in racetrack memory devices due to their ability to control the motion of the domain walls [33-35]. In addition, the magnetic properties of NTs and NWs have been exploited during the past two decades and understood to a greater extent. Now it is time to bring new challenges to the field by building nanostructures consisting of both NT and NW segments in a single nanostructure. Such nanostructures are a new type of 1D materials that have great potential to become building blocks for advanced magnetic devices. The properties of these nanostructures are expected to be hybridized between NTs and NWs. However, except in this thesis there is no experimental report that investigates the fabrication and magnetic properties of cylindrical nanostructures comprised of both NT and NW segments, in spite of a few theoretical reports [34, 35]. Neumann *et al.* [34] predicted that in nanostructures with wire-tube morphology different reversal modes can be induced in each segment by choosing the right geometrical parameters and they observed a kink in the hysteresis curve which is an indication of the partial pinning of the domain wall at the interface between NT and NW and will be discussed in detail in Chapter 3. In addition, Salazar *et al.* [35] showed that the tube segment reverses its magnetization before the wire segment, allowing a control of the magnetic domain walls' motion between the two segments. For more detail about these nanostructures see Chapter 3.

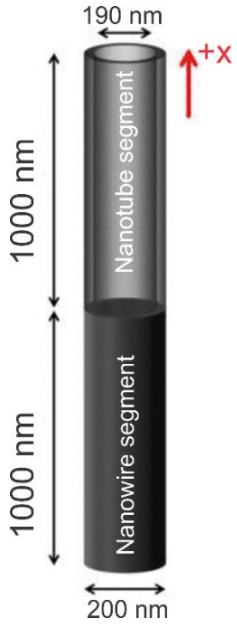


Figure 1.4: Geometrical characterization of a wire-tube nanostructure. Adapted from [36].

1.3.3 High anisotropy hcp Co-Pt based NWs

A number of studies have been reported on arrays of soft magnetic NWs such as Ni, Fe, Ni-Fe etc. [6-8] for the applications where strong shape anisotropy is desired. Strong shape anisotropy leads to an orientation of the magnetization along the length of the NW. While such magnetic configuration competes with magnetostatic interaction in NW arrays result in a reduction of the effective longitudinal anisotropy [37].

Co-based alloys are an integral part of modern magnetic recording media such as hard disk drive (HDD) due to their excellent magnetic properties. Alloying Co with metals like Pt enhances its intrinsic magnetic properties such as MCA. In addition it shows excellent chemical stability, higher coercivity and resistance against corrosion which makes such alloys suitable candidates for magnetic data storage devices. Due to the size-confinement trend in magnetic storage devices, it is reasonable to expect that the Co-Pt alloy nanostructures such as NWs and NTs would replace their counterparts in future. As mentioned, hcp Co-Pt is a well-known magnetic material with high MCA, it is comparable to or even stronger than the shape anisotropy in magnetic NWs [13, 14]. In many cases, MCA of hcp phase favors the easy magnetization axis perpendicular-to-the-NW axis [1, 38]. Thus, the effective anisotropy energy is determined by the competition between shape and MCA, resulting in a near energy balance, and consequently to an order of magnitude decrease in the effective anisotropy. However, it is acceptable when magnetization easy axis perpendicular to the NWs long axis is desirable. Moreover, it is possible to tune the preferred magnetization direction, magnetization reversal mechanisms and magnetic domains structure in Co-Pt NWs by accurately control the crystallographic structure of hcp crystallites in the NWs [19, 39, 40].

1.4 Magnetic Properties of 1D Nanostructures

1.4.1 Magnetic domains configurations in NWs

A sample of a ferromagnetic material larger than critical size (R_{coh}) is not magnetized homogeneously but consists of several domains (regions of uniform magnetization). They are separated by domain walls, region where the magnetization direction changes gradually. The demagnetization field reduces by the formation of magnetic domains, on the other hand exchange energy is increased due to the gradient in the magnetization. Thus magnetic domain configuration in soft magnetic NWs is due to the competition of these two energies. The most common domain wall structure found in soft magnets NWs is head-to-head (or tail-to-tail) domain wall, where magnetic domains are aligned along the length of the NW, with magnetization pointing towards (or away) from each other [41]. There are two distinct structures in head-to-head domain wall, namely transverse and vortex domain wall as shown in Figure 1.5 (a) and (b). Which of these two are lowest energy depends on the length and diameter of the NW as shown in Figure 1.5 (c). However, head-to-head domain walls are only stable in NWs with strong shape anisotropy and/or uniaxial anisotropy along the length of the NW. In the presence of significant MCA in the out-of-plane directions, other domain patterns can be observed in NWs. For materials such as Pt/Co/Pt trilayers with strong perpendicular anisotropy (1×10^6 J/m^3), domain magnetization is oriented along the anisotropy direction. In such material NWs, the domain walls are nearly ideal Bloch or Neel walls [42, 43] and a periodic dark-and-bright contrast along the length of the NW can be observed in magnetic force microscope (MFM) images as shown in Figure 1.5 (d) and (e). Details about the periodic magnetic domains structures in Co-Pt NWs can be found in Chapter 4, 5 and 6.

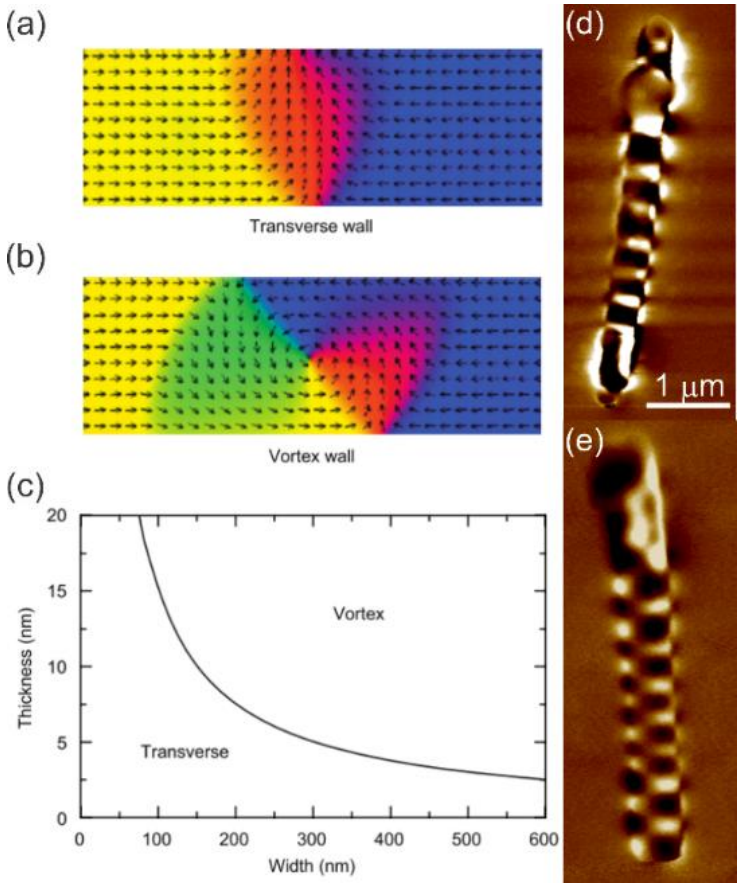


Figure. 1.5: Spin structures of (a) transverse and (b) vortex domain walls. Which of these structures yields the lowest total energy is a function of the aspect-ratio, described by the phase boundary in (c) adapted from [41]. (d) and (e) MFM contrast of periodic domain structure in Co-Pt NWs [39].

1.4.2 Magnetization reversal modes in nanowire and nanotubes

Coercivity is one of the most important properties of magnetic nanostructures from the point of view of their applications, and an understanding of the coercivity mechanism is a constant challenge for researchers. Measuring the angular dependence of the coercivity (ADC) for the nanostructures provides information about the underlying mechanisms of the magnetization reversal (MR) [44]. Different MR modes, such as coherent rotation, vortex or transverse mode have been discussed in cylindrical NWs (and NTs) under the framework of analytical calculations [45-47]. In coherent reversal mode all magnetic moments simultaneously rotates; the vortex mode (V mode), where magnetic moment rotates progressively via propagation of a vortex domain wall (this mode is frequently called curling reversal mode); and transverse mode (T mode), where magnetic moments rotates progressively via propagation of a transverse domain wall as shown in Figure 1.6. Where w_T and w_V represent the domain wall widths of a transverse and vortex domain wall, respectively.

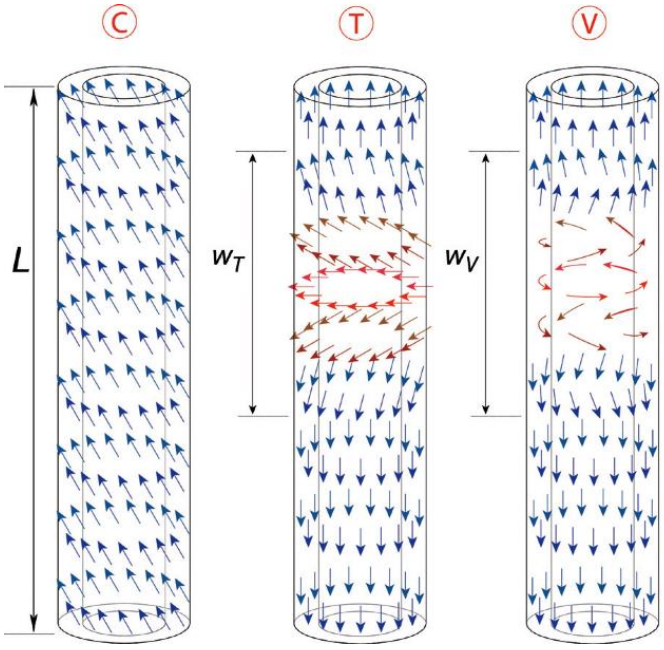


Figure 1.6: Different MR modes: Coherent (C), Transverse (T) and Vortex (V) modes. w_T and w_V represent the domain wall widths of a transverse and vortex domain wall, respectively. Adapted from [2].

Significant progress achieved in the analytical theory over the past few years has allowed investigating MR in cylindrical shaped NWs with diameter of several tens of nanometres and length several micrometres. Stoner and Wohlfarth [48] have reported the angular dependence of the nucleation field for a coherent MR:

$$H_n^C = -\frac{2(K_{sh}(L) + K_{mca})}{2\mu_0 M_s}\frac{\sqrt{1-t^2+t^4}}{1+t^2} \qquad (1.7)$$

Where $t = (\tan(\theta))^{\frac{1}{3}}$, θ is the angle between applied magnetic field and nanostructure long axis, K_{mca} is the MCA constant and $K_{sh}(L) = \frac{1}{4}\mu_0 M_s^2[1-3N_z(L)]$ is the shape anisotropy constant with N_z corresponds to the demagnetizing factor along z-axis of the nanostructure, M_s is the saturation magnetization, and L is the length of the NW/NT. For NWs the demagnetization factor along z-axis N_z of the general prolate ellipsoid of revolution is given by [49],

$$N_z(L) = \frac{xyz}{2}\int_0^\infty \frac{(z^2+\delta)^{-1}}{\sqrt{(x^2+\delta)(y^2+\delta)(z^2+\delta)}}d\delta, \quad (1.8)$$

Where x, y and z represent the semi-minor axis and semi-major axis, respectively with condition x=y<z, thus N_x=N_y=(1-N_z)/2. However, for high aspect-ratio NTs, the demagnetizing factor was proposed by Escrig *et al.* [50] and is given by

$$N_z(L) = \frac{d}{L(1-\beta^2)}\int_0^\infty \frac{1-e^{-\frac{2yL}{d}}}{y^2}[J_1(y) - \beta J_1(\beta y)]^2\, dy, \qquad (1.9)$$

Where J_1 is the Bessel function of the first kind and order one, and $\beta=d_i/d_o$, where d_i and d_o are the inner and outer tube diameters, respectively. According to the Stoner Wohlfarth model [48], the ADC can then be estimated from the nucleation field, by [2]

$$H_c^C(\theta) = \begin{cases} |H_n^C(\theta)|, & 0 \le \theta < \dfrac{\pi}{4} \\ 2\left|H_n^C\left(\theta = \dfrac{\pi}{4}\right)\right| - |H_n^C(\theta)|, & \dfrac{\pi}{4} \le \theta \le \dfrac{\pi}{2} \end{cases} \qquad (1.10)$$

Small nanostructures with diameter comparable to exchange length can rotate their magnetization via coherent MR and above Eq. 1.7 predicts that coercivity decreases as a function of the applied magnetic field angle in this mode. However, for high aspect-ratio nanostructures, the MR proceed through nucleation and propagation of a domain wall either vortex or transverse domain wall. Typically domain wall widths vary from ~40 to 100 nm depending on the geometry of the NW [2]. The angular dependence of coercivity for T mode was estimated by an adapted Stoner Wohlfarth model proposed by Escrig *et al.* [51]. This model assumes a high aspect-ratio system can be divided into two regions one which reverses by a transverse domain wall, and the other one with an effective volume that reverses by coherent rotation, they both will have an equivalent nucleation field which can be estimated by

$$H_n^T = -\frac{2(K_{sh}(w_T) + K_{mca})}{2\mu_0 M_s}\frac{\sqrt{1-t^2+t^4}}{1+t^2} \qquad (1.11)$$

Where w_T is the region of the transverse domain wall and the ADC for transverse mode can be estimated from Eq. 1.11.

The nucleation field for the V mode in an elongated prolate spheroid was first suggested by Aharoni [52] and extended for ADC of NTs and NWs by [53] and [54], respectively.

$$\begin{cases} H_n^V(\theta)\cos(\theta-\psi) = (N_x(L)\sin^2(\psi) + N_z(L)\cos^2(\psi) - \zeta - \xi[3\cos^2(\psi)-1])M_s \\ H_n^V(\theta)\sin(\theta-\psi) = ([N_x(L) - N_z(L) - \xi]\dfrac{\sin(2\psi)}{2})M_s \end{cases} \qquad (1.12)$$

Where $\zeta = \frac{4q^2L_{ex}^2}{d^2}, \xi = \frac{K_{mca}}{\mu_0 M_s^2}$, and q satisfies [55]:

$$\frac{qJ_0(q) - J_1(q)}{qY_0(q) - Y_1(q)} = \frac{\beta q J_0(\beta q) - J_1(\beta q)}{\beta q Y_0(\beta q) - Y_1(\beta q)}, \qquad (1.13)$$

Where J_p and Y_p is the Bessel function of the first and second kind, respectively, and order p. Where ψ is the angle between magnetization and nanostructure long axis. Considering the wire/tube symmetry, one has $N_x=N_y=(1-N_z)/2$. The coercivity in the V mode is very close to the absolute value of the nucleation field, and we can therefore use the approximation $H_c^V = -H_n^V$,

In many cases the effective magnetic anisotropy of NWs includes mainly the shape

anisotropy, and MCA. Both these anisotropy components can be included in analytical calculations by using the *effective* anisotropy concept, with the value fitted to experimental data. For example, [56] and [57] fitted experimentally measured ADC to analytical models based on transverse and vortex mode to associate the coercivity mechanism in Co-based NWs with possible occurrence of these processes. Additionally, the fitted effective anisotropy constant (K_{eff}) can be used to further explain the magnetization behaviour of the NWs. The study of the reversal mode in Co-Pt nanostructures is particularly exciting because their crystal structure introduces a very significant energy term that makes the MR mechanism certainly more complex. Since the exact knowledge about MR mechanism in NWs is very important in many areas of the applications. Please see Chapter 3 and 4 for further detail about reversal modes.

1.5 Characterization of Nanomagnets

It is crucial both from a fundamental as well as an application point of view to understand and control the magnetic behaviour of small magnetic elements. This requires special experimental tools to characterize the magnetic properties. The collective magnetic properties such as hysteresis loop can be obtained by standard techniques. However, it is important to characterize the individual as well as array behaviour of the nanomagnets with special techniques, and only then some of the following questions can be answered: what is the magnetization configuration (i.e. magnetic domain) of an individual nanomagnets? How they are interacting between each other in array? How does an individual and array of nanomagnets switch their magnetization? Finally, what is the variability of these properties from element to element?

The collective magnetic information can be characterized by vibration sample magnetometry (VSM), first-order reversal curves (FORC) can obtain information about interaction between the nanomagnets as well as switching field distribution in arrays [58], the MR mechanisms can be understood by ADC, information about the crystal inhomogeneities in the sample can be obtained with ferromagnetic resonance (FMR) measurements [59]. Due to variation between individual elements, the characterization of an individual element can be washed out in the measurements of ensembles. Therefore, some sophisticated spatially resolved techniques for instance MFM which allow the investigation of the magnetic properties of individual elements can be used. A combination of these techniques allows one to fully reconstruct the complete magnetization distribution and fully understand the mechanism of magnetization switching.

1.5.1 Magnetic force microscopy

Magnetic force microscopy (MFM) is a powerful technique for studying the magnetic domains in nanostructures with a high spatial resolution (~10 nm) in ambient conditions using a simple method for sample preparation [60-62]. MFM records the magnetostatic forces or force component gradient between a magnetic sample and a small magnetic tip with typical radius of curvature 10-50 nm as shown in Figure 1.7.

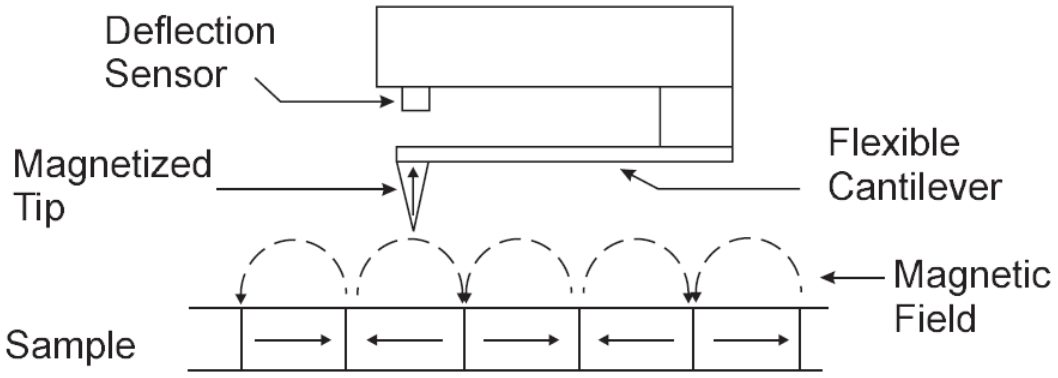


Figure 1.7: a magnetic tip interacts with the magnetic stray field of the sample. The changes in the status of the cantilever are measured by the deflection sensor, and recorded to generate the image. Adapted from [63].

In principle a flexible cantilever beam with a sharp tip on its one end is brought close to the sample surface, typically ten to few hundred nanometres, the magnetic interactions between the tip and the sample can give rise to a change of the cantilever status such as resonance frequency. As the MFM tip (cantilever) raster across the sample, these changes can be used to form a two-dimensional image. As the MFM detects the force component gradient between the MFM tip and magnetic sample. The magnetic force acting on a tip can be written as

$$F_{t-s} = \frac{\partial \mathrm{E}}{\partial \mathrm{r}'} = \int d^3r' \int d^3r'' M(r')H(r'', r') \qquad (1.14)$$

Where M (r$'$) is the tip magnetization at position r$'$ inside the tip, while H(r$''$,r$'$) is the sample stray field at position r$'$ generated by the magnetic moment at position r$''$ inside the sample. The magnetic force (or force component gradient) between the tip and the sample depends on both the tip and the sample moment distribution and the separation between them. For example a force component gradient above the center of a transition of a longitudinal recording medium with a long dipole tip as shown in Figure 1.7 can be written as

$$F'_{mag} \approx \frac{1}{(a+z)^2} \qquad (1.15)$$

Where z is the tip-sample separation, and a is the transition width, of the order of 100 nm. When the tip-sample separation is of the order of 100 nm the magnetic force gradient decays slower than electrostatic and van der Waals forces, thus at well separation between tip and sample later forces can be ignored and the magnetic force gradient can be accurately calculated.

High sensitivity can be achieved in the tapping mode of operation in which cantilever is oscillating near its resonance frequency. As shown in Figure 1.8, the sample is scanned twice: the sample topography is obtained in the tapping mode and magnetic contrast is subsequently obtained in the lift mode at certain height h. Throughout this thesis Veeco

dimension 3100 from digital instruments were used.

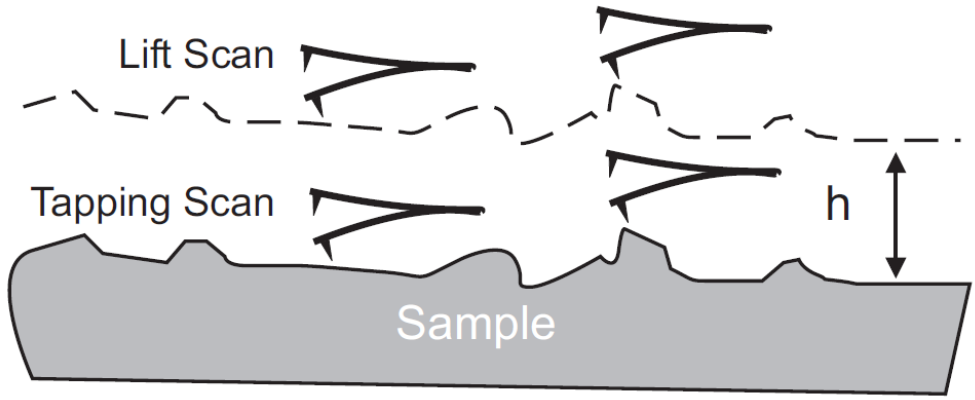


Figure 1.8: Tapping/lift mode (dual), first tapping scan is used to obtain the sample's topography, which in the lift scan magnetostatic interactions are recorded.

1.5.2 First-order reversal curves (FORCs) measurements

Typically magnetization processes of NWs are studied through the analysis of global hysteresis loops to determine their characteristics such as coercivity and remanence. Further details of the magnetic interactions between NWs can be determined by studying multiple minor hysteresis loops, so-called Henkel plots. However, for determination of quantitative magnetic interaction between NWs first-order reversal curves (FORCs) are performed. The FORC measurements not only include interactions as a whole, but also allow one to separate the mean field interaction effect (i.e. the interactions between NWs) from local effects (exchange-like). In particular, the FORC method has proved to be extremely valuable in addressing the role of the distinct crystallographic orientations present in NWs by taking into consideration the switching field distribution [64, 65]. Recent advancement in understanding of FORC diagrams have made it possible to track individual NWs switching in their arrays [66]. Additionally, FORC measurements also give information on the distribution of internal coercivities which are important for studying of the reversible and irreversible contributions present in the overall magnetization switching. The switching field distributions can accurately be extracted from FORC measurements which can further supply valuable information about magnetic anisotropies of individual entities.

The FORC method was initially based on the classical Preisach model [58], in which hysteresis was described as a set of elementary processes called "mathematical hysterons" and characterized by a coercive H_c and bias H_u field as shown in Figure 1.9, most FORC analysis include several different approaches, either based on physical hypothesis [67] or on mathematical distribution [68].

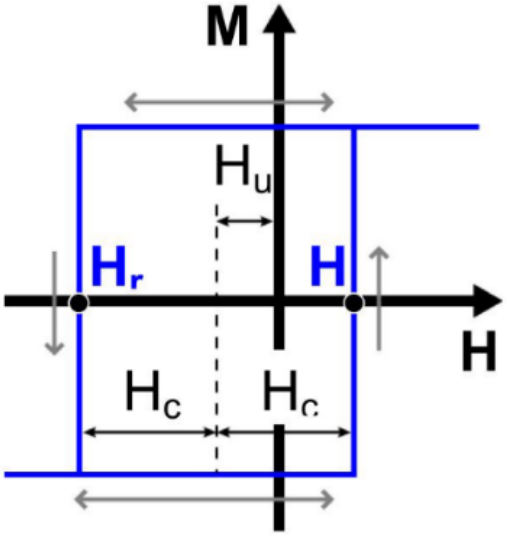


Figure 1.9: Mathematical hysteron from the classical Preisach model [67].

During the FORC measurements the system is first magnetically saturated; then, H is reduced to the so-called reversal field (H_r); finally M is measured from H_r up to the maximum field H_{max}. To obtain a complete set of FORCs M(H,H_r), these measurements are then repeated by increasing H_r from $-H_{max}$ to H_{max} in steps of $H_{max}/50$. The insets of Figures 1.10 show the FORCs of selected sample.

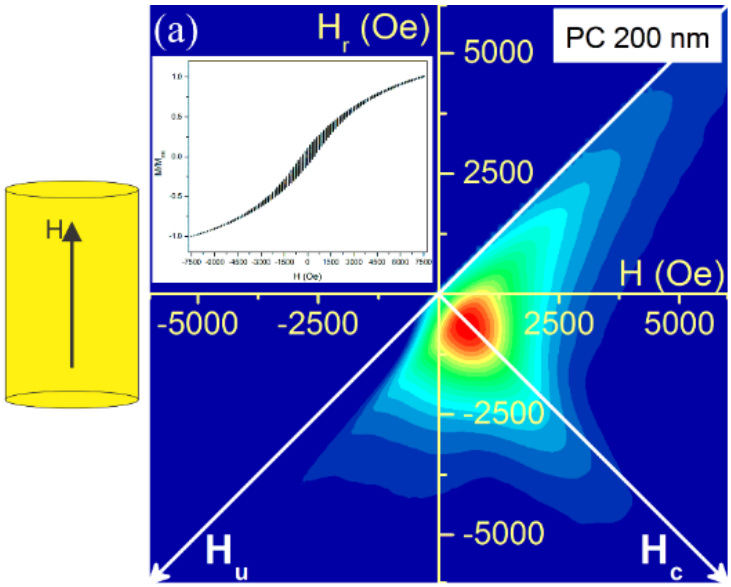


Figure 1.10: FORC measurements (insets) and FORC diagrams of the Co-Pt NWs arrays when the applied field is (a) parallel to the Co-Pt NW's long axis for PC membrane.

The FORC distribution, ρ_{FORC}, is then obtained by taking a second-order mixed derivative of M(H,H_r) [58]:

$$\rho\ (H, H_r) = -\frac{1}{2}\frac{\partial^2 M(H, H_r)}{\partial H \partial H_r}, for\ (H > H_r) \qquad (1.16)$$

The ρ_{FORC} is usually represented as a contour coloured plot, called FORC diagram as shown in Figure 1.10, with a scale ranging from red (maximum value of ρ) to blue (minimum value of ρ). From the FORC measurements one can extract individual coercivity of the nanoparticles (H_c) and the magnetostatic interactions field (H_u) between the nanoparticles in arrays. To read the H_c and H_u parameters directly from the FORC diagram, it is convenient to perform a change of coordinates, to define coercivity field axis (H_c) and an interaction field axis (H_u)

$$H_c = \frac{H - H_r}{2}, \qquad H_u = -\frac{H + H_r}{2} \qquad (1.17)$$

The magnetostatic interactions can then be measured as the half width (ΔH_u) of the FORC distribution along the H_u direction [67]. Using the moving Preisach model [58], that takes into consideration the interactions between the individual magnetic elements, one can approximate the interaction field at saturation as:

$$H_{in,sat} = 2\sigma_{in} - \kappa, \quad (1.18)$$

Where σ_{in} and κ are the local and mean interaction fields, respectively [67]. A positive (negative) value of κ would correspond to a mean interaction field parallel (antiparallel) to M. For example, an array of high aspect-ratio soft magnetic NWs favors antiparallel interaction field between each element, due to strong demagnetizing field produced by the array. The presence of a sharp contour (red) in FORC diagram in Figure 1.10 indicates the existence of dominant local magnetostatic interactions σ_{in} (exchange-like) parallel to NWs long axis in arrays. Further details on the FORC measurement on NWs can be found in Chapter 5.

1.5.3 Ferromagnetic resonance (FMR) measurements

Ferromagnetic resonance (FMR) is a useful technique for measuring the dynamic magnetic properties of ferromagnetic NWs. It yields direct information about the homogeneous (and inhomogeneous) precession mode of the NWs which can be related to the average anisotropy magnitude [59]. The precessional motion of a ferromagnetic material with magnetization M about an applied external magnetic field H is known as the FMR. In the physical process of resonance, the energy is absorbed from radio frequency (r_f) transverse magnetic field h_{rf}, which occurred when frequency matched with the microwave frequency (ω). The precessional frequency depends on the sample properties and the strength of the applied magnetic field. Thus, it allows us to measure almost all the important parameters of the material: Curie temperature, relaxation mechanism, effective anisotropy, total magnetic moment and others. In addition, the width of the resonance peak (referred to as linewidth), visible if the r_f absorption is recorded as a function of an external field, and can be related to the losses of the precessional energy due to damping in the magnetic system.

Before we start describing FMR conditions one needs to understand the dynamic properties of a ferromagnetic material which can be determined by Landau Lifshitz Gilbert (LLG) equation

$$\frac{d\vec{M}}{dt} = -\gamma\vec{M} \times \left(\overrightarrow{H_{eff}} - \frac{\alpha}{\gamma M_s}\frac{d\vec{M}}{dt}\right) = -\gamma\vec{M} \times \overrightarrow{H_{eff,o}} + \frac{\alpha}{M_s}\vec{M} \times \frac{d\vec{M}}{dt} \quad (1.19)$$

where $\gamma = \frac{g\mu_B}{\hbar}$ is the gyromagnetic ratio and $\alpha = \frac{G}{\gamma\mu_o M_s}$ is the dimensionless Gilbert damping constant and G is the Gilbert damping parameter. $\overrightarrow{Heff,o}$ is the overall effective magnetic field which is a sum of a static magnetic field ($\vec{H}$), a dynamic magnetic field (h_{rf}) and internal magnetic field ($H_{eff} = \frac{2K_{eff}}{\mu_o M_s}$). The effective anisotropy constant (K_{eff}) consists of various magnetic anisotropies in the material such as shape anisotropy, and MCA. In this equation the first part describes the torque acting on M which leads to the rotation of the M towards the direction of the external magnetic field (H) as shown in Figure 1.11 (a). The damping (α) in the second part causes a decay in the precessional motion which by applying a dynamic magnetic field becomes continuous as shown in Figure 1.11 (b). A FMR condition for a simple case (single domain magnetic particle) with magnetization M under applied field H along the z-direction in a microwave cavity can be given by Kittle formalism [69]

$$\hbar\omega = g\mu_B\sqrt{[H + (N_x - N_z)M][H + (N_y - N_z)M]} \quad (1.20)$$

where N_x, N_y, and N_z are the demagnetization factors along x, y, and z directions, respectively, and g is the Lande factor and μ_B is the Bohr magneton. ω is the microwave frequency

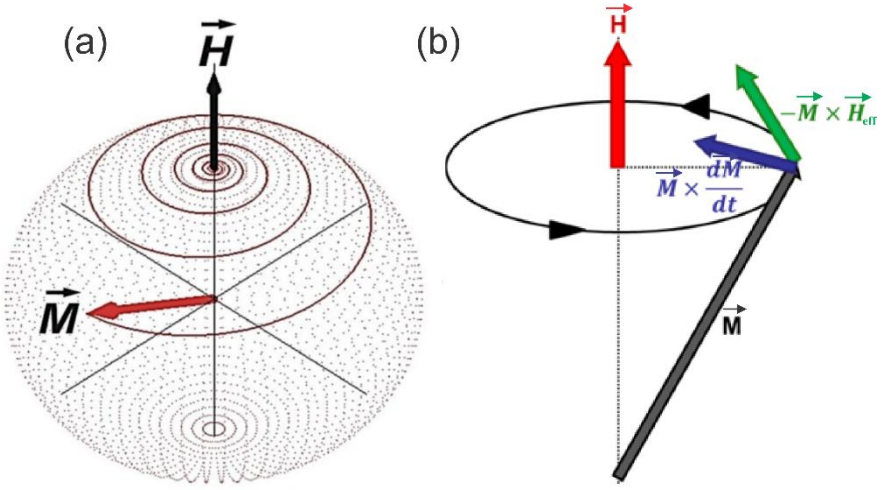


Figure 1.11: (a) Motion of $\vec{M}$ under constant $\vec{H}$ (b) Torque component exerted on the magnetization $\vec{M}$ by rotational field $\vec{H}$. Adapted from [70].

Smit and Beljers [71] proposed a method to extract information of FMR measurements from free energy by obtaining minimum energy term. The free energy density equation for an array of NWs in the presence of an external magnetic field at angle (θ_H) from NW axis in spherical coordinate can be written as

$$E = -MH(sin\theta sin\theta_H \cos(\varphi - \varphi_H) + cos\theta cos\theta_H) + K_{eff} sin^2\theta \quad (1.21)$$

Where φ is an azimuthal angle and K_{eff} is the effective anisotropy constant of NWs. Minimum energy condition

$$E_\theta = \frac{\partial E}{\partial \theta} = 0 \quad (1.22)$$

$$E_\theta = -MH(cos\theta sin\theta_H \cos(\varphi - \varphi_H) - sin\theta cos\theta_H) + K_{eff} sin2\theta = 0 \quad (1.23)$$

The FMR dispersion relation can be obtained from above equation

$$(\frac{\omega}{\gamma})^2 = [Hcos(\theta - \theta_H) + H_{eff} cos^2\theta][Hcos(\theta - \theta_H) + H_{eff} cos2\theta] \quad (1.24)$$

The dispersion relation (ω/γ) depends upon the angle between the external magnetic field and easy magnetization axis and effective anisotropy field of the NWs. There are certain factors which can affect the FMR frequency for instance shape anisotropy and the MCA. In the case of shape anisotropy different geometrical shaped samples have different demagnetizing factors. In case of MCA, the magnetization process is different when the magnetic field is applied along different crystallographic directions and this anisotropy reflects the crystal symmetry of the particular crystal system (see Section **1.2.1.2 magnetocrystalline anisotropy**). Thus, different crystal orientations significantly affect the above-mentioned dispersion relation. As it was mentioned previously, the effective anisotropy field H_{eff} comes from the combination of shape and MCA. By modelling MR curves (see Section **1.4.2 Magnetization reversal modes in nanostructures**) the contributions to H_{eff} and hence the anisotropy constants can be determined from measurements. But it should be noted that MR curves include unsaturated regimes, where magnetic domains might be present. The domain switching is determined by external contributions such as pinning centers or impurities, which in turn makes it challenging for modelling. Methods that are rely on saturated samples for example FMR, circumvent these disadvantages. The homogeneous and inhomogeneous contribution to the FMR linewidth is a combined effect of the exchange interactions and the spin-orbital coupling and can be extracted from the following relation [72]

$$\Delta H_{pp} = \Delta H_{inhomo} + \Delta H_{homo} = \Delta H_{inhomo} + \frac{2}{\sqrt{3}} \alpha \frac{\omega}{\gamma} \quad (1.25)$$

Where ΔH_{pp} is the FMR linewidth. In this thesis FMR measurements on Co-Pt NWs embedded into AAO membrane were performed in frequency X-band ($\frac{\omega}{2\pi}$~9.41 GHz) using a reflection cavity microwave spectrometer (Bruker Elexsys E500) and details can be found in Chapter 5.

1.5.4 Micromagnetic simulation

Micromagnetic simulation can be used to help explaining experimental observation, and to understand the domain formation process in magnetic nanostructures. The simulation were performed by solving the LLG Eq. (1.19) [73]. The effective anisotropy field is defined as

$$H_{eff} = \frac{\partial E}{\partial M} \quad (1.26)$$

Where E is the total magnetic energy density including the exchange energy, anisotropy energy, Zeeman energy, and magnetostatic energy (demagnetizing energy). Detail about the micromagnetic simulation is presented in Chapter 3, 5 and 8.

1.6 Fabrication of Nanomagnets

1.6.1 Template-assisted electrodeposition

NWs and NTs can be fabricated by a wide range of different methods, for instance nano-lithography technique [74-76], chemical vapour deposition [77], molecular self-assembly [78], template filling by sol-gel technique [79], hydrothermal synthesis [80], and template-assisted electrodeposition [25, 81, 82]. Typically, the above-mentioned techniques require expensive equipment and/or time-consuming processes. However, the template-assisted electrochemical deposition is an efficient and cost effective method for growing high density and high aspect-ratio arrays of NWs and NTs [21, 24] with a precise control over their characteristics [26, 27]. Electrodeposition gives possibility to deposit different materials with high aspect-ratio that are densely and continuously packed and possess a high crystallinity [83]. The widely used commercially available templates for electrodeposition are AAO and polycarbonate (PC) membranes and were utilized to synthesis Co-Pt nanostructures in this thesis.

The AAO membranes are prepared by two step anodization of aluminum foil in acidic conditions [84]. Cylindrical pores with different diameters perpendicular to the aluminum foil surface can be obtained by choosing appropriate conditions e.g. anodization voltage. The separation between the pores can also be adjusted with anodization voltage with appropriate acidic environment [85]. The AAO membranes are an excellent choice for electrodeposition of nanostructures (NWs, NTs etc.) due to their tunability of pore dimension, good mechanical strength, thermal stability and ordered pores with high density (10^9-10^{11} pores/cm^2) [86].

However, the PC membranes are prepared with a completely different process which involves nuclear track etch process. The high energy ions are bombarded on a polycarbonate film producing pores which further chemically etched, etching process determined the size of the pores. The PC membranes have been extensively used in fabrication of metal and oxide nanostructures [87, 88]. However, the pores in the PC membrane are misaligned perpendicularly to the membrane plane and the majority of the pores are tilted randomly by a few degrees with respect to the normal of the membrane plane, due to the nature of fabrication of the PC membrane. Different characteristics of all commercial templates used in this thesis to deposit Co-Pt nanostructures are shown in the following Table 1.

Table 1: AAO and PC membranes with different diameters used in this thesis.

Diameter ϕ (nm)	Membrane	Nominal pore diameter $D_p \pm \sigma$ (nm)	Pore separation $D_c \pm \sigma$ (nm)	Chapters
200	AAO	240 ±20	356±22	3,4,5,7
200	PC	226 ±10	570±140	5
80	PC	77 ±10	418±189	6
50	PC	52 ±8	300±110	6
15	PC	18 ±8	170±100	6

Electrodeposition process of Co-Pt NW fabrication into AAO and PC membranes is schematically presented in Figure 1.12. Electrodeposition of metals requires that one side (bottom side) of the membrane is in contact with a conductive metallic layer. This can be achieved with vacuum deposition technique for example sputtering of a gold (Au) layer on the membranes as shown in Figure 1.12 (a) and (c). The thickness of the Au layer is typically 100-200 nm and should be strongly adhered to the membrane.

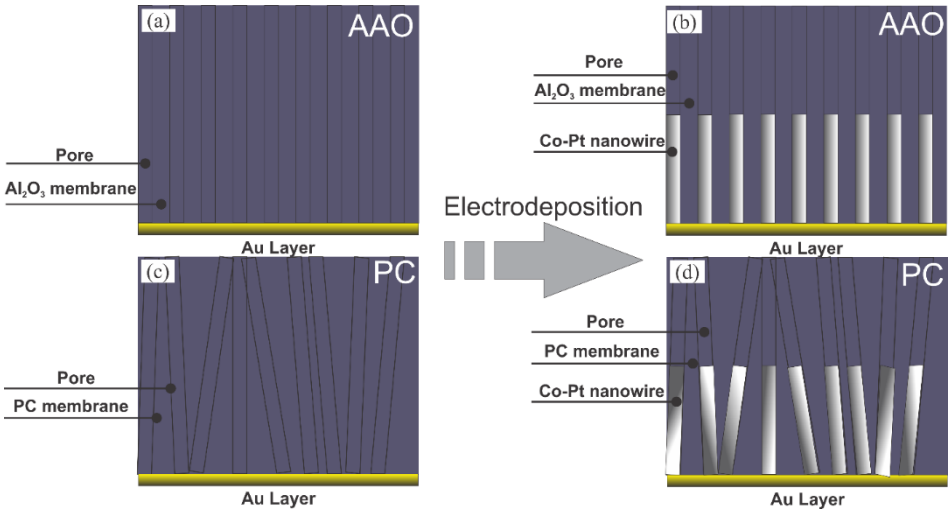


Figure 1.12: (a) and (c) Schematic image of the AAO and PC membrane, respectively. (b) and (c) schematic of NWs fabricated after electrodeposition into AAO and PC membranes, respectively.

In electrochemical cell the Au coated side of the membrane where the metal will be deposited is the cathode, also known as the working electrode, the anode, or counter electrode is a Pt mesh and third electrode is a reference electrode as shown in Figure 1.13. After the electrodeposition Co-Pt NWs can be fabricated into the membranes as shown in Figure 1.12 (b) and (d). The electrodeposition of metal ions is explained in detail in the following.

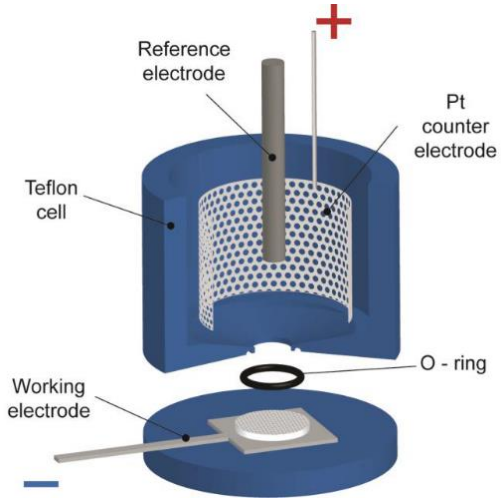


Figure 1.13: Schematic of the electrochemical cell for the electrodeposition of Co-Pt NWs.

The general reaction for the process of metal reduction can be written as

$$M^{n+} + ne \rightarrow M^0$$

Where M represents a metal ion and thus reduction takes part in the charge transfer process. The amount of electric charge which taking part in the reaction are represented by ne. For the deposition of one metal atom, one needs n electrons, i.e. a charge of Q=ne Coulombs. Measuring the current (I) that passes through the circuit during the deposition process one can estimate the deposited metal mass (m) from the Faraday's law of electrolysis:

$$m = \frac{QA_w}{nF} \qquad (1.27)$$

Where A_w is the atomic weight of the metal and F is the Faraday constant (96485 C/mol). This equation helps to estimate the amount of material, deposited during time of the electrodeposition process provided most of the electrical current is used to reduce metal ions.

Despite the simplicity of electrodeposition operation, many parameters such as the deposition modes (Potentiostatic or alternating current mode) [89], the electrodeposition voltage [83], metal ion concentration [90], and the electrolyte pH [91, 92] need to be optimized in order to obtain the required magnetic properties of the NWs. In potentiostatic mode (dc) a constant potential is applied, so the current transient monitored allows one to control the deposition charge involved in the metal reduction reaction. It is well-known that the dc mode under controlled conditions can produce NWs with better crystallinity and faster growth [16]. In this thesis we have chosen the dc method for the preparation of Co-Pt nanostructures into AAO and PC membranes using a three-electrode cell, as shown in Figure 1.13. In addition, electrodeposition of NWs consists of noble metal and base metal whose standard potentials are far away from each other and require high diligence in choosing appropriate electrodeposition parameters to allow co-deposition [83]. More detail about electrodeposition process is given in Chapter 3, 4, 5, 6 and 7.

Chapter 2

Aims and Hypothesis

2.1 Description of the Problem

Nanomagnetism and spintronics are relatively young and emerging branches in the field of nanotechnology. However, extraordinary achievements have been made in these fields, for example advances in the magnetic materials and nanomagnetism have helped tremendously in increasing the magnetic data storage capacity of HDDs from 1 kB/in^2 in early 1960 to 1.34 TB/in^2 in 2014. Over this period of time, the area of one magnetic bit used to store information has decreased in size (now ~40 nm) by about nine order to magnitudes; it is now so tiny that it is reaching the fundamental limit (superparamagnetic limit) that are difficult or too expensive to overcome. A number of alternatives to the magnetic disk drive have been suggested. Among them racetrack memory devices seems to be potential candidates and close to the realization. Such devices are based on one-dimensional (1D) ferromagnetic nanostructures with magnetic domain walls which can be moved with the help of a spin polarized current. Thus, a large research effort has been put forward to investigate such ferromagnetic nanostructures with special geometries e.g., nanowires (NWs), and nanotubes (NTs). Apart from possible application in data storage devices these nanostructures have been proven to be potential candidates for microwave devices [93], chemical sensors [94], light emitters [95], and for biological applications e.g. cell manipulation and hyperthermia to treat cancer [96].

As for any magnetic system, the overall peculiarity of such nanostructures and hence their suitability for a particular application would be determined by their effective magnetic anisotropy which is dependent on many factors such as geometry, crystal structure, crystal orientation, grain size and the magnetostatic interactions between the elements. Only intensive research on influence of each parameter can provide answers to many fundamental physical questions such as magnetic domain structure and magnetization reversal behaviour in 1D nanostructures. Efforts have been made to understand the magnetic domain structure, magnetization reversal and magnetization switching behaviour to utilize these nanostructures in above-mentioned novel applications [83, 97]. However, a considerable space is left for further improvement of these properties and will be highlighted in this thesis.

In the past several years, template-assisted electrodeposition has been widely used for the synthesis of a large variety of ferromagnetic nanostructures, especially NWs and NTs made of several different materials. It provides a full control over parameters to manipulate the

microstructure, morphology and size of the nanostructures. However, deep understanding of electrodeposition process is required to obtained nanostructure properties suitable for specific applications. Co-Pt alloy with hcp crystal structure is a suitable magnetic material for a variety of applications due to its high MCA. As-deposited Co-Pt alloys can exhibit either a disordered fcc-based (L_{11}-CoPt) or a hcp-based $D0_{19}$-Co_3Pt crystal structure depending on the composition of the nanostructure and the formation conditions. Fcc- and hcp-based structures consist of atomic stacking sequences of ….ABCABC….and …ABAB…, respectively, along the direction normal to the close-packed plane. The crystal structure of Co-Pt alloy nanostructures is known to vary between the two stacking types and may also exist as a mixture of both. The Co_3Pt hcp structure is a well-known magnetic material with a large MCA (K_u=1x10^6 J/m^3), comparable to or even stronger than the shape anisotropy ($\pi\mu_o M_s^2$=4x10^5 J/m^3) in their nanostructures. Thus, it is important to understand the underlying synthesis parameters to fabricate hcp Co-Pt nanostructures to obtain large MCA.

2.2 Purpose and Goals of the Thesis

We believe that the best way to tailor the magnetic properties of magnetic nanostructures towards specific applications is (1) first to understand the influence of individual anisotropies contributing to the effective anisotropy and (2) by tailoring and optimizing the contributions of each anisotropy to obtain suitable magnetic properties. Our final goal was to obtain magnetic properties of Co-Pt nanostructures suitable for applications such as racetrack memory devices. To reach this objective, several sub-objectives were in focus:

1. The magnetic properties of NTs and NWs have been exploited during the past two decades and understood to a greater extent. The most common MR mechanisms observed in NTs and NWs are the vortex [98] and transverse reversal modes [47], respectively. Landeros *et al.* [98] showed that the vortex domain wall nucleation is favorable for NTs with diameter larger than 50 nm, while in NWs, with similar diameter, mainly transverse domain wall nucleation is observed [47]. The first goal of the thesis was to fabricate and investigate the complex morphologies of the 1D nanostructures consist of a pair of NT and NW segments with diameter larger than 50 nm. This new type of 1D nanostructures with tube-wire morphology can provide control over the nucleation of a domain wall and thus magnetization reversal mechanisms. Therefore, these nanostructures are potential candidates for applications like racetrack memory devices where it is necessary to control the motion of the domain walls [33-35] in nanostructure.

   The properties of these nanostructures are expected to be hybridized between NTs and NWs. However, there is no experimental report that investigates the fabrication and magnetic properties of cylindrical nanostructures comprised of both NT and NW segments, in spite of a few theoretical reports [34, 35]. More detail on this topic can be found in the following article:

   Muhammad Shahid Arshad, Darja Pečko, Sašo Šturm, Juan Escrig, Matej Komelj, Paul McGuiness, Spomenka Kobe, Kristina Žužek Rožman. “Angular

dependence of the coercivity in electrodeposited Co-Pt nanostructures with a tube-wire morphology". IEEE Trans. Magn. **2014**, 50, 1-4.

2. It is well-known that the size and the geometry of the magnetic domains in the 1D nanostructures are set by a competition between different anisotropies e.g. shape anisotropy and MCA. The shape anisotropy is defined by the elongated shape of the NWs and takes the form $2\pi M_s$ for NWs with aspect-ratio (length/diameter) larger than 15. However, the evaluation of the MCA is rather complex and depends on many factors e.g. crystal structure, grain sizes and grain (crystallite) orientation and so on. As mentioned, the crystal structure of Co-Pt NWs can easily vary between fcc and hcp structure due to very close atomic stacking sequences and their identification is very complicated due to similar d-values. Moreover, it is possible that there is a crystallographic texturing of grains which can significantly influence the magnetic properties of NWs depending on the MCA easy magnetization axis. Thus, the present study was focused on effect of MCA on magnetic domains and magnetization reversal of Co-Pt nanowires. Moreover, it was anticipated that the effective anisotropy constant (K_{eff}) which depends on shape and MCA can be extracted by comparing the angular dependence of the coercivity with analytical calculation. In many cases, the MCA of the hcp phase favors the easy magnetization axis (c-axis) perpendicular to the NW long axis. It can trigger a new physical phenomena such as a periodic domain structure suitable for racetrack memory devices. More details on this topic can be found in the following article:

   Muhammad Shahid Arshad, Sašo Šturm, Janez Zavašnik, Juan Escrig, Alvaro Espejo, Paul J. McGuiness, Spomenka Kobe, and K. Žužek Rožman. "Effect of magnetocrystalline anisotropy on the magnetic properties of electrodeposited Co-Pt nanowires". *J Nanopart Res*, **2014**, 16, 1-16.

3. As already mentioned, the crystal structure of the Co-Pt alloy nanostructures are sensitive to the chemical composition between cobalt and platinum and according to the Co-Pt phase diagram if Co content is around 80 at% the crystal structure will have a pure hcp structure. The chemical composition of the Co-Pt nanostructure can be controlled with metal concentrations in the electrolyte. Hcp Co-Pt is a well-known magnetic material with a high MCA (K_u=1x10^6 J/m^3), comparable to, or even stronger than, the shape anisotropy ($\pi\mu_o M_s^2$=4x10^5 J/m^3) in magnetic NWs. Furthermore, it is also known that grains crystal orientation and the texturing in the Co-Pt nanostructures can be controlled with membrane pore diameter and the current density. It is possible that there is a competition between shape anisotropy and MCA due to the specific orientations of the crystallites (grains) in Co-Pt nanostructures. Kept this in mind we fabricated Co-Pt NWs and found that hcp c-axis orientation can slightly vary which can significantly influence switching field distribution and magnetic domain configuration. We propose an "oblivious growth" mechanism for Co-Pt NWs produced via potentiostatic electrodeposition into commonly used, ordered-alumina and disordered-polycarbonate membranes with similar pore diameters (≈200 nm). We also studied in detail the interpretation of periodic domain structure in Co-Pt NWs. We have

found that transverse stripe (TS) and longitudinal stripe (LS) domain configuration is most energetically favorable. Further information can be found in our following article:

> **Muhammad Shahid Arshad**, Mariana P Proenca, Špela Trafela, Volker Neu, Ulrike Wolff, Sven Stienen, Manuel Vazquez, Spomenka Kobe, and Kristina Žužek Rožman, "Oblivious growth mechanism of high perpendicular anisotropic Co-Pt nanowire arrays: role of crystal orientation (c-axis) on Switching Field Distribution and Magnetic Domain configurations", Journal of Physics D: Applied Physics (Submitted).

4. After thoroughly exploiting the magnetic properties of Co-Pt nanostructures with diameters 200 nm, we move to diameters below 100 nm to study their magnetic properties. As already mentioned, if one of the dimensions of NWs is comparable to exchange length, interesting magnetic properties can appear. Moreover, for ultra-high density racetrack memory devices, NWs with diameter as small as 15 nm are required. The central aim of this work was to fabricate Co-Pt NWs with diameter below 100 nm and obtain periodic domain structure as in 200 nm diameter NWs keeping the similar electrodeposition parameters.
   In membranes with large interpore separation, one can exclude the magnetostatic interaction between the NWs, thus the intrinsic magnetic behaviour of the NWs can be extracted from their arrays. Thus for this study, we used low packing density polycarbonate membranes with diameters below 100 nm (80, 50, and 15 nm) to investigate the effect of the microstructure on the magnetic properties of the Co-Pt NWs. We have demonstrated that microstructural study obtained in individual Co-Pt NWs of each diameter can explained the magnetic hysteresis loops and also their magnetic domain structure. The details about this study are in the following article:

   > **Muhammad Shahid Arshad**, Janez Zavašnik, Sašo Šturm, Paul J. McGuiness, Spomenka Kobe, and Kristina Žužek Rožman. "Microstructure and Magnetic Properties of Electrodeposited Co-Pt Nanowires (NWs) with diameters below 100 nm". IEEE Mag. Let., **2014**, 5, 1-4.

5. The magnetic properties of 1D nanostructures are governed by the collaborative behaviour of shape and MCA. It is well-known that materials like hcp Co-Pt with strong MCA can surpass shape anisotropy and thus drive the magnetization process in nanostructures. However, it is important to look at the other side of the picture e.g. nanostructures with negligible MCA and strong shape anisotropy. It is believed that in such 1D nanostructures the magnetic domain structure and other magnetic properties would be completely different. For the proof of concept we investigated shape-anisotropy-governed fcc equiatomic Fe-Pd NW and found a single domain structure with magnetization along the length of the NWs. Details about this can be found in the following article:

   > Darja Pečko, **Muhammad Shahid Arshad**, Sašo Šturm, Spomenka Kobe and Kristina Žužek Rožman, "Magnetization-Switching Study of fcc Fe-Pd Nanowire and Nanowire Arrays Studied by In-Field Magnetic Force Microscopy," IEEE Trans. Magn., **2015**, 51, 1-4.

As a result, this study comprised a multidisciplinarity of competence, including material science, chemistry and physics.

Chapter 3

Angular Dependence of the Coercivity in Electrodeposited Co-Pt Nanostructures with a Tube-Wire Morphology

In this Chapter, article entitled "Angular dependence of the coercivity in electrodeposited Co-Pt nanostructures with a tube-wire morphology", by **Muhammad Shahid Arshad,** Darja Pečko, Sašo Šturm, Juan Escrig, Matej Komelj, Paul J. McGuiness, Spomenka Kobe, Kristina Žužek Rožman, [33] is presented. For this article the author performed electrodeposition of Co-Pt nanostructures, SEM characterization for morphology analysis, sample preparation for TEM, hysteresis loop and angular dependence of coercivity measurements and micromagnetic simulation study on Co-Pt nanostructures with tube-wire morphology.

In this article we have introduced a new type of nanostructures with a tube-wire morphology for possible applications in racetrack memory devices due to their ability to control the motion of domain walls [33-35].

A special feature, a kink in the hysteresis of these nanostructures was observed which was found to be due to the partial pinning of the domain walls at the interface between tube and wire segment. It was also found that in such nanostructures different reversal modes can be induced in each segment by choosing the right geometrical parameters. Moreover, it was shown that the tube segment reverses its magnetization before the wire segment, allowing a control of the magnetic domain walls' motion between the two segments.

In conclusion in these nanostructures it is possible to choose MR mechanism and they have potential for applications where control over domain wall motion is required such as racetrack memory devices.

Some of the simulation work was completed after the publication of the following article, so we are presenting this data here. It is important to mention that the following results should be treated as supplementary data and should be read after the following article.

For this purpose micromagnetic simulations with NMAG simulator were performed [73]. Figure 3.1 (a) shows the schematic image of the nanostructure with tube-wire morphology. Figure 3.1 (b) shows the snapshot of the micromagnetic simulation under a certain external magnetic field (field when kink appear in hysteresis loop); it was observed that the domain wall was induced at a free end of the tube segment which propagate to the transition region between the tube and wire segments, where the domain wall pinned under certain range of external magnetic field. Figure 3.1 (c) shows the hysteresis loop of a tube-wire nanostructure. Two distinct Barkhausen jumps can be clearly seen defining a kink that originates from the tube segment reversing its magnetization first, then the wire segment. Further analysis showed that a vortex domain wall formed at the tube end moves rapidly and propagates through the tube segment, stops at interface between tube and wire (partial pinning) and then propagate through wire segment (see inset in Figure 3.1 (c)). It was also observed that when the wire segment was long enough, a transverse domain wall propagates through wire segment first and the tube segment.

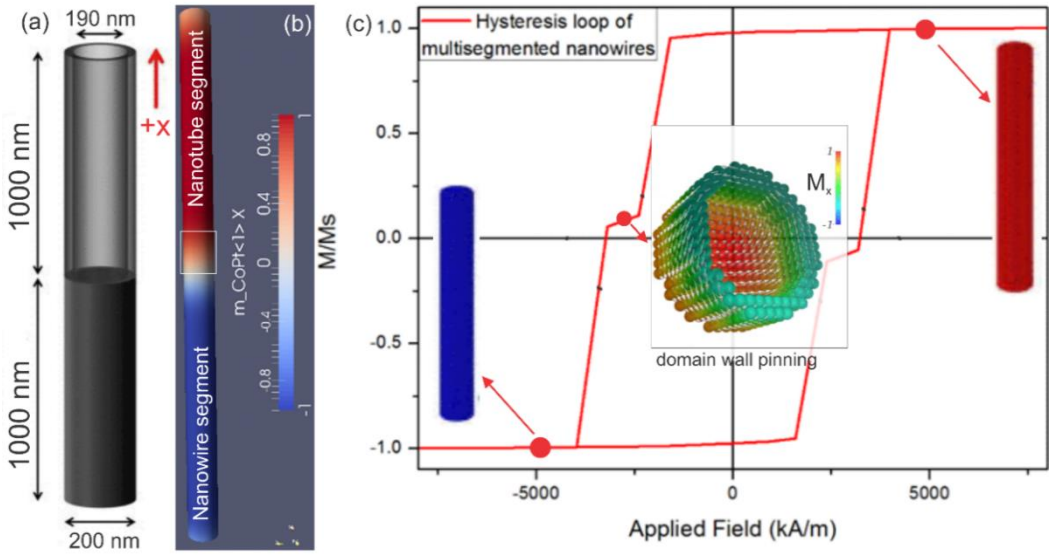


Figure 3.1: (a) geometrical characterization of a wire-tube nanostructure. (b) Micromagnetic simulation results of nanostructure with tube-wire morphology showing domain pinning at the interface between tube and wire. (c) Hysteresis curve for a Co-Pt wire-tube nanostructure when a magnetic field is applied along its axis. The central snapshot shows the vortex domain wall that appears between the two segments of the nanostructure.

Angular dependence of the coercivity in electrodeposited Co-Pt nanostructures with a tube-wire morphology

Muhammad Shahid Arshad[1,2], Darja Pečko[1,2], Sašo Šturm[1], Juan Escrig[3], Matej Komelj[1], Paul J. McGuiness[1], Spomenka Kobe[1,4], and K. Žužek Rožman[1]

[1]Jožef Stefan Institute, Department for Nanostructured Materials K7, Ljubljana, Slovenia
[2]Jožef Stefan International Postgraduate School, Ljubljana, Slovenia
[3]Universidad de Santiago de Chile (USACH), Departamento de Física, and Center for the Development of Nanoscience and Nanotechnology (CEDENNA), Av. Ecuador 3493, 9170124 Santiago, Chile
[4]Center of Excellence on Nanoscience and Nanotechnology (CENN Nanocenter), Ljubljana, Slovenia

Corresponding author: Muhammad Shahid Arshad (shahid.arshad@ijs.si)

We have fabricated Co-Pt cylindrical nanostructures comprised of a pair of nanotube and nanowire segments via direct electroplating into anodic alumina (AAO) membranes. The fabrication of such nanostructures is possible due to the penetration of sputtered gold (Au) nanoparticles inside the template, which serve as nucleation spots. The current transient monitored during the deposition process allowed us to distinguish between the nanotube and nanowire formation regime during the electrodeposition. In this work we report on the systematic changes in the angular dependence of the coercivity behavior due to the change in the length of the nanowire segment of these nanostructures, while keeping the nanotube segment constant. Considering the range of parameters studied, we found that the tube segment always reverses its magnetization through a vortex domain wall, whereas the nanowire segment reverses its magnetization through a transverse domain wall. Our results are in good agreement with literature. The possibility to alter the magnetization reversal mode in such nanostructures provides an attractive way to control the motion of the magnetic domain walls.

***Index Terms*—Angular dependence of the coercivity, Co-Pt alloy, magnetization reversal, multisegmented nanostructures.**

I. Introduction

The ever-increasing desire for smaller sensors and actuators has motivated a large research effort to fabricate magnetic nanostructures with different geometries [1]. In particular, special attention has been focused on one-dimensional (1D) ferromagnetic materials such as nanowires and nanotubes to address not only fundamental physical questions [2, 3], but also for technological reasons, owing to their potential applications in biosensors and other magnetic devices [1]. In the past few years, template-assisted electrodeposition (ED) has been widely used for the synthesis of a large variety of ferromagnetic nanostructures comprising of nanowires [4, 5] and nanotubes [4, 6] made of several different materials.

Coercivity is one of the most important properties of magnetic nanostructures from the point of view of their applications, and an understanding of the coercivity mechanism is a constant challenge for researchers. Measuring the angular dependence of the coercivity (ADC) for the nanostructures provides information about the underlying mechanisms of the magnetization reversal (MR) [2]. MR mechanisms are very sensitive to morphology of the nanostructures, thus different MR modes can be induced by simply changing the geometrical parameters [7]. The most common MR mechanisms in nanotubes and nanowires are the vortex and transverse reversal modes [2, 3]. Landeros *et al.* [2] showed that the vortex domain wall nucleation is favorable for nanotubes with diameters larger than 50 nm, while in nanowires, mainly transverse domain wall nucleation is observed for diameters of ≈50 nm [8] (of course, depending also on the material that form the nanostructures).

The MR modes in nanotubes and nanowires have been exploited during the past two decades and understood to a greater extent. Now it is time to bring new challenges to the field by building nanostructures consisting of both nanotube and nanowire segments in a single nanostructure. Such nanostructures are a new type of 1D materials that have great potential to become building blocks for advanced magnetic devices. The properties of these nanostructures are expected to be hybridized between nanotubes and nanowires. However, there is no experimental report that investigates the angular dependence of the magnetic properties of cylindrical nanostructures comprised of both nanotube and nanowire segments, in spite of a few theoretical reports on the magnetic properties of similar morphology nanostructures [9, 10]. Neumann *et al.* [9] predicted that in nanostructures with wire-tube morphology different reversal modes can be induced in each segment by choosing the right geometrical parameters and they observed a kink in the hysteresis curve which will be discussed later. In addition, Salazar *et al.* [10] showed that the tube segment reverses its magnetization before the wire segment, allowing a control of the magnetic domain walls' motion between the two segments.

Following these ideas, in this report we have synthesized Co-Pt nanostructures consisting of a pair of nanotube and nanowire segments and investigated systematic changes in the angular dependence of the coercivity behavior by changing the length of the nanowire segment.

II. Experimental Details

Porous alumina (AAO) membranes (Whatman Anapore Co.) with pore diameters of ≈200 nm were used for the electrodeposition of the Co-Pt based nanostructures. The AAO

This is the author's version of an article that has been published in the IEEE Transactions on magnetics. Changes were made to this version by the publisher prior to publication. The final version of record is available at 10.1109/TMAG.2014.2320911

membranes are ≈65 μm thick with an average spacing between the pores of ≈125 nm. A gold (Au) layer (≈100 nm) was sputtered on one surface of the AAO membrane to make it conductive and used as the working electrode (cathode) in a three-electrode cell. The electrolyte consisted of 80 mmol/dm^3 of Co-sulphamate ($Co(SO_3NH_2)_2$) and 20 mmol/dm^3 of Pt-p-salt ($Pt(NH_3)_2(NO_2)_2$), while ammonium citrate ($(NH_4)_2C_6H_6O_7$) (20 mmol/dm^3) and glycin (NH_2CH_2COOH) (0.2 mmol/dm^3) were used as the complexing agents. The pH of the electrolyte was set to 8 using ammonia. A Pt mesh electrode was used as the anode, and potentiostatic conditions with -2.1 V against a reference electrode of Ag/AgCl were used to deposit metal ions into the pores of the AAO membrane to obtained an average composition of $Co_{65\pm3}Pt_{35\pm3}$ with the crystal structure of face centered cubic intermixed with hexagonal close packed (fcc+hcp) as presented in another study [11].

Fig. 1 shows the current-time (*i*-*t*) transients for a sample deposited for 60 mins. At the beginning of the deposition a high current is obtained (i_C = 44 mA) due to the charging of the electrical double layer (stage 1), which is followed by a nucleation process on the bottom of the pore (stage 2). The constant current in stage 3 (see the inset of fig.1) corresponds to nanotube growth for t ≈ 600 s, which is continued with the current decrease indicating the nanowire growth (stage 4). This abrupt decrease in the cathodic current when the transition from the nanotube to the nanowire occurred was also observed by Motoyama *et al.* [12]. Herein, Au sputtering controls the formation of the Co-Pt nanotubes. During the sputtering step some Au nanoparticles (NPs) were attached to the inner walls of the AAO template. According to our previous study [13], the sputtered Au NPs entered about 1 μm into the pores of AAO template. A possible mechanism for the deposition of the nanotube/nanowire junction can be deduced and is schematically presented in fig. 1. The ED of Co-Pt initiates on the Au NPs that entered the AAO pores during the sputtering step and therefore serve as preferential sites. Later, the ED continues on the new freshly as-deposited Co-Pt particles around the pore walls and in the pore axial directions [14]. Under this confinement the Co-Pt nanotubes were deposited, with the approximate wall thickness of ~30 nm. The growth of the nanotube with a nearly constant wall thickness is continued as long as the Au NPs are present in the AAO template (<1 μm, t <600 s). When there are no more Au NPs present in the AAO template (>1 μm, t >600 s), the nanotubes inside the pores grow thicker and eventually the nanowires are formed. A similar observation in the growth mechanism of nanotubes/nanowires junctions was made by [4] and [12].

The morphology of the individual Co-Pt nanostructure was studied by transmission electron microscopy (TEM; JEOL JEM-2010F). To obtain individual nanostructures, the AAO membrane was dissolved in an aqueous solution of 10-M NaOH and the nanostructures were released using a centrifuge. The Co-Pt nanostructures were then dispersed in absolute ethanol and sprinkled onto TEM Cu-grids and dried. A field-emission-gun scanning electron microscope (FEG-SEM; JSM-7600F) study provided information about the aspect ratio of the nanostructures. The magnetic measurements were performed using a vibrating sample magnetometer (VSM) at RT. For the magnetic hysteresis loops the field (H_a) was swept in the range ±875 kA/m and the applied field angle was increased with respect to the long axis (z-axis) of the nanostructures in 20^o steps after each measurement.

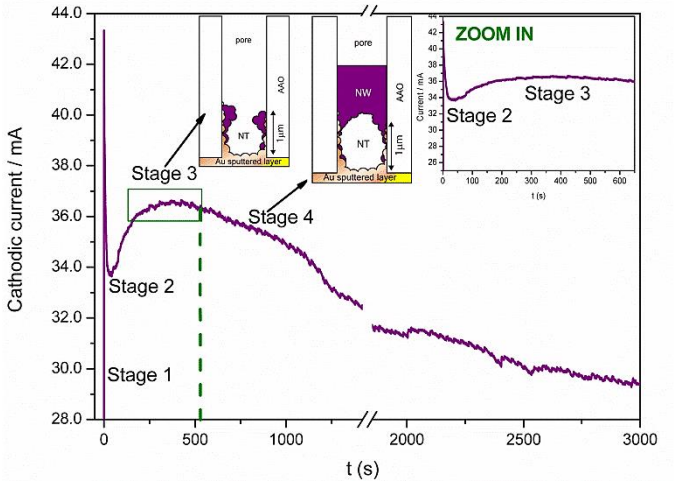


Fig. 1. Cathodic current transients during the deposition of Co-Pt nanotubes+nanowires in the AAO/Au template. The inset shows the the initial region (t < 600 s) of the *i*–*t* curve.

III. Results and Discussion

Fig. 2 (a) shows a TEM image of a Co-Pt sample fabricated for 60 mins of electrodepostion, taken after the removal of the template. It is clear that the nanostructure formed consists of a nanotube (≈1 μm) at the bottom and a nanowire segment at the top. The obtained 1D nanostructure maintains a diameter of ≈200nm, like pores size of the AAO template. Fig. 2(b) represents the resultant morphology of the nanostructure. Their geometrical parameters are defined as the external and internal radii of nanotube segment, R and a, respectively, and the total length is L, which includes the wire segment (length h) and the tube segment (length h'≈1 μm). The ratio β=a/R is defined such that β=0 represents a solid cylinder and β→1 corresponds to a very narrow tube. The tube wall thickness was found to be around 30 nm, thus β=0.9 was considered for all cases. In addition, we defined η=h/L, so that a nanotube is represented by η=0 while a multisegmented system considers η ≠ 0. Table 1 shows five different samples deposited for different times of electrodeposition (t).

Table 1. Time of electrodeposition, t, lengths, L, of the whole nanostructures, geometrical parameters, and reversal modes for the nanostructures obtained from different shapes of $H_c(\theta)$ curves. In the fourth column, "v" stands for "vortex domain wall" and "t" for "transverse domain wall". Note that the capital letters represent the reversal modes that are dominant in the measured θ range.

Sample	t (mins)	L (μm)	h=L-1	η=h/L	Reversal modes
S1	10	1	0	0	V
S2	20	2	1	0.5	V-t
S3	30	3	2	0.7	v-T
S4	60	6	5	0.85	v-T
S5	200	20	19	0.95	T

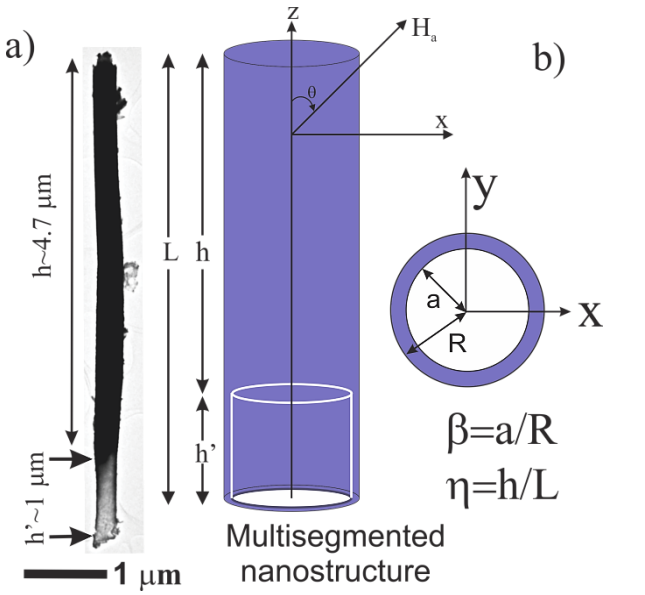


Fig. 2. (a) TEM micrograph showing a nanostructure composed of nanotube (h'~1 μm) and nanowire (h~4.7 μm) segments (b) Illustration of a nanostructure composed of a nanotube at the bottom and a nanowire at the top with defined geometrical parameters β and η.

Fig. 3 shows the magnetic hysteresis loops measured for sample S1 (η=0) and S2 (η =0.5) at an applied field angle of θ=90°. We observed a kink in the hysteresis curve (see the insets of fig.3) for S2, whereas there is no kink present for the S1. Neumann *et al.* [9] interpreted this kink as partial pinning of the domain wall as it moves at the interface between the nanotube and the nanowire segment. This phenomenon was observed in all samples with $0 < \eta \leq 0.95$. This effect can be further enhanced by introducing two different coercivity materials in the two segments [9].

To investigate the MR processes of multisegmented Co-Pt nanostructure arrays with a diameter ≈200 nm, measurements of the ADC were performed. Fig. 4 shows the results of the ADC, $H_c(\theta)$, for the Co-Pt nanostructure arrays for five different samples (S1-S5) with different lengths of nanowire segment (h). The corresponding SEM micrographs show the overall lengths of the nanostructures. The shapes of the H_c (θ) curves are determined by the underlying MR mechanisms in the nanostructures [15]. For example, in sample (S1), in fig. 4, the coercivity increases with the increasing angle at which the external field is applied, thus showing an almost monotonic behavior. This behavior of the ADC is a signature for the MR process through the nucleation and propagation of a vortex domain wall [16]. However, the opposite H_c (θ) behavior was observed for sample (S5), which corresponds to a MR through the nucleation and propagation of a transverse domain wall [8].

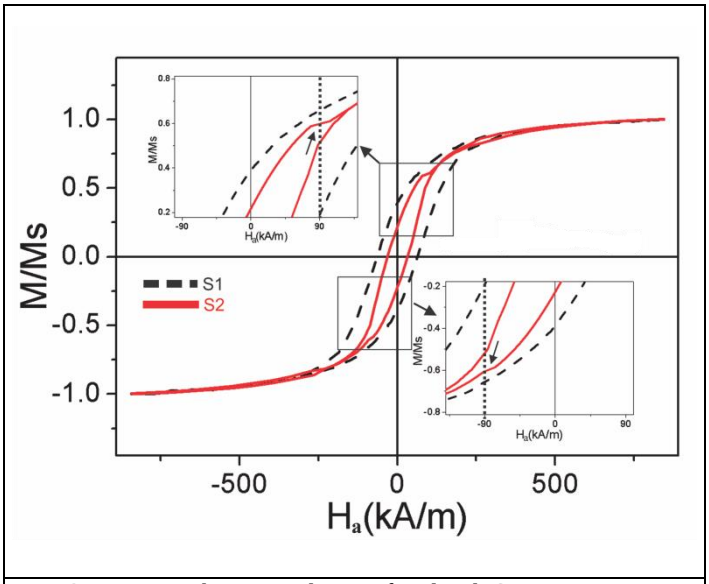


Fig. 3. Magnetic hysteresis loops of ordered Co-Pt nanostructure arrays with d = 200 nm, measured at angle θ = 90° of the external field for sample S1 (dotted curve) and S2 (line curve).

In addition, the H_c (θ) behavior is not monotonic for samples (S2-S4) with intermediate lengths, 1 < L < 20 μm. This behavior has been observed previously for nanowires [3, 17] and nanotubes [18, 19], and it has been interpreted as arising due to the transition between two different magnetization reversal modes. To summarize, measurements of the ADC revealed that the MR transforms from a vortex domain wall nucleation (S1) to a transverse domain wall nucleation (S5) by changing the geometrical parameter η from 0 to 0.95. Furthermore, a crossover is observed between two modes of MR when the samples have intermediate lengths 1 < L < 20 μm. For more details see table 1. Additionally, our results are in good agreement with the theoretical observations obtained by Neumann *et al.* [9] and Salazar *et al.* [10] for similar morphologies.

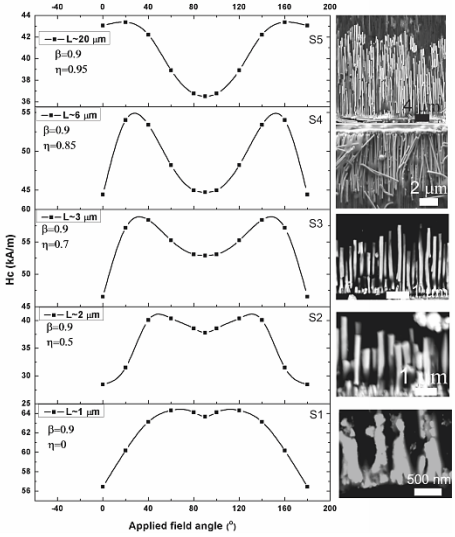


Fig. 4. Measurements of the ADC for five different samples (S1-S5)

with different lengths of the nanowire segment. The corresponding SEM micrographs show the overall length of the five samples.

IV. Conclusion

In conclusion, we have fabricated Co-Pt nanostructures with a pair of nanotube and nanowire segments via an electrodeposition process. Such a morphology is obtained due to the Au NP inclusion (≈1 μm) into the pores of the AAO template. We have observed a kink in the hysteresis curves corresponding to a partial pinning of the domain wall at the interface between the tube and wire segments. The angular dependence of the coercivity behavior for such nanostructures was observed by increasing the length of the nanowire segment. Considering the range of parameters studied, we found that the tube segment always reverses its magnetization through a vortex domain wall, whereas the nanowire segment reverses its magnetization through a transverse domain wall. In the intermediate lengths there is an interplay between the two reversal modes. Our results are in accordance with the literature and provide guidelines for predicting the MR of Co-Pt nanostructures with a pair of alternating nanotube and nanowire segments and will be helpful for their utilization in future applications. Further detailed crystal-structure studies and associated anisotropies will be investigated together with micromagnetic modeling in future work.

Acknowledgment

This project was funded by the Slovenian Research Agency (ARRS) under project number PR-04442. In Chile, we acknowledged support from FONDECYT under project 1110784, Grant ICM P10-061-F by Fondo de Innovación para la Competitividad-MINECON and Financiamiento Basal para Centros Científicos y Tecnológicos de Excelencia, under project FB0807.

References

[1] L. A. Bauer, N. S. Birenbaum and G. J. Meyer, "Biological applications of high aspect ratio nanoparticles," *J. Mater. Chem.* vol. 14, pp. 517-526, 2004.

[2] P. Landeros, S. Allende, J. Escrig, E. Salcedo, D. Altbir and E. E. Vogel, "Reversal modes in magnetic nanotubes," *Appl. Phys. Lett.* vol. 90, pp. 102501-102503, 2007.

[3] R. Lavín, C. Gallardo, J. L. Palma, J. Escrig and J. C. Denardin, "Angular dependence of the coercivity and remanence of ordered arrays of Co nanowires," *J. Magn. Magn. Mater.* vol. 324, pp. 2360-2362, 2012.

[4] J. Fu, S. Cherevko and C.-H. Chung, "Electroplating of metal nanotubes and nanowires in a high aspect-ratio nanotemplate," *Electrochem. Commun.* vol. 10, pp. 514-518, 2008.

[5] V. Vega, T. Böhnert, S. Martens, M. Waleczek, J. M. Montero-Moreno, D. Görlitz, V. M. Prida and K. Nielsch, "Tuning the magnetic anisotropy of Co-Ni nanowires: comparison between single nanowires and nanowire arrays in hard-anodic aluminum oxide membranes," *Nanotechnology* vol. 23, pp. 465709-465709, 2012.

[6] Xiu-Feng Han, Shahzadi Shamaila, J.-Y. C. Rehana Sharif, Hai Rui Liu and a. D. P. Liu, "Structural and Magnetic Properties of Various Ferromagnetic Nanotubes," *Adv. Mater.* vol. 21, pp. 6, 2009.

[7] A. P. Chen, J. Gonzalez and K. Y. Guslienko, "Domain walls confined in magnetic nanotubes with uniaxial anisotropy," *J. Magn. Magn. Mater.* vol. 324, pp. 3912-3917, 2012.

[8] M. P. Proenca, C. T. Sousa, J. Ventura, J. P. Araujo, J. Escrig and M. Vazquez, "Crossover between magnetic reversal modes in ordered Ni and Co nanotube arrays," *SPIN* vol. 02, pp. 1250014-1250020, 2012.

[9] R. F. Neumann, M. Bahiana, N. M. Vargas, D. Altbir, S. Allende, D. Görlitz and K. Nielsch, "Domain wall control in wire-tube nanoelements," *Appl. Phys. Lett.* vol. 102, pp. 202407-202412, 2013.

[10] D. Salazar-Aravena, R. M. Corona, D. Goerlitz, K. Nielsch and J. Escrig, "Magnetic properties of multisegmented cylindrical nanoparticles with alternating magnetic wire and tube segments," *J. Magn. Magn. Mater.* vol. 346, pp. 171-174, 2013.

[11] M Shahid Arshad, K. Žužek Rožman, Sašo Šturm, Janez Zavašnik, Alvaro P. Espejo, Juan Escrig, Matej Komelj, Paul J. McGuiness and S. Kobe, "Effect of magnetocrystalline anisotropy on the magnetic properties of electrodeposited Co-Pt nanowires ", Submitted for Publication.

[12] M. Motoyama, Y. Fukunaka, T. Sakka and Y. H. Ogata, "Initial stages of electrodeposition of metal nanowires in nanoporous templates," *Electrochim. Acta* vol. 53, pp. 205-212, 2007.

[13] N. Kostevšek, K. Ž. Rožman, D. Pečko, B. Pihlar and S. Kobe, "A comparative study of the electrochemical deposition kinetics of iron-palladium alloys on a flat electrode and in a porous alumina template," *Electrochim. Acta* vol. 125, pp. 320-329, 2014.

[14] D. Yang, G. Meng, S. Zhang, Y. Hao, X. An, Q. Wei, M. Ye and L. Zhang, "Electrochemical synthesis of metal and semimetal nanotube-nanowire heterojunctions and their electronic transport properties," *Chem. Commun. (Cambridge, U. K.)* vol. 17, pp. 1733-1735, 2007.

[15] G. C. Han, B. Y. Zong, P. Luo and Y. H. Wu, "Angular dependence of the coercivity and remanence of ferromagnetic nanowire arrays," *J. Appl. Phys.* vol. 93, pp. 9202-9207, 2003.

[16] J. Escrig, M. Daub, P. Landeros, K. Nielsch and D. Altbir, "Angular dependence of coercivity in magnetic nanotubes," *Nanotechnology* vol. 18, pp. 445706, 2007.

[17] S. Goolaup, N. Singh, A. O. Adeyeye, V. Ng and M. B. A. Jalil, "Transition from coherent rotation to curling mode reversal process in ferromagnetic nanowires," *EPJ B* vol. 44, pp. 259-264, 2005.

[18] J. Escrig, J. Bachmann, J. Jing, M. Daub, D. Altbir and K. Nielsch, "Crossover between two different magnetization reversal modes in arrays of iron oxide nanotubes," *Phys. Rev. B* vol. 77, pp. 214421-214428, 2008.

[19] J. Bachmann, J. Escrig, K. Pitzschel, J. M. M. Moreno, J. Jing, D. Görlitz, D. Altbir and K. Nielsch, "Size effects in ordered arrays of magnetic nanotubes: Pick your reversal mode," *J. Appl. Phys.* vol. 105, pp. 07B521-507B524, 2009.

Chapter 4

Effect of Magnetocrystalline Anisotropy on the Magnetic Properties of Electrodeposited Co-Pt Nanowires

In this Chapter, the article entitled "Effect of magnetocrystalline anisotropy (MCA) on the magnetic properties of electrodeposited Co-Pt nanowires" by **Muhammad Shahid Arshad,** Sašo Šturm, Janez Zavašnik, Alvaro P. Espejo, Juan Escrig, Matej Komelj, Paul J. McGuiness, Spomenka Kobe, Kristina Žužek Rožman, [39] is presented. The author contribution to this article is electrodeposition of Co-Pt nanowires, SEM+EDS analysis for morphology and compositional analysis, sample preparation for XRD and TEM analysis, magnetic characterizations, MFM measurements and MFM images interpretation.

The purpose of this article was to evaluate the effect of MCA on magnetic properties of Co-Pt NWs. Co-Pt NWs are transition metals nanomagnets created by d-electrons exchange interactions, which can develop strong spin-orbital coupling, thus present high MCA which can play a significant role in magnetic properties of the nanowires.
It was found that the Co-Pt NWs consist of intermixed hcp and fcc crystal structures with strong crystallographic texturing. The MCA easy axis of hcp ([001]-c-axis) and fcc ([111]) were found to be aligned perpendicular to NW along axis. Perpendicular easy magnetization axis was due to perpendicular arrangement of MCA. Thus, the shape and MCA are in competition with each other which reduced the effective anisotropy constant K_{eff}= 2.6 x 10^4 J/m^3, it is an important parameters for determining the static and dynamic magnetic properties of Co-Pt NWs. The competition between the shape and MCA was found to be responsible for periodic domain structure in individual Co-Pt NWs. We also studied magnetic domain configuration in Co-Pt NWs under applied magnetic field with home-made MFM stage.
To conclude, in Co-Pt NWs MCA strongly affects the magnetization easy axis, MR and magnetic domain structure.

Effect of magnetocrystalline anisotropy on the magnetic properties of electrodeposited Co-Pt nanowires

Muhammad Shahid Arshad[1,2], Sašo Šturm[1], Janez Zavašnik[1], Alvaro P. Espejo[3], Juan Escrig[3], Matej Komelj[1], Paul J. McGuiness[1], Spomenka Kobe[1,2,4], and K. Žužek Rožman[1]

[1]Jožef Stefan Institute, Department for nanostructured materials K7, Ljubljana, Slovenia

[2]Jožef Stefan International Postgraduate School, Ljubljana, Slovenia

[3]Departamento de Física, Universidad de Santiago de Chile (USACH), and Center for the Development of Nanoscience and Nanotechnology (CEDENNA), Av. Ecuador 3493, 9170124 Santiago, Chile

[4]Center of Excellence on Nanoscience and Nanotechnology (CENN Nanocenter), Ljubljana, Slovenia

E-mail: shahid.arshad@ijs.si

Telephone: +386 1 4773 178
Fax: +386 1 4773 221

Abstract

We report on the influence of the magnetocrystalline anisotropy on the easy magnetization axis, magnetization reversal and magnetic domain configurations of electrodeposited Co-Pt nanowires with length of 4-6 μm and a diameter of 250 nm. The transmission electron microscopy and the X-ray diffractions revealed that the nanowires are composed of an intermixture of *hcp* and *fcc* textured crystal structures. The crystallographic orientation of both phases was such that the [00$\bar{1}$] of the *hcp* phase and the of the *fcc* phase are pointing almost perpendicular to the nanowire axis. This observation allows us to understand the perpendicular easy magnetization axis of the nanowire arrays measured with vibrating sample magnetometry. Analytical calculations of the angular dependence of the coercivity revealed that the magnetization reversal changes from vortex to transverse mode at applied field angle $\theta=30^{o}$. Fitting of the experiment to these calculations results in a perpendicular *effective* anisotropy constant (K_{eff}= 2.6 x 10^4 J/m^3) in nanowires which can be ascribed to the strong magnetocrystalline anisotropy. Furthermore, the magnetic domain configurations of individual nanowires of length range $4 < L < 6$ μm are studied using magnetic force microscopy. This reveals a spatial magnetization modulation along the length of the nanowires which was found to be length dependent. Such an intrinsic modulation is attributed to the competition between the magnetocrystalline anisotropy and the shape anisotropy in the nanowires. We believe this interplay between anisotropies gives rise to a magnetic configuration involving vortex-like structure with alternating chirality along the length of the nanowires.

Keywords: Co-Pt nanowire arrays, single Co-Pt nanowire, effective magnetic anisotropy, angular dependence of the coercivity, magnetization reversal modes, periodic magnetic domains, magnetization of a single Co-Pt nanowire.

This is the author's version of an article that has been published in Journal of Nanoparticle Research. Changes were made to this version by the publisher prior to publication. The final version of record is available at 10.1007/s11051-014-2688-4

Introduction

The ever-increasing desire for smaller sensors, actuators and in the increase of data storage density has motivated large research effort to scale down the size of the components and to investigate different geometries of magnetic materials. In particular, special attention has been focused on one-dimensional (1D) magnetic nano-materials such as nanowires and nanotubes to address not only fundamental physical questions, such as magnetic domain configurations (Y. Henry et al. 2001) and magnetization reversal processes (Landeros et al. 2007), but also for technological reasons, owing to their potential applications in biosensors (Ning et al. 2010; Bauer et al. 2004) and magnetic memory devices (L.Sun et al. 2005).

The electrochemical deposition of nanowires into anodic alumina (AAO) membranes is an efficient and cost effective method for growing high density and high aspect ratio arrays of nanowires (Fu et al. 2008; Vega et al. 2012) with precise control over their characteristics (Martin 1994, 1996). Despite the simplicity of electrodeposition operation, many parameters such as the deposition modes (dc/ac mode) (Zhang et al. 2007), the electrodeposition voltage (Schlörb et al. 2010), metal ion concentration (Yang et al. 2000), and the electrolyte pH (Khurshid et al. 2009; Fashen Li et al. 2004) need to be optimized in order to obtain the required magnetic properties of the nanowires. It is well known that the dc mode under controlled conditions can produce nanowires with better crystallinity and faster growth (Pan et al. 2005). In addition, electrodeposition of nanowires consist of noble metal and base metal whose standard potential are far away from each other require high diligence in choosing appropriate electrodeposition parameters to allow co-deposition (Schlörb et al. 2010).

Co-Pt-based alloys with high magnetocrystalline anisotropy are suitable magnetic material for a variety of applications, including high density recording media (Irshad et al. 2012) and magnetic actuators for micro-electro-mechanical systems (MEMS) (Zana et al. 2004). Co-Pt alloys nanostructures can exhibit either a metastable disordered phase (fcc-based $L1_1$-CoPt (Sayama et al. 2011)), hcp based B_h-CoPt (Ohtake et al. 2013) or a hcp-based $D0_{19}$-Co_3Pt (Harp et al. 1993) crystal structure depending on the formation conditions. Fcc- and hcp-based structures respectively consist of atomic stacking sequences of ABCABC….and ABAB… along the direction normal to the close-packed plane. The crystal structure of Co-based alloy nanostructures is known to easily vary between the two structures and may consist of a mixture of the two (Bolzoni et al. 1984; Zhang et al. 2006; Aboaf et al. 1983; Ohtake et al. 2013). Co-Pt hcp structure is a well-known magnetic material with high magnetocrystalline anisotropy, comparable to or even stronger than the shape anisotropy in magnetic nanowires (Zana et al. 2004; Bran et al. 2013). In many cases, magnetocrystalline anisotropy of hcp phase favours easy magnetization axis perpendicular-to-the-nanowire axis (Cho et al. 2006; Yu et al. 2013b). Thus, the effective anisotropy energy is determined by the competition between shape and magnetocrystalline anisotropies. Therefore, it is possible to tune the preferred magnetization direction, magnetization reversal mechanisms and magnetic domains structure in Co-Pt nanowires by accurately control the crystallographic structure and volume ratio of fcc and hcp crystals in the nanowires (Xianghua et al. 2009).

Different magnetization reversal modes, such as coherent rotation, vortex or transverse mode have been discussed in cylindrical nanowires (and nanotubes) under the framework of analytical calculations (Lavin et al. 2009a; Lavin et al. 2010; Lavín et al. 2012). In coherent reversal mode all magnetic moments simultaneously rotates; the vortex wall, where magnetic moment rotates progressively via propagation of a vortex domain wall (this mode is frequently called curling reversal mode); and transverse wall, where magnetic moments rotates progressively via propagation of a transverse domain wall. Significant progress achieved in the analytical theory over the past few years has allowed investigating magnetization reversal in cylindrical shape nanowires with diameter of several tens of nanometres and length several micrometres. Magnetic anisotropy of nanowires can include the shape anisotropy, and magnetocrystalline anisotropy. All these anisotropy components can be included in analytical calculations by using the *effective* anisotropy concept, with the value fitted to experimental data. For example, (Vivas et al. 2012b) and (Vivas et al. 2012a) fitted experimentally measured angular dependence of coercivity to analytical models based on

transverse and vortex mode to associate the coercivity mechanism in Co-based nanowires with possible occurrence of these processes. Additionally, the fitted effective anisotropy constant can be used to further explain the magnetization behaviour of the nanowires. Since the exact knowledge about magnetization reversal mechanism in nanowires is very important in many areas of the applications.

Magnetic force microscopy (MFM) is a powerful technique for studying the magnetic domains in nanostructures with a high spatial resolution using a simple method for sample preparation (Sorop et al. 2003; Y. Henry et al. 2001; Zuwei Liu et al. 2008). In spite of few MFM reports on individual Co-Pt nanowires (Hassel et al. 2006), a detailed MFM study on individual Co nanowires with hcp crystal structure was reported by (Y. Henry et al. 2001; Zuwei Liu et al. 2008). A periodic dark and bright MFM contrast along the length of the nanowire was observed. This contrast was interpreted as the signature of a single domain state, with the magnetization modulation along the length of the nanowire (Ivanov et al. 2013). From theoretical point of view (Gerd Bergmann et al. 2008; Fert and Piraux 1999; Kristof M Lebecki and Donahue 2010), this magnetization modulation originates from the competition between the magnetocrystalline anisotropy and the shape anisotropy in the nanowires. The right interpretation of this contrast is not yet clear and even conflicting in some reports (Gerd Bergmann et al. 2008; Kristof M Lebecki and Donahue 2010). For example, in (Gerd Bergmann et al. 2008), it is found in the thin wire limit that the angle between the magnetization and the wire axis is modulated sinusoidally along the length of the wire axis to lower the magnetic energy. Whereas, (Kristof M Lebecki and Donahue 2010) performed micromagnetic simulations and found even lower energy state with vortex-like configuration along the length of the nanowires. Recently, an experimental report (Zuwei Liu et al. 2008) on single crystal hcp Co nanowires with periodic domain structure was explained on the basis of analytical model by (Gerd Bergmann et al. 2008) assuming the thin wire limit. We and (Kristof M Lebecki and Donahue 2010) believe this assumption simply doesn't hold in observed nanowires with diameter larger than 50 nm as exchange length doesn't exceed 10 nm. We believe we have model system which can explain the theoretical results of (Kristof M Lebecki and Donahue 2010). However, in (Zuwei Liu et al. 2008) magnetization modulation is commented to arise from the competition between magnetocrystalline and shape anisotropy. But no study for nanowires with different length and/or diameter was provided to fully clarify the matter. In this study we have systematically investigated the variation of the magnetization modulation with the length of the nanowires. Additionally, all the experimental published reports with such a domain pattern were reported on single crystalline hcp Co nanowires (Y. Henry et al. 2001; Zuwei Liu et al. 2008). Thus, the question about the existence of such magnetic domain structure in polycrystalline nanowires still remains open.

In this study we have investigated potentiostatically electrodeposited Co-Pt nanowires with a diameter of 250 nm and a length of 4-6 μm. The microstructure, which consists of Co-Pt textured fcc and hcp phases in a crystallographic relationship, was investigated by means of X-ray diffraction (XRD) and Selected area electron diffraction pattern (SAED). On the basis of detailed TEM analysis, we have been able to describe the possible growth mechanism of Co-Pt nanowires. The anisotropy interplay coming from the different crystalline phases and the shape of the nanowires were found to influence the easy magnetization axis and thus was also the reason for the periodic domain structure observed in a single Co-Pt nanowire. However, there are conflicting interpretations of periodic domain structure in nanowires in literature; we shed a light on the possible domain configurations in our Co-Pt nanowires. Additionally, a systematic study on different lengths of the individual Co-Pt nanowires was performed to understand the balance between the magnetocrystalline and shape anisotropy. Here we present a good agreement between experimental and analytical calculations for investigation of the magnetization reversal mode in Co-Pt nanowire arrays. A crossover between two distinct magnetization reversal mechanisms was found as a function of the angle at which the external field is applied. A home-made MFM stage with permanent magnet was employed to investigate the magnetic domain configuration in different magnetic fields. The obtained knowledge about the magnetization easy axis, coercivity mechanism and domain structure in connection with the crystal structure and geometry of the Co-Pt-based nanowires is important for their advanced applications.

Experimental details

Porous alumina (AAO) membranes (Whatman Anapore Co.) with average pore diameters of ≈ 250±30 nm were used for the electrodeposition of the Co-Pt alloy based nanowires. The AAO membranes are ≈65 μm thick with an average distance between the pores (center to center) of ≈360±30 nm. A gold (Au) layer (≈100 nm) was first sputtered to one surface of the AAO membrane to make it conductive. Then, on the same surface, Au was electrodeposited for 10 mins to completely cover the pores so as to use it as the working electrode (cathode) in a three-electrode cell. The electrolyte consisted of 80 mmol of Co-sulphamate ($Co(SO_3NH_2)_2$) and 20 mmol of Pt-p-salt ($Pt(NH_3)_2(NO_2)_2$), while ammonium citrate ($(NH_4)_2C_6H_6O_7$) (20 mmol) and glycin (NH_2CH_2COOH) (0.2 mmol) were used as the complexing agents. The pH of the electrolyte was set to 8 by using ammonia. A Pt mesh electrode was used as the anode, and potentiostatic conditions with -2.1 V against a reference electrode of Ag/AgCl were used to deposit metal ions into the pores of the AAO membrane. The time of the electrodeposition that determines the length of the nanowires was fixed 60 mins.

The morphology, composition and crystal structure of the electrodeposited Co-Pt nanowire arrays were characterized by scanning electron microscopy (SEM; JSM-7600F) and X-ray diffraction (XRD) (PANalytical X'pert Pro), respectively. The XRD patterns were acquired in a θ-2θ setup by employing Cu-$K_{\alpha 1}$ radiation (λ=1.54056 Å). A zero-background sample holder was used for the XRD measurements. To obtain individual nanowires the AAO membrane was dissolved in an aqueous solution of 10-M NaOH and the nanowires were released using a centrifuge. The Co-Pt nanowires were then dispersed in absolute ethanol and sprinkled onto TEM Cu-grids and dried. The microstructure, crystal structure and the ordering between the crystallites of an individual Co-Pt nanowire was studied by (TEM; JEOL JEM-2010F). The TEM was equipped with an energy-dispersive X-ray spectrometer (EDXS) to determine the composition of the individual Co-Pt nanowires. High-resolution transmission electron microscopy (HRTEM) images were taken on appropriate regions of the nanowire. Selected-area electron-diffraction (SAED) pattern analyses were used to determine the crystal structure and the local ordering of crystallites of an individual Co-Pt nanowire.

Room temperature hysteresis loops and the angular dependence of the coercivity (ADC) measurements of Co-Pt nanowire arrays were performed using a Vibrating Sample Magnetometer (VSM). For the hysteresis loops the external magnetic field was swept in the range ±875 kA/m. For the ADC measurements, where $\theta=0^o$ means the applied field is parallel to the nanowire long axis and 90^o perpendicular (in-plane orientation, considering the AAO surface) to them. The applied field angle was increased with respect to the long axis of the nanowires in 20^o steps after each measurement and the coercivity was determined as a function of the angle between applied field and the nanowires orientation. For MFM measurements a drop of ethanol containing Co-Pt nanowires was placed on a clean Si wafer and then dried. After a single nanowire was selected, a commercial scanning probe microscope (Digital Instruments Dimension 3100) was used for the MFM measurements. The MFM cantilever (Nanoworld MFMR type probe) was used in the lift mode. The tip magnetization direction was perpendicular to the plane of the Si substrate on which the nanowire was horizontally placed. For the *in-situ* magnetic field MFM measurements a home-made stage after (Bran et al. 2009) was used. The external field was applied perpendicular to the long axis of the nanowire.

Results and discussion

Morphological, compositional and structural characterization

Fig. 1 shows a SEM cross-sectional image of the Co-Pt nanowires arrays embedded in an AAO membrane. The nanowires are robust, erected, regular cylinders with a length of 4-6 μm and a diameter of 250±20 nm. Although the time of electrodeposition was fixed (60 mins) different length of the nanowires is due to heterogeneous nucleation of the nanowires inside the membrane. The diameter of the Co-Pt nanowires is consistent with the pore size of the AAO membrane. The aspect ratio (length/diameter) of the nanowires is ≈20-30. As seen from the SEM image, the filling

factor is estimated to be close to 100%. The SEM-EDXS analysis shows that the composition of the nanowires corresponds to Co and Pt with an average composition of $Co_{65\pm3}Pt_{35\pm3}$.

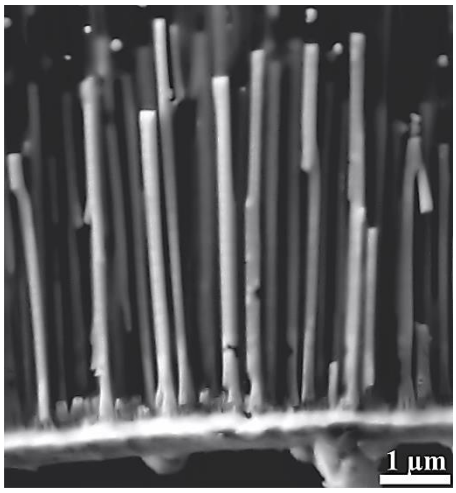


Fig. 1 SEM cross-sectional view of an AAO membrane filled with Co-Pt nanowires for L ≈4-6 µm.

The XRD pattern of the Co-Pt nanowire arrays embedded in the AAO membrane using the θ-2θ configuration in the range between 30º and 80º is shown in Fig. 2. The peak at 2θ≈38.2º corresponds to the deposited Au film used as the cathode, while the rest of the peaks relate to the Co-Pt alloy. The XRD diffractogram of the nanowires consist of intermixture of fcc and hcp phases. $CoPt_3$ *fcc* (ICSD#107047) and CoPt *fcc* (ICSD#624782) were identified for nanowire arrays with peaks corresponding to the $(111)_{fcc}$, $(200)_{fcc}$ and $(220)_{fcc}$ crystal planes. Two Co_3Pt_{hcp} (ICSD#102626) phase peaks were also identified at the angles 2θ≈40.48º and 46.13º corresponding to the $(100)_{hcp}$ and $(101)_{hcp}$ crystal planes, respectively. The diffraction peak at 2θ≈40.48º corresponding to the $(100)_{hcp}$ Co-Pt plane, is higher than expected for a polycrystalline sample (see ICSD#102626). This indicates strong crystallographic texturing along the $(100)_{hcp}$ crystal plane in the Co-Pt nanowires. The grain sizes were estimated to be ≈8 nm for fcc and ≈9 nm for hcp phases using the Scherrer formula (Cullity and Stock 2001).

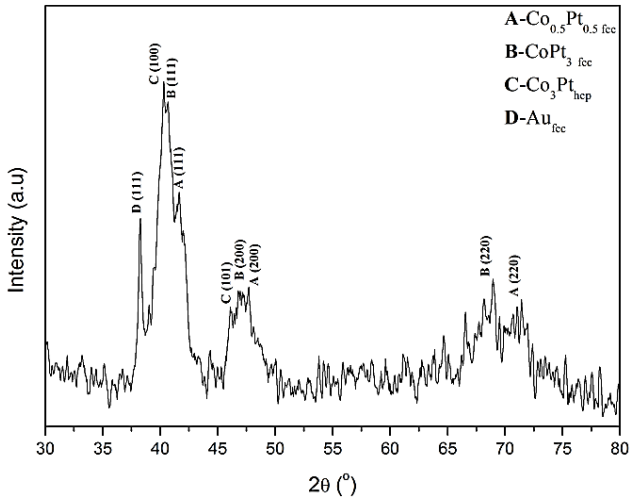


Fig. 2 XRD recorded on Co-Pt nanowire arrays inside the AAO templates.

Fig. 3a shows a TEM micrograph of an individual Co-Pt nanowire with a length of 5.5 µm and a diameter of ≈250 nm. The semi-transparent region at the bottom of the nanowire corresponds to a tube-like morphology, which is gradually converted into a nanowire after ≈1 µm in length. The observed tube-like morphology is the result of the uneven Au sputtered layer on the membrane, where Au nanoparticles enters into the pores of the template about ≈1 µm as we observed in our previous study (Kostevšek et al. 2014) and explained in detail elsewhere (Arshad et al. 2014). The deposition preferentially starts at these circular Au step edges, which have the ability to catalyse the electron transfer (Bowling et al. 1989) thus forming a tube-like morphology. When there are no more Au present in the AAO template (>1 µm), the nanotubes inside the pores grow thicker and eventually the nanowires are formed. A similar observation in the growth mechanism of nanotubes/nanowires junctions was made by (Fu et al. 2008) and (Motoyama et al. 2007).

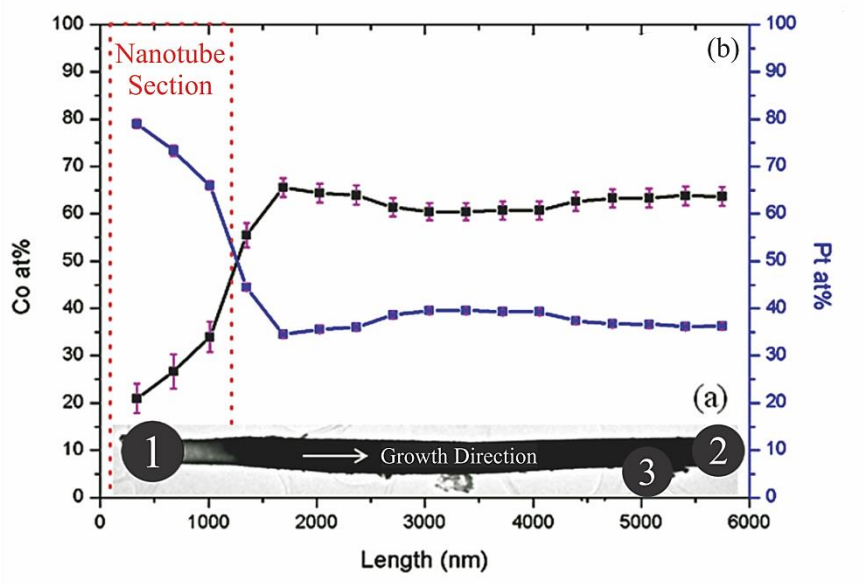


Fig. 3 (**a**) TEM micrograph of an individual Co-Pt nanowire. (**b**) Graph showing the EDXS composition analysis along the growth direction of the single Co-Pt nanowire. The marked circles 1, 2, and 3 in **Fig. 3a** are where additional TEM analyse were made. These circles will be discussed in later sections.

In order to trace the changes in the Co/Pt composition ratio, a TEM-EDXS analysis was performed along the growth direction of the wire as shown in Fig. 3b. At the start of the wire, the overall composition is Pt rich ($CoPt_3$) containing a Co content ≈ 20 at. %, similar to what we had observed in Co-Pt nanotubes (Rožman K Ž et al. 2009), while along the growth direction the Co/Pt ratio gradually increases until after the first 1 µm reaches the equilibrium composition of ≈ $Co_{65\pm3}Pt_{35\pm3}$. The observed ratio is then preserved to the end of the wire growth, without a significant deviation from the equilibrium composition.

In Fig. 4a the SAED ring-pattern recorded from the bottom part of the wire (circle 1 in Fig. 3a) shows that the tube section of the wire is composed of randomly oriented grains. The crystal structure of the tube section was determined by comparing the experimental SAED pattern with a simulation, based on $CoPt_3$ fcc (a=0.385 nm) that matches perfectly, as shown in Fig. 4a. This indicates that the nanowire growth process starts at several nucleation sites. No traces of hcp phase in this region of the nanowire are observed. Fig. 4b shows the HRTEM image after filtering representing elongated-shaped grains with an average size of ≈10 nm, which is consistent with the XRD measurements.

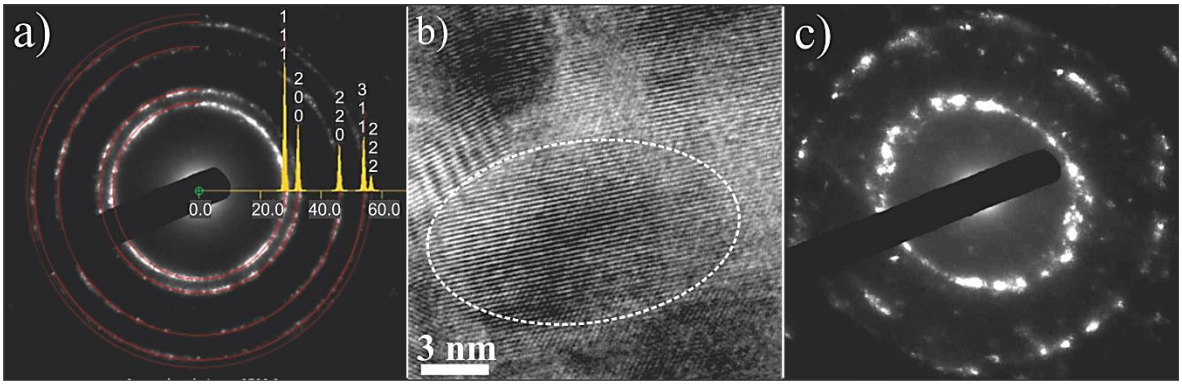


Fig. 4 (**a**) SAED ring pattern recorded from the bottom part (circle 1 in **Fig. 3a**) of the nanowire compared with the $CoPt_3$ fcc simulation. (**b**) HRTEM image taken at the bottom part of the nanowire shows an average grain size of ≈10 nm. (**c**) SAED pattern recorded from the end-of-growth of the wire (circle 2 in **Fig. 3a**), showing a combination of hcp and fcc phases.

The upper part of the Co-Pt nanowire is much thicker, and so not transparent for electrons. Therefore, the SAED patterns were taken from those areas of the wire where the specimen was sufficiently thin (circle 2 and 3 in Fig. 3a). The SAED pattern taken from the end-of-growth of the wire (circle 2 in Fig. 3a), shown in Fig. 4c, consists of sharp, partially interrupted rings and isolated arcs, resulting in elliptical elongation of the central ring. We believe that the elongation of the central ring could be the combined result of the preferred orientation of the crystallites in the sample and the presence of both hcp and fcc phases. To verify the possible presence of both phases we used a rotational averaging (RA) procedure on SAED pattern shown in Fig. 4c. In RA the intensities on the SAED micrograph are evenly distributed by rotating the diffraction pattern around the central dot (Mitchell 2008). The resulting image (inverted contrast) after the RA procedure can be seen in Fig. 5a (right half). The intensity profile over the most intense rings (marked with a square in Fig. 5a) is shown in Fig. 5b. From the intensity profile we can see that the SAED pattern is composed of three intensity peaks instead of just two, as would be expected for the fcc Co-Pt (see Fig. 4a). To correlate these peaks with the possible hcp and fcc mixture, we simulated SAED patterns for the CoPt fcc phase with a lattice parameter a=0.374 nm (ICSD #624782) and for hcp phase with lattice parameters a=0.257 nm and c=0.419 nm (ICSD #102626), as shown in Fig. 5c. Both phases were calculated together in a 50:50 ratio to produce the simulated SAED pattern of a mixture of two crystallographically un-related phases, as shown in Fig. 5c. The intensity profile over such a produced SAED pattern indeed showed very similar patterns made with three distinct peaks that perfectly match with the experimental data, as shown in Fig. 5b. This indicates that the upper part of the nanowire consists of intermixture of fcc and hcp phase. Such coexistence of the fcc and hcp phases in the Co-Pt system was also reported by other authors for similar chemical compositions (Eagleton et al. 2005; Aboaf et al. 1983; Wang et al. 2010; Ohtake et al. 2013). The SAED pattern analysis confirmed and explained the XRD data, showing the disordered growth of the fcc phase during the nucleation of the nanowire, followed by a intermixture of the hcp and fcc phases.

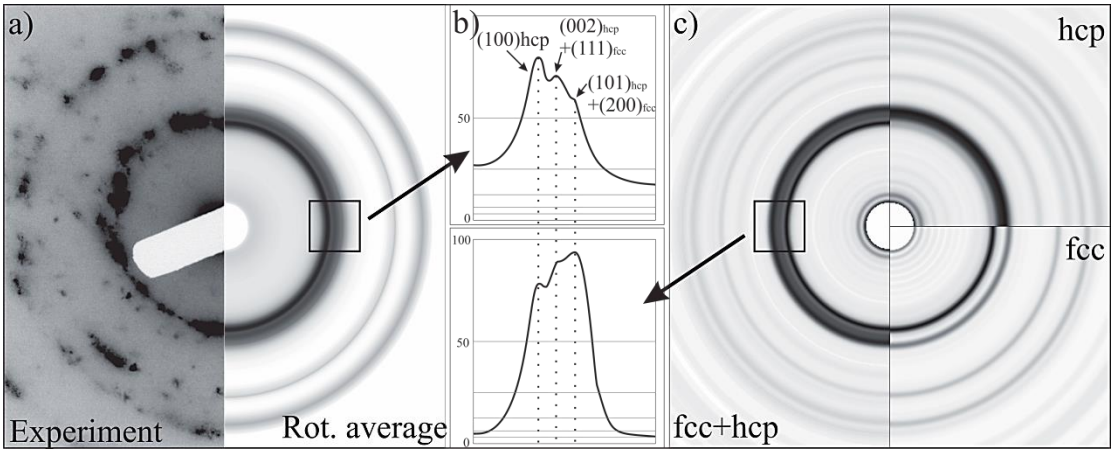


Fig. 5 (**a**) Experimental SAED pattern in inverted contrast recorded over the nanowire section (circle 2 in **Fig. 3a**) and rotational average of the same SAED pattern (right half). (**b**) (Top) Intensity profile over the diffraction rings of experimental SAED pattern (squared area) and compared to the same area of intensity profile over simulated SAED (bottom). (**c**) Simulation of diffraction rings of: CoPt fcc, Co-Pt hcp and fcc+hcp intermixture in a 50:50 ratio.

Further analyses were made for the relative orientation of the crystallites with the help of single crystal diffraction simulations. In Fig. 6a SAED pattern, recorded over the circle 3 in Fig. 3a, shows enhanced diffraction spots indicate a preferential orientation of the grains, contrary to the random distribution of the grains as evidenced by the diffraction ring in Fig. 4a. The diffraction spots of the fcc phase are aligned with the diffraction spots of the hcp phase, as shown in Fig. 6a. This indicates that the possible arrangement of both phases would be such that the $[00\bar{1}]$ of the hcp and the [111] of the fcc phase are pointing perpendicular to the nanowire axis and most probably rotate along the circumference of the nanowire. From the crystallographic relation between hcp and fcc phases, the contact-plane between the crystallites was deduced to be $(110)_{hcp} \parallel (02\bar{2})_{fcc}$, such arrangement is possible due to similar atomic arrangements and interatomic distances with misfit of 2 % in the contact planes as can be seen in Fig. 6b.

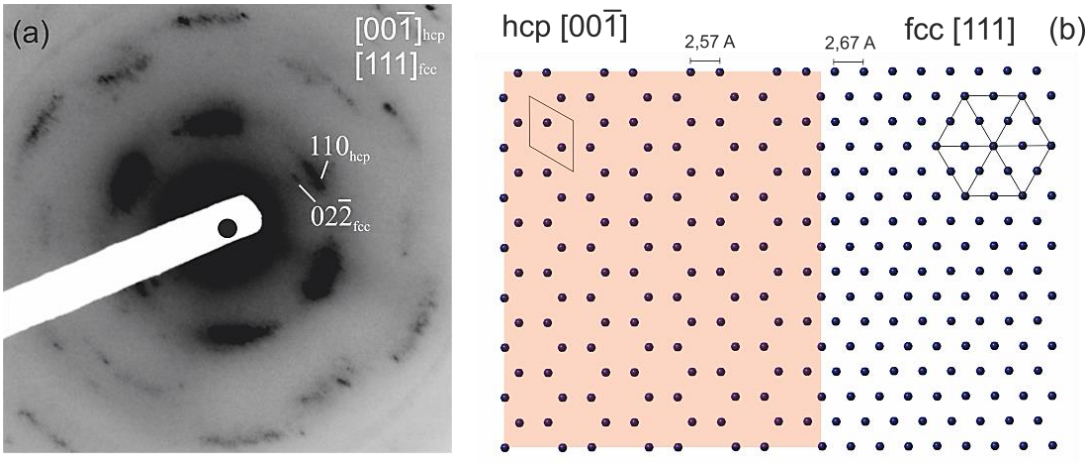


Fig. 6 (**a**) Experimental SAED pattern (marked circle 3 in **Fig 3a**) with index planes. (**b**) The reconstruction of the atomic structures for fcc and hcp arrangements when zone axis is along $[00\bar{1}]_{hcp}$ and $[111]_{fcc}$.

The detailed TEM analysis allowed us to understand the formation mechanism of Co-Pt nanowires in the AAO membrane. The electrodeposition of polycrystalline nanowires occur due to the coalescence nucleation process

proposed by (Tian et al. 2003) into the nanopores of the AAO membrane. Co and Pt are high melting point metals $T_{m,Co}$≈1495 ^{o}C and $T_{m,Pt}$ ≈1768 ^{o}C, respectively, and have high binding energies favouring the aggregation of atoms into small 3D clusters. The diffusion of electrodeposited atoms along the surface is restricted due to the high cohesive energy of these metals, resulting in the nucleation, growth and coalescence of many 3D grains during deposition, thereby forming the Co-Pt polycrystalline nanowires with small grain size (≈10 nm). Furthermore, these small grains start to align themselves to achieve textured structure due to the small volume and rigid walls of the AAO membranes (Florian et al. 2007). It is well known that smaller is the lateral diameter of the pores sooner the aspect ratio for the textured structure is reached (Florian et al. 2007). In our case after the first 1 μm of wire growth, two principal phenomena happen simultaneously: (1) the composition becomes Co rich to accommodate fcc and hcp solid solution in the nanowires and (2) the aspect ratio increases and so the surface energy increases. The preferred crystallographic orientation follows the tendency of minimization of the surface energy during the electrodeposition process. The preferred $[111]_{fcc}$ and $[00\bar{1}]_{hcp}$ crystal planes perpendicular to the axis of the nanowire correspond to the lowest energy configurations. Furthermore, similar interatomic distances in the hcp and fcc phases with misfit of 2% in the observed orientation $(110)_{hcp} \parallel (02\bar{2})_{fcc}$ are the driving force that allows epitaxial overgrowing of the hcp and fcc phases.

Magnetic characterization

The room temperature hysteresis loops of the as-deposited Co-Pt nanowire arrays when the field was applied parallel (∥) and perpendicular (⊥) to the axis of the wires is shown in Fig. 7. The squareness ($SQ=M_R/M_s$) values of 0.11 and 0.3 respectively were measured for the parallel and the perpendicular field directions. Low SQ appears to be common to all arrays, obtained using commercial alumina template (Ciureanu et al. 2005). A coercivity of about ≈44.3 kA/m was observed for both field directions for Co-Pt nanowire arrays. The coercivity and SQ values are close for both field directions indicating that the easy axis of the magnetocrystalline anisotropy is not parallel to that of the shape anisotropy. The shape of the hysteresis curves shows that the easy magnetization axis is perpendicular to nanowire long axis. The alignment of easy axis can be specified by the sign of ΔH_s, where $\Delta H_s = H_s^{per} - H_s^{para}$ (Ciureanu et al. 2005). Here H_s^{para} is the saturation field when the magnetic field is applied parallel to the nanowire axis and H_s^{per} is the saturation field when the magnetic field is applied perpendicular to the nanowire axis. The negative sign of ΔH_s indicates the easy axis orientation perpendicular to nanowire axis and vice versa. A value of ΔH_s ≈ -200 kA/m is obtained from Fig. 7 for Co-Pt nanowire arrays representing perpendicular easy magnetization axis.

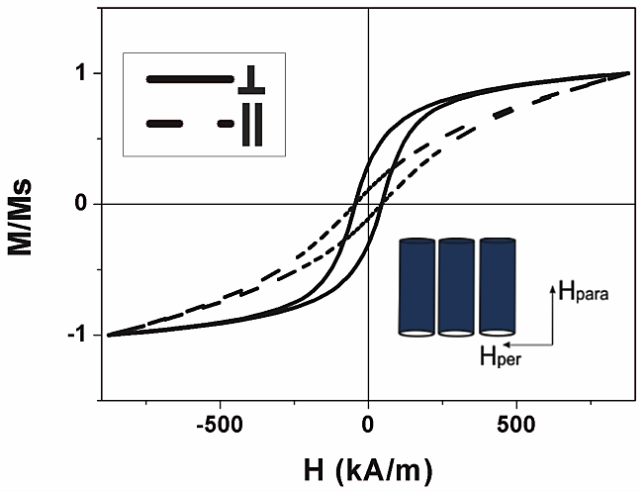


Fig. 7 Hysteresis loops of the Co-Pt nanowire arrays when field was applied parallel (dotted curve) and perpendicular (solid curve) to the long axis of the wire. (Inset) schematic view of the applied field direction w.r.t. the

nanowire's axis.

This behaviour can be explained by taking into consideration all the anisotropies present in the nanowire arrays. The main contributions to the effective anisotropy field H_{eff} are the shape anisotropy, the dipolar interactions between the nanowires, and the magnetocrystalline anisotropy (Escrig et al. 2007). The shape anisotropy for the case of infinitely long nanowires, takes the form $2\pi M_s$. The saturation magnetization $\mu_o M_s$ (≈1.15 T) for Co-Pt nanowires examined in this article was calculated by (Mallet et al. 2004) for similar composition. Dipolar interactions in a densely packed nanowire arrays play a key role and can even govern the magnetic properties of the entire ensemble in some cases (Vázquez et al. 2005; Carignan et al. 2007; Raposo et al. 2000; Sorop et al. 2004). Due to the high filling factor (almost 100%) in our case, where a small distance separates the nanowires (≈360 nm), large dipolar interactions between nanowires can be expected. First, we take a magnetostatic anisotropy H_{ms} by considering only the contribution of the shape anisotropy and the dipolar interactions between the nanowires (De La Torre Medina et al. 2009; Netzelmann 1990; Encinas-Oropesa et al. 2001)

$$H_{ms} = 2\pi Ms(1 - 3P) \quad \ldots(1)$$

where packing factor-P $= \frac{\pi}{2\sqrt{3}}(\frac{wire\ diameter}{interwire\ distance})^2$ (G. Kartopu et al. 2011) and M_s respectively are the membrane-packing factor and saturation magnetization. This model yields a demagnetizing factor parallel to the axis of the wire equal to the packing factor (P) of the membrane and a factor equal to $(1 - P)/2$ in the perpendicular direction (Dahmane et al. 2006; Encinas-Oropesa et al. 2001). Therefore, with a packing factor of 35% the demagnetization factor in the direction parallel to the nanowire is 0.35, whereas in the perpendicular direction it is 0.32, indicating the parallel and perpendicular curves in Fig. 7 should be very similar. The observed disagreement might be attributed to the additional anisotropy, i.e. the magnetocrystalline anisotropy which plays a significant role in modifying the hysteresis loop in both field directions. A similar phenomenon was reported by (Forster et al. 2002), they concluded that it is important to take into consideration the specific arrangement of the magnetocrystalline anisotropy in the nanowires. Thus, the orientation of magnetocrystalline anisotropy easy axis with respect to nanowire axis greatly influence the overall magnetic behaviour of the nanowires, therefore we have to take into consideration the magnetocrystalline anisotropy contribution into effective anisotropy H_{eff} (De La Torre Medina et al. 2009; Vega et al. 2012),

$$H_{eff} = H_{ms} - H_{mca} = 2\pi Ms(1 - 3P) - \frac{1}{2} < H_{mca} > \quad \ldots \quad (2)$$

According to the literature for Co-Pt system the magnetocrystalline anisotropy easy axis is along $[111]_{fcc}$ for fcc and along $[00\bar{1}]_{hcp}$ for hcp phases, respectively (Razee et al. 1997; Razee et al. 2001). Since the observed texturing of the crystallites in Co-Pt nanowires is in the $[111]_{fcc}$ and $[00\bar{1}]_{hcp}$ direction which is found to be pointing perpendicular to the nanowires long axis, thus the magnetocrystalline anisotropy is the largest perpendicular to the wire long axis. Recently, Ivanov et al (Yu et al. 2013a) simulated that when the angle of the magnetocrystalline anisotropy easy axis with the nanowire axis is larger than 70^o the magnetocrystalline anisotropy competes with shape anisotropy. Furthermore, (Zana et al. 2004) have shown that the magnetocrystalline anisotropy of Co-Pt hcp phase can be stronger than shape anisotropy and can significantly modify the magnetization easy axis orientation. Thus large contribution from magnetocrystalline anisotropy results in perpendicular magnetization axis for Co-Pt nanowire arrays. Our observation is in accordance with many other reports on different material nanowire arrays consisting of intermixture of fcc and hcp structure (De La Torre Medina et al. 2009; Vega et al. 2012; Rosa et al. 2012). The coercivity values (44.3 kA/m) were found to be higher than those for fcc Co-Pt (Shamaila et al. 2008) and closer to those obtained for Co-Pt nanowires with the hcp structure (Cortés et al. 2013) for similar nanowire dimensions indicating that probably hcp is the dominant phase in our Co-Pt nanowires. Although, (Shamaila et al. 2008) also found perpendicular magnetization axis for Co-Pt nanowire arrays (fcc structure) with similar dimension but they

concluded this orientation is due to high magnetostatic interactions between the nanowires. This might be possible because the interwire distance between the nanowires in their case is D=250 nm which is 100 nm smaller than our case. Small separation between the nanowires can significantly modify the hysteresis loops (Vázquez et al. 2005; Carignan et al. 2007).

Magnetization reversal mechanism for Co-Pt nanowire arrays

It is well known that in magnetic nanowires (as well as nanotubes) three distinct magnetization reversal modes (Coherent C, Vortex ,V and Transverse T mode) are possible, details can be find here (Lavin et al. 2009a; Lavin et al. 2010; Lavín et al. 2012; Escrig et al. 2008). It was pointed out by (Landeros et al. 2007) the coherent reversal mode is only favourable for very short magnetic nanostructures where the length of the nanostructure is comparable with domain wall width. The measurement of the angular dependence of the coercivity (ADC) $H_c(\theta)$ elucidates the mechanisms of magnetization reversal in nanostructures. The $H_c(\theta)$ in vortex reversal mode exhibits a monotonic increase of the coercivity field w.r.t. the angle at which field is applied (upto $\theta = 90^o$) and vice versa for the transverse reversal mode. Fig. 8 (solid dots) shows the experimental results of $H_c(\theta)$ for Co-Pt nanowire arrays. The $H_c(\theta)$ variation with increasing applied field angle is found to be non-monotonic, it increases from 0 to 20º and then decreases in the range $20º < \theta < 90º$. Thus, indicating a crossover in the mechanism of magnetization reversal depending on the angle of the applied field.

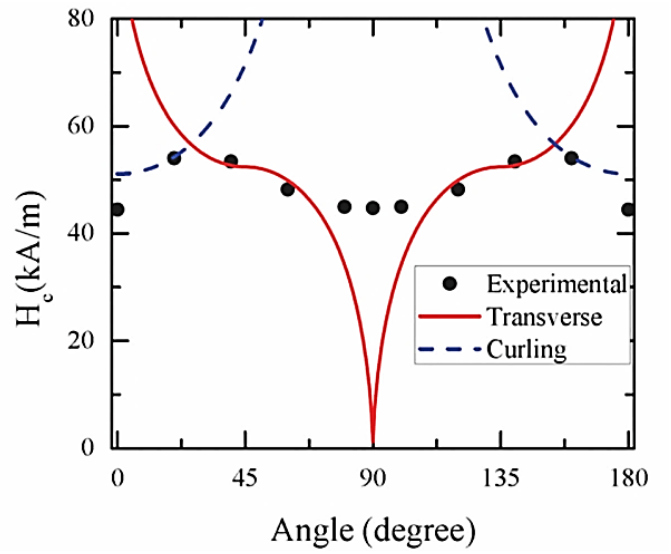


Fig. 8 Comparison between experiment and analytical calculations for the ADC for the Co-Pt nanowire arrays. Solid dots correspond to the experimental data while the lines correspond to the analytical calculations. Dotted line to the vortex (curling) reversal mode and solid line to the transverse reversal mode.

(Lavin et al. 2010) performed $H_c(\theta)$ measurements on Co nanowire arrays and found a non-monotonic behaviour which they explained by a transition from one reversal mode to another. Similar observation was also done in magnetic nanotubes by (Allende et al. 2008; Albrecht et al. 2011). We analysed our results for the $H_c(\theta)$ by comparing them with analytical models (Lavín et al. 2012; Lavin et al. 2009b) to investigate the magnetization reversal processes of Co-Pt nanowire arrays. The parameters used for the analytical calculations are the geometric parameters (length~5 µm and diameter~250 nm), the saturation magnetization, $\mu_o M_s$ =(≈1.15 T) at room temperature, exchange constant $A=1.6 \times 10^{-11}$ J/m and an effective anisotropy constant of $K_{eff}= 2.6 \times 10^4$ J/m^3 perpendicular to nanowire long axis. It is important to mention that K_{eff} was used as free variable to fit the experimental data with analytical model to include any variation in the composition, morphology and the size of the

nanowires, and the calculated K_{eff} is very close to Co-Pt system. The dotted line in Fig. 8 is a result of the analytical model for $H_c(\theta)$, calculated with the vortex mode, and the solid line is for transverse mode. From Fig. 8 we observed that the theoretical curves match very well with the experimental data. Thus from this good agreement, we can identify for the Co-Pt nanowire arrays there is a transition from vortex to transverse reversal mode when the applied field angle is around $\theta=30^o$. It is worth mentioning that the crossing point between the vortex and transverse mode in Co-Pt nanowires is same for the experimental data and analytical results, and there is a good agreement between the experimental and calculated coercivity values. The only differences between the experiments and the theoretical results occur for angles near $\theta=90^o$. The difference at higher angles might be due to the small angle variation during experiment which can give rise to considerable differences in the coercivity. Moreover, it should be noted that the analytical model used for the calculations does not consider the dipolar interactions between the nanowires that might also be the reason of this difference.

In order to understand the origin of this crossover from vortex to transverse mode in Co-Pt nanowire arrays, one has to look at the morphology of the nanowires. TEM analysis revealed that the nanowires consist of a nanotube segment at the bottom with 1 μm length which is followed by the formation of full cylinder. The detailed study of magnetization reversal for Co-Pt cylindrical nanostructures with tube-wire morphology was presented elsewhere (Arshad et al. 2014). For intermediate length (presented in this study), the tube-segment always reverse its magnetization through a vortex, whereas nanowire-segment reversed through transverse reversal mode. Thus, we can safely attribute this crossover of reversal mode in Co-Pt nanowires with this dimension to the different morphologies in the nanowires. Our results are in good agreement with the theoretical predictions of (Neumann et al. 2013) and (Salazar-Aravena et al. 2013) for similar morphologies. (Shamaila et al. 2008) and (Gao et al. 2006) investigated the angular dependence of the coercivity in Co-Pt nanowire arrays with fcc crystal structure and found out the vortex reversal mode perceived in similar dimensions. Despite the fact that they also explained angular dependence of the coercivity, it is just a qualitative explanation and not the quantitative understanding such as the one we proposed in this report. Here we would like to emphasize the important role played by the crystalline structure and its orientation, as it significantly affects the magnetization reversal mode as also proposed by (Yu et al. 2013a).

Magnetic domain configuration in individual Co-Pt nanowires

Fig. 9 a-c shows the MFM measurement on individual Co-Pt nanowires at remanence state on Si substrate with similar diameter and length changes between $6 > L > 4$ μm (length range investigated in this study). The variation in the diameter between these nanowires is below 10%, in the range of standard deviation of pore size distribution of the template. There is a slight difference in diameter along the length of each nanowire which is attributed to the nature of the template. All the MFM images for each length were taken at a constant scan height of 60 nm. Difference in the substrate contrast is due to the different MFM tips with small variation in resonance frequency, changing the oscillation amplitude, thus the interaction between tip and substrate. This small difference in resonance frequency doesn't influence alot on the contrast from the nanowires due to strong coupling. All nanowires in Fig. 9 a-c arguably show a periodic dark and bright MFM contrast along their lengths. For the sake of simplicity here we have ignored the effect of nanotube segment in the nanowires (see TEM analysis).

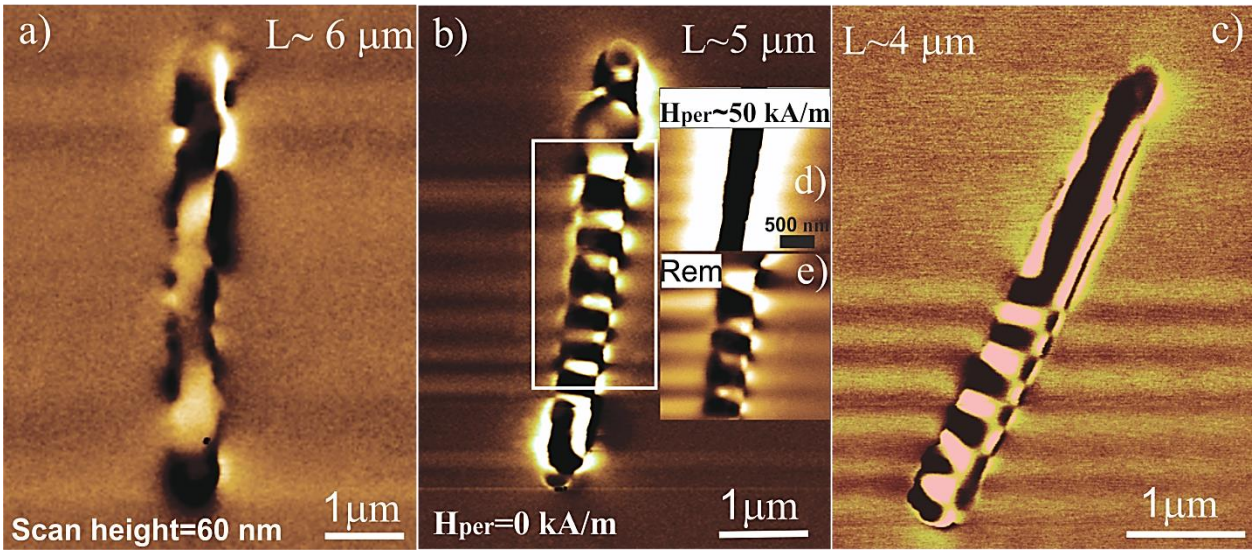


Fig. 9 (a)-(c) The experimental MFM images of individual Co-Pt nanowires with diameter 250 nm and length 6 > L > 4 μm. (**d**) Saturation magnetization state of an individual Co-Pt nanowire at an applied field of $H_{per} \approx$ 50 kA/m. (**e**) Remanent magnetization of an individual Co-Pt nanowire.

The observed MFM contrast can be well understood if one considers the magnetization modulates along the length of the nanowires (Y. Henry et al. 2001; Zuwei Liu et al. 2008; Kristof M Lebecki and Donahue 2010). The average period of the modulation (between two dark or bright regions) for all lengths of the nanowires is plotted in Fig. 10a. For nanowires with length 4 and 5 μm, modulation was found to be w ≈ 350-450 nm while for nanowire with length 6 μm, modulation is much larger W ≈ 1300 nm. It is important to note that the modulation is consistent along the length for 5 μm nanowire which can be attributed to a delicate balance between the involved anisotropies. From theoretical point of view (Gerd Bergmann et al. 2008; Fert and Piraux 1999), this magnetization modulation originates from the competition between the magnetocrystalline anisotropy and the shape anisotropy in the wire. In many cases, a MFM image consists of complementary dark and bright contrast spanning the two ends of the nanowire was observed (Y. Henry et al. 2001), suggesting that the magnetization is along the wire axis, thus shape anisotropy is predominant. For our case where the magnetocrystalline anisotropy is significantly larger especially due to the preferential orientation of the hcp phase, pointing perpendicular to the nanowire axis, the magnetocrystalline anisotropy tends to align the magnetization in the plane perpendicular to the axis of the nanowire, whereas the shape anisotropy tends to align them parallel to the wire axis. As a result of this competition, the magnetization deviates from the axis of the wire and modulates within the plane spanned by the axis of the wire and the vertical axis for energy minimization. This problem was investigated theoretically by many authors (Gerd Bergmann et al. 2008; Erickson and Mills 2009; Kristof M Lebecki and Donahue 2010). In (Gerd Bergmann et al. 2008), it is found in the thin wire limit that the angle between the magnetization and the wire axis is modulated sinusoidally along the length of the wire axis to lower the magnetic energy. Whereas (Kristof M Lebecki and Donahue 2010) performed micromagnetic simulations and found even lower energy state with vortices along the length of the nanowires, they call it *z*-vortex and *y*-vortex. Either of the mentioned vortex state or both can prevail in the nanowire depending on the material and geometrical parameters. As the diameter of our nanowires is much larger (250 nm) than exchange length we believe that the thin wire limit does not hold. However, existence of *y*-vortex and *z*-vortex explained by (Kristof M Lebecki and Donahue 2010) might be relevant to our case. Both states are energetically quite close but the MFM contrast from both vortices states is slightly different. In *y*-vortices state the periodic MFM contrast is along the length of the nanowires whereas in *z*-vortices state periodic contrast can be along

the radial side of the nanowires, similar to what we have observed in our nanowires as shown in Fig.9 a-c. However, *y*-vortices state can be compared with so called partial Landau-Kittel stripe domain structure found in thin films (Kronmuller and Fahnle 2003). The period of modulation (w) for the case of nanowires with *y*-vortices state can be given by following expression (Kristof M Lebecki and Donahue 2010)

$$w(\mathrm{r}) = 2\sqrt{\frac{4\sqrt{A\,\mathrm{K}_{eff}}\,2r}{\frac{(\mathrm{f}(\alpha)4\,\mu_o \mathrm{M}_s^2)}{\pi^3} + 2\,\alpha^2 \mathrm{K}_{eff}}} \quad \ldots\ldots(3)$$

Where exchange constant A=1.6 x 10^{-11} J/m, 2r= 250 nm diameter of the nanowire, $\mu_o M_s$ =≈1.15 T saturation magnetization, α=0.34 normalized surface charge size (can have value between 0.34 and 0.4) depends on the radius of the nanowires, value used best fit in our case, f (α)=0.292 is related to an infinite sum, see Eq. 9.16 in (Kronmuller and Fahnle 2003), effective anisotropy constant of K_{eff}= 2.6 x 10^4 J/m^3 which we have calculated from angular dependence of the measurement. The period of the modulation was calculated to be ~350 nm, which is very close to our experimental values for nanowires with length 4 and 5 μm as shown in Fig.10 (a). However, much larger periodicity in nanowire with length of 6 μm cannot be explained by the periodic *y*-vortices states, it might be consistent with *z*-vortices state mixed with complex structure as was observed by (Yu et al. 2013b). Nanowire with length 4 μm also showed an elongated modulation in the upper part of the nanowire which can also be attributed to the existence of *z*-vortices state in this part. In TEM analysis it was found that the possible arrangement of the crystallites in the nanowires is along the circumference of the cylinder which can result in accumulation of surface charges in such a way that vortex-like state is most favourable. The schematic of *y*-vortices state is presented in Fig.10b-c. Fig.10b should not be misinterpreted with sinusoidal state, trough and crest here is showing the accumulation of surface charges corresponding to the magnetization modulation along the length of the nanowire. We believe that we have a model system, which can describe the theoretical work of (Kristof M Lebecki and Donahue 2010). This vortex-like configuration along the length of the nanowire has also been reported in simulations of amorphous microwires with circular anisotropy (Stoleriu et al. 2012). Experimentally (Yu et al. 2013b) has reported rather complex vortex structure along the length of the nanowire. Further work is needed to fully understand this magnetic domain pattern in the nanowires, in experimental point of view the focus must be based on the complex microstructure of the nanowires, including important factors such as the pinning from the grain boundaries between the fcc and hcp crystallites.

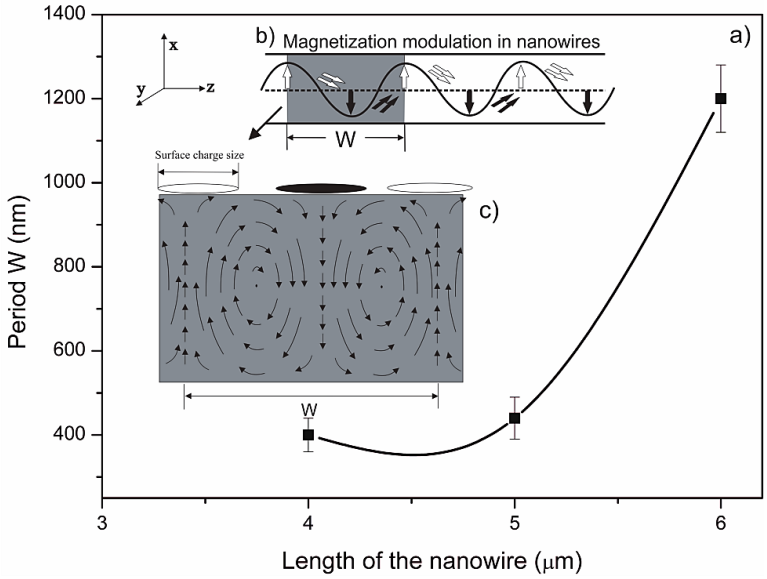


Fig. 10 (a) Graph showing the period of modulation for different nanowire lengths **(b)** Schematic showing the magnetization (indicated by black and white arrows) modulates along the wire axis. **(c)** Schematic in xz-cross section of a nanowire with y-vortices state.

From the literature it was found that, some authors (Y. Henry et al. 2001) couldn't re-observe this domain pattern after the application of external magnetic field and some could (Zuwei Liu et al. 2008). For the completeness MFM images were taken for different values of the external magnetic field perpendicular to the axis of the wire. When the absolute value of the applied magnetic field reaches a value high enough (H_{per}≈ 50 kA/m) to overcome all the anisotropies, the magnetization of the nanowire switches to its saturation state, as shown in Fig. 9d. We estimated the saturation field (H_o) by the analytical expression $H_o = \frac{2K_{eff}}{M_s}$ (B D Cullity and Graham 2009), where K_{eff} =2.6 x 10^4 J/m^3 (from analytical calculation) and $\mu_o M_s$ =≈1.15 T saturation magnetization, the H_o was calculated to be 45 kA/m, which is very close to the experimental value of the saturation field (≈50 kA/m) for a single Co-Pt nanowire. Therefore, it can be safely concluded that the effective anisotropy constant (K_{eff}) is accurately estimated from the analytical calculations. Finally, when the applied field was reduced from saturation magnetization to zero, the magnetization gradually reduced to its most energetically stable state as shown in the Fig. 9e.

Conclusion

We have performed a detailed structural and magnetic study on arrays and individual Co-Pt nanowires synthesized in AAO template via electrodeposition with diameter of 250 nm and length of 4-6 μm. During electrodeposition nanowires were found to nucleate as nanotubes due to the Au nanoparticles inclusion (≈1 μm) into the pores of the AAO template. The crystal structure study revealed that the nanowires mostly consist of an intermixture of *hcp* and *fcc* phases. A detailed TEM investigation showed that the nanowires have a double texturing in the $[111]_{fcc}$+$[00\bar{1}]_{hcp}$ directions and the contact plane between both phases is found to be $(110)_{hcp} \parallel (02\bar{2})_{fcc}$ which is attributed to similar atomic arrangements and interatomic distances with misfit of ≈2%. The c-axis of the *hcp* and [111] of the *fcc* phase was found to textured perpendicular to the long axis of the nanowire and strongly influence the effective anisotropy of Co-Pt nanowires. Thus, the perpendicular easy magnetization axis is attributed to the strong contribution from magnetocrystalline anisotropy in nanowires. Based on good agreement between the angular dependence of the coercivity and the analytical calculations, a transition from vortex to transverse reversal mode was identified around $\theta=30^o$, which we believe is due to tube-wire morphology of the nanowires. Fitting of the experiment to the analytical

calculations revealed a perpendicular *effective* anisotropy constant (K_{eff}= 2.6 x 10^4 J/m^3) in nanowires which further used to investigate the magnetic behaviour of an individual nanowires. Furthermore, systematic MFM measurements on individual Co-Pt nanowires in length range 4 < L < 6 μm revealed a periodic domain configurations along the length of the nanowires. Combined results with microstructural study revealed that such domain configurations indeed originate from the competition between the shape anisotropy and the magnetocrystalline anisotropy. We also found that only nanowire with length ≈5 μm show consistent periodic domain structure along the length of the nanowires which can be attributed to a delicate balance between magnetocrystalline anisotropy and shape anisotropy. By comparing the experimental results with micromagnetic simulations (from literature), we believe such periodic domain structure in the nanowires is due to *y*-vortices state which is mixed with *z*-vortices state in some cases. We are currently studying the micromagnetic simulations through our knowledge about crystallographic orientations in Co-Pt nanowires to fully explain and understand this phenomenon. Finally, the nanowire was found to return to its same initial magnetization modulation after reducing the external saturation magnetic field (50 kA/m) perpendicular to the axis of the nanowire. Our results provide a deep insight in the magnetic properties of Co-Pt nanowires with strong magnetocrystalline anisotropy and thus make them useful for possible applications in nanoelectronics.

Acknowledgements

This project was funded by the Slovenian Research Agency (ARRS) under project number PR-04442. In Chile, we acknowledged support from FONDECYT under project 1110784, Grant ICM P10-061-F by Fondo de Innovación para la Competitividad-MINECON and Financiamiento Basal para Centros Científicos y Tecnológicos de Excelencia, under project FB0807. CONICYT Ph.D. Program Fellowships is also acknowledged.

References

Aboaf JA, Herd SR, Klokholm E (1983) Magnetic properties and structure of cobalt-platinum thin films. IEEE Trans Magn 19:1514-1519

Albrecht O, Zierold R, Allende S, Escrig J, Patzig C, Rauschenbach B, Nielsch K, Gorlitz D (2011) Experimental evidence for an angular dependent transition of magnetization reversal modes in magnetic nanotubes. J Appl Phys 109:093910-093915

Allende S, Escrig J, Altbir D, Salcedo E, Bahiana M (2008) Angular dependence of the transverse and vortex modesin magnetic nanotubes. EPJ B 66:37-40

Arshad MS, Pečko D, Šturm S, Escrig J, Komelj M, McGuiness PJ, Kobe S, Rožman KŽ (2014) Angular dependence of the coercivity in electrodeposited Co-Pt nanostructures with a tube-wire morphology IEEE Transactions on Magnetics DOI 101109/TMAG:20142320911 Accepted for Publication

B D Cullity, Graham CD (2009) Introduction to Magnetic Materials. Second Ed. edn. John Wiley & Sons, Inc., Hoboken, New Jersey

Bauer LA, Birenbaum NS, Meyer GJ (2004) Biological applications of high aspect ratio nanoparticles. J Mater Chem 14:517-526

Bolzoni F, Leccabue F, Panizzieri R, Pareti L (1984) Magnetocrystalline anisotropy and phase transformation in Co-Pt alloy. IEEE Trans Magn 20:1625-1627

Bowling RJ, Packard RT, McCreery RL (1989) Activation of highly ordered pyrolytic graphite for heterogeneous electron transfer: relationship between electrochemical performance and carbon microstructure. J Am Chem Soc 111:1217-1223

Bran C, Butenko AB, Kiselev NS, Wolff U, Schultz L, Hellwig O, Rößler UK, Bogdanov AN, Neu V (2009) Evolution of stripe and bubble domains in antiferromagnetically coupled $[(Co/Pt)_8/Co/Ru]_{18}$ multilayers. Phys Rev B 79:024430-024434

Bran C, Ivanov YP, Trabada DG, Tomkowicz J, del Real RP, Chubykalo-Fesenko O, Vazquez M (2013) Structural Dependence of Magnetic Properties in Co-Based Nanowires: Experiments and Micromagnetic Simulations. IEEE Trans Magn 49:4491-4497

Carignan L-P, Lacroix C, Ouimet A, Ciureanu M, Yelon A, Ménard D (2007) Magnetic anisotropy in arrays of Ni, CoFeB, and Ni/Cu nanowires. J Appl Phys 102:023905-023915

Cho JU, Wu J-H, Min JH, Ko SP, Soh JY, Liu QX, Kim YK (2006) Control of magnetic anisotropy of Co nanowires. J Magn Magn Mater 303:e281-e285

Ciureanu M, Beron F, Clime L, Ciureanu P, Yelon A, Ovari TA, Cochrane RW, Normandin F, Veres T (2005) Magnetic properties of electrodeposited CoFeB thin films and nanowire arrays. Electrochim Acta 50:4487-4497

Cortés M, Gómez E, Vallés E (2013) Electrochemical growth of CoPt nanowires of different aspect ratio and their magnetic properties. J Electroanal Chem 689:69-75

Cullity BD, Stock SR (2001) Elements of X-Ray Diffraction. 3rd Ed. edn. Prentice-Hall Inc. New Jersey,

Dahmane Y, Cagnon L, Voiron J, Pairis S, Bacia M, Ortega L, Benbrahim N, Kadri A (2006) Magnetic and structural properties of electrodeposited CoPt and FePt nanowires in nanoporous alumina templates. J Phys D: Appl Phys 39:4523-4528

De La Torre Medina J, Darques M, Piraux L, Encinas A (2009) Application of the anisotropy field distribution method to arrays of magnetic nanowires. J Appl Phys 105:023909-023918

Eagleton TS, Mallet J, Cheng X, Wang J, Chien C-L, Searson PC (2005) Electrodeposition of Co_xPt_{1-x} Thin Films. J Electrochem Soc 152:C27-C31

Encinas-Oropesa A, Demand M, Piraux L, Ebels U, Huynen I (2001) Effect of dipolar interactions on the ferromagnetic resonance properties in arrays of magnetic nanowires. J Appl Phys 89:3

Erickson RP, Mills aDL (2009) Theory of the undulating magnetic ground state of cylindrical cobalt nanowires. Phys Rev B 80:214410-214418

Escrig J, Altbir D, Jaafar M, Navas D, Asenjo A, Vázquez M (2007) Remanence of Ni nanowire arrays: Influence of size and labyrinth magnetic structure. Phys Rev B 75:184429-184434

Escrig J, Bachmann J, Jing J, Daub M, Altbir D, Nielsch K (2008) Crossover between two different magnetization reversal modes in arrays of iron oxide nanotubes. Phys Rev B 77:214421-214428

Fashen Li, Tao Wang, Ren L, Sun J (2004) Structure and magnetic properties of Co nanowires in self-assembled arrays. J Phys: Condens Matter 16:8053-8060

Fert A, Piraux L (1999) Magnetic nanowires. J Magn Magn Mater 200:338-358

Florian M, Joachim B, Shafqat K, Maria Eugenia Toimil M, Christina T, Hartmut F (2007) Preferred growth orientation of metallic fcc nanowires under direct and alternating electrodeposition conditions. Nanotechnology 18:135709-135716

Forster H, Schrefl T, Dittrich R, Suess D, Scholz W, Tsiantos V, Fidler J, Nielsch K, Hofmeister H, Kronmuller H, Fischer S (2002) Magnetization reversal in granular nanowires. IEEE Trans Magn 38:2580-2582

Fu J, Cherevko S, Chung C-H (2008) Electroplating of metal nanotubes and nanowires in a high aspect-ratio nanotemplate. Electrochem Commun 10:514-518

G. Kartopu, O. Yalc, K. L. Choy, R. Topkaya, S. Kazan, Akta B (2011) Size effects and origin of easy-axis in nickel nanowire arrays. J Appl Phys 109:033909-033901

Gao TR, Yin LF, Tian CS, Lu M, Sang H, Zhou SM (2006) Magnetic properties of Co–Pt alloy nanowire arrays in anodic alumina templates. J Magn Magn Mater 300:471-478

Gerd Bergmann, Jia G. Lu, Yaqi Tao, Thompson RS (2008) Frustrated Magnetization in Co nanowires: Competition between crystal anisotropy and demagnetization energy. Phys Rev B 77:054415-054420

Harp GR, Weller D, Rabedeau TA, Farrow RFC, Toney MF (1993) Magneto-optical Kerr spectroscopy of a new chemically ordered alloy: Co_3Pt. Phys Rev Lett 71:2493-2496

Hassel C, Brands M, Lo FY, Wieck AD, Dumpich G (2006) Resistance of a Single Domain Wall in $(Co/Pt)_7$ Multilayer Nanowires. Phys Rev Lett 97:226805-226810

Irshad MI, Ahmad F, Mohamed NM (2012) A review on nanowires as an alternative high density magnetic storage media. AIP Conf Proc 1482:625-632

Ivanov PY, Vivas LG, Asenjo A, Chuvilin A, Chubykalo-fesenko O, Vázquez M (2013) Magnetic structure of a single-crystal hcp electrodeposited cobalt nanowire. Europhys Lett 102:17009-17014

Khurshid H, Huang YH, Bonder MJ, Hadjipanayis GC (2009) Microstructural and magnetic properties of CoPt nanowires. J Magn Magn Mater 321:277-280

Kostevšek N, Rožman KŽ, Pečko D, Pihlar B, Kobe S (2014) A comparative study of the electrochemical deposition kinetics of iron-palladium alloys on a flat electrode and in a porous alumina template. Electrochim Acta 125:320-329

Kristof M Lebecki, Donahue MJ (2010) Comment on "Frustrated magnetization in Co nanowires: Competition between crystal anisotropy and demagnetization energy". Phys Rev B 82:096401-096401

Kronmuller H, Fahnle M (eds) (2003) Micromagnetism and the Microstructure of Ferromagnetic Solids. Cambridge University Press, Cambridge, UK

L.Sun, Y.Hao, C.L.Chien, Searson aPC (2005) Tuning the properties of magnetic nanowires. IBM Journal of Research and Developement 49:79 - 102

Landeros P, Allende S, Escrig J, Salcedo E, Altbir D, Vogel EE (2007) Reversal modes in magnetic nanotubes. Appl Phys Lett 90:102501-102503

Lavin R, Denardin JC, Escrig J, Altbir D (2009a) Angular dependence of magnetic properties in Ni nanowire arrays. J Appl Phys 106:103903-103901-103905

Lavin R, Denardin JC, Escrig J, Altbir D, Cortes A, Gomez H (2009b) Angular dependence of magnetic properties in Ni nanowire arrays. J Appl Phys 106:103903-103905

Lavin R, Denardin JC, Espejo AP, Cortes A, and Gomez H (2010) Magnetic properties of arrays of nanowires: Anisotropy, interactions, and reversal modes. J Appl Phys 107:09B504-509B507

Lavín R, Gallardo C, Palma JL, Escrig J, Denardin JC (2012) Angular dependence of the coercivity and remanence of ordered arrays of Co nanowires. J Magn Magn Mater 324:2360-2362

Mallet J, Yu-Zhang K, Chien C-L, Eagleton TS, Searson PC (2004) Fabrication and magnetic properties of fcc Co_xPt_{1-x} nanowires. Appl Phys Lett 84:3900-3902

Martin CR (1994) Nanomaterials: A Membrane-Based Synthetic Approach. Science 266:1961-1966

Martin CR (1996) Membrane-Based Synthesis of Nanomaterials. Chem Mater 8:1739-1746

Mitchell DRG (2008) DiffTools: Electron diffraction software tools for DigitalMicrograph™. Microsc Res Tech 71:588-593

Motoyama M, Fukunaka Y, Sakka T, Ogata YH (2007) Initial stages of electrodeposition of metal nanowires in nanoporous templates. Electrochim Acta 53:205-212

Netzelmann U (1990) Ferromagnetic resonance of particulate magnetic recording tapes. J Appl Phys 68:1800-1808

Neumann RF, Bahiana M, Vargas NM, Altbir D, Allende S, Görlitz D, Nielsch K (2013) Domain wall control in wire-tube nanoelements. Appl Phys Lett 102:202407-202412

Ning G, Hongjun W, Eui-Hyeok Y (2010) An experimental study on ferromagnetic nickel nanowires functionalized with antibodies for cell separation. Nanotechnology 21:105107-105115

Ohtake M, Suzuki D, Kirino F, Futamoto M (2013) Metastable Ordered Phase Formation in CoPt and Co_3Pt Alloy Thin Films Epitaxially Grown on Single-Crystal Substrates. IEICE Transactions on Electronics E96-C:1460-1468

Pan H, Liu B, Yi J, Poh C, Lim S, Ding J, Feng Y, Huan CHA, Lin J (2005) Growth of Single-Crystalline Ni and Co Nanowires via Electrochemical Deposition and Their Magnetic Properties. J Phys Chem B 109:3094-3098

Raposo V, Garcia JM, González JM, Vázquez M (2000) Long-range magnetostatic interactions in arrays of nanowires. J Magn Magn Mater 222:227-232

Razee SSA, Staunton JB, Ginatempo B, Bruno E, Pinski FJ (2001) Ab initio theoretical description of the dependence of magnetocrystalline anisotropy on both compositional order and lattice distortion in transition metal alloys. Phys Rev B 64:014411-014415

Razee SSA, Staunton JB, Pinski FJ (1997) First principles theory of magnetpcrystalline anisotropy of disordered alloys: Application to Cobalt Platinum. Phys Rev B 56:8082-8091

Rosa WO, Vivas LG, Pirota KR, Asenjo A, Vázquez M (2012) Influence of aspect ratio and anisotropy distribution in ordered CoNi nanowire arrays. J Magn Magn Mater 324:3679-3682

Rožman K Ž, Šturm S, McGuiness PJ, K aS (2009) Hard Magnetic Co-Pt-Based Nanotubes Produced via Direct Electroplating. IEEE Trans Magn 45:4413-4416

Salazar-Aravena D, Corona RM, Goerlitz D, Nielsch K, Escrig J (2013) Magnetic properties of multisegmented cylindrical nanoparticles with alternating magnetic wire and tube segments. J Magn Magn Mater 346:171-174

Sayama J, Shimatsu T, Nemoto H, Okamoto S, Kitakami O, Aoi H (2011) Temperature dependence of the magnetic properties of $L1_1$-type Co–Ni–Pt ordered alloy films for thermally assisted recording media. J Appl Phys 110:013918-013923

Schlörb H, Haehnel V, Khatri MS, Srivastav A, Kumar A, Schultz L, Fähler S (2010) Magnetic nanowires by electrodeposition within templates. Phys Status Solidi B 247:2364-2379

Shamaila S, Sharif R, Riaz S, Ma M, Khaleeq-ur-Rahman M, Han XF (2008) Magnetic and magnetization properties of electrodeposited fcc CoPt nanowire arrays. J Magn Magn Mater 320:1803-1809

Sorop T, Untiedt C, Luis F, Kröll M, Raşa M, de Jongh L (2003) Magnetization reversal of ferromagnetic nanowires studied by magnetic force microscopy. Phys Rev B 67:1-8

Sorop TG, Nielsch K, Göring P, Kröll M, Blau W, Wehrspohn RB, Gösele U, De Jongh LJ (2004) Study of the magnetic hysteresis in arrays of ferromagnetic Fe nanowires as a function of the template filling fraction. J Magn Magn Mater 272-276:1656-1657

Stoleriu L, Pinzaru C, Stancu A (2012) Micromagnetic analysis of switching and domain structure in amorphous metallic nanowires. Appl Phys Lett 100:122404-122408

Tian M, Wang J, Kurtz J, Mallouk TE, Chan MHW (2003) Electrochemical Growth of Single-Crystal Metal Nanowires via a Two-Dimensional Nucleation and Growth Mechanism. Nano Lett 3:919-923

Vázquez M, Pirota K, Torrejón J, Navas D, Hernández-Vélez M (2005) Magnetic behaviour of densely packed hexagonal arrays of Ni nanowires: Influence of geometric characteristics. J Magn Magn Mater 294:174-181

Vega V, Böhnert T, Martens S, Waleczek M, Montero-Moreno JM, Görlitz D, Prida VM, Nielsch K (2012) Tuning the magnetic anisotropy of Co-Ni nanowires: comparison between single nanowires and nanowire arrays in hard-anodic aluminum oxide membranes. Nanotechnology 23:465709-465709

Vivas LG, Escrig J, Trabada DG, Badini-Confalonieri GA, Vázquez M (2012a) Magnetic anisotropy in ordered textured Co nanowires. Appl Phys Lett 100:252405-252409

Vivas LG, Vazquez M, Escrig J, Allende S, Altbir D, Leitao DC, Araujo JP (2012b) Magnetic anisotropy in CoNi nanowire arrays: Analytical calculations and experiments. Phys Rev B 85:035439-035443

Wang N, Zhang J, Wang C, Shen TH (2010) A study on phase relations and texture of $Co_{1-x}Pt_x$ ($0.09<x<0.86$) nanowire arrays. Mater Lett 64:2530-2533

Xianghua H, Qingfang L, Jianbo W, Shiliang L, Yong R, Ronglin L, Fashen L (2009) Influence of crystal orientation on magnetic properties of hcp Co nanowire arrays. J Phys D: Appl Phys 42:095005-095009

Y. Henry, K. Ounadjela, L. Piraus, S. Dubois, J.-M. George, Duvail aJ-L (2001) Magnetic anisotropy and domain patterns in electrodeposited cobalt nanowires. EPJ B 20:35-44

Yang S, Zhu H, Yu D, Jin Z, Tang S, Du Y (2000) Preparation and magnetic property of Fe nanowire array. J Magn Magn Mater 222:97-100

Yu PI, Vázquez M, Chubykalo-Fesenko O (2013a) Magnetic reversal modes in cylindrical nanowires. J Phys D: Appl Phys 46:485001-485012

Yu PI, Vivas LG, Asenjo A, Chuvilin A, Chubykalo-fesenko O, Vázquez M (2013b) Magnetic structure of a single-crystal hcp electrodeposited cobalt nanowire. EPL (Europhysics Letters) 102:17009-17014

Zana I, Zangari G, Park J-W, Allen MG (2004) Electrodeposited Co–Pt micron-size magnets with strong perpendicular magnetic anisotropy for MEMS applications. J Magn Magn Mater 272–276:E1775-E1776

Zhang J, Jones GA, Shen TH, Donnelly SE, Li G (2007) Monocrystalline hexagonal-close-packed and polycrystalline face-centered-cubic Co nanowire arrays fabricated by pulse dc electrodeposition. J Appl Phys 101:054310-054315

Zhang J, Li W, Jones GA, Shen TH (2006) Composition-dependent structural and magnetic properties of $Co_{1-x}Pt_x$ ($0.09 <= x <= 0.86$) nanowire arrays. J Appl Phys 99:08Q502-503

Zuwei Liu, Pai-Chun Chang, Chia-Chi Chang, Evgeniy Galaktionov, Gerd Bergmann, Lu JG (2008) Shape Anisotropy and Magnetization Modulation in Hexagonal Cobalt Nanowires. Adv Funct Mater 18:1573-1578

Chapter 5

An Oblivious Growth Mechanism for High-Magnetic-Anisotropy hcp Co-Pt Nanowire Arrays: The Role of the Crystal Orientation in the Switching-Field Distribution and the Magnetic-Domain Configuration

In this Chapter, the article entitled "An oblivious growth mechanism for high-magnetic-anisotropy hcp Co-Pt nanowire arrays: the role of the crystal orientation in switching-field distribution and magnetic domain configuration", by Muhammad Shahid Arshad, Mariana P Proenca, Špela Trafela, Volker Neu, Ulrike Wolff, Sven Stienen, Manuel Vazquez, Spomenka Kobe, and K. Žužek Rožman, Journal of Physics D: Applied Physics (Submitted) is presented. For this article the author performed statistical analysis for pore diameter and pore separation on AAO and PC membranes, SEM+EDS analysis on Co-Pt nanowires, sample preparation for XRD experiment and data analysis, hysteresis loop measurement and determination of effective anisotropy constant, data analysis of FORC and FMR measurements, MFM measurements and micromagnetic simulations for MFM data interpretation.

This work aimed to synthesis Co-Pt NWs with hcp crystal structure into most widely used commercially available membranes and to perform comparative study on both membranes for the switching field distribution and magnetic domain structure in Co-Pt NWs.

In this study, Co-Pt NWs were potentiostatically electrodeposited into the most widely used polycarbonate and alumina membranes with $D_p \approx 200$ nm. The large pore diameter of the membrane ($D_p > D_o$) and the deposition conditions were chosen to obtain Co-Pt NWs with a hcp crystal structure and a c-axis orientation perpendicular to the NW long axis. We successfully prepared the samples with hcp c-axis perpendicular to NWs long axis, what we did not anticipated is the variation in the c-axis orientation from NW to NW.

We have proved that the small variations in the orientation of the c-axis in the perpendicular plane of the NWs' long axis can be possible due to "oblivious" electrodeposition, including a small fluctuation in the deposition conditions, like the pore diameter, pore shape etc. Hcp Co-Pt NWs have strong MCA, and thus even small fluctuations in the c-axis orientations can significantly affect the magnetic properties of the Co-Pt NWs, such as the switching-field distribution observed with FORC measurements.The large FMR linewidth helped us to estimate the spread of the c-axis orientation and effective anisotropy constant for Co-Pt NWs. We observed three distinct groups of magnetic domains which supports our hypothesis of variation in the orientation of the c-axis. We performed simulation work and found that the TS and LS magnetic domain structure are most energetically suitable.

The conclusion of this work is that small fluctuations in the electrodeposition process can slightly modify hcp c-axis orientation which can further influence switching field distribution and magnetic domain structure of such NWs. In order to improve the magnetic properties of the high anisotropy NWs fabricated with electrodeposition into commercially available membranes one has to pay very close attention to hcp c-axis orientation which is ignored in many cases.

An oblivious growth mechanism for high-magnetic-anisotropy hcp Co-Pt nanowire arrays: the role of the crystal orientation in the switching-field distribution and the magnetic-domain configuration

Muhammad Shahid Arshad[1,2], Mariana P Proenca[3], Spela Trafela[1,2], Volker Neu[4], Ulrike Wolff[4], Sven Stienen[5], Manuel Vazquez[6], Spomenka Kobe[1,2,7], and Kristina Žužek Rožman[1]

[1] Jožef Stefan Institute, Department for nanostructured materials K7, Ljubljana, Slovenia

[2] Jožef Stefan International Postgraduate School, Ljubljana, Slovenia

[3] IFIMUP and IN—Institute of Nanoscience and Nanotechnology and Departamento Fisica e Astronomia, Universidade Porto, Rua do Campo Alegre 687, 4169-007 Porto, Portugal

[4] IFW Dresden, Institute for Metallic Materials, P.O. Box 270116, 01171 Dresden Germany

[5] Helmholtz-Zentrum Dresden-Rossendorf, Bautzner Landstraße 40001328 Dresden, Germany

[6] Instituto de Ciencia de Materiales de Madrid, CSIC, 28049 Madrid, Spain

[7] Center of Excellence on Nanoscience and Nanotechnology (CENN Nanocenter), Ljubljana, Slovenia

Corresponding author e-mail: shahid.arshad85@gmail.coms

Telephone: +386 1 4773 178
Fax: +386 1 4773 221

Abstract

We propose an "oblivious growth" mechanism for Co-Pt nanowires (NWs) produced via potentiostatic electrodeposition into commonly used, ordered-alumina and disordered-polycarbonate membranes with similar pore diameters (≈200 nm). The pore diameter of the membranes and the deposition conditions were chosen such that the Co-Pt NWs fabricated into both membranes had a hcp crystal structure with a strong texturing of the c-axes in the direction perpendicular to the NWs' long axes; this effect was more pronounced in the alumina membranes. Hcp Co-Pt is a well-known magnetic material with a high magnetocrystalline anisotropy (MCA) (K_u=1x10^6 J/m^3), comparable to, or even stronger than, the shape anisotropy ($\pi\mu_o M_s^2$=4x10^5 J/m^3) in magnetic NWs. Due to the oblivious growth mechanism, hcp Co-Pt NWs have a small variation in the c-axes orientations in the plane perpendicular to the NWs' long axes. Magnetic characterizations suggested that the small variation in the orientation of the hcp c-axis plays an important role in the effective anisotropy field, which subsequently influences the switching-field distribution and the magnetic domain structure of the Co-Pt NWs. This study accentuate that the characterization of individual NW can be washed out in the measurements of ensembles, thus the quantitative analysis of the hcp c-axis for high-anisotropy materials is essential to control the functional properties of NWs.

Keywords: Co-Pt NW arrays, single Co-Pt NWs, complex FORC diagram, switching-field distribution, FMR measurements, magnetocrystalline anisotropy, longitudinal stripe domain, periodic magnetic domains, transverse stripe domain.

1. Introduction

Recently, special attention has been focused on one-dimensional (1D) ferromagnetic materials such as nanowires (NWs) to address not only fundamental physical questions, such as anisotropies (shape, magnetocrystalline), magnetic domain configurations [1] and magnetization reversal processes, but also for technological reasons, owing to their potential applications in racetrack memory devices [2]. A racetrack memory is a ferromagnetic NW where the information is stored along the length of the wire, as a sequence of magnetic domains. By applying short pulses of spin-polarized current, it is possible to move the magnetic domain walls in one dimension along the length of the NWs, reaching the read and write heads [2]. A great deal of research has been focused on soft magnetic NWs exhibiting just shape anisotropy, such as permalloy ($Ni_{80}Fe_{20}$), and some promising results have been obtained [3, 4]. However, there are some limitations on memory density in soft magnetic NWs due to (1) fewer domain walls and (2) domain-wall expansion due to the spin-polarized current [2, 5]. According to the roadmap for racetrack memory devices [2], materials with a large magnetocrystalline anisotropy (MCA), e.g., Co-Pt, Co-Ni, Co-Fe, can overcome these limitations. Thus, a high MCA material provides another degree of freedom (crystal structure and its orientation), although it comes with some new challenges that will be discussed here.

Co-Pt NWs can exhibit either a metastable disordered phase (fcc-based $L1_1$-CoPt [6]), a hcp-based B_h-CoPt [7] or a hcp-based $D0_{19}$-Co_3Pt [8]) crystal structure, depending on the relative amounts of Co and Pt as well as the formation conditions. A Co-rich Co-Pt favours the hcp structure and is a well-known magnetic material with a high MCA ($K_u=1x10^6$ J/m^3), comparable to (or even stronger than) the shape anisotropy ($\pi\mu_o M_s^2=4x10^5$ J/m^3) in magnetic NWs [9]. Hongyu *et al.* [10] reported that it is possible to generate a variety of preferential growth orientations in hcp NWs by varying either the pore diameter (D_p) of the membrane or the deposition current density. A determination of the exact critical diameter D_o (which is equal to $4\frac{\gamma_a-\gamma_b}{f_{\infty,a}f_{\infty,b}}$, where γ and f are the surface and interface energies, respectively, see equation 4 in [10]) for the change of the preferential growth orientation is a difficult task, since it depends on the surface and interface energies, which further depend on many unknown factors, e.g., the electrolyte, the substrate and the impurities in the NWs [10]. However, in this work we used the pore diameter $D_p\approx200$ nm, which is larger than the critical diameter for Co-based NWs and so a preferential crystal orientation (c-axis) that is perpendicular to the NWs' long axes can be expected. For example, Henry *et al.* [1] observed, by means of dark-field transmission electron microscopy images, that for hcp Co NWs with diameters $D_p<50$ nm, the hcp c-axis lies parallel to the wire long axis, while for NWs with a diameter $D_p>50$ nm, the hcp c-axis was found to be perpendicular to the NW's long axis. Thus, it is possible that the MCA and the shape anisotropy are in competition with each other and so trigger interesting physical phenomena in NWs. It is important to note that the MCA of the polycrystalline NWs depends on the preferred orientation of the enclosed crystallites. Forster *et al.* [11] and Ivanov *et al.* [12] investigated the magnetization reversal of hcp Co NWs made up of grains with different orientations with respect to the wires' long axes, using the finite-element method; their results showed that the granular structure and the orientation of the crystallites should be taken into account. There are some experimental reports about hcp Co NWs where the orientation of the c-axis plays an important role in the magnetization-reversal process [13]. Thus, it is possible to tune the magnetization and the magnetization reversal of Co-Pt hcp NWs by controlling the crystal (c-axis) orientation [13]. Therefore, it is important to characterize the orientation of the c-axis in high-anisotropy materials like Co-Pt, not only qualitatively but also quantitatively.

It is important to note that the effective magnetic behaviour of arrays of NWs is determined by the magnetic anisotropy of the individual NWs, i.e., the shape and MCA contributions, together with the magnetostatic interactions between the NWs in the arrays [14]. First-order reversal-curve (FORC) measurements are the first choice for a quantitative magnetostatic interaction analysis, since they not only include the interactions as a whole, but also make it possible to

separate the mean-field interactions (i.e., dipolar, like the interactions between the NWs) from local interaction effects (i.e., exchange-like). In particular, the FORC method has also proved to be extremely valuable in addressing the role of the specific crystallographic orientations (c-axis) present in NWs [15, 16]. The switching-field distributions can be accurately extracted from FORC measurements, which can supply additional valuable information about the magnetic anisotropies for individual entities in the system [17].

Ferromagnetic resonance (FMR) measurements on NWs can yield direct information about the homogeneous (and inhomogeneous) precession mode of the NWs, which is related to the magnitude of the effective magnetic anisotropy [18] that will give additional information about crystal orientations (c-axis) in the NWs. An analysis of the FMR linewidth can also provide detailed information about the inhomogeneities in the sample that come from the crystal disorientations (c-axis), the dimensions and the anisotropies, etc. [18].

There have been a few magnetic-force microscopy (MFM) studies of individual Co-Pt NWs, e.g., [19], and a detailed MFM study of individual hcp Co NWs with different crystal orientations was reported in [1]. Henry *et al.* [20] observed a periodic dark-and-bright MFM contrast along the length of the NW, which was attributed to the competition between the MCA and the shape anisotropy in the NWs. This MFM contrast was interpreted as transverse-stripe (TS) and longitudinal-stripe (LS) domain states on the basis of the minimization of the energy. In another report [21] on hcp Co single-crystal NWs with the c-axis almost perpendicular to the NW's long axis the periodic contrast was explained on the basis of vortex domains with an opposite chirality along the length of the NW to minimize the magnetic energy. Thus, the exact interpretation of this contrast is not yet clear, and even conflicting in some reports [22, 23]. The MFM measurements on Co-Pt NWs presented here are an extension of our previous investigation [24]. We believe that the introduction of a model system can provide a mature insight into this topic and can further highlight the influence of the c-axis orientation on the magnetic-domain configurations in high-anisotropy NWs. Although most of the experimental reports related to this contrast [25] explained the magnetization modulation as arising from the competition between the MCA and the shape anisotropy, no systematic study of NWs with different orientations of the c-axis was conducted so far to fully clarify this matter. In this study we have investigated the variation of the magnetization modulation in Co-Pt NWs with the change in the orientation of the c-axis. Additionally, all the experimental published reports with periodic domain patterns were reported on single-crystal hcp Co NWs [1, 21, 25]. Thus, the question about the existence of such a magnetic domain structure in polycrystalline Co-Pt NWs remains open.

In this study we investigated Co-Pt NWs that were potentiostatically electrodeposited into the most widely used polycarbonate and alumina membranes with D_p~200 nm. The large pore diameter of the membrane ($D_p > D_o$) and the deposition conditions were chosen to obtain Co-Pt NWs with a hcp crystal structure and a c-axis orientation perpendicular to the NW long axis in order to study the competition between the shape and the MCA. We have proved that the small variations in the orientation of the c-axis in the perpendicular plane of the NWs' long axes can be possible due to "oblivious" electrodeposition, including a small fluctuation in the deposition conditions, like the pore diameter, etc. In hcp Co-Pt NWs the MCA is stronger than the shape anisotropy, and thus even small fluctuations in the c-axis orientations can significantly affect the magnetic properties of the Co-Pt NWs, such as the switching-field distribution and the FMR linewidth, etc. However, it is important to characterize the individual behaviour of the NWs to answer questions like what is the variability of magnetic properties from NW to NW? The anisotropy interplay coming from the slight variation in the orientation of the c-axis and the competition between the shape anisotropy and the MCA in hcp Co-Pt NWs were found to strongly influence the magnetic-domain structures of individual Co-Pt NWs. It is our aim to highlight the importance of the influence of the hcp c-axis orientation in high-anisotropy materials such as hcp Co-Pt NWs and thus the need for their quantitative analysis to fully understand and improve the final magnetic properties of these NWs.

2. Methods

Porous anodic aluminum oxide (AAO) (Whatman Anapore® Co.) and polycarbonate (PC) membranes (Whatman Nuclepore® Co.) with pore diameters of ≈ 200 nm were used for the electrodeposition of the Co-Pt NWs. The AAO membranes are ≈65 μm thick, while the PC membranes are 30 μm. Figure 1 (a) and (d) shows typical SEM images of the AAO and PC membranes (top view) to provide a clear indication of the distribution of the pores. In order to check the homogeneity of the pore diameters and the interpore separations a statistical analysis was performed on both membranes and the results are shown in figure 1(b), (c), (e) and (f). Figure 1 (b) and (e) shows that the pore diameters of the AAO and PC membranes, with an average pore diameter of D_p=240 ±20 nm and D_p=226 ±11 nm, respectively. The small standard deviation in the PC membrane shows that there is relatively less variation in the pore diameters in the PC membranes. Figure 1 (c) and (f) shows an analysis of the interpore separation (center to center) for the AAO and PC membranes, respectively, with an average pore separation of D_c=356±22 nm and D_c=570±140 nm. It is clear from figure 1 (d) that there is a large spatial distribution of pores in the PC membrane, with a large standard deviation (≈140 nm), which is a characteristic of PC membranes.

For the electrodeposition of the Co-Pt NWs, a gold (Au) layer (≈100 nm) was first sputtered on one side of both membranes to make them conductive. Then, on the same surface, Au was electrodeposited for 10 mins to completely cover the pores, so as to use it as the working electrode (cathode) in a three-electrode cell. In order to avoid Co-Pt nanotube formation, as observed in a previous study [24], the gold NWs were electrodeposited for 10 mins prior to the main deposition of the Co-Pt NWs. The electrolyte consisted of 80 mmol of Co-sulphamate ($Co(SO_3NH_2)_2$) and 20 mmol of Pt-p-salt ($Pt(NH_3)_2(NO_2)_2$), while ammonium citrate ($(NH_4)_2C_6H_6O_7$) (20 mmol) and glycin (NH_2CH_2COOH) (0.2 mmol) were used as complexing agents. The pH of the electrolyte was set to 8 using ammonia. A Pt mesh electrode was used as the anode, and potentiostatic conditions with -2.1 V against a reference electrode of Ag/AgCl were used to deposit metal ions into the pores of the membranes. The time of the electrodeposition that determines the length of the NWs was 60 mins for the AAO membranes and 40 mins for the PC membranes in order to keep the length of the NWs the same. The reason for the rapid growth of the Co-Pt NWs into the PC membrane can be attributed to the rapid mass transport due to the small thickness (30 μm) of the PC membrane in comparison to the AAO membrane (65 μm).

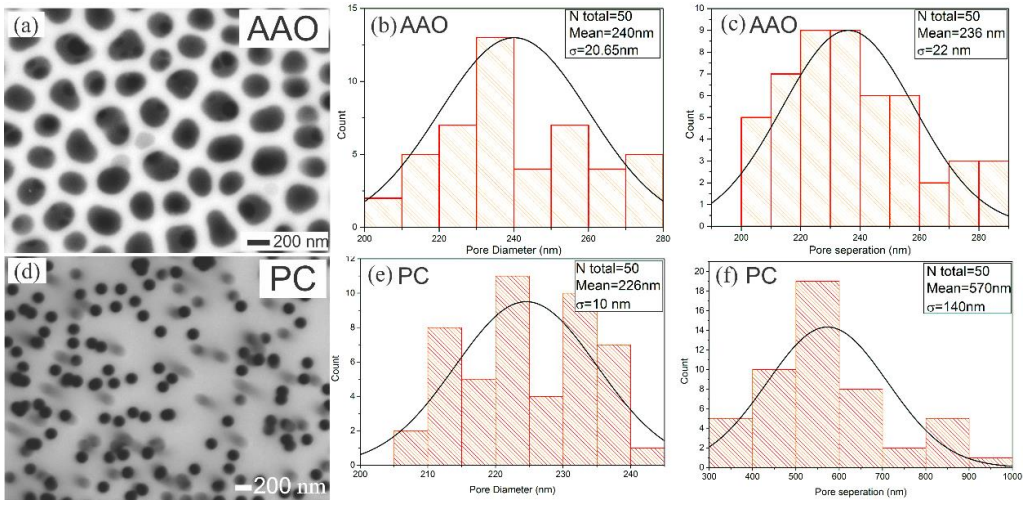


Figure 1. (a) SEM image of AAO membrane (top view). Statistical analysis on AAO membrane for (b) pore diameter (D_p) and (c) pore separation (D_c). (d) SEM image of PC membrane (top view). Statistical analysis on PC membrane for (e) pore diameter (D_p) and (f) pore separation (D_c).

The morphology, composition and crystal structure of the electrodeposited Co-Pt NW arrays were characterized by scanning electron microscopy (SEM; JSM-7600F) and XRD (PANalytical X'pert Pro). The SEM was equipped with an energy-dispersive X-ray spectrometer (EDXS) to determine the composition of the Co-Pt NWs. The XRD patterns

were acquired in a θ-2θ setup by employing Cu-$K_{\alpha 1}$ radiation (λ=1.54056 Å). A zero-background sample holder was used for the XRD measurements. Room-temperature hysteresis loops and FORC measurements of the Co-Pt NW arrays were performed using a vibrating-sample magnetometer (VSM, LOT-Oriel and EZ7). The hysteresis loops and the FORC measurements were obtained with the external magnetic field applied parallel (out-of-plane orientation, with respect to the membrane surface) and perpendicular (in-plane orientation, with respect to the membrane surface) to the NW's long axis. The FMR measurements on the Co-Pt NWs embedded into the AAO membrane were performed in the frequency X-band ($\frac{\omega}{2\pi}$~9.41 GHz) in a reflection-cavity microwave spectrometer using a Bruker Elexsys E500 spectrometer. The FMR measurements were performed in both the out-of-plane and in-plane orientations. The frequency was fixed and consistent with the geometry of the used microwave cavity. A field modulation of 1 mT (100 KHz) was used for detection purposes. To dissolve the AAO and PC membranes an aqueous solution of 10-M NaOH and dichloromethane was used and then the NWs were released using a centrifuge. The Co-Pt NWs were dispersed in absolute ethanol, and for the MFM measurements a drop of ethanol containing the Co-Pt NWs was placed on a clean Si wafer and then dried. After a single NW was selected, a commercial scanning probe microscope (Digital Instruments Dimension 3100) was used. The MFM measurements were performed in the lift mode using a cantilever from Nanoworld (MFMR type probe). All the MFM images were taken at a constant scan height of 100 nm. The direction of the tip's magnetization was perpendicular to the plane of the Si substrate on which the NW was horizontally placed.

3. Results and discussion

3.1 Basic characterizations, microstructure and growth mechanism of Co-Pt NWs

Figure 2 (a) and (b) shows a SEM cross-sectional image of the Co-Pt NW arrays embedded in the AAO and PC membranes. In the AAO membrane the NWs are robust and vertically erected with a length of 6±2 μm and a diameter consistent with the pore-diameter analysis. The aspect ratio (length/diameter) of the NWs lies in the range ≈25-35. As seen from the SEM image, the filling factor is estimated to be close to 100%. Figure 2 (b) shows a SEM image of the Co-Pt NW arrays after they are partially removed from the PC membrane. It is clear that the NWs are robust, vertically erected, and regular cylinders with a length of 6±1 μm and a diameter consistent with the pore-diameter analysis. However, the NWs in the PC membrane are misaligned perpendicularly to the membrane plane and the majority of the NWs are tilted randomly by a few degrees with respect to the normal of the membrane plane, due to the nature of the PC membrane. It is important to mention that the effect is exaggerated in figure 2 (b) due to the partial removal of the PC membrane. Figure 2 (a) and (b) are backscattered SEM images where the bright contrasts at the bottom of the Co-Pt NWs are Au NWs with a length of ≈1 μm in both membranes. The reasons for the deposition of the Au NWs in membrane are (1) it avoids the formation of nanotube segment at the bottom of the NWs, as previously reported in [24], and (2) it avoids Co-Pt NWs dendrite formation in the AAO membrane, as seen in figure 2 (a).

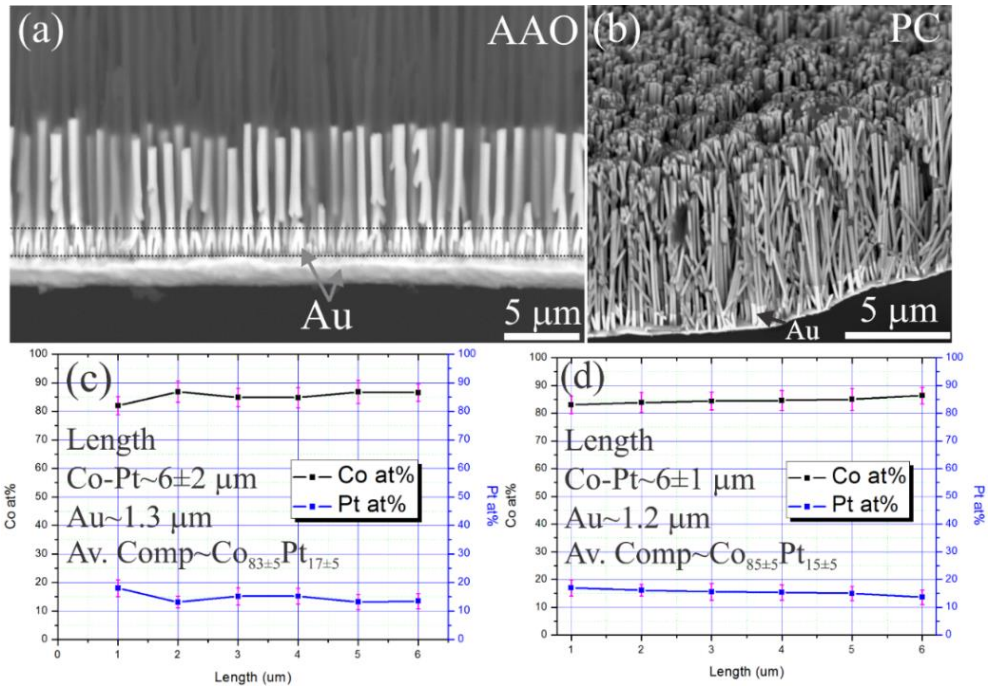


Figure. 2 SEM cross-sectional view of (a) an AAO membrane filled with Co-Pt NWs with lengths ~6±2 μm (b) a PC membrane filled with Co-Pt NWs with lengths ~6±1 μm. SEM-EDX analysis along the length of the Co-Pt NWs prepared in (c) AAO and (d) PC membranes.

The SEM-EDXS analysis for the Co-Pt NWs into the AAO and PC membranes is shown in figure 2 (c) and (d), respectively. In the AAO and PC membranes the composition of the NWs corresponds to Co and Pt with an average composition of $Co_{83\pm5}Pt_{17\pm5}$ and $Co_{85\pm5}Pt_{15\pm5}$, respectively. It is worth mentioning that a very consistent composition was obtained along the length of the NWs in both membranes.

The XRD patterns of the Co-Pt NW arrays embedded in the PC and AAO membranes using the θ-2θ configuration in the range between 30° and 100° are shown in figure 3(a) and (b), respectively. Figure 3 (c) and (d) show the NW arrangements into the PC and AAO membranes, respectively. The experimental results were compared with literature XRD data for Au (ICSD#180868) and Co_3Pt_{hcp} (ICSD#102626). The blue dotted lines show the literature data for the Co-Pt hcp crystal structure. The XRD patterns of the Co-Pt NWs from both membranes exhibit a textured hcp polycrystalline structure. In the case of Co-Pt NWs deposited into the PC membrane the (100), (101), (110), (112), and (201) peaks are present, as shown in figure 3 (a). According to the literature data for Co_3Pt_{hcp} (ICSD#102626), the peak intensity of (101) must be three times higher than (100), which is not the case in figure 3 (a), indicating that there is a strong texturing in the Co-Pt NWs along the (100) direction in the PC membrane. However, the Co-Pt NWs embedded into the AAO membrane exhibit only (100) and (110) reflections, as shown in figure 3 (b). The nomenclature of the missing peaks in figure 3 (b) can be realized using the expression $(hkl)|_{l\neq0}$, thus, the c-axis of the hcp Co-Pt NWs is not in the Bragg condition. Furthermore, the Rietveld-refinement method was used to investigate the crystallographic texturing [26] in the Co-Pt NWs. It is important to note that the Co-Pt $(103)_{hcp}$ and $Au(222)_{fcc}$ peaks overlap at 2θ=81.71° and were not included in the refinement. The green line at the bottom of figure 3 shows the Rietveld-refinement fitted graph for the AAO membrane and the orange dotted line is the residual graph. The analysis indicates a strong crystallographic texturing of the c-axis perpendicular to the Co-Pt NWs long axes in both membranes; however, the effect is more pronounced in the AAO membrane. Although it is hard to prove, the misalignment of the Co-Pt NWs with respect to the PC membrane's normal might be the reason for the appearance of the additional peaks, e.g., the (101) in figure 3 (a). A peak-width analysis was performed by fitting a pseudo-Voigt type-I function, and the average grain size was estimated using the Scherrer equation [27]. The grain sizes were estimated to be ≈7 nm and ≈12 nm for Co-Pt NWs into the PC and AAO membranes, respectively.

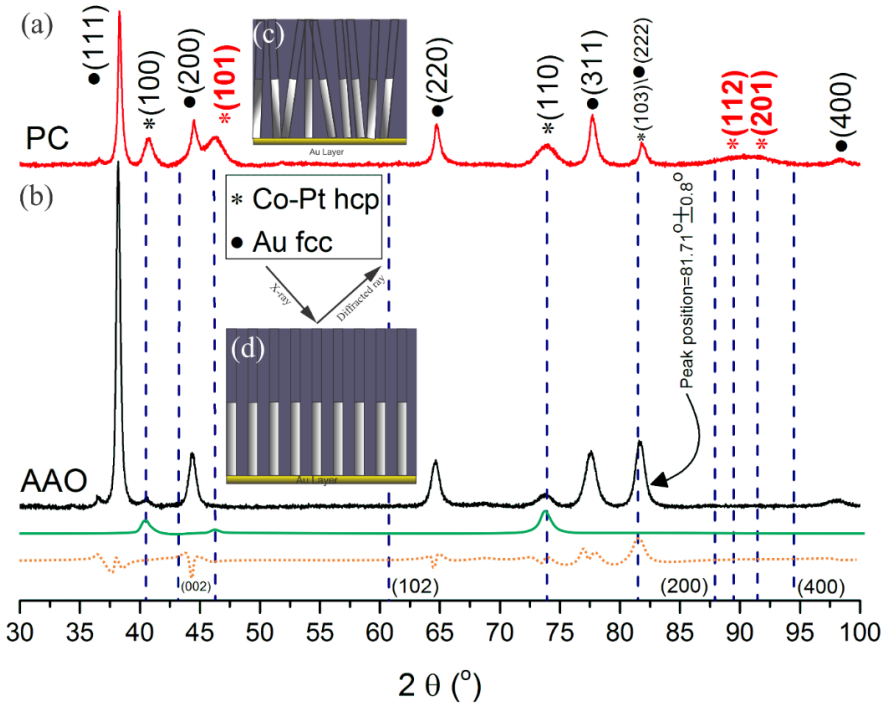


Figure. 3 XRD recorded on Co-Pt NW arrays embedded inside the (a) PC and (b) AAO membranes. Blue dotted lines are literature data for the Co-Pt hcp crystal structure. Schematic of Co-Pt NWs embedded inside the (c) PC and (d) AAO membranes

In detail, as the composition of the Co-Pt NWs in both membranes is Co rich, the most favourable hcp crystal structure was observed in the XRD data, as seen in figure 3. The Rietveld analysis of the XRD data and our previous experience [24, 28] allowed us to understand the growth mechanism of the Co-Pt NWs in both membranes. For this we considered a single, cylinder-shaped pore with a diameter D_p, as shown in the top view in figure 4 (a1). It is well known that the electrodeposition of NWs mostly occurs due to the coalescence-nucleation process proposed by [29] into the pores of the membranes. Co and Pt are high-melting-point metals ($T_{m,Co}$≈1495 ºC and $T_{m,Pt}$ ≈1768 ºC), which favours the aggregation of small 3D clusters, resulting in a random nucleation at the edges of the gold NW, as shown in figure 4 (a2). The reason for this kind of nucleation is the existence of a most energetically favourable site for the charge transfer [30]. The preferred crystallographic orientation follows the tendency of minimization of the surface energies of different crystal planes during the nucleation and growth processes of NWs [31]. In hcp crystal-structure materials like Co-Pt, the c-axis [001] is the lowest-energy crystal planes [32], and if the condition for the pore diameter (D_p>D_o, equation 4 in [10]) is satisfied, it grows perpendicular to the nucleation plane (pore wall). Due to the spatial confinement of the pores, the [001] crystal planes perpendicular to the pore wall grow larger, as shown in figure (a3). As a result, most of the grains point the c-axis [001] perpendicular to the NWs' long axes, as shown in figure (a4). Such growth phenomena have also been reported for other materials with a hcp crystal structure [33]. Furthermore, the crystallographically textured structure due to the pores' diameter (D) and the rigid walls of the membrane is explained in [10, 31]. According to the growth theory presented in [10], the conditions are suitable for the c-axis to be perpendicular to NWs' long axes, as seen in the XRD data (figure 3), but still the c-axes of all the NWs may not be pointing in the same direction due to the fact that the NWs grow independently in the membrane. Such an electrodeposition process may be termed "oblivious electrodeposition": in such a system the NWs are unaware of the c-axis orientation of the neighbouring NWs. Therefore, the c-axis can misalign among the NWs in the array by a certain number of degrees in the plane perpendicular to NWs' long axes. This is vital information for high MCA materials like Co-Pt as it can significantly affect the magnetic properties.

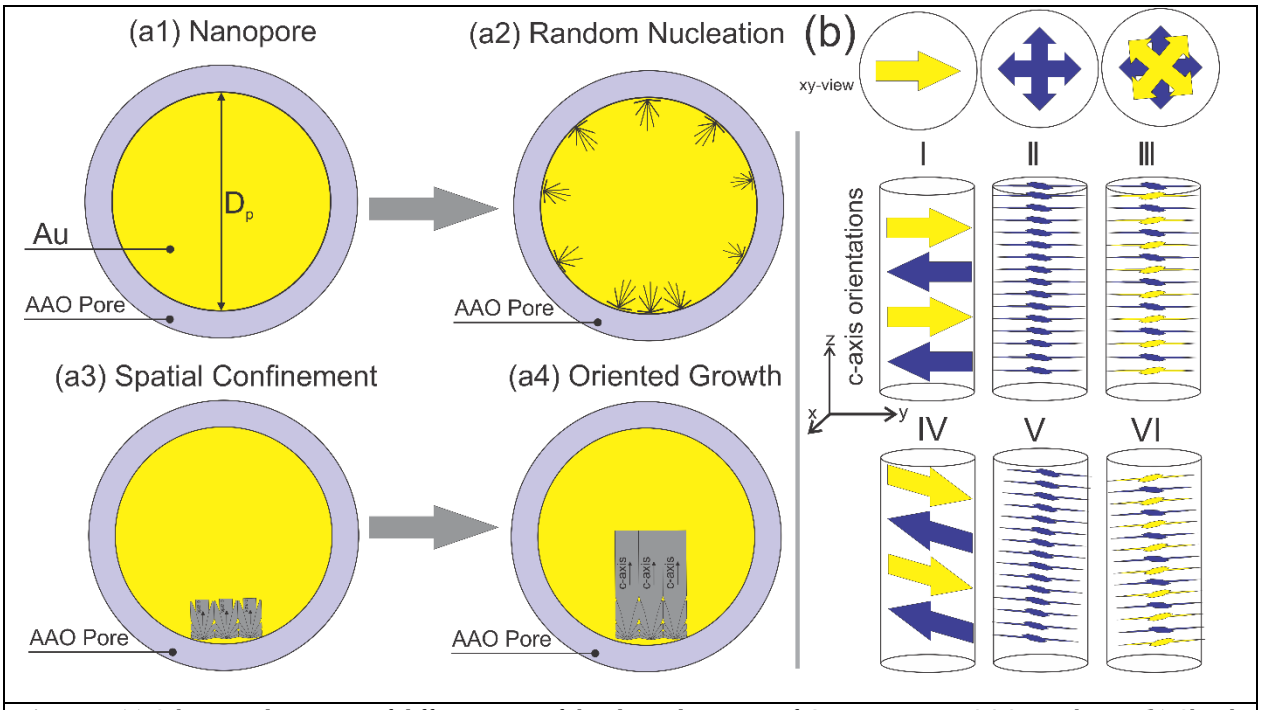


Figure. 4 (**a**) Schematic description of different steps of the electrodeposition of Co-Pt NWs into AAO membrane. (b) Sketch of NW with three different orientations of the c-axis. (I) whole NW has a c-axis perpendicular to the long axis (uniaxial); (II) c-axis orientation is in two directions but always perpendicular to the long axis (biaxial). (III) c-axis has a random orientation. Last row shows the possibility of the c-axis being in I II and III, respectively, tilted by a small angle.

Furthermore, we propose a few different possible orientations of the c-axis in the plane perpendicular to NWs' long axes, as shown in figure 4(b) I-VI. It is important to mention that all these c-axis orientations give rise to similar XRD diffraction patterns observed in figure 3. (I) whole NW has a single c-axis perpendicular to the long axis (uniaxial); (II) c-axis orientation is in two direction, but always perpendicular to the long axis (biaxial); and (III) isotropic c-axis orientation (random orientation of c-axis) in the plane perpendicular to the NW's long axis. Last row (IV), (V) and (VI) in figure 4(b) showing the possibility of the c-axis being in I II and III tilted at small angles with respect to the NWs' long axes. This can happen due to small fluctuations in the electrodeposition conditions, such as pore diameter, etc. It is important to mention that each of these c-axis orientations given in figure 4 (b) will play a different role in the MCA with respect to the effective anisotropy field of the NW arrays and thus the magnetic properties. To summarize, figure 5 (a) shows a schematic of the AAO membrane with the Au substrate as well as the Au NWs at the bottom. After the oblivious electrodeposition of the Co-Pt NWs the c-axis is oriented along the short axis of the NW due to the deposition conditions, as observed from the XRD pattern (figure 3) shown in figure 5 (b). Figure (c) shows a set of four NWs with slightly different c-axis orientations, as indicated by the arrows.

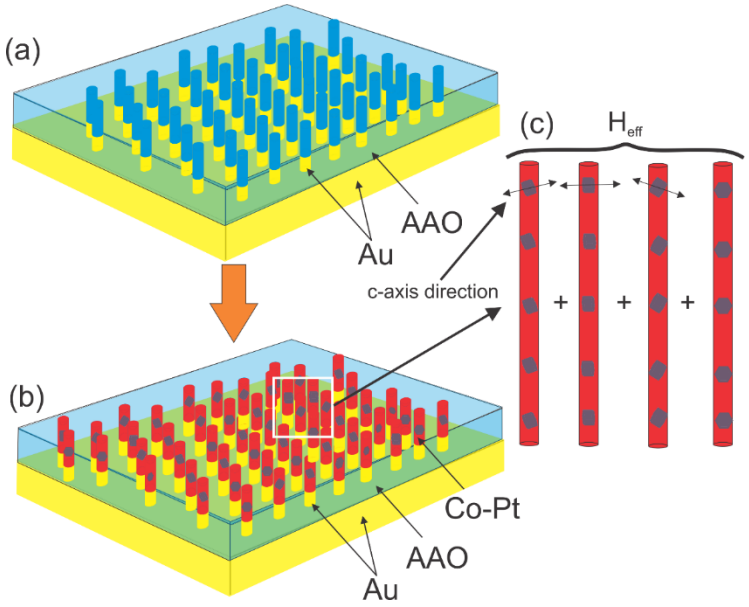


Figure. 5 (a) A schematic of the AAO membrane and Au substrate as well as Au NWs at the bottom. (b) Co-Pt NWs grow with small variations in the orientation of the c-axis of hcp. (c) Shows sample of four NWs with small variations of the c-axes.

3.2 Magnetic characterization

The room-temperature normalized hysteresis loops of the as-deposited Co-Pt NW arrays in the AAO and PC membranes, when the field was applied parallel (black solid line) and perpendicular (red solid line) to the NW long axis, is shown in figure 6 (a) and (b), respectively. The shapes of the hysteresis curves show that the easy magnetization axis is perpendicular to the NW long axis in both membranes. The squareness (SQ) ($m_r=M_R/M_s$) values of 0.076 (0.162) and 0.086 (0.15) were measured for the parallel and the perpendicular field directions for the AAO and PC membranes, respectively. A coercivity of about ≈400 Oe was observed for both field directions for the Co-Pt NW arrays in both samples. The coercivity and SQ values are similar for both field directions and both membranes exhibit analogous behaviours, indicating that the Co-Pt NWs have similar lengths, diameters and crystal structures. The small coercivity and the SQ values can also indicate that the MCA is in competition with the shape anisotropy, which significantly reduces the effective anisotropy.

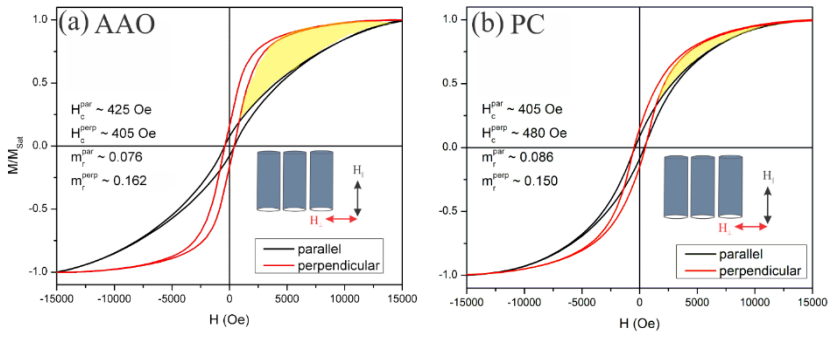


Figure 6 Normalized room-temperature hysteresis loops of the Co-Pt NW arrays when the field was applied parallel (black solid line) and perpendicular (red solid line) to the long axis of the wire in (a) AAO and (b) PC membrane. (Inset) schematic view of the applied field direction with respect to the NW's axis.

Although the coercivity and SQ values are similar for both membranes, there is an obvious difference between these two samples, e.g., the effective anisotropy, the yellow highlighted area in figure 6 (a), is larger than figure 6 (b). This behaviour can be explained by taking into consideration the crystal texture in these samples. According to the literature for the Co-Pt hcp system the MCA easy axis is along the $[001]_{hcp}$ (c-axis) direction [11]. Since the observed texturing of the crystallites in the Co-Pt NWs (figure 3) in both membranes is in the $[001]_{hcp}$ direction, which is found to be pointing perpendicular to the NWs' long axes, the MCA is in competition with the shape anisotropy. Compared with the PC sample, the AAO sample exhibited a stronger texturing, as shown in figure 3, which means relatively more crystalline grains with their c-axes perpendicular to NW long axis can be found in the AAO sample. Thus, the total effective anisotropy can be investigated to explain the differences between these samples. The effective anisotropy constant (K_{eff}) can be estimated using [13]

$$K_{eff} = \frac{M_s}{m_{tot}} \int_0^{m_{tot}} H_{\perp} dm - \frac{M_s}{m_{tot}} \int_0^{m_{tot}} H_{\parallel} dm \qquad (1)$$

where M_s is the saturation magnetization, m_{tot} is the total magnetic moments of the sample when it is magnetized to saturation and $H_{\parallel}$ and $H_{\perp}$ are the applied field parallel and perpendicular to the axis of the NW, respectively. The saturation magnetization $\mu_o M_s$ ($\approx 8x10^5$ A/m) for the Co-Pt NWs examined in this article was taken from [34]. Co-Pt in the hcp structure is a well-known magnetic material with a high MCA ($K_u=1x10^6$ J/m^3), comparable to (or even stronger than) the shape anisotropy ($\pi\mu_o M_s^2=4x10^5$ J/m^3) in magnetic NWs [9]. The K_{eff} calculated from expression (1) is larger for the PC sample ($6.75x10^4$ J/m^3) than the AAO sample ($2.34x10^4$ J/m^3). As in the AAO membrane there is stronger texturing of the c-axis perpendicular to the NW long axis than the PC membrane, in this case the MCA and the shape anisotropy tend to align the magnetic moment in different directions, and this competition decreases the K_{eff}. The above results indicate that Co-Pt NW arrays with the same crystal structure, but slightly different textures, exhibit different effective anisotropies. It is clear that the crystal texture plays an important role in the process of magnetization in the Co-Pt NW arrays and the MCA induced by the crystallographic orientation influences the magnetization and demagnetization processes. Considering that in reality there are crystal disfigurements even in the same array of NWs (oblivious electrodeposition in the previous section), there is a need for further study in order to understand the final properties of the Co-Pt NW arrays, and which will be investigated in this paper. It is important to mention that the obtained K_{eff} ($2.34x10^4$ J/m^3) for the AAO membrane is very close to our previously reported value ($4x10^4$ J/m^3) using another method [24]. Our observations are in accordance with many other reports on Co-based NW arrays consisting of hcp structures [13, 35]. The coercivity values were found to be higher than those for fcc Co-Pt [36] and closer to Co-Pt NWs with the hcp structure [37]. Shamaila *et al.* [36] also found a perpendicular magnetization axis for the Co-Pt NW arrays (fcc structure) with similar dimensions, but their results were attributed to the large magnetostatic interactions between the NWs. The main contributions to the effective anisotropy field H_{eff} are the shape anisotropy, the dipolar interactions between the NWs, and the MCA [38]. Therefore, in order to probe the effect of the magnetostatic interactions between the NWs in the AAO and PC membranes we performed FORC measurements, which will be discussed in the next section.

3.3 First-Order Reversal Curves (FORCs) of Co-Pt NW arrays

First-order reversal curves (FORCs) were measured with a magnetic field (H) applied parallel and perpendicular to the wire axis in the AAO and PC membranes. During the FORC measurements the system is first magnetically saturated at 15 kOe; then, H is reduced to the so-called reversal field (H_r); finally, M is measured from H_r up to the maximum field H_{max}. In this work we used H_{max} values of 8 and 7.5 kOe for the NWs electrodeposited into the AAO and PC membranes, respectively. To obtain a complete set of FORCs, $M(H,H_r)$, these measurements are then repeated by increasing H_r from $-H_{max}$ to H_{max} in steps of $H_{max}/50$. The insets of figures 7 (a)-(d) show the FORCs of selected samples. The FORC distribution, ρ_{FORC}, is then obtained by applying a second-order mixed derivative of $M(H,H_r)$ [39]. The ρ_{FORC} is usually represented as a contour coloured plot, called a FORC diagram, with a scale ranging from red (maximum value of ρ) to blue (minimum value of ρ). From the FORC measurements we can extract the individual coercivities (H_c) of the NWs and the magnetostatic interactions (H_u) between the NWs in their arrays. To read the H_c

and H_u parameters directly from the FORC diagram, it is convenient to perform a change of coordinates, to define a coercivity field axis (H_c) and an interaction field axis (H_u) as shown in figure 7 (a)-(d). The magnetostatic interactions can then be measured as the half width (ΔH_u) of the FORC distribution along the H_u direction [40]. Using the moving Preisach model [39], that takes into consideration the interactions between the individual magnetic elements, we can approximate the interaction fields at saturation as:

$$H_{in,sat} = 2\sigma_{in} - \kappa, \quad (2)$$

where σ_{in} and κ are the local and the mean interaction fields, respectively [41].

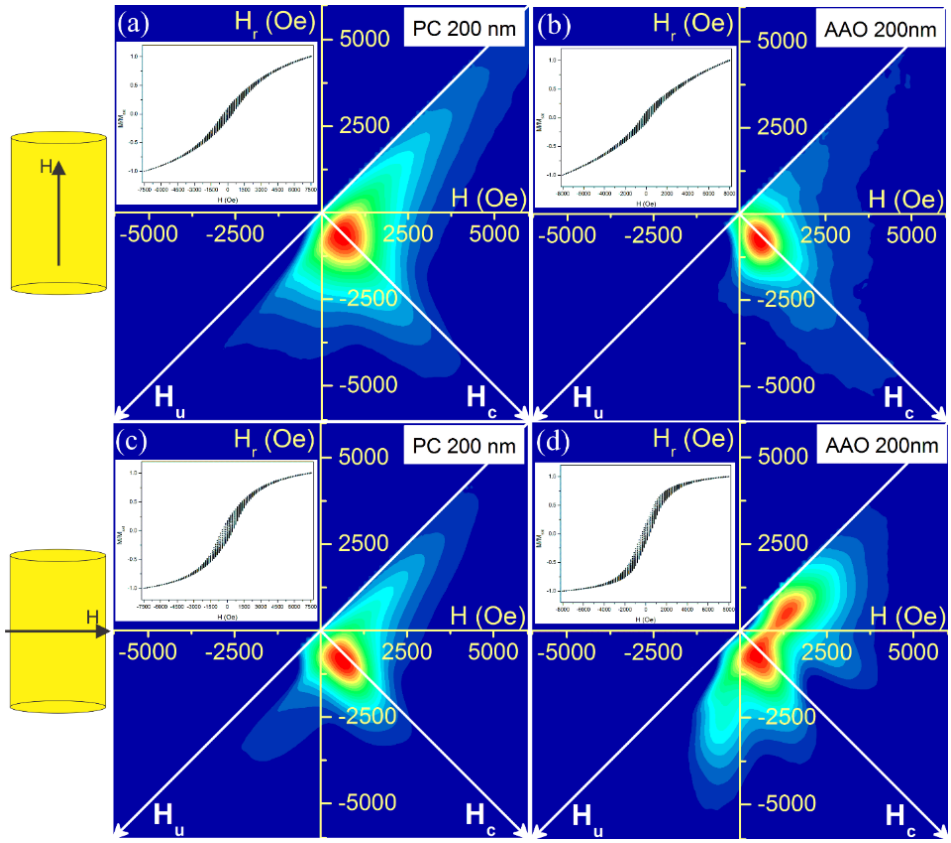


Figure. 7 FORC measurements (insets) and FORC diagrams of the Co-Pt NW arrays when the applied field is (a,b) parallel and (c,d) perpendicular to the NW's long axis for both membranes.

Figure 7 (a)-(d) shows selected FORC diagrams of the Co-Pt NW arrays when the applied field is parallel and perpendicular to the wires' long axes in the PC and AAO membranes, respectively. Analysing the FORC diagrams, we can see the presence of a sharp peak along both applied field directions for the NWs electrodeposited in the PC membrane, but an anisotropic behaviour when using the AAO membrane. In particular, the FORC diagram in figure 7 (d) shows complex magnetic behaviour, evidencing the existence of two different switching-field distributions shifted along the H_u axis. To better understand this effect, we studied the magnetostatic interactions present in the NW array by analysing the cross-sections of the FORC diagrams along the H_u axis (Figure 8). The inset in figure 8 evidences the existence of sharp peaks in the H_u profile, when the magnetic field is applied parallel to the NWs' long axes. These are ascribed to the dominance of the local magnetostatic (exchange-like) interactions in the NW arrays [41, 42], being stronger for the NWs electrodeposited into the PC membranes (broader peak). However, when the magnetic field is applied perpendicular to the wires' axis, the two different membranes show different magnetic behaviours. For the PC membranes, again, local magnetostatic (exchange-like) interactions prevail, as a sharp peak is observed in figure 8.

These interactions, however, are smaller along the perpendicular direction (the sharper peak in figure 8) than those observed along the parallel direction of the applied magnetic field (the broader peak in the inset of figure 8). On the other hand, the NWs electrodeposited into the AAO membrane evidence two distinct peaks on the H_u profile, when the magnetic field is applied perpendicular to the NWs' axes. These two peaks show the existence of two individual FORC distributions, shifted by the interaction field, suggesting the existence of two different magnetic behaviours that are interacting between themselves, which can be attributed to a mixture of hard and soft magnetic phases [43] or different crystal (c-axis) orientations in the Co-Pt NWs in the AAO membrane. As the XRD results did not show evidence of the presence of two crystallographic phases in the Co-Pt NWs in the AAO membrane, the most plausible explanation would be the different c-axis orientation of the MCA in the NWs. Moreover, the absence of such behaviour in the PC membrane can be attributed to the small standard deviation of the pore diameter (half of AAO), which means less variation of the c-axis orientation in the PC membrane. Therefore, it is vital to further investigate the crystal disfigurement (or disorientations) in Co-Pt NWs electrodeposited in the AAO membranes, and this will be addressed in the following sections.

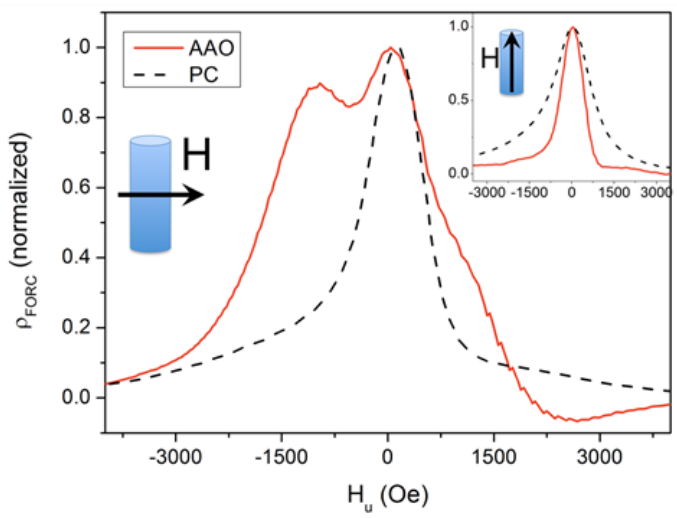


Figure 8. Cross-sections of the FORC diagrams along the H_u axis for the NWs in the AAO (red solid lines) and PC (black dashed lines) membranes, when the magnetic field is applied perpendicular to the NWs' long axes. Inset shows the results obtained when the magnetic field is applied parallel to the NWs' long axes.

3.4 Ferromagnetic resonance (FMR) measurements for the Co-Pt NW arrays in the AAO membrane

Ferromagnetic resonance (FMR) yields direct information about the homogeneous (and inhomogeneous) precession mode of the NWs, which can be related to the crystal orientation and subsequently to the effective anisotropy magnitude [44]. The FMR measurements were performed in two geometries so as to fully cover all the possible angles: (i) the φ-scan, in which the external field always lies in a plane perpendicular to the NWs' long axes (in order to obtain the whole perpendicular plane the sample was rotated by 360° in the external field), as shown in figure 9(a) and (a1); and (ii) the Φ-scan, in which the sample was rotated to an orientation parallel to the long axes of the NWs, as shown in figure 8 (b) and (b1). While it is hard to align the sample inside the microwave cavity, we chose an angular range of 200° for this orientation. Figure 9 (c) and (d) shows the angular-dependent FMR measurement results for an AAO membrane in the in-plane (IP) and out-of plane (OOP) rotations, respectively. To better understand the FMR results, the intensity of the FMR signal was displayed as polar contour plots where the red (blue) colour shows the maximum positive (negative) values of the FMR signal's intensity. It is worth mentioning that the applied field was swept down to the saturation field, which is 12 kOe for the OOP and 10 kOe for the IP measurements. However, for the sake of clarity, only the FMR data up to 5 kOe are shown in figures 9 (c) and (d). Following the FMR intensity in the OOP

case (figure 9 (d)), it is clear that the hard magnetic axis of the NW lies parallel to the NW's long axis (90°), indicated by the higher resonance field in that direction. Corresponding to this result, the majority of the Co-Pt grains have their c-axes oriented in the film's plane (perpendicular to the NW's long axis) as expected from the XRD data (figure 3(b)). The IP measurement shown in figure 9 (c) has a 2-fold magnetic anisotropy, which proves the coercivity variation, as shown by the black dotted line. The origin of the 2-fold anisotropy lies in the strong texturing in the plane perpendicular to the NWs' long axes, with slight c-axis disorientations.

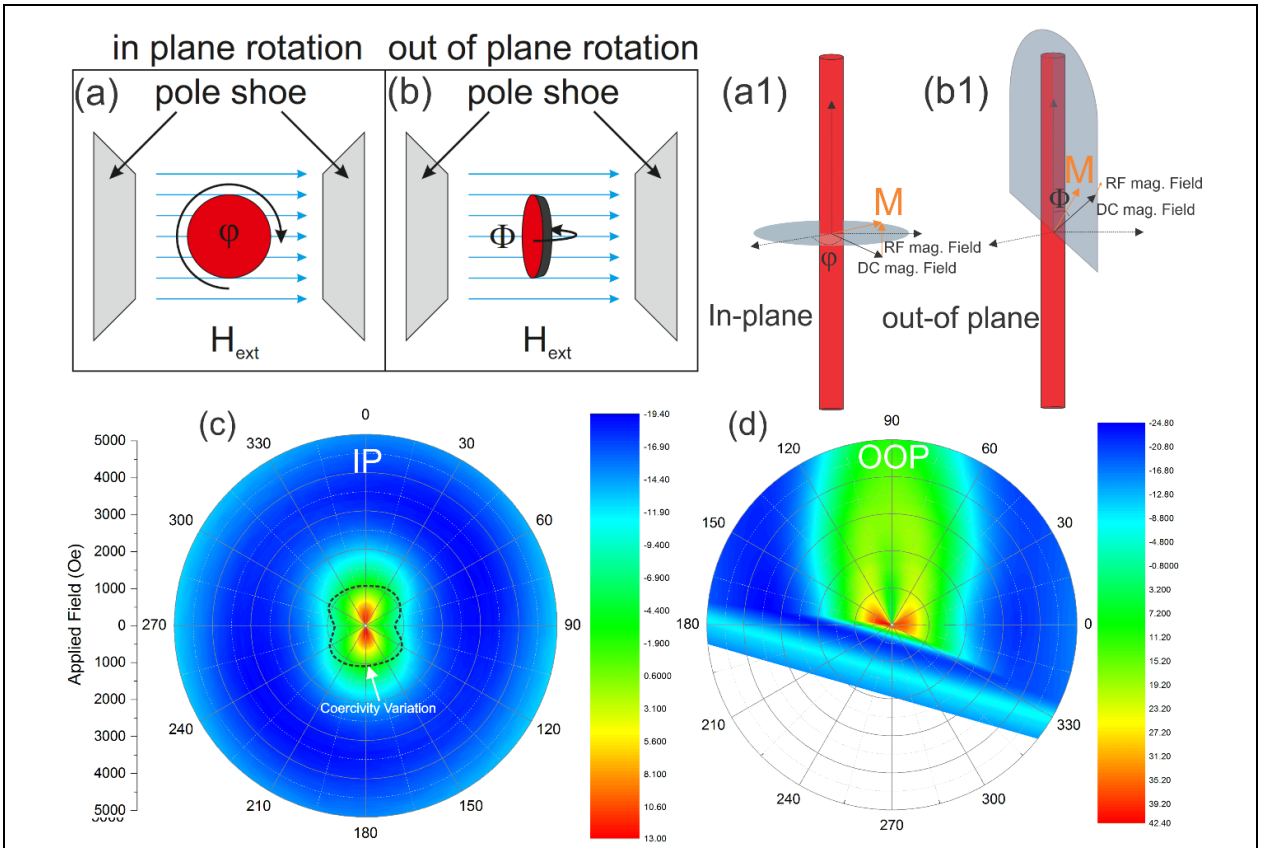


Figure. 9 Schematic diagram of two different orientations for the FMR measurements on the AAO membrane. (a,a1) the φ-scan, in which the external field always lies in a plane perpendicular to the NWs' long axes. (b,b1) the Φ-scan, in which the sample was rotated to an orientation parallel to the long NWs' axes. (c) FMR results for in-plane (IP) rotation, IP coercivity (H_c) is represented by a black dotted line (d) FMR results for out-of-plane (OOP) rotation.

The slight variation in the c-axis orientations result in different resonance fields, which correspond to different switching-field distributions, as also seen in the FORC measurements (see figure 7 (d)). In both geometries for the Co-Pt NWs a very broad FMR linewidth (~6 kOe) was observed, which indicates that the system consists of a large number of small grains with slightly different anisotropies, different c-axis orientations, or both. In such a case the linewidth broadening may be expressed as an inhomogeneity line broadening (ILB) and is frequency independent. For large inhomogeneities in the sample, the precession becomes localized and the FMR spectrum approaches that of a local precession on independent grains [18]. With respect to the ILB, the FMR spectrum comes from the superposition of many local FMR profiles arising from the different orientations of the c-axis in each grain in the NWs. It is worth mentioning that inhomogeneities are also the basis for two magnon scattering (TMS) processes [45], also a contributor to the FMR linewidth broadening. In a TMS process, local inhomogeneities such as size variation (length and diameter), non-uniform grain-to-grain anisotropy, and grain boundaries, can break the orthogonality between the driven FMR mode and other degenerate spin-wave modes.

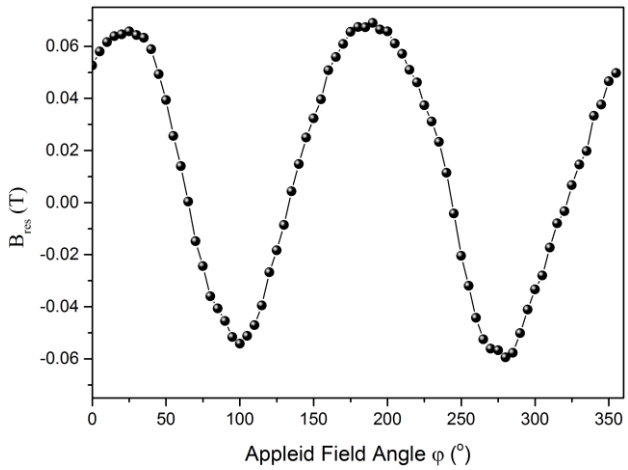


Figure. 10 FMR resonance fields for the IP measurement, determined by fitting the experimental data.

Although the quantification of the inhomogeneities will require further analysis of the FMR data, it is strongly believed that the observed large linewidth shown in figure 9 (c) is mainly due to disorientations of the c-axis in the IP configuration (figure 5 (c)). However, the homogeneous and inhomogeneous contributions to the FMR linewidth are a combined effect of the exchange interactions and the spin-orbital coupling, and can be extracted from the following relation [46]

$$\Delta H_{pp} = \Delta H_{inhomo} + \Delta H_{homo} = \Delta H_{inhomo} + \frac{2}{\sqrt{3}}\alpha\frac{\omega}{\gamma} \qquad (3)$$

where ΔH_{pp} is the FMR linewidth, $\gamma = \frac{g\mu_B}{\hbar}$ is the gyromagnetic ratio, $\alpha = \frac{G}{\gamma\mu_o M_s}$ is the dimensionless Gilbert damping constant, G is the Gilbert damping parameter, and ω is the microwave frequency. It seems that a broad linewidth is a common characteristic of high MCA materials like Co-Pt [47]. These results allow us to conclude that there is a variation in the orientation of the c-axis in the plane perpendicular to the NW's long axis. The exact magnitude of the effective anisotropic field was hard to determine because of two factors: (1) the FMR signal is partially below zero and (2) the very large linewidth. However, for an estimation of the effective anisotropy field we fitted the experimental data with a deviated Lorentz function to determine the resonance fields, as shown in figure 10. From these results we have obtained an effective anisotropy field of about 120 mT (≈95.5 kA/m) and hence the effective anisotropy constant K_{eff} ≈4x10^4 J/m^3, which is in agreement with our previous findings using a different method [24].

3.5 Magnetic domain configuration in individual Co-Pt NWs

Individual Co-Pt NWs were obtained after dissolving the AAO membrane to perform zero-field MFM measurements. More than 45 Co-Pt NWs were investigated, from which selective results are shown here. The MFM measurements on the Co-Pt NWs presented here are an extension of our previous investigation [24]. The NWs are categorized into three distinct groups, depending on the similarity in their MFM contrast. The Co-Pt NWs in figure 11 (a)-(g) show a periodic dark-and-bright MFM contrast along their lengths. The observed MFM contrast can be well understood if we consider that the c-axis lies perpendicular to the NWs' long axes. In the case when a MFM image consisting of a complementary dark-and-bright contrast spanning the two ends of the NW is observed [48], this suggest that the magnetization is along the length of the wire, and thus the shape anisotropy dominates. In the present case the magnetization modulation originates from the competition between the MCA and the shape anisotropy in the wire. The MCA tends to align the magnetization in the plane perpendicular to the NW long axis, whereas the shape anisotropy tends to align them parallel to the wire's long axis. It is clear from figure 11 (a)-(g) that in hcp Co-Pt NWs the MCA is significantly larger than the shape anisotropy due to the preferential orientation of the c-axis, pointing perpendicular to the long axis of the NW (figure 3 (b)). In figure 11 (a) the dark-and-bright contrast reveals a rapid alternation of pairs of diametrically opposed

dark-and-bright contrasts along the lengths of the NWs; however, in figure 11 (d), this alternation is also along the short axis of the NWs. We believe that both contrasts originate from the same magnetic state (transverse stripes, TS—figure 11 (d)) of the NWs and will be discussed later. It is important to note that in figure 11 (a) and (d) the magnetization modulation is consistent along the length of the NWs, which can be attributed to a uniaxial c-axis orientation along the whole length of the NWs (see figure 4 (b)). However, in other NWs in figure 11 there is a slight variation in the magnetization modulation, which can be ascribed to a variation in the c-axis orientation in some segments of the NWs. For example, the lower segment of figure 11 (b) and (c) is believed to have a TS magnetic configuration; however, the upper part reveals a longitudinal stripes configuration (LS—figure 11 (i)).

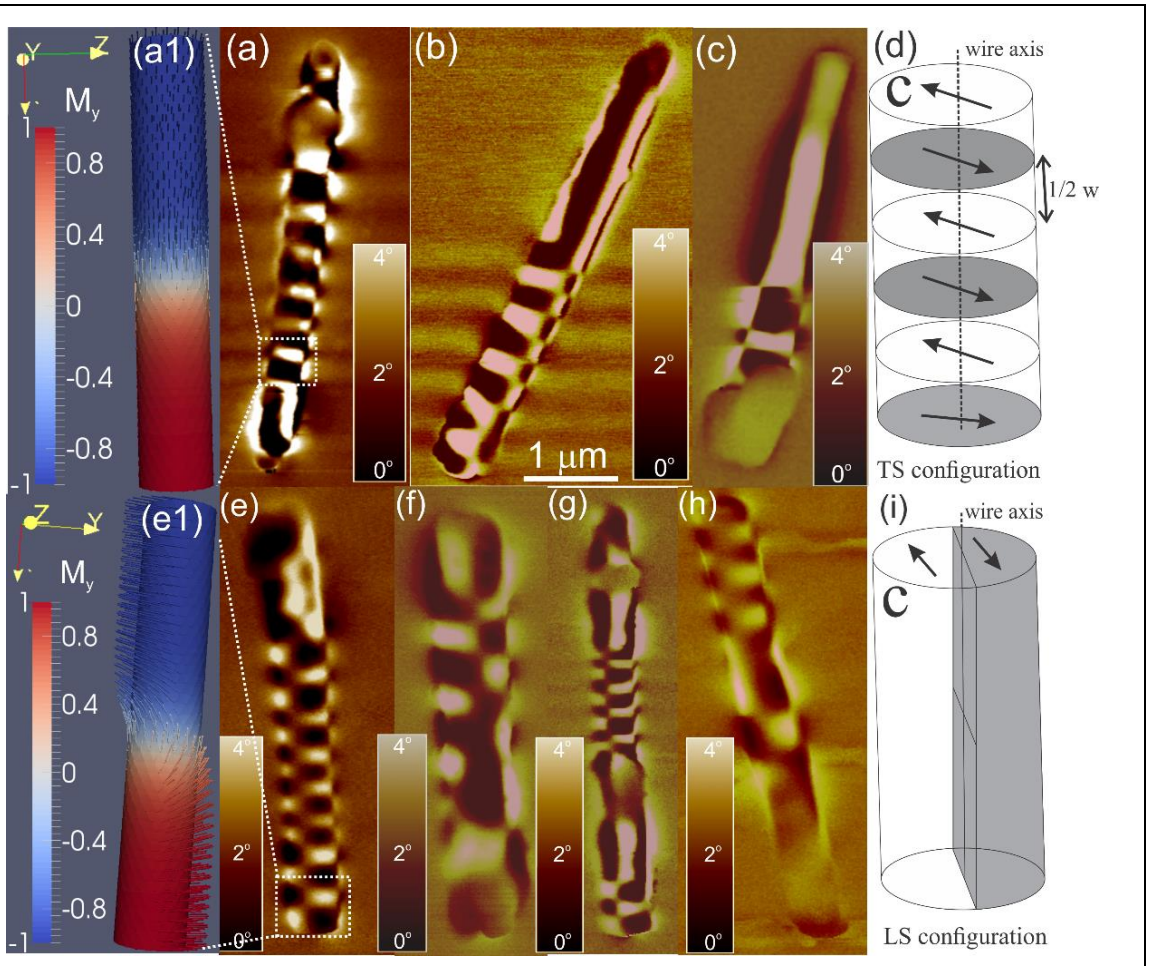


Figure. 11 (a)-(c) and (e)-(h) The experimental MFM images of individual Co-Pt NWs with a diameter of ~250 nm. Upper row shows dark-and-bright contrast along the length of the NW, while in the lower row the contrast is along the short axis of the NW. (a1) and (d1) NMAG simulation images of the magnetization profile in a small segment of the NW at two different angles (90º). (d) and (i) transverse stripe and longitudinal stripe configuration. Figure 11 (a) and (b) are reproduced with permission from Copyright Clearance Center, 2015, under license number 3734280795078.

The average period of the modulation between two dark or bright regions (w_{ave}) for all the NWs in figure 11 is found to be relatively small (≈400 nm); it is believed to minimize the demagnetization energy and is plotted as square points in figure 12. The period of the modulation is seen to depend monotonically on the wire's diameter (D) and can be successfully described using an adapted partial Landau-Kittle stripe-domains equation [23], as shown by the solid line in figure 12. There is an excellent agreement between the calculated and the experimental periods of the modulation (w). More detail about this topic can be found in our previous publication [24]. The periodic domain structures in the NWs have been under intense investigation by many groups, but unfortunately most of the reports are theoretical in nature [22, 23, 49], thus there is a need for further experimental work. Possible applications of periodic domain

structures can be found in spintronics, since the periodic character will introduce gaps in the spin-wave dispersion relation [49]. With the application of an external magnetic field it is possible to tune the nature of the gaps, and subsequently the dispersion relation, which is of great interest from the point of view of device applications.

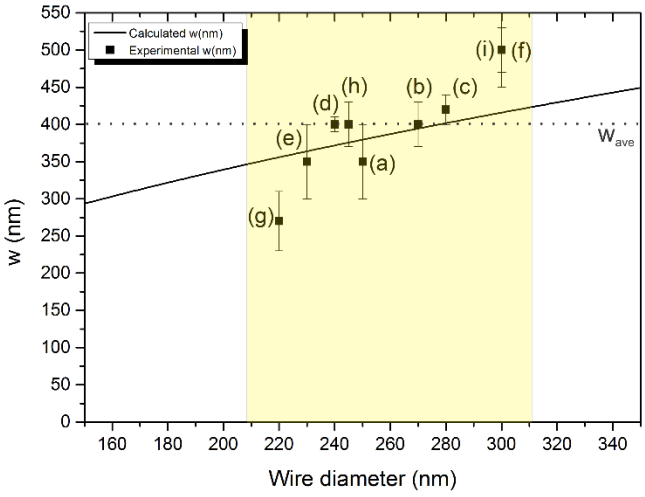


Figure. 12 Period of the modulation (w) of the periodic domain structures of Co-Pt NWs as a function of wire diameter. Calculated (solid line) and experimental (square points).

Another set of NWs with similar MFM contrast (a stripe-like domain structure) along their length was observed as shown in figure 13 (a)-(e). A strong similarity exists between the NWs in figure 13 (a)-(e) and hcp (0001) Co films with a strong out-of-plane crystal anisotropy (K_u) and a thickness larger than 50 nm [50]. In such films, perpendicularly magnetized, stripe-shaped domains oriented up and down with a 180° Bloch wall in between were observed [50], strongly correlated with figure 13 (a)-(e). These MFM contrasts qualitatively resemble the longitudinal invariant magnetic configuration (LS) shown in figure 11 (i).

In figure 13 (f)-(k) an alternating dark-and-bright contrast is seen across the NW diameter with an elongation along the length of the NW. For instance, in figure 13 (j) the MFM contrast changes alternatively along the whole length of the NW. The period of modulation (1 μm) in these NWs is much larger than the previously observed wires (figure 11). This contrast can be attributed to a c-axis orientation tilt at a small angle from the perpendicular plane of the NW's long axis. Ivanov *et al.* [21] have performed MFM measurements on hcp Co NWs and found a similar contrast, which was explained using micromagnetic simulations as an asymmetric, vortex-like configuration with an alternating chirality along the length of the NW, and we find their explanation plausible also for our case. Thus, in these NWs the c-axis orientation is tilted at a certain angle from perpendicular to the NW's long axis, as shown in figure 4 (b), and will not be discussed further here.

Moreover, three-dimensional finite-element calculations with the Nmag simulation tool [51] on a magnetic cylinder, carrying a uniaxial transverse crystal anisotropy $K_u=1\text{x}10^6$ J/m^3 with other material parameters $A=1.6\text{x}10^{-11}$ A/m and $M_s\approx 8\text{x}10^5$ A/m are currently in progress. The simulation results, so far, on a small cylinder (diameter=10 nm, length=60 nm) have already shown that the TS configuration is indeed the lowest energy state, as shown in figure 11 (a1), which is in excellent agreement with the present observations. It is also shown that due to the physical rotation of the NWs the MFM contrast can change (figure (a1) and (e1)), which may explain the contrasts in figure (a) and (e). Interestingly, the simulation data have also shown that the TS and LS configurations have almost equal magnetic energies, although TS appears to be the most favoured for the NWs in figure 11 and LS in the NWs in figure 13 (a)-(e). This may also explain why these two configurations simultaneously exist in a NW, as shown figure 11 (b) and (c). Further work is indeed needed to fully understand these magnetic domain patterns in the NWs. From the experimental point of view, the focus must be based on the complex microstructure of the NWs and the exact knowledge of the c-axis orientation of hcp crystallites. To summarize, a small variation in the c-axis orientation in hcp Co-Pt NWs can

significantly influence the magnetic domains and the magnetization processes, e.g., the switching-field distribution and the FMR linewidth, as described in previous sections.

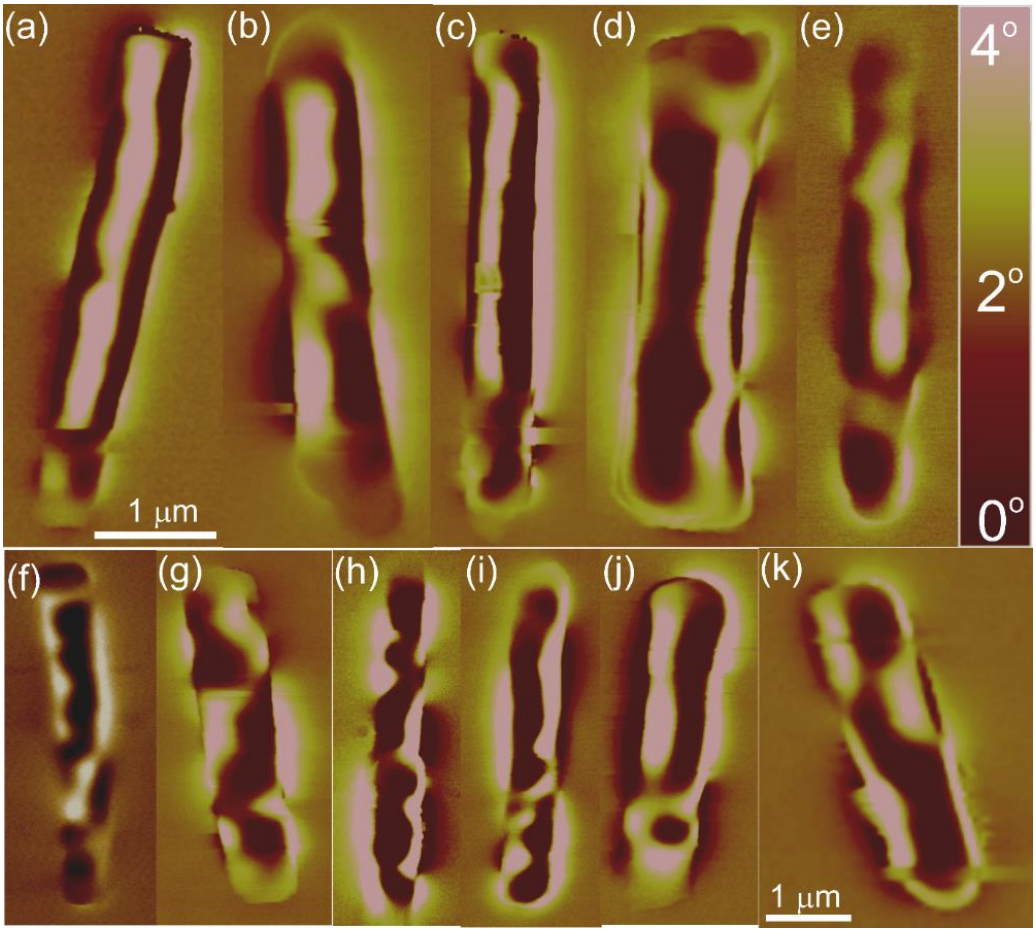


Figure 13 a-k Experimental MFM images of individual Co-Pt NWs with a diameter of ~250 nm. Upper row shows a stripe-like contrast along the whole length of the NW, while in the lower row alternating dark-and-bright contrast along the short axis of the NW is observed.

4. Conclusion

In conclusion, we found that the preferential orientation of the hcp c-axis in Co-Pt NWs can be adjusted to be perpendicular to the NWs' long axes by choosing a large pore diameter ($D_p \approx 240$) and the right deposition conditions (e.g., a high Co content in the electrolyte). Small variations in the orientation of the hcp c-axis in the perpendicular plane of the NWs' long axes are due to the "oblivious" electrodeposition, including a small deposition fluctuation, e.g., the pore diameter, etc. Hcp Co-Pt NWs have a high MCA, which is stronger than the shape anisotropy, thus small fluctuations in the c-axis orientations can significantly affect the magnetic properties of the Co-Pt NWs. Therefore, the characterization of an individual element can be washed out in the measurements of ensembles. This study highlights the importance of the influence of the hcp c-axis orientation in high-anisotropy materials and the need for their quantitative analysis in order to fully understand and improve their final magnetic properties. The results of the micromagnetic simulations so far indicate that the TS and LS domain structures are the most energetically favourable states when the MCA and the shape anisotropy are at 90°, while at reduced angles, the vortex-like domain structure

becomes more favourable. Indeed, more work needs to be done in this area to fully understand the magnetic domain structures in NWs with a strong perpendicular MCA.

Acknowledgements

This work was funded by the Slovenian Research Agency (ARRS) under project number PR-04442 and funding from Communidad de Madrid under project Nanofrontmag S2103/MIT-2850. M. P. Proenca acknowledges FCT for grant SFRH/BPD/84948/2012 supported by funding POPH/FSE. Arshad would like to thank Dr. Jana Fercic, Asst. Prof. Aleksander Recnik, Asst. Prof. Nina Daneu, and Jure Strle for fruitful discussions about the XRD results and the preparation of the MFM substrate.

References

[1] Y. Henry, K. Ounadjela, L. Piraus, S. Dubois, J.-M. George and Duvail a J-L 2001 *Magnetic anisotropy and domain patterns in electrodeposited cobalt nanowires EPJ B* **20** 35-44

[2] Parkin S and Yang S-H 2015 *Memory on the racetrack Nat Nano* **10** 195-198

[3] Hayashi M, Thomas L, Rettner C, Moriya R and Parkin S S P 2007 *Direct observation of the coherent precession of magnetic domain walls propagating along permalloy nanowires Nat. Phys.* **3** 21-25

[4] Hayashi M, Thomas L, Rettner C, Moriya R, Jiang X and Parkin S S P 2006 *Dependence of Current and Field Driven Depinning of Domain Walls on Their Structure and Chirality in Permalloy Nanowires Phys. Rev. Lett.* **97** 207205

[5] Allenspach R and Jubert P O 2006 *Magnetic domain walls in nanowires Mrs Bull* **31** 395-399

[6] Sayama J, Shimatsu T, Nemoto H, Okamoto S, Kitakami O and Aoi H 2011 *Temperature dependence of the magnetic properties of $L1_1$-type Co–Ni–Pt ordered alloy films for thermally assisted recording media J. Appl. Phys.* **110** 013918-013923

[7] Ohtake M, Suzuki D, Kirino F and Futamoto M 2013 *Metastable Ordered Phase Formation in CoPt and Co_3Pt Alloy Thin Films Epitaxially Grown on Single-Crystal Substrates IEICE T Electron* **E96-C** 1460-1468

[8] Harp G R, Weller D, Rabedeau T A, Farrow R F C and Toney M F 1993 *Magneto-optical Kerr spectroscopy of a new chemically ordered alloy: Co_3Pt Phys. Rev. Lett.* **71** 2493-2496

[9] Zana I, Zangari G, Park J-W and Allen M G 2004 *Electrodeposited Co–Pt micron-size magnets with strong perpendicular magnetic anisotropy for MEMS applications J. Magn. Magn. Mater.* **272-276** E1775-E1776

[10] Hongyu S, Xiaohong L, Yan C, Defeng G, Yanwu X, Wei L, Baoting L and Xiangyi Z 2009 *Diameter- and current-density-dependent growth orientation of hexagonal CdSe nanowire arrays via electrodeposition Nanotechnology* **20** 425603

[11] Forster H, Schrefl T, Dittrich R, Suess D, Scholz W, Tsiantos V, Fidler J, Nielsch K, Hofmeister H, Kronmuller H and Fischer S 2002 *Magnetization reversal in granular nanowires IEEE Trans. Magn.* **38** 2580-2582

[12] Ivanov Y P, Vázquez M and Chubykalo-fesenko O 2013 *Magnetic reversal modes in cylindrical nanowires J. Phys. D: Appl. Phys.* **46** 485001-485012

[13] Xianghua H, Qingfang L, Jianbo W, Shiliang L, Yong R, Ronglin L and Fashen L 2009 *Influence of crystal orientation on magnetic properties of hcp Co nanowire arrays J. Phys. D: Appl. Phys.* **42** 095005-095009

[14] Escrig J, Altbir D, Jaafar M, Navas D, Asenjo A and Vázquez M 2007 *Remanence of Ni nanowire arrays: Influence of size and labyrinth magnetic structure Phys. Rev. B* **75**

[15] Pirota K R, Béron F, Zanchet D, Rocha T C R, Navas D, Torrejón J, Vazquez M and Knobel M 2011 *Magnetic and structural properties of fcc/hcp bi-crystalline multilayer Co nanowire arrays prepared by controlled electroplating J. Appl. Phys.* **109** 083919

[16] Clime L, Zhao S-Y, Normandin F and Veres T 2007 *Characterization of ferromagnetic nanowires by partial first order reversal curves J. Appl. Phys.* **102** 063903

[17] Dobrotă C-I and Stancu A 2015 *Tracking the individual magnetic wires' switchings in ferromagnetic nanowire arrays using the first-order reversal curves (FORC) diagram method Physica B: Condensed Matter* **457** 280-286

[18] McMichael R D, Twisselmann D J and Kunz A 2003 *Localized Ferromagnetic Resonance in Inhomogeneous Thin Films Phys. Rev. Lett.* **90** 227601

[19] Hassel C, Brands M, Lo F Y, Wieck A D and Dumpich G 2006 *Resistance of a Single Domain Wall in (Co/Pt)$_7$ Multilayer Nanowires Phys. Rev. Lett.* **97** 226805-226810

[20] Henry Y, Ounadjela K, Piraux L, Dubois S, George J M and Duvail J L 2001 *Magnetic anisotropy and domain patterns in electrodeposited cobalt nanowires European Physical Journal B* **20** 35-54

[21] Ivanov Y P, Vivas L G, Asenjo A, Chuvilin A, Chubykalo-fesenko O and Vázquez M 2013 *Magnetic structure of a single-crystal hcp electrodeposited cobalt nanowire Europhys. Lett.* **102** 17009-17014

[22] Gerd Bergmann, Jia G. Lu, Yaqi Tao and Thompson R S 2008 *Frustrated Magnetization in Co nanowires: Competition between crystal anisotropy and demagnetization energy Phys. Rev. B* **77** 054415-054420

[23] Kristof M Lebecki and Donahue M J 2010 *Comment on "Frustrated magnetization in Co nanowires: Competition between crystal anisotropy and demagnetization energy" Phys. Rev. B* **82** 096401-096405

[24] Arshad M S, Šturm S, Zavašnik J, Espejo A, Escrig J, Komelj M, McGuiness P, Kobe S and Rožman K 2014 *Effect of magnetocrystalline anisotropy on the magnetic properties of electrodeposited Co–Pt nanowires J Nanopart Res* **16** 1-16

[25] Zuwei Liu, Pai-Chun Chang, Chia-Chi Chang, Evgeniy Galaktionov, Gerd Bergmann and Lu J G 2008 *Shape Anisotropy and Magnetization Modulation in Hexagonal Cobalt Nanowires Adv. Funct. Mater.* **18** 1573-1578

[26] Rietveld H 1969 *A profile refinement method for nuclear and magnetic structures J. Appl. Crystallogr.* **2** 65-71

[27] Cullity B D and Stock S R 2001: Prentice-Hall Inc. New Jersey)

[28] Arshad M S, Pecko D, Sturm S, Escrig J, Komelj M, McGuiness P J, Kobe S and Rozman K Z 2014 *Angular Dependence of the Coercivity in Electrodeposited Co-Pt Nanostructures With a Tube-Wire Morphology IEEE Trans. Magn.* **50** 1-4

[29] Tian M L, Wang J U, Kurtz J, Mallouk T E and Chan M H W 2003 *Electrochemical growth of single-crystal metal nanowires via a two-dimensional nucleation and growth mechanism Nano Lett.* **3** 919-923

[30] Motoyama M, Fukunaka Y, Sakka T and Ogata Y H 2007 *Initial stages of electrodeposition of metal nanowires in nanoporous templates Electrochim. Acta* **53** 205-212

[31] Florian M, Joachim B, Shafqat K, Maria Eugenia Toimil M, Christina T and Hartmut F 2007 *Preferred growth orientation of metallic fcc nanowires under direct and alternating electrodeposition conditions Nanotechnology* **18** 135709-135716

[32] Zhang J-M, Wang D-D and Xu K-W 2006 *Calculation of the surface energy of hcp metals by using the modified embedded atom method Appl. Surf. Sci.* **253** 2018-2024

[33] Podlogar M, Richardson J J, Vengust D, Daneu N, Samardžija Z, Bernik S and Rečnik A 2012 *Growth of Transparent and Conductive Polycrystalline (0001)-ZnO Films on Glass Substrates Under Low-Temperature Hydrothermal Conditions Adv. Funct. Mater.* **22** 3136-3145

[34] Mallet J, Yu-Zhang K, Chien C-L, Eagleton T S and Searson P C 2004 *Fabrication and magnetic properties of fcc Co_xPt_{1-x} nanowires Appl. Phys. Lett.* **84** 3900-3902

[35] Vega V, Böhnert T, Martens S, Waleczek M, Montero-Moreno J M, Görlitz D, Prida V M and Nielsch K 2012 *Tuning the magnetic anisotropy of Co-Ni nanowires: comparison between single nanowires and nanowire arrays in hard-anodic aluminum oxide membranes Nanotechnology* **23** 465709-465709

[36] Shamaila S, Sharif R, Riaz S, Ma M, Khaleeq-ur-Rahman M and Han X F 2008 *Magnetic and magnetization properties of electrodeposited fcc CoPt nanowire arrays J. Magn. Magn. Mater.* **320** 1803-1809

[37] Cortés M, Gómez E and Vallés E 2013 *Electrochemical growth of CoPt nanowires of different aspect ratio and their magnetic properties J. Electroanal. Chem.* **689** 69-75

[38] Escrig J, Altbir D, Jaafar M, Navas D, Asenjo A and Vázquez M 2007 *Remanence of Ni nanowire arrays: Influence of size and labyrinth magnetic structure Phys. Rev. B* **75** 184429-184434

[39] Mayergoyz I D 1985 *Hysteresis models from the mathematical and control theory points of view J. Appl. Phys.* **57** 3803-3805

[40] Béron F, Ménard D and Yelon A 2008 *First-order reversal curve diagrams of magnetic entities with mean interaction field: A physical analysis perspective J. Appl. Phys.* **103** 07D908

[41] Béron F, Clime L, Ciureanu M, Ménard D, Cochrane R W and Yelon A 2008 *Magnetostatic Interactions and Coercivities of Ferromagnetic Soft Nanowires in Uniform Length Arrays J. Nanosci. Nanotechnol.* **8** 2944-2954

[42] Proenca M P, Ventura J, Sousa C T, Vazquez M and Araujo J P 2014 *Angular first-order reversal curves: an advanced method to extract magnetization reversal mechanisms and quantify magnetostatic interactions Journal of physics. Condensed matter : an Institute of Physics journal* **26** 116004

[43] Garcia J, Prida V M, Vivas L G, Hernando B, Barriga-Castro E D, Mendoza-Resendez R, Luna C, Escrig J and Vazquez M 2015 *Magnetization reversal dependence on effective magnetic anisotropy in electroplated Co-Cu nanowire arrays J Mater Chem C* **3** 4688-4697

[44] Medina J D, Piraux L, Govea J M O and Encinas A 2010 *Double ferromagnetic resonance and configuration-dependent dipolar coupling in unsaturated arrays of bistable magnetic nanowires Phys. Rev. B* **81**

[45] Mo N, Green J J, Krivosik P and Patton C E 2007 *The low field microwave effective linewidth in polycrystalline ferrites J. Appl. Phys.* **101** 023914

[46] Youssef J B and Brosseau C 2006 *Magnetization damping in two-component metal oxide micropowder and nanopowder compacts by broadband ferromagnetic resonance measurements Phys. Rev. B* **74** 214413

[47] Mo N, Hohlfeld J, ul Islam M, Brown C S, Girt E, Krivosik P, Tong W, Rebei A and Patton C E 2008 *Origins of the damping in perpendicular media: Three component ferromagnetic resonance linewidth in Co–Cr–Pt alloy films Appl. Phys. Lett.* **92** 022506

[48] Darja Pecko, Muhammad Shahid Arshad, Saso Sturm, Spomenka Kobe and Kristina Zuzek Rozman 2015 *Magnetization-switching study of fcc Fe-Pd Nanowire and Nanowire Arrays studied by In-Field Magnetic Force Microscopy IEEE Trans. Magn.* **PP** 1-1

[49] Erickson R P and Mills D L 2009 *Theory of the undulating magnetic ground state of cylindrical cobalt nanowires Phys. Rev. B* **80**

[50] Hehn M, Padovani S, Ounadjela K and Bucher J P 1996 *Nanoscale magnetic domain structures in epitaxial cobalt films Phys. Rev. B* **54** 3428-3433

[51] Fischbacher T, Franchin M, Bordignon G and Fangohr H 2007 *A Systematic Approach to Multiphysics Extensions of Finite-Element-Based Micromagnetic Simulations: Nmag URL: http://nmag.soton.ac.uk/nmag/ IEEE Trans. Magn.* **43** 2896-2898

Chapter 6

Microstructure and Magnetic Properties of Electrodeposited Co-Pt Nanowires (NWs) with Diameters below 100 nm

In this Chapter, article entitled "Microstructure and magnetic properties of electrodeposited Co-Pt nanowires (NWs) with diameters below 100 nm", by **Muhammad Shahid Arshad,** Janez Zavašnik, Sašo Šturm, Paul J. McGuiness, Spomenka Kobe, Kristina Žužek Rožman, [40] is presented. The author contribution to this article is statistical analysis on pore diameter and pore separation of PC membranes, electrodeposition of Co-Pt NWs into three different membranes with diameters 80, 50 and 15 nm, Sample preparation for TEM measurement and data analysis, hysteresis loop measurements and data interpretation, MFM measurements and interpretation of domain structure.
As shown in previous chapters we thoroughly exploited the magnetic properties of Co-Pt nanostructures with diameters 200 nm, in this article we move to diameters below 100 nm. It is well-known that if one of the dimensions of the NWs is reduced to exchange length (~10 nm), interesting magnetic properties can appear. Moreover, for ultra-high density racetrack memory devices, NWs with diameter as small as 30 nm are required.

The central aim of this work was to fabricate Co-Pt NWs with diameter below 100 nm and obtain a similar periodic domain structure as observed in 200 nm. In membranes with large interpore separation, one can exclude the magnetostatic interaction between the NWs, thus the intrinsic magnetic behaviour of the NWs can be extracted from their arrays. Thus for this study, we used low packing density polycarbonate membranes with diameters below 100 nm (80, 50, and 15 nm) to investigate the effect of the microstructure on the magnetic properties of the Co-Pt NWs. We have observed that the crystallographic texturing becomes more pronounced with reduced diameter. This observation made us believe that the pore diameter plays a significant role in texturing of NWs. We observed for NWs with diameter 15 nm the transformation from polycrystalline to single crystal along their length. We have demonstrated that microstructural study obtained in individual Co-Pt NWs of each diameter can explained the magnetic hysteresis loops and also their magnetic domain structure. We were not able to obtain periodic domain structure as dense as in Co-Pt 200 nm but the closest we got was for 80 nm diameter.

This is the author's version of an article that has been published in IEEE MAGNETICS LETTERS. Changes were made to this version by the publisher prior to publication. The final version of record is available at http://dx.doi.org/10.1109/LMAG.2014.2362106

Current Topics

Microstructures and Magnetic Properties of Electrodeposited Co-Pt Nanowires with diameters below 100 nm

Muhammad Shahid Arshad[1,2*], Janez Zavašnik[3], Sašo Šturm[1], Paul McGuiness[1], Spomenka Kobe[1,4*], and Kristina Žužek Rožman[1]

[1]*Jožef Stefan Institute, Department for Nanostructured Materials K7, Ljubljana, Slovenia*
[2]*Jožef Stefan International Postgraduate School, Ljubljana, Slovenia*
[3]*Centre for Electron Microscopy and Microanalysis (CEMM), Ljubljana, Slovenia*
[4]*Center of Excellence on Nanoscience and Nanotechnology (CENN Nanocenter), Ljubljana, Slovenia*
** Member, IEEE*

Corresponding author: Muhammad Shahid Arshad (shahid.arshad@ijs.si)

Abstract— We have investigated the effect of the microstructure on the magnetic properties of Co-Pt nanowires (NWs) with diameters of 15, 50 and 80 nm. These Co-Pt NWs were fabricated by using polycarbonate membranes with different pore diameters via direct electrodeposition. A detailed transmission-electron-microscopy analysis revealed that the Co-Pt NWs transform from a polycrystalline to a single-crystalline-like structure along the growth direction of the NWs. The selected-area electron-diffraction investigation of the Co-Pt NWs with 50-nm diameters revealed a fcc-dominant crystal structure, while the 15- and 80-nm NWs were composed of an intermixture of fcc and hcp phases. This investigation allows us to understand the magnetic hysteresis loops of the Co-Pt NW arrays. Furthermore, the magnetic domains of the individual Co-Pt NWs were studied with magnetic force microscope (MFM) and the MFM contrasts for the 50- and 80-nm diameter NWs are interpreted as consisting of *z*-vortices.

Index Terms— Current Topics, Cobalt alloys, Magnet wire, Magnetic hysteresis, Magnetic anisotropy, Magnetic domains.

I. Introduction

The ever-increasing desire for smaller sensors, actuators and improved data-storage densities have motivated a large research effort to reduce the size of components (T. Thurn-Albrecht et al. 2000). In particular, special attention has been focused on one-dimensional (1D) ferromagnetic materials such as nanowires (NWs) to address not only fundamental physical questions, but also for technological reasons, owing to their potential applications in biosensors (Bauer et al. 2004) and ultra-high-density magnetic storage media (Chu et al. 2005).

In the past several years, electrodeposition into polycarbonate (PC) membranes has been widely used for the synthesis of a large variety of ferromagnetic nanostructures, especially NWs (Tian et al. 2003) made of several different materials. Co-Pt alloy NWs have been investigated for many applications, including high-density recording media (Chu et al. 2005) and magnetic actuators for micro-electro-mechanical systems (MEMS) (Zana et al. 2004). As-deposited Co-Pt alloys can exhibit either a disordered phase (fcc-based $L1_1$-CoPt (Sayama et al. 2011)) or a hcp-based $D0_{19}$-Co_3Pt (Harp et al. 1993) crystal structure, depending on the composition of the nanostructure and the formation conditions. Fcc- and hcp-based structures consist of the atomic stacking sequences ….ABCABC….and …ABAB…, respectively, along the direction normal to the close-packed plane. The crystal structure of Co-Pt alloy nanostructures is known to vary between the two stacking types and may also exist as a mixture (Aboaf et al. 1983). The Co_3Pt hcp structure is a well-known magnetic material with a large magnetocrystalline anisotropy (MCA), comparable to, or even stronger than, the shape anisotropy in NWs (Zana et al. 2004). In many cases, the MCA of the hcp phase favours the easy magnetization axis perpendicular to the NW axis (Cho et al. 2006; Ivanov Yu et al. 2013). However, in polycrystalline fcc structure NWs, the shape anisotropy determines the easy magnetization axis. Furthermore, texturing in the Co-Pt NWs along the easy magnetization axis increases the MCA contribution, thereby reducing the field required to reach saturation magnetization and improve the device's performance (Cho et al. 2006).

The ground-state magnetic domains and domain walls in NWs are the subject of extensive research due to their potential applications in racetrack memory devices (Parkin et al. 2008). However, most published reports have investigated the magnetic domains in pure Co NWs (Ivanov Yu et al. 2013). This means that questions about the magnetic structure in Co-based alloy NWs with different Co contents remain open.

In this study we have investigated Co-Pt NWs fabricated by electrodeposition into the pores of PC membranes with 15-, 50- and 80-nm diameters. The magnetic properties of the NWs with different diameters were investigated and explained on the basis of different anisotropy interplays, resulting from the preferred orientation of the crystalline phases and the shape of the NWs.

II. Experimental Details

Low-porosity PC membranes (Whatman Nuclepore® Co.) with pore diameters of ≈15, 50 and 80 nm were used for the electrodeposition of the Co-Pt-based NWs. A gold (Au) layer

Copyright (c) 2014 IEEE. Personal use is permitted. For any other purposes, permission must be obtained from the IEEE by emailing pubs-permissions@ieee.org.

This is the author's version of an article that has been published in this journal. Changes were made to this version by the publisher prior to publication.
The final version of record is available at http://dx.doi.org/10.1109/LMAG.2014.2362106

(≈100 nm) was sputtered on one surface of the PC membrane to make it conductive and then used as the working electrode (cathode) in a three-electrode cell. The electrolyte consisted of 80 mmol/dm^3 of Co-sulphamate ($Co(SO_3NH_2)_2$) and 20 mmol/dm^3 of Pt-p-salt ($Pt(NH_3)_2(NO_2)_2$), while ammonium citrate ($(NH_4)_2C_6H_6O_7$) (20 mmol/dm^3) and glycin (NH_2CH_2COOH) (0.2 mmol/dm^3) were used as the complexing agents. The pH of the electrolyte was set to 8 using ammonia. A Pt mesh electrode was used as the anode, and potentiostatic conditions with -2.1 V against a reference electrode of Ag/AgCl were used to deposit the metal ions into the pores of the PC membrane to obtain the Co-Pt NWs. Thirty minutes of electrodeposition were sufficient for the deposition of NWs and this time was fixed for all the experiments.

A field-emission-gun scanning electron microscope (FEG-SEM; Jeol JSM-7600F) was used to study the PC membrane and also provided us information about the morphology of the NWs. The composition and crystal structure of the Co-Pt NWs were investigated with a transmission electron microscope (TEM; JEOL JEM-2010F). To obtain individual NWs, the PC membrane was dissolved in dichloromethane and the NWs were released using an ultrasound bath. The Co-Pt NWs were then dispersed in absolute ethanol and sprinkled onto Cu-grids and dried. The chemical compositions of the Co-Pt NWs were determined with an energy-dispersive X-ray spectrometer (EDXS). The crystal structures and the local ordering of the crystallites of the Co-Pt NWs were determined using the selected-area-electron-diffraction (SAED) technique.

The magnetic measurements were performed using a vibrating-sample magnetometer (VSM) at RT. For the magnetic hysteresis loops the field was applied perpendicular and parallel to the NW axis direction in the range of ±1200 kA/m. For the magnetic force microscopy (MFM) measurements a drop of ethanol containing Co-Pt NWs was placed on a clean Si wafer and then dried. After a single NW was selected, a commercial scanning probe microscope (Digital Instruments Dimension 3100) was used for the MFM measurements. The MFM cantilever (Nanoworld MFMR type probe) was used in lift mode. The tip magnetization direction was perpendicular to the plane of the Si substrate, on which the NW was placed horizontally. All the MFM images of the NWs were obtained at a constant scanning height of ≈60 nm.

III. Results and Discussion

Fig. 1 (a) shows a SEM image of a typical low-porosity PC membrane (top view) with a diameter 80 nm to provide a clear indication of the distribution of the pores. It is clear that the pore diameters of the membrane are consistent but the interpore distances have a broad distribution. In order to check the homogeneity of the pores' diameters and the interpore separations a statistical analysis was performed on a PC membrane with diameters of 15, 50 and 80 nm and the results are shown in **Table. 1**. Fig. 1 (b) shows an SEM image of the Co-Pt NW arrays grown in the PC membrane with an 80-nm diameter. It is clear that the NWs are robust, erect, regular cylinders with a length of 2–4 μm and a diameter of 80±8.7 nm, which is consistent with the pore diameters of the membrane. A similar length was observed for the other diameters (15 and 50 nm) as well. However, the NWs are misaligned perpendicularly to the PC membrane plane and the majority of the NWs are tilted randomly by a few degrees with respect to the normal to the membrane plane.

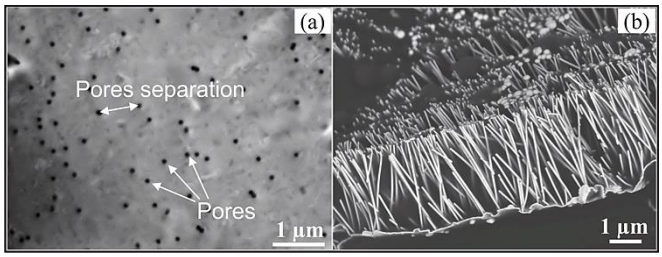


Fig. 1. (a) SEM image of PC membrane with 80-nm diameter pores. (b) SEM image of Co-Pt NWs grown in PC membrane with 80 nm diameter.

The analysis of the PC membrane in **Table 1** explained that the average interpore separation between the NWs is much larger (~6x) than the wire diameters, and so we can consider that the dipolar interaction between the NWs is smaller than the shape anisotropy and the MCA (Laroze et al. 2007), which is explained later.

Table 1. Diameter of the pores ϕ (nm), interpore separation d (nm), composition, at.%, crystal structure, magnetization easy axis (EA), H_c (kA/m) and SQ of Co-Pt NWs

ϕ (nm)	d (nm)	Comp.(at %)	Cryst. Struct.	EA	(H_c∥ / H_c⊥) (kA/m)	SQ∥/SQ⊥
80±8.7	418±189	$Co_{73\pm5}Pt_{27\pm5}$	hcp+fcc	⊥	26.2/30	0.1/0.17
50±7.8	254±114	$Co_{42\pm2}Pt_{58\pm2}$	fcc	∥	15.7/ 20.5	0.3/0.18
15±5.1	129±43	$Co_{95\pm2}Pt_{5\pm2}$	hcp+fcc	⊥	52/38.5	0.17/0.28

Fig. 2 (a) shows a TEM image of a Co-Pt NW with a 15-nm diameter after the removal of the PC membrane. It is clear that the diameter is uniform along the length of the NW. The SAED patterns Df1 and Df2 were recorded from the corresponding marked areas on the NW shown in Fig. 2 (a). The Df1 pattern, exhibiting complete, closed diffraction rings, indicates a large quantity of randomly oriented crystallites, composing one single NW, while Df2 corresponds to a single-crystal-like diffraction pattern. The enlarged Df1 area in Fig. 2 (b) reveals that the average grain size is ≈10 nm, which is found to gradually increase along the growth direction of the NW. In order to determine the crystal structure of the nanowire Df1 was fitted to the Co-Pt fcc simulated rings, which match well (see Fig.2). It is important to note that some of the intensities in Df1 do not fit to the Co-Pt fcc simulation rings and correspond to the Co-Pt hcp phase. For instance, one can see in Fig. 2 (b), the white parallel lines represent the Co-Pt hcp stacking faults, which also contribute to the diffraction rings. Df2 was taken in the zone axis $[100]_{fcc}$ and the corresponding fcc crystal planes are presented in Fig. 2. Such an analysis indicates that the growth of the NW starts with random nucleation, which gradually transitions into a single-crystal-like NW at the conclusion of the growth. The growth mechanism of such NWs is well described in (Huang et al. 2010).

Copyright (c) 2014 IEEE. Personal use is permitted. For any other purposes, permission must be obtained from the IEEE by emailing pubs-permissions@ieee.org.

This is the author's version of an article that has been published in this journal. Changes were made to this version by the publisher prior to publication.
The final version of record is available at http://dx.doi.org/10.1109/LMAG.2014.2362106

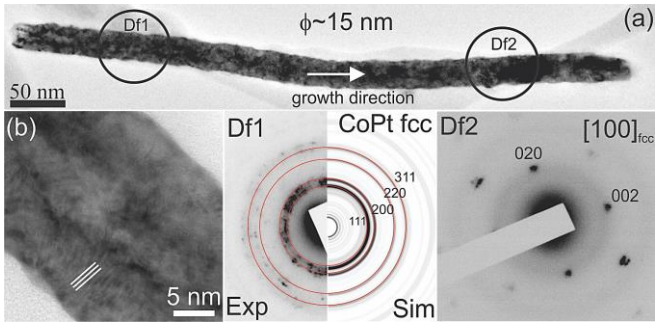


Fig. 2. (a) TEM micrograph of 15-nm diameter NW with corresponding SAED patterns (Df1 and Df2) taken along the growth direction of the NW. (b) Enlarged area of Df1, showing the size of the individual grains.

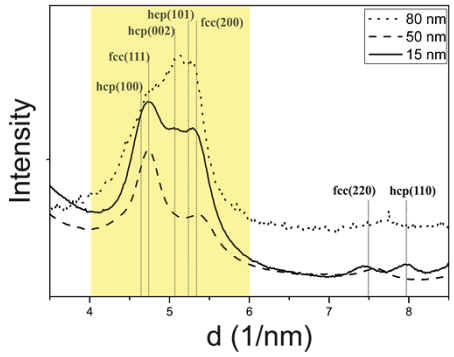


Fig. 3. Intensity profile of the rotational average of the SAED patterns for Co-Pt NWs with 15-, 50- and 80-nm diameters.

The crystal phases of the Co-Pt NWs with 15-, 50- and 80-nm diameters were determined by rotational averaging of the SAED patterns, as shown in Fig. 3. This is because we can easily distinguish between the Co-Pt fcc and hcp phases using their d-values. Such an analysis revealed that Co-Pt NWs with a 50-nm diameter have only the Co-Pt fcc phase present, as evidenced by only two fcc peaks in the highlighted region of Fig. 3, whereas NWs with 15- and 80-nm diameters consist of an intermixture of fcc and hcp phases. A further analysis of the Co-Pt NW with a 50-nm diameter revealed that the $[111]_{fcc}$ crystal directions are orientated at an angle ≈50° with respect to the NWs' axes (not shown here). The observed crystal structures for the Co-Pt NWs with 15-, 50-, and 80-nm diameters are in accordance with the Co-Pt phase diagram (Wang et al. 2010). The composition of the NWs can be influenced by the template geometry due to the different diffusion rates of the ions into different pore geometries. For instance, the 15-nm diameter NWs are Co rich (see Table 1) due to the slow diffusion of the large Pt ions into the nanopores. However, we observed an anomaly in the 50-nm diameter NWs, where the Co composition is lower than the 80-nm diameter NWs. We believe such anomalies can be explained on the basis of interacting parameters between the mass transport and the reduction of ions, such as the number of active nucleation sites and field of electrical double layer.

Fig. 4 (a), (b) and (c) show the hysteresis loops measured for Co-Pt NW arrays with 15-, 50- and 80-nm diameters in two field directions. For the Co-Pt NW arrays with 15- and 80-nm diameters, a clear perpendicular easy magnetization axis was obtained; this is in contrast to the 50-nm diameter NWs, where isotropic hysteresis loops were observed. According to the TEM analysis in the 15- and 80-nm NWs the c-axis of the hcp phase is preferably orientated perpendicular to the NWs axis. Thus, the perpendicular magnetization easy axis can be attributed to the strong hcp MCA. However, for the Co-Pt NWs with the 50-nm diameter, the fcc phase was obtained with the MCA easy axis (which is along the [111] crystal direction (Razee et al. 1997)) at ≈50° with respect to the NW axis. The isotropic behavior can be ascribed to the competition between the MCA and the shape anisotropy. It is important to note that for all the diameters of the NWs, there is competition between the MCA and the shape anisotropy.

The highest coercivity (see Table 1) was obtained for the Co-Pt NWs with a 15-nm diameter, which is expected due to the presence of the hcp phase having a high MCA and probably a single-domain structure, due to the small diameter. The lowest coercivity was found for the 50-nm diameter NWs, which can be attributed to the existence of the fcc phase with a low MCA. A low SQ ($=M_r/M_s$) was observed for all the diameters, which appears to be common to all the arrays obtained using commercial membranes (Ciureanu et al. 2005).

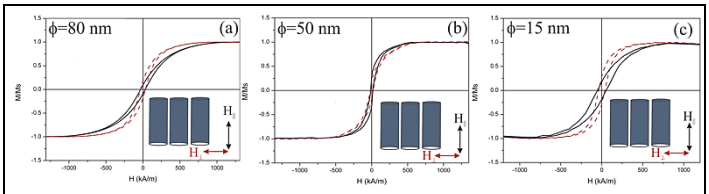


Fig. 4. (a), (b) & (c) Magnetic hysteresis loops of the Co-Pt NW arrays with d = 80, 50 and 15 nm, respectively, measured with an applied field parallel (solid line) and perpendicular (dotted line) to the NWs axis.

Fig. 5 (a)-(g) shows the AFM/MFM measurements on individual Co-Pt NWs with 15-, 50- and 80-nm diameters at the remanence state with two magnetization directions of the tip. In Fig. 5 (a) & (b) it is clear that the MFM contrast is complementary and there is a periodic dark and bright MFM contrast in the middle part of the NW. In contrast, at the two edges of the NW, the dark and bright contrast is along the radial direction, similar to what was observed along the whole length of the 50-nm diameter NW, as shown in Fig. 5 (c) & (d). It has been demonstrated with micromagnetic simulations in NWs with competition between the shape anisotropy and the MCA and a diameter below 150 nm that they can have *z*-vortex magnetization states as the ground state (Kristof M Lebecki et al. 2010). A schematic of the *z*-vortex is presented in Fig. 5 (h). The periodic MFM contrast in Fig. 4 (a)–(d) can be originated from the *z*-vortex state with different chirality and/or from the interfaces between the vortices (Ivanov Yu et al. 2013). The vortex state usually has a closed flux configuration (CurlM=0) and it is difficult to observe with MFM, but the z-vortex state of the NWs with a strong magnetocrystalline anisotropy can be observed by MFM due to the asymmetry of the vortex shell (Ivanov Yu et al. 2013). A vortex-like domain structure has also been observed experimentally by some other authors (Ivanov Yu et al. 2013) for Co NWs. Note that the contrast in Fig. 5 (c)

Copyright (c) 2014 IEEE. Personal use is permitted. For any other purposes, permission must be obtained from the IEEE by emailing pubs-permissions@ieee.org.

This is the author's version of an article that has been published in this journal. Changes were made to this version by the publisher prior to publication.
The final version of record is available at http://dx.doi.org/10.1109/LMAG.2014.2362106

and (d) at point 2 remains the same, which can be ascribed to the strong interaction between the tip and the NW. In Fig. 5 (f) and (g) a uniform, dark MFM contrast was observed along the length of the 15-nm diameter NW, which was not reversed upon the reversal of the tip magnetization, except on the two edges. Such a contrast has been ascribed to the susceptibility contrast. Further simulation work would be needed to fully understand these magnetic domain configurations in Co-Pt NWs; with this in mind, micromagnetic modeling is planned for the future.

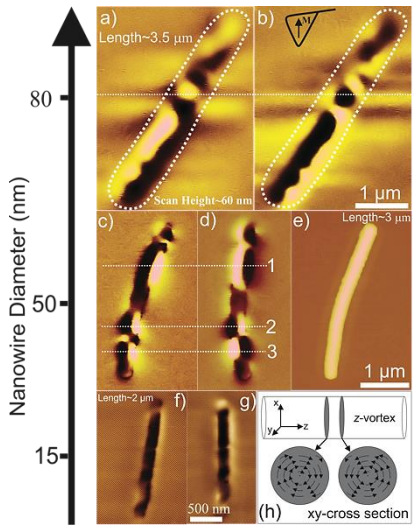


Fig. 5. (a)-(g) The experimental AFM/MFM images of individual Co-Pt NWs at the remanent magnetization state with diameters of 15, 50 and 80 nm and with two different magnetization directions (±x) of the MFM tip. (h) Schematic of the z-vortex state.

IV. Conclusion

The conclusions are listed below:

1. We found in Co-Pt NWs with 15-, 50- and 80-nm diameters that the shape anisotropy and MCA are in competition with each other and the magnetic properties (easy axis, coercivity and magnetic domains) are predominantly influenced by the crystal structure (MCA) of the NWs.
2. The observed magnetic-domain structures in the 50- and 80-nm diameter NWs are interpreted as the presence of a non-symmetrical *z*-vortex state. Susceptibility contrast was found in the 15-nm diameter NW.

Acknowledgment

This project was funded by the Slovenian Research Agency (ARRS) under project number PR-04442.

References

Aboaf JA, Herd SR, Klokholm E (1983), "Magnetic-Properties and Structure of Cobalt Platinum Thin-Films." *IEEE Trans Magn*, vol. 19, no. 4, pp. 1514-1519, doi: 10.1109/Tmag.1983.1062575.

Bauer LA, Birenbaum NS, Meyer GJ (2004), "Biological applications of high aspect ratio nanoparticles." *J Mater Chem*, vol. 14, no. 4, pp. 517-526, doi: 10.1039/B312655b.

Cho JU, Wu J-H, Min JH, Ko SP, Soh JY, Liu QX, Kim YK (2006), "Control of magnetic anisotropy of Co nanowires." *J Magn Magn Mater*, vol. 303, no. 2, pp. e281-e285, doi: 10.1016/j.jmmm.2006.01.082.

Chu SZ, Inoue S, Wada K, Kurashima K (2005), "Fabrication of integrated arrays of ultrahigh density magnetic nanowires on glass by anodization and electrodeposition." *Electrochim Acta*, vol. 51, no. 5, pp. 820-826, doi: 10.1016/j.electacta.2005.03.075.

Ciureanu M, Beron F, Clime L, Ciureanu P, Yelon A, Ovari TA, Cochrane RW, Normandin F, Veres T (2005), "Magnetic properties of electrodeposited CoFeB thin films and nanowire arrays." *Electrochim Acta*, vol. 50, no. 22, pp. 4487-4497, doi: 10.1016/j.electacta.2005.02.011.

Harp GR, Weller D, Rabedeau TA, Farrow RFC, Toney MF (1993), "Magneto-optical Kerr spectroscopy of a new chemically ordered alloy: Co_3Pt." *Phys Rev Lett*, vol. 71, no. 15, pp. 2493-2496, doi: 10.1103/PhysRevLett.112.068103.

Huang XH, Li GH, Sun GZ, Dou XC, Li L, Zheng LX (2010), "Initial Growth of Single-Crystalline Nanowires: From 3D Nucleation to 2D Growth." *Nanoscale Res Lett*, vol. 5, no. 6, pp. 1057 - 1062, doi: 10.1007/s11671-010-9602-5.

Ivanov Yu P, G. VL, A. A, A. C, O. C-f, M. V (2013), "Magnetic structure of a single-crystal hcp electrodeposited cobalt nanowire." *Europhys Lett*, vol. 102, no. 1, pp. 17009-17014, doi: 10.1209/0295-5075/102/17009.

Kristof M Lebecki, Donahue MJ (2010), "Comment on “Frustrated magnetization in Co nanowires: Competition between crystal anisotropy and demagnetization energy”." *Phys Rev B*, vol. 82, no. 9, pp. 096401-096405, doi: 10.1103/PhysRevB.82.096401.

Laroze D, Escrig J, Landeros P, Altbir D, Vazquez M, Vargas P (2007), "A detailed analysis of dipolar interactions in arrays of bi-stable magnetic nanowires." *Nanotechnology*, vol. 18, no. 41, pp. 415708-415714, doi: 10.1088/0957-4484/18/41/415708.

Parkin SSP, Hayashi M, Thomas L (2008), "Magnetic Domain-Wall Racetrack Memory." *Science*, vol. 320, no. 5873, pp. 190-194, doi: 10.1126/science.1145799.

Razee SSA, Staunton JB, Pinski FJ (1997), "First-principles theory of magnetocrystalline anisotropy of disordered alloys: Application to cobalt platinum." *Phys Rev B*, vol. 56, no. 13, pp. 8082-8090, doi: 10.1103/PhysRevB.56.8082.

Sayama J, Shimatsu T, Nemoto H, Okamoto S, Kitakami O, Aoi H (2011), "Temperature dependence of the magnetic properties of $L1_1$-type Co–Ni–Pt ordered alloy films for thermally assisted recording media." *J Appl Phys*, vol. 110, no. 1, pp. 013918-013923, doi: 10.1063/1.3608123.

T. Thurn-Albrecht, J. Schotter, G. A. Kastle, N. Emley, T. Shibauchi, L. Krusin-Elbaum, K. Guarini, C. T. Black, M. T. Tuominen, Russell aTP (2000), "Ultrahigh density nanowire arrays grown in self-assembled diblock copolymer templates." *Science*, vol. 290, no. pp. 4, doi: 10.1126/science.290.5499.2126.

Tian ML, Wang JU, Kurtz J, Mallouk TE, Chan MHW (2003), "Electrochemical growth of single-crystal metal nanowires via a two-dimensional nucleation and growth mechanism." *Nano Lett*, vol. 3, no. 7, pp. 919-923, doi: 10.1021/Nl034217d.

Wang N, Zhang J, Wang C, Shen TH (2010), "A study on phase relations and texture of Co1−xPtx (0.09<x<0.86) nanowire arrays." *Mater Lett*, vol. 64, no. 22, pp. 2530-2533, doi: 10.1016/j.matlet.2010.07.040.

Copyright (c) 2014 IEEE. Personal use is permitted. For any other purposes, permission must be obtained from the IEEE by emailing pubs-permissions@ieee.org.

This is the author's version of an article that has been published in this journal. Changes were made to this version by the publisher prior to publication.
The final version of record is available at http://dx.doi.org/10.1109/LMAG.2014.2362106

Zana I, Zangari G, Park J-W, Allen MG (2004),
"Electrodeposited Co–Pt micron-size magnets with strong perpendicular magnetic anisotropy for MEMS applications."
J Magn Magn Mater, vol. 272-276, no. 0, pp. E1775-E1776,
doi: 10.1016/j.jmmm.2003.12.990.
Copyright (c) 2014 IEEE. Personal use is permitted. For any other purposes, permission must be obtained from the IEEE by emailing pubs-permissions@ieee.org.

Chapter 7

Magnetization-Switching Study of fcc Fe-Pd Nanowire and Nanowire Arrays Studied by In-Field Magnetic Force Microscopy

In this Chapter, the article, "Magnetization-switching study of fcc Fe-Pd Nanowire and Nanowire Arrays studied by In-Field Magnetic Force Microscopy.", By Darja Pečko, **Muhammad Shahid Arshad**, Sašo Šturm, Spomenka Kobe, Kristina Žužek Rožman, [37] is presented. For this article the author performed sample preparation for MFM measurement and interpretation of MFM images, statistical analysis on MFM measurements to determine the magnetostatic interactions between NWs.

The purpose of this article was to study the magnetic structure and magnetostatic interaction for soft magnetic NWs. The magnetic properties of 1D nanostructures are governed by the collaborative behaviour of shape and MCA. It is well-known that materials like hcp Co-Pt with strong MCA can surpass shape anisotropy and thus drive the magnetic domain structure and other magnetic processes in nanostructures. However, it is important to look at the other side of the picture e.g. nanostructures with negligible MCA and strong shape anisotropy. It is believed that in such 1D nanostructures the magnetic domain structure and other magnetic properties would be driven by shape anisotropy. For the proof of concept we investigated shape-anisotropy-governed fcc equiatomic Fe-Pd NW and found a single domain structure with magnetization along the length of the NWs. We have found that in dense assemblies of soft magnetic Fe-Pd NWs, the dipolar interactions between the NWs are strong and can modify the hysteresis properties (e.g., coercivity, remanence and switching-field distribution) of such NWs. Such NWs are attractive for applications where pronounced shape anisotropy is necessary such as logic devices and the advantage of having an equiatomic composition in the Fe-Pd NW enables the transformation of the fcc crystal structure into the L_{10}, which has a high MCA energy (1.8 MJ/m^3) that is beneficial from the application point of view.

The conclusion of this study is that soft magnetic Fe-Pd NWs have single domain structure and the dipolar interactions strongly influence their magnetic behaviour.

Magnetization-switching study of *fcc* Fe-Pd Nanowire and Nanowire Arrays studied by *In-Field* Magnetic Force Microscopy

Darja Pečko[1,2], Muhammad Shahid Arshad[1,2], Sašo Šturm[1], Spomenka Kobe[1,3], K. Žužek Rožman[1]

[1]Jožef Stefan Institute, Department for Nanostructured Materials K7, Ljubljana, Slovenia
[2]Jožef Stefan International Postgraduate School, Ljubljana, Slovenia
[3]Center of Excellence on Nanoscience and Nanotechnology (CENN Nanocenter), Ljubljana, Slovenia

Corresponding author: Darja Pečko (darja.pecko@ijs.si)

Using electrodeposition into anodic aluminium oxide (AAO) membranes we have successfully fabricated near-equiatomic $Fe_{48\pm3}Pd_{52\pm3}$ nanowires (NWs) with diameters of ≈ 200 nm and lengths of ≈ 3.5 μm. XRD and TEM/SAED analyses revealed that the as-deposited NWs are isotropic and polycrystalline with an average crystal size of 5 nm and have an *fcc* crystal structure. Magnetic force microscopy (MFM) on a single Fe-Pd NW revealed its single-domain behaviour with the easy axis of magnetization along the long axis of the NW. The magnetization-switching behaviour of a single Fe-Pd NW studied with MFM suggested a square-shaped magnetization curve (M/M_S=1) with $H_{C\|}$ ≈ 3.2 kA/m. Additionally, by using *in-field* MFM techniques, the effects of dipolar interactions in an Fe-Pd array of NWs still embedded in the AAO were determined. It was found that the dipolar interactions greatly reduce the parameters of the magnetization hysteresis loop, such as the coercivity, the remanence and the switching-field distribution of the Fe-Pd NW array.

***Index Terms*— Fe-Pd alloy NWs, magnetic NWs, easy axis, shape anisotropy, magnetostatic interactions**

I. Introduction

The ever-increasing demands for greater storage capacity in magnetic-recording-media devices are leading to great efforts in the development of innovative magnetic materials [1].

An ultra-high-density magnetic recording medium requires the lateral size of the information bits to be as small as possible, without reaching the superparamagnetic limit [1]. One way to avoid the superparamagnetic limit is by using patterned perpendicular media, where one information bit corresponds to one single-domain, nanosized particle or so-called nanomagnet. In this case, each bit would be composed of a single, large-aspect particle [2]. For this reason, magnetic nanowires (NWs) of different materials were investigated [3-5]. NWs are particularly attractive due to their pronounced shape anisotropy, which orients the magnetic moments along the NW's longitudinal axes, forming a high-density perpendicular magnetic recording medium with small switching fields and a high thermal stability [4]. An array of such nanomagnets could lead to an ultra-high storage density of 1 Tbit/in^2 [6]. In the past decade the synthesis of one-dimensional nanostructures by means of electrochemical deposition into the pores of an anodic aluminium oxide template (AAO) has attracted a great deal of scientific interest because of many outstanding features, such as low price and the suitability of producing NWs into ordered and regular AAO templates, having a high pore density (10^9–10^{11} cm^2) over large surface areas (several square centimetres) [4, 7-9].

Magnetic force microscopy (MFM) has been shown to be a useful tool for the evaluation of magnetic domain structures, magnetization hysteresis loops on a local scale and for gaining an insight into the dipolar interactions between the NWs [6]. In dense assemblies, the dipolar interactions between the NWs are strong and can modify the hysteresis properties (e.g., coercivity, remanence and switching-field distribution) of the NWs [10].

Up to now, most of the MFM studies on ferromagnetic NWs applicable for magnetic recording media were based on single-metal Ni or Co NWs [3-5], whereas in this study we have focused on *fcc* Fe-Pd alloy-based nanowires with an equiatomic composition. Such NWs are attractive for applications in magnetic storage devices due to the pronounced shape anisotropy and the advantage of having an equiatomic composition in the Fe-Pd NW enables the transformation of the *fcc* crystal structure into the $L1_0$, which has a high magnetocrystalline anisotropy (MCA) (1.8 MJ/m^3) [11] that is beneficial from the application point of view. In this series of experiments we deposited equiatomic $Fe_{48\pm3}Pd_{52\pm3}$ NWs and an *in-field* MFM study was performed to investigate the magnetization switching of a single Fe-Pd NW. Additionally, the dipolar interactions' influence on the magnetic properties of such NWs still embedded in the AAO template were investigated.

II. Experimental Details

The depositions of the Fe-Pd NWs were performed from an electrolyte containing 200-mM $FeCl_3$, 30-mM $PdCl_2$, 0.4-M $(NH_4)_2C_6H_6O_7$ and 0.5-M NH_3(aq) for the pH adjustment to 9. The Fe-Pd NWs were electrochemically deposited in commercially available AAO membranes (Whatman, Anapore, pore diameter d = 200 nm, interpore separation a = 360 nm). The conductivity of the membranes was achieved by first sputtering the back side of the membrane with 600 nm of Au, which was followed by the electrochemically deposited Au NW. The AAO template was then glued with a Cu-tape on the Al-foil sheet and used as a cathode. A circular platinum mesh was used as a counter electrode. The $Fe_{48\pm3}Pd_{52\pm3}$ NWs with a length of 3.5 μm were deposited at –1.1 V and measured vs. a Ag/AgCl/3 M KCl// at room temperature for 900 s.

The Fe-Pd NWs were characterized using a field-emission-gun scanning electron microscope (FEG-SEM) JEOL JSM-7600F equipped with an Oxford Instruments INCA system for energy-dispersive X-ray spectroscopy (EDXS) with a 20-mm^2 silicon drift detector (SDD). To obtain individual NWs the AAO

This is the author's version of an article that has been published in the IEEE Transactions on Magnetics. Changes were made to this version by the publisher prior to publication. The final version of record is available at 10.1109/TMAG.2015.2449773

membrane was dissolved in an aqueous solution of 10-M NaOH and the NWs were released using a centrifuge. For the TEM investigation, the NWs after the removal of the AAO template were mixed with the two-component epoxy glue and gently applied between two Si wafers. These stacks were further cut and polished using a dimple-grinder. The final, thin, electron-transparent, specimen foil was obtained by ion milling in a Baltec RES010. The NWs were examined with a JEM-2010F transmission electron microscope (TEM). The crystal structure of the as-deposited Fe-Pd NWs inside the alumina templates were investigated by XRD using a diffractometer (D4 Endeavor, Bruker AXS, Karlsruhe, Germany) with Bragg-Brentano geometry, a Cu-Kα radiation source and a Sol-X energy-dispersive detector.

For the MFM measurements a drop of ethanol containing Fe-Pd NWs was placed on a clean Si wafer and then dried. After a single NW was selected, a commercial scanning probe microscope (Digital Instruments Dimension 3100) was used for the MFM measurements. The MFM cantilever (Nanoworld MFMR-type probe) was used in the lift mode. The tip magnetization direction was perpendicular to the plane of the Si substrate on which the NW was horizontally placed. For the *in-field* MFM measurements a home-made stage after [12] was used. The external field was applied with a permanent magnet (H_{max}~240 kA/m) in the direction parallel to the NW's long axis. The NWs remained embedded in the AAO template to study the dipolar interactions between them. The AAO template with Fe-Pd NW was fixed with resin to the Si-wafer [2] and the AAO template and Au were polished away with the tripod (MultiPrep System Allied) until the tops of the Fe-Pd NWs were reached. The lengths of the NWs were checked with the FEG-SEM. The magnetic properties of the as-deposited NWs were measured using a MicroSense model FCM 10 with magnetic fields in the range $\pm$1200 kA/m.

III. Results and Discussion

Fig.1. (a) shows a FEG-SEM image of an array of ≈ 3.5-μm-long and ≈200-nm-thick Fe-Pd NWs with a consistent composition of $Fe_{48\pm3}Pd_{52\pm3}$ along the whole lengths of the NWs. The crystal structure of the Fe-Pd NWs was evaluated by XRD and TEM/SAED (selected-area electron diffraction). Fig.1. (b) shows the XRD diffractogram of an array of $Fe_{48\pm3}Pd_{52\pm3}$ NWs embedded in the AAO template recorded from the top of the membrane in order to avoid the high Au signal, from the template's bottom side. The XRD diffractogram of the as-deposited NWs consists of the *fcc* Fe-Pd phase with reflections (111), (200), (220) and (311) (taken from the card PDF-021440). Comparing the peak intensities, no preferred crystal texturing was observed in the Fe-Pd NWs. Using the Scherrer equation the size of the crystallites of the as-deposited Fe-Pd NWs was calculated to be around 5 nm.

Fig.2. shows a TEM image of a single, as-deposited $Fe_{48\pm3}Pd_{52\pm3}$ NW and selected-area electron diffraction (SAED) patterns performed on two spots along the length of the NWs (marked with 1, 2). From the TEM micrograph it was confirmed that an as-deposited Fe-Pd NW consists of randomly oriented nanocrystals with an average size of ≈ 5 nm. The most probable crystal structure of the NW was determined by comparing the experimental SAED pattern with a calculated one (simulated in the white background of 1 and 2), based on the *fcc* Fe-Pd crystal structure with a cell parameter a = 3.67 Å [13]. The experimental SAED pattern matches with the calculated SAED pattern.

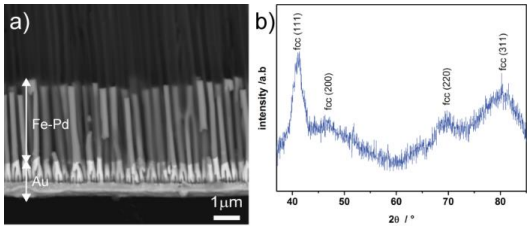


Fig. 1. FEG-SEM image (a) and the XRD diffractogramm (b) of an array of $Fe_{48\pm3}Pd_{52\pm3}$ NWs in embedded in the AAO tempate.

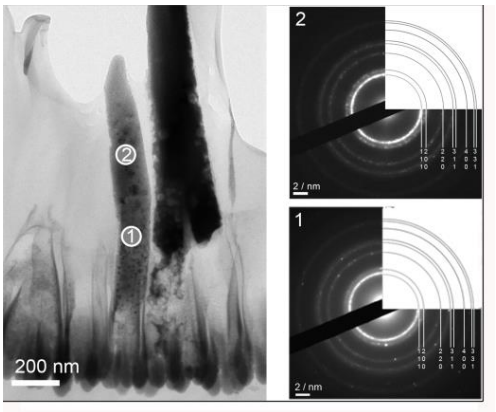


Fig. 2. TEM image and SAED patterns from spots (1 and 2) on a single $Fe_{48\pm3}Pd_{52\pm3}$ NW.

Fig.3. (a) & (b) show the AFM and MFM images of a single, as-deposited $Fe_{48\pm3}Pd_{52\pm3}$ NW with a length of 3.5 μm at a scan height of 100 nm. MFM response is recorded in Fig.3. (b), which exhibits a complementary dark and bright contrast at the extremities of the nanowire, a characteristic for a single-domain nanowire with the magnetization orientated along the length of the nanowire [1]. Notice that there is dark contrast around bright contrast at the top edge of the nanowire; this observation substantiates the presence of stray field in the vicinity of the nanowire which can also be imaged by MFM. Same is true for the bottom part of the nanowire. A slight dark contrast in the middle region of the nanowire was also observed, which was inverted when the tip magnetization was reversed (not shown here), thus the contrast is magnetic in origin. This contrast might be originated from small diameter modulation in this region of the nanowire as shown in inset FEG-SEM images, similar observation have been reported by other authors [14].

In order to investigate the magnetization-switching behaviour of a single $Fe_{48\pm3}Pd_{52\pm3}$ NW a set of *in-field* MFM experiments were performed, as shown in Fig.4. Such experiments revealed the whole hysteresis loop of a single $Fe_{48\pm3}Pd_{52\pm3}$ NW with the field applied parallel (Fig.4.) to the long axis of the NWs. From Fig.3 (b), MFM image of the Fe-Pd nanowire in zero applied field (say "virgin state") is presented in the middle of the hysteresis loop in Fig.4. After a high magnetic field (H_{sat}=16 kA/m) was applied, parallel to the nanowires' long axis, nanowire was fully saturated in opposite direction. At the remanence point (M_R) the MFM image was identical to the saturation point (M_S), which is typical for single-domain particles exhibiting a square-shaped hysteresis loop. The

coercivity of a single Fe-Pd nanowire was determined using small external field steps in the negative direction and the coercivity field is calculated when dM/dH change its sign or in other words when the MFM contrast just reversed. In Fig.4 such state was found at –3.3 kA/m as shown by arrow, where a flip of the magnetization was observed. We continue applying field in negative direction till –16 kA/m, no noticeable change in contrast was observed. Similar coercivity field was observed in positive field direction as well (not shown here).

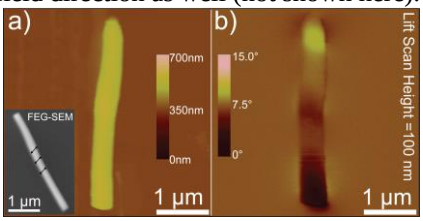


Fig. 3. AFM (a) and MFM (b) images of single $Fe_{48\pm3}Pd_{52\pm3}$ NW (d = 200 nm, L = 3.5 µm) in the demagnetized state. Inset in Fig.3 (a) represents the FEG-SEM image of the investigated $Fe_{48\pm3}Pd_{52\pm3}$ NW.

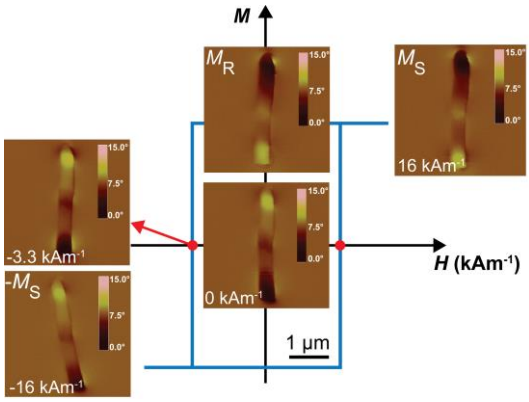


Fig.4. MFM images of single $Fe_{48\pm3}Pd_{52\pm3}$ NW (d = 200 nm, L = 3.5 µm) at the different applied fields that were parallel to the long NW's axis.

We also studied the magnetostatic interactions between the NWs in an array using the *in-field* MFM with the applied magnetic field in the direction parallel to the long NWs' axes. The length of the NWs is same as individual NW (L = 3.5 µm) showing single magnetic domain behaviour as shown in Fig.3 (b). Fig.5. (a) & (b) show the typical 10× 10 µm^2 AFM and MFM images (remanence state), respectively, obtained from the top surface of the $Fe_{48\pm3}Pd_{52\pm3}$ NWs array still embedded in the AAO membrane. In order to keep track the same area of the template a reference point is marked by the arrow as shown in Fig.5 (a) & (b). In Fig.5 (b) the spot sizes (dark and bright) are larger than the nominal diameters (200 nm) of the NW, because the MFM tip measures the NWs' dispersive stray fields resulting in a continuous, typical, labyrinth domain structure, as expected for a hexagonal array to maintain neighbouring bits with antiparallel magnetization and to minimize the inter NW dipolar field energy [15]. As only two distinguishable MFM spots (dark and bright spots) at the two edges of the single NWs were identified in Fig.3 (b), we believe that the dark spots in Fig.5 (b) indicate the magnetization pointing "up" and the bright spots indicate the magnetization pointing "down". Therefore, the local MFM-based hysteresis loop can be calculated by counting the number of NWs in the "up" and "down" states. The MFM normalized magnetization can be written as

$$\frac{M^{MFM}(H)}{M_S^{MFM}} = \frac{n_{up} - n_{down}}{n_{up} + n_{down}} \quad (1)$$

where n_{up} and n_{down} are the number of NWs with up and down states, respectively. M_S^{MFM} is the effective saturation magnetization (total number of NWs in the image), while $M^{MFM}(H)$ is the effective magnetization at an applied magnetic field H. The MFM coercive field can be extracted from the image where the number of NWs with "up" and "down" states is the same (n_{up}= n_{down}). The remanence state can be obtained from the MFM image at zero applied magnetic field.

$$\frac{M^{MFM}(0)}{M_S^{MFM}} \quad (2)$$

In the case when there is no interaction present between neighbouring NWs at the remanence state all the wires should point in the same direction ("up" or "down") [16]. However, due to the magnetostatic interactions among the NWs, the distribution of the states (up and down) changes and a patterned domain structure (i.e., labyrinth domains) is observed (see Fig.5 (b)). Typically, in a hexagonal lattice with an interwire separation (a ~ 2d) two of the six nearest neighbours will align their magnetization "up" and four will align "down", or vice versa [2, 16].

In order to obtain more detailed information about the magnetization reversal (switching) of the NWs, a series of MFM images were recorded at different magnetic fields parallel to the NW axes, as shown in Fig.5 (c) to (f). At the remanence state (H = 0 kA/m) in Fig.5 (b), careful analysis revealed that in many cases four of the NWs have magnetization "down" and two are aligned "up", as expected in a typical hexagonal arrangement. Later, after applying a field of –50 kA/m (Fig.5 (c)) successive switching of the NWs into dark ("up" state) was observed. When external magnetic field was increased more, more nanowires turn to dark and finally when the field of –240 kA/m (Fig.5 (f)) was applied all the nanowires turned dark (saturated state). We also observed interconnected switching of the NWs indicates strong interactions among the neighbouring NWs e.g. in Fig. 5 (a) to (f) we have selected three nanowires (aligned in a line) enclosed by a square, at remanence state all nanowires are dark (up state), when applied of –100 kA/m was applied one of the NW (leading NW from the top) turn bright as shown in Fif.5 (d) which switch dark again after application of field of –240 kA/m. Please note that the small bright islands in Fig.5 (f) are regions where NWs are missing as shown by the circles in Fig.5 (a) to (f), we believe that the observed contrast is induced due to the neighbouring NWs.

The MFM-based hysteresis curve was obtained by analysing 10 MFM images at different applied field values, 5 of which are presented in Fig.5 (b)–(f). A bulk magnetization curve with an applied field along the length of the NWs in similar field range was obtained with the VSM on the same batch of the sample. Fig.6 shows a comparison between the bulk magnetization curve and the MFM hysteresis curve for the array of NWs. Good agreement between the MFM and the VSM measurements was obtained at higher applied field values however, there is a noticeable difference in the low applied field values (near coercivity field values). This difference in the

coercivity values might be due to a small scanning area (10 × 10 μm^2) in the MFM as compared to VSM measurement done on bulk sample (2 x 2 mm^2). However, the good agreement between the hysteresis curves suggested that there is large switching field distribution which results in low remanence and coercivity and possible reason would be strong magnetostatic interactions between the NWs.

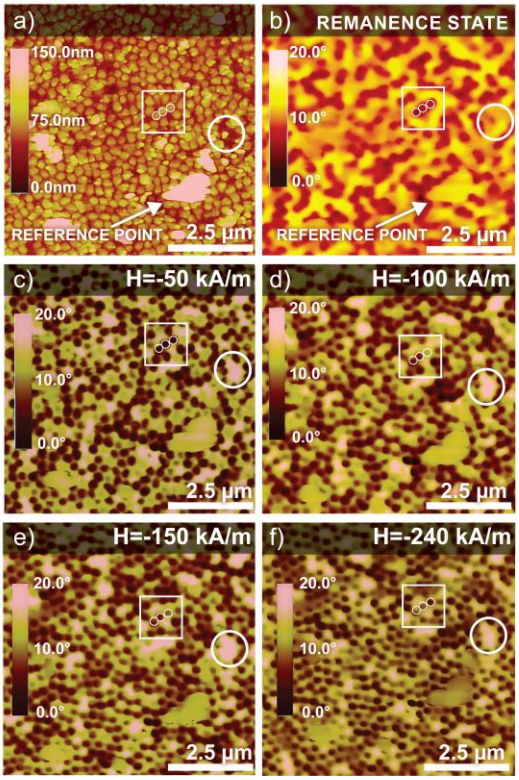


Fig. 5. AFM and MFM images from the top of an array of $Fe_{48\pm3}Pd_{52\pm3}$ NWs ($d \approx 200$ nm, $L = 3.5$ μm) filled in the AAO template: AFM (a) and MFM (b) image of the 10 × 10 μm^2 area in the demagnetized state, MFM images of 10 × 10 μm^2 area after applying the external magnetic field perpendicular to the NWs tops: –50 kA/m (c), –100 kA/m (d) and –240 kA/m (e).

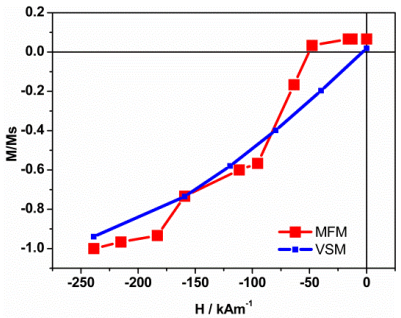


Fig. 6. Comparison of the *in-field* MFM magnetization curves with the ones obtained with VSM measurmenst of an array of $Fe_{48\pm3}Pd_{52\pm3}$ NWs.

IV. Conclusion

Single-domain, 200-nm-thick and 3.5-μm-long *fcc* NWs with a consistent composition of $Fe_{48\pm3}Pd_{52\pm3}$ were deposited into a commercial AAO template. We have shown that by applying the field in the direction parallel to the NW's axis we were able to flip the magnetization ($H_{CII} \approx 3.3$ kA/m). The MFM study of the magnetostatic interactions revealed that the NWs are strongly coupled. For ultra-high-density storage media, NWs with smaller dimensions would be needed. The objective of the present study was to investigate the magnetic domain structure, the local magnetization switching behaviour of the shape-anisotropy-governed Fe-Pd NW and the magnetic interactions in such a NW array. The next step will be focused on the synthesis of equiatomic Fe-Pd NWs into our own AAO templates with a smaller diameter (up to 70 nm), with the present work serving as a reference.

Acknowledgment

This work was supported by Slovenian Research Agency (ARRS). The authors would also like to acknowledge to Medeja Gec for the preparation of the TEM and MFM sample.

References

[1] Y. Henry, K. Ounadjela, L. Piraux, S. Dubois, J. M. George and J. L. Duvail, "Magnetic anisotropy and domain patterns in electrodeposited cobalt nanowires," *The European Physical Journal B - Condensed Matter and Complex Systems* vol. 20, pp. 35-54, 2001.
[2] K. Nielsch, R. B. Wehrspohn, J. Barthel, J. Kirschner, S. F. Fischer, H. Kronmüller, T. Schweinböck, D. Weiss and U. Gösele, "High density hexagonal nickel nanowire array," *J. Magn. Magn. Mater.* vol. 249, pp. 234-240, 2002.
[3] K. Nielsch, F. Müller, G. Liu, R. B. Wehrspohn, U. Gösele, S. F. Fischer and H. Kronmüller 2000 In: *Electrochemical Society Proceedings*,
[4] A. S. Samardak, E. V. Sukovatitsina, A. V. Ognev, L. A. Chebotkevich, R. Mahmoodi, S. M. Peighambari, M. G. Hosseini and F. Nasirpouri 2012 In: *Journal of Physics: Conference Series*: IOP Publishing) p 012011
[5] T. Wang, Y. Wang, Y. Fu, T. Hasegawa, F. S. Li, H. Saito and S. Ishio, "A magnetic force microscopy study of the magnetic reversal of a single Fe nanowire," *Nanotechnology* vol. 20, pp. 105707, 2009.
[6] M. R. Tabasum, F. Zighem, J. De La Torre Medina, A. Encinas, L. Piraux and B. Nysten, "Magnetic force microscopy study of the switching field distribution of low density arrays of single domain magnetic nanowires," *J. Appl. Phys.* vol. 113, pp. -, 2013.
[7] H. Schlörb, V. Haehnel, M. S. Khatri, A. Srivastav, A. Kumar, L. Schultz and S. Fähler, "Magnetic nanowires by electrodeposition within templates," *Phys. Status Solidi B* vol. 247, pp. 2364-2379, 2010.
[8] H. Liu, F. Wang, Y. Zhao, J. Liu, K. C. Park and M. Endo, "Synthesis of iron–palladium binary alloy nanotubes by template-assisted electrodeposition from metal-complex solution," *J. Electroanal. Chem.* vol. 633, pp. 15-18, 2009.
[9] V. Vega, T. Böhnert, S. Martens, M. Waleczek, J. M. Montero-Moreno, D. Görlitz, V. M. Prida and K. Nielsch, "Tuning the magnetic anisotropy of Co–Ni nanowires: comparison between single nanowires and nanowire arrays in hard-anodic aluminum oxide membranes," *Nanotechnology* vol. 23, pp. 465709, 2012.
[10] K. Nielsch, R. B. Wehrspohn, J. Barthel, J. Kirschner, U. Gösele, S. F. Fischer and H. Kronmüller, "Hexagonally ordered 100 nm period nickel nanowire arrays," *Appl. Phys. Lett.* vol. 79, pp. 1360-1362, 2001.
[11] M. S. Viqueira, S. E. Garcia, S. E. Urreta, G. P. Lopez and L. M. Fabietti, "Hysteresis Properties of Hexagonal Arrays of FePd Nanowires," *IEEE Trans. Magn.* vol. 49, pp. 4498-4501, 2013.
[12] C. Bran, A. B. Butenko, N. S. Kiselev, U. Wolff, L. Schultz, O. Hellwig, U. K. Rößler, A. N. Bogdanov and V. Neu, "Evolution of stripe and bubble domains in antiferromagnetically coupled multilayers," *Phys. Rev. B* vol. 79, pp. 024430, 2009.
[13] E. Burzo and P. Vlaic, "Magnetic properties of iron-palladium solid solutions and compounds," *Journal of optoelectronics and adavnced materials* vol. 12, pp. 1869-1878, 2010.
[14] K. Pitzschel, J. Bachmann, S. Martens, J. M. Montero-Moreno, J. Kimling, G. Meier, J. Escrig, K. Nielsch and D. Görlitz, "Magnetic reversal of cylindrical nickel nanowires with modulated diameters," *J. Appl. Phys.* vol. 109, pp. -, 2011.
[15] K. Nielsch, R. B. Wehrspohn, J. Barthel, J. Kirschner, U. Gosele, S. F. Fischer and H. Kronmuller, "Hexagonally ordered 100 nm period nickel nanowire arrays," *Appl. Phys. Lett.* vol. 79, pp. 1360-1362, 2001.
[16] F. Zighem, T. Maurer, F. Ott and G. Chaboussant, "Dipolar interactions in arrays of ferromagnetic nanowires: A micromagnetic study," *J. Appl. Phys.* vol. 109, pp. 2011.

Chapter 8

Miscellaneous Results

In this Chapter, the research work under progress is presented. Section 1 we introduce the simulation results where the current induced domain wall motion in Co-Pt nanowires (NW) with periodic domain structure was studied. In Section 2 we present the NWs with artificial notches to introduce the domain-wall pinning effect. We have successfully demonstrated that in Co-Pt NWs with 50 nm diameter, a notch of a half the size of the NW diameter is enough to pin a domain wall at the notch-site. At the end in Section 3 magnetization switching behaviour of a single domain Co-Pt NW is presented.

8.1 Current Induced Domain-Wall Movement in Cylindrical Co-Pt Nanowires: Theoretical Approach

Magnetic HDDs have been the prime repository of digital data for more than a half century. Over this period, the area of one magnetic bit used to store information has decreased in size (now ~40 nm) by about nine order to magnitudes; it is now so tiny that it is reaching the fundamental limit that is difficult or too expensive to overcome. A number of alternatives to the magnetic disk drive have been suggested. Among them racetrack memory devices seems to be potential candidates and close to the realization. Such devices are based on magnetic NWs with magnetic domains which can be moved with the help of spin polarized current.

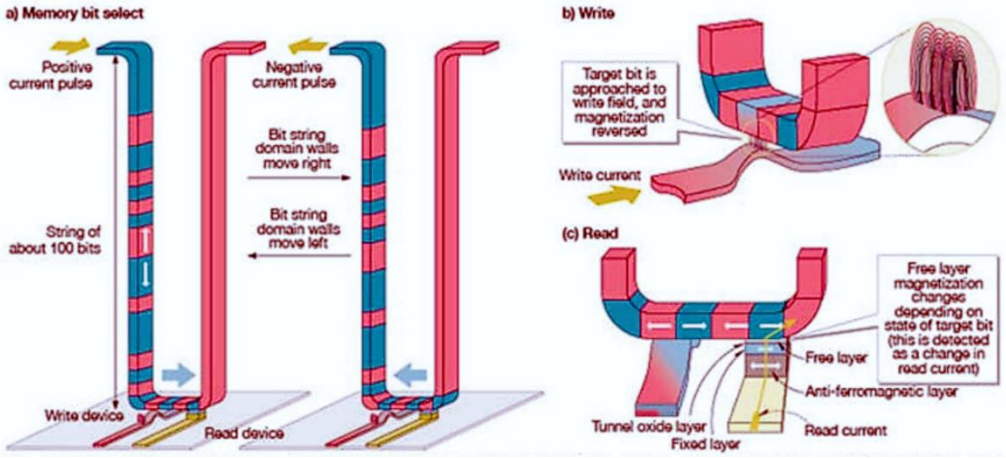


Figure 8.1: Schematic diagram of a racetrack memory operation (a) selecting, (b) writing and (c) reading a memory bit. By applying a negative (or positive) current pulse to the

NW, the magnetic domain walls move to the left (right) in the diagram, controlling in this way the access to the data stored along the wire. Adopted from [99].

One of such ideas are racetrack memory devices, where information is stored in the form of magnetic domains with opposite magnetization along the length of the nanowires. One of the fascinating points of such devices is that domains in nanowires can move forward or backward depending on the current directions. Many researchers believe that such devices have the potential to keep the Moore's law going and big IT companies like IBM are funding research on racetrack memory devices. [4] The main features of such devices are enlisted below

1. Non-volatile (information remains stored even if there is no power, such as HDD and flash).

2. Higher Density (up to 10x information in comparison to HDD can be stored).

3. Super Speed (reading and writing of information would be equivalent or higher than SRAM).

4. Universal Memory devices (such devices can replace all types of memory devices such as SRAM, DRAM and flash memory).

For such devices to function properly it is necessary to have 1) magnetic domains with opposite magnetization as shown by red and blue boxes in Figure 8.1, and 2) it is also important to efficiently manipulate domains and domain walls with external current. In the present thesis, the Co-Pt nanostructures have been synthesized into polycarbonate (PC) as well as AAO membranes with diameter range from 15-200 nm. We have studied the magnetic domains in such Co-Pt nanowires and investigated their magnetization reversal. We have utilized micromagnetic simulations (NMAG) to understand the nature of magnetization and magnetization reversal in such nanowires. For further details we suggest readers to read our published articles [39, 40].

8.1.1 Current induced domain wall motion in periodic magnetic domains in Co-Pt nanowires

Periodic domains structure observed with MFM along the length of the Co-Pt NWs and their interpretations are shown in Figure 8.2 (a) to (i). In Figure 8.2 (a) the dark-and-bright contrast reveals a rapid alternation of pairs of diametrically opposed dark-and-bright stripes along the lengths of the NWs; however, in Figure 8.2 (e), this alternation is also along the short axis of the NWs. We believe that both contrasts originate from the same magnetic state (transverse stripes, TS—Figure 8.2 (d)) of the NWs. However, in other NWs in Figure 8.2 there is a slight variation in the magnetization modulation, for example, the lower segment of Figure 8.2 (b) and (c) is believed to have a TS magnetic configuration; however, the upper part reveals a longitudinal stripes configuration (LS—Figure 8.2 (i)). Further detail about this topic can be found in Chapter 5 of this thesis. Moreover, the three-dimensional finite-element calculations with the NMAG simulation tool [73] on a magnetic cylinder, carrying a uniaxial transverse crystal anisotropy K_u=1x10^6 J/m^3 with

other material parameters $A=1.6\text{x}10^{-11}$ A/m and $M_s \approx 8\text{x}10^5$ A/m are currently in progress. The simulation results, so far, on a small cylinder (diameter=10 nm, length=60 nm) have already shown that the TS configuration is indeed the lowest energy state, as shown in Figure 8.2 (a1), which is in excellent agreement with the present MFM observations. It is also shown that due to the physical rotation of the NWs the MFM contrast can change (Figures 8.2 (a1) and (e1)), which may explain the different contrasts in Figures 8.2 (a) and (e). Interestingly, the simulation data have also shown that the TS and LS configurations have almost equal total magnetic energies, although TS appears to be the most favored and in some NWs LS is present as shown in Figure 8.2 (a)-(e). This may also explain why these two configurations simultaneously exist in a NW, as shown Figures 8.2 (b) and (c). Magnetic domain structure presented in Figure 8.2 is ideal for a racetrack memory devices.

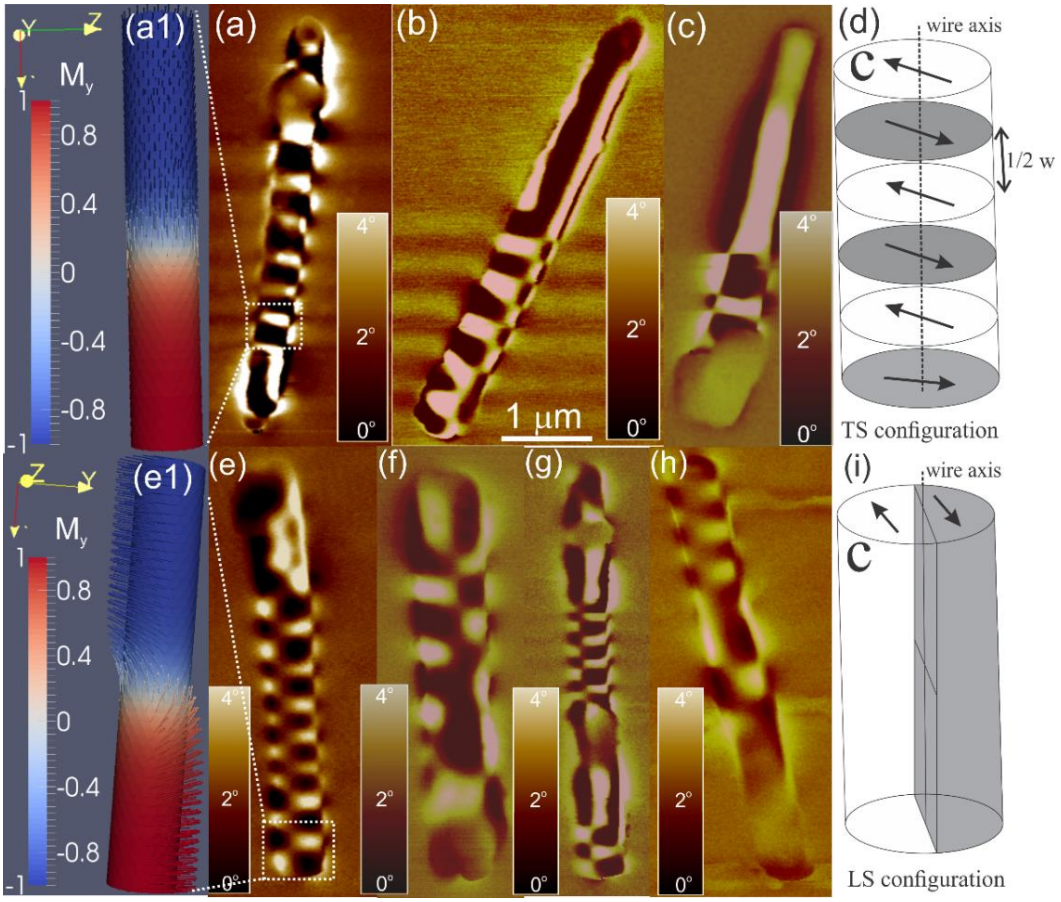


Figure. 8.2: (a)-(c) and (e)-(h) The experimental MFM images of individual Co-Pt NWs with a diameter of ~250 nm. Upper row shows dark-and-bright contrast along the length of the NW, while in the lower row the contrast is along the short axis of the NW. (a1) and (d1) NMAG simulation images of the magnetization profile in a small segment of the NW at two different angles (90°). (d) and (i) TS and LS configuration, respectively.

Furthermore, we perform a micromagnetic simulation for the current induced domain wall motion to move these domains along the length of Co-Pt NWs. For this purpose, 5 ns pulses of spin polarized current were applied with the different current densities along the length of the NWs, as shown in Figure 8.3. When a spin polarized current is applied through the Co-Pt NW, the domain wall moves in the direction of the conduction electron flow due to the localized momentum transfer from the spin transfer torque as shown in Figure 8.3. A minimum current density for the domain wall in this configuration to overcome its intrinsic pinning was found to be $1x10^{11}$ A/m^2, whereby the domain wall remains static with a current density that is lower than this value. Upon increasing the current density values, domain wall moves in the direction of conduction electron depending on the polarity. In Figure 8.3 there are two columns starting from top (current density 0 A/m^2). It was observed that the domain walls move in left (or right) direction depending upon the positive (or negative) polarity of applied current density through Co-Pt NWs as shown in Figure 8.3.

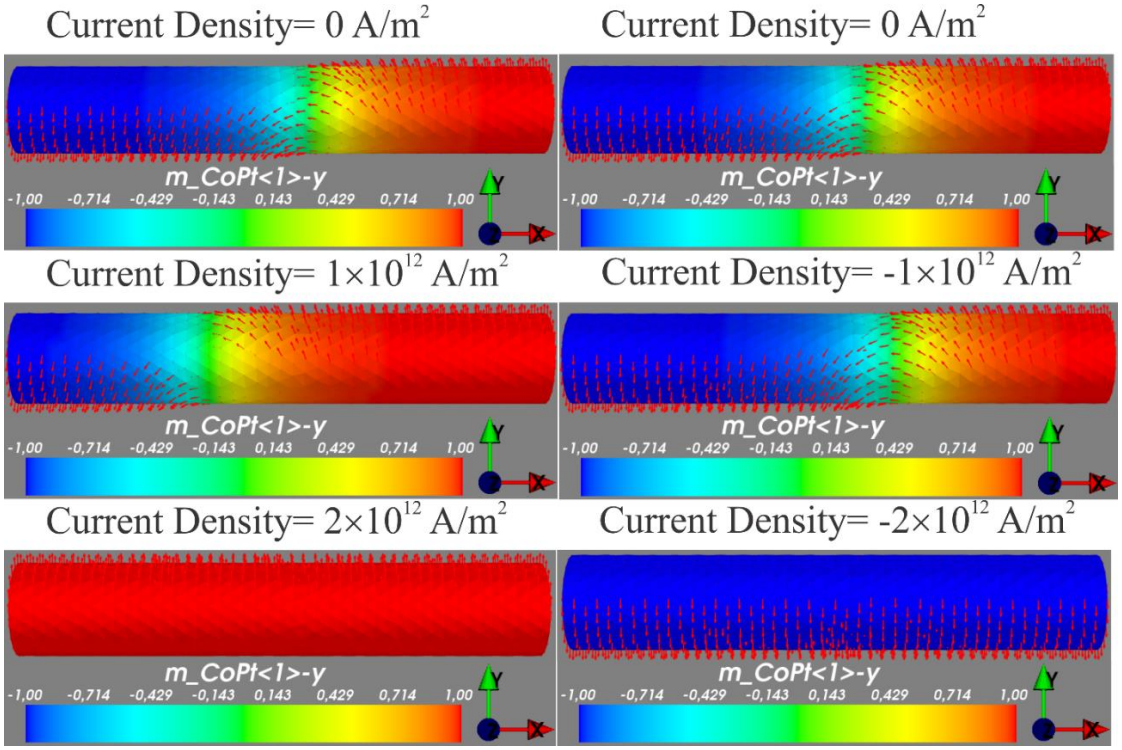


Figure 8.3: Micromagnetic simulation results for spin polarized current induced domain wall motion in Co-Pt NWs.

8.2 A Domain-Wall-Pinning Mechanism in Notched Cylindrical Electrodeposited Co-Pt Nanowires

In the present study, artificial notches along the length of the Co-Pt NWs were introduced to form sites for the domain-wall-pinning. We have synthesized Co-Pt NWs in polycarbonate (PC) membranes with a diameter of ≈50 nm via potentiostatic electrodeposition. Transmission electron microscope (TEM) study has shown the presence

of a textured fcc crystal phase with the [111] crystal planes almost perpendicular to NW long axis as described in Figure 8.4 (a) and (b).

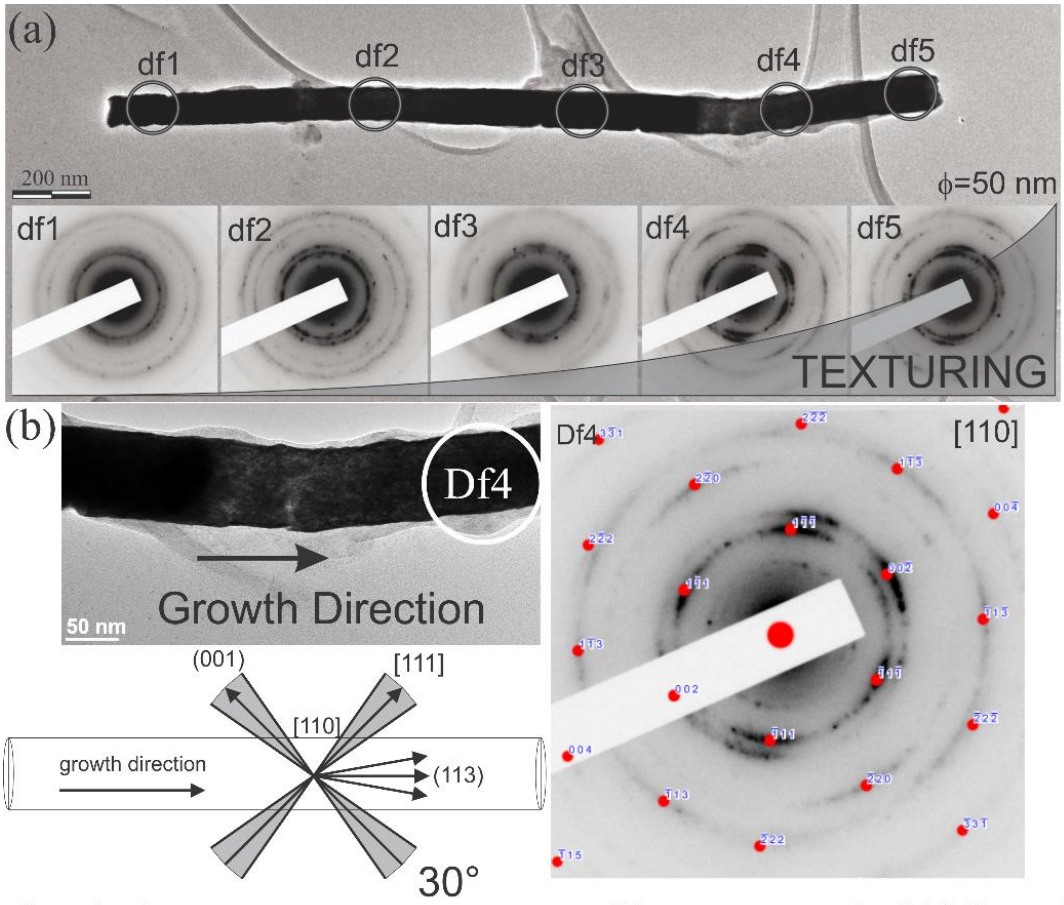


Figure 8.4: (a) Transmission electron microscopy on Co-Pt NW with diameter of 50 nm. Selected area diffraction pattern (df1-df5) along the length of the Co-Pt NW. Texturing is increasing along the length of the Co-Pt NW. (b) an analysis to calculate the angle between [111] crystal plan which is easy magnetization axis of fcc crystal phase and growth direction (nanowire long axis) [113].

MFM imaging was applied to observe the magnetic domain patterns on the basis of the magnetization profile of the NWs lying horizontally on specially prepared Si substrates, used to locate the NWs under the MFM. We observed a uniform dark contrast along the length of the Co-Pt NW indicating a single domain state, due to the texturing of [111] crystal planes (easy magnetization axis) perpendicular to NW long axis. In comparison to the previous Section periodic domain structure is favorable when the Co-Pt NWs have a hcp crystal structure. A focused ion beam (FIB) was used to produce such notches with different sizes and shapes along the lengths of the NWs. We have successfully pinned the domain walls in the Co-Pt NWs at the notches with a depth of almost half of the NWs' diameters, as shown in Figure 8.5. These notches can act as controlling sites for domain wall motion in racetrack memory devices. The nature of the domain wall is

expected to be a transverse domain wall. Some anomalous domain behaviour near the notches appeared, as seen at the bottom of the NW in Figure 8.5, which may have its origin in the crystal defects and/or surface modification due to notch preparation. However, further optimization of the notches in the Co-Pt NWs is necessary in order to utilize them for racetrack memory devices. Moreover, micromagnetic simulations (NMAG) of the notched NWs were performed on a magnetic cylinder, carrying a cubic crystal anisotropy $K=2\text{x}10^5$ J/m^3 with other material parameters $A=1.3\text{x}10^{-11}$ A/m and $M_s \approx 12\text{x}10^5$ A/m. The dimensions of the NW are the same as in experiment (length~2 μm and diameter~50 nm) and a notch of about depth~25 nm and width~25 nm was introduced in the simulation. We relax the system to its magnetic ground state by solving the LLG equation and found that there was a transverse domain wall formed at the notch site as shown in Figure 8.5 (d). Figure 8.5 (e) and (f) are zoom-in of the simulation showing formation of the transverse domain wall at the notch site as evident by the arrows pointing outward. Thus it concludes that by introducing the notches along the length of the Co-Pt NWs one can introduce transverse domain wall at pinning sites. This method of controlling the domain walls have been applied to permalloy NWs also and useful results have been obtained [31, 100].

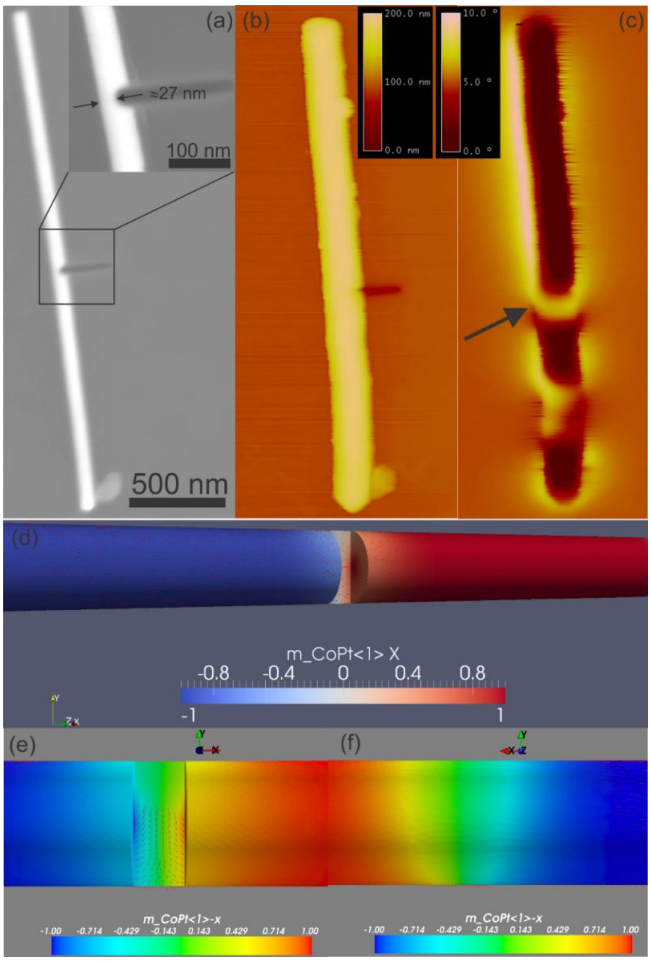


Figure 8.5: (a) SEM image of the Co-Pt nanowire (length~2 μm and diameter~50 nm) with a notch in the middle, (inset) close-up image of the notch area. (b) AFM image (c) MFM image. (d) micromagnetic simulation on cylindrical Co-Pt NW with same dimension as in experiment with notch half the size of the wire diameter. (e) and (f) simulation showing

formation of the transverse domain wall at the notch site as evident by the arrows pointing outward.

8.3 Magnetization Switching Behaviour of Individual Single Domain Co-Pt Nanowire

In Figure 8.6 (a) a SEM image (Backscattered electron-BSE image) of the fcc $Co_{40\pm3}Pt_{60\pm3}$ NW with length ~ 1 µm and diameter 200 nm is shown. A non-magnetic part of the membrane is attached to the one end of the Co-Pt NW. Figure 8.6 (b) shows the topology of this single Co-Pt NW. In the MFM image in Figure 8.6 (c), the NW appears in a uniform dark contrast along the length of the wire. As we know, if the magnetic interaction between tip and sample is attractive, the MFM image will show dark contrast. Thus, a uniform dark contrast means that the magnetization direction within the wire is the same as tip magnetization over the whole length under no external field.

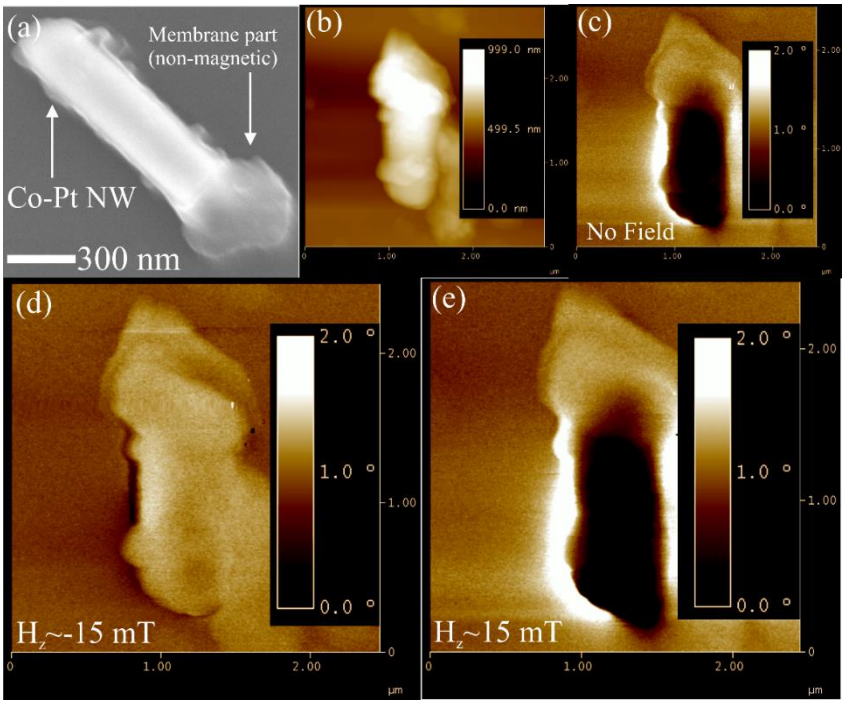


Figure 8.6: (a) The SEM image of the Co-Pt NW with length ~1µm and diameter 200 nm with non-magnetic part of membrane is attached to the top end of the nanowire (BSE image). (b) AFM picture showing the topology of an individual Co-Pt nanowire (height image). (c) MFM picture of Co-Pt NW under no external field showing uniform dark contrast (phase image). (d) and (e) MFM images under negative and positive external magnetic field (±15 mT) respectively.

At small external magnetic field -15 mT all the magnetic moments get aligned with the field shown by the uniform bright contrast in phase image as shown in Figure 8.6 (d). On application of the opposite field of 15 mT the observed contrast turned

completely dark, depicting uniform magnetic charges in opposite direction as shown in Figure 8.6 (e). Thus Co-Pt NWs with 1 μm length and 200 nm diameter rapidly switch its magnetization under external applied field of 15 mT, such NWs can be applicable in sensors and/or magnetic recording media. Further work needs to be done with micromagnetic simulation to understand in detail the local magnetization reversal mechanism of this NW.

Chapter 9

Summary and Conclusions

In this Chapter we summarize the main conclusions and achievements accomplished throughout this thesis, at the end outlook on the future perspectives are given.

The main focal points for this thesis were fabrication, material characterization and understanding the underlying physical phenomena with theoretical calculations to utilize Co-Pt nanostructures for possible applications. Figure 9.1 presents the visual summary of the interesting results obtained in this thesis.

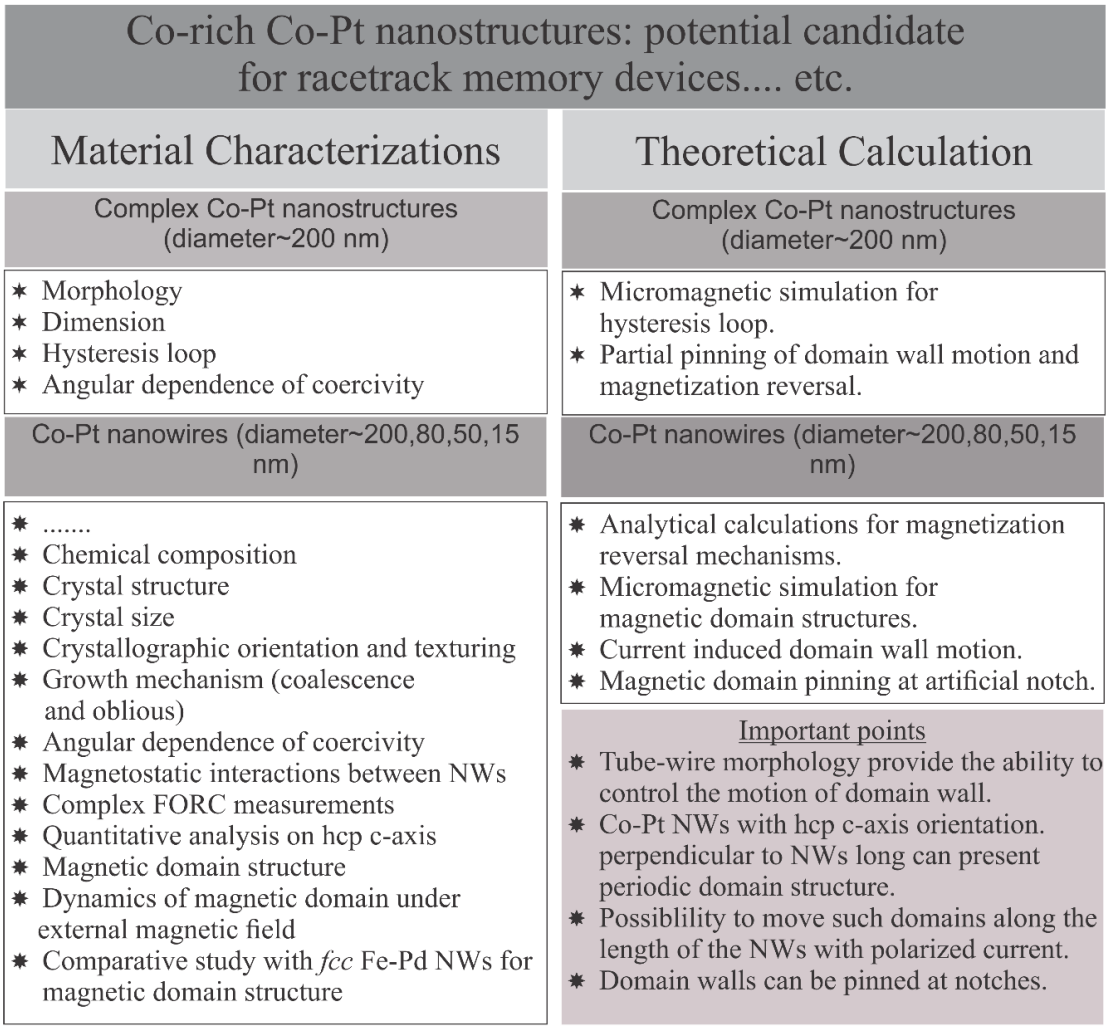


Figure 9.1: Visual summary of the thesis.

The thesis was divided into three main domains,

1. The fabrication and characterization of a new type of complex nanostructures with tube-wire morphology.
2. The investigation of the growth mechanism and the influence of MCA and c-axis orientation on magnetic properties of hcp Co-Pt NWs. Determination of effective anisotropy constant, K_{eff} for Co-Pt NWs which further used to explain magnetic properties of such NWs. The quantitative analysis was performed to determine variation in the hcp c-axis orientation.
3. Comparison of magnetic domain structure between nanowires with different predominate anisotropies i.e. hard magnetic Co-Pt NWs and soft magnetic Fe-Pd.

First we fabricated Co-Pt nanostructures with a pair of nanotube and nanowire segments (with different lengths) via a potentiostatic electrodeposition process. Such a morphology is obtained due to the Au nanoparticles inclusion (≈1 µm) into the pores of the AAO template. A kink in the hysteresis curves was observed which is attributed to a partial pinning of the domain wall at the interface between the tube and wire segments. Considering the range of parameters studied, we found that the tube segment always reverses its magnetization first, through a vortex domain wall, whereas the nanowire segment reverses its magnetization through a transverse domain wall. In the intermediate wire lengths (η=0.5-0.8) there is an interplay between the two reversal modes. Thus, this provides the possibility to tune the reversal mode in such nanostructures by adjusting the geometrical parameters. Our results are in accordance with the theoretical predictions and provide guidelines for envisaging the magnetization reversal of Co-Pt nanostructures with a pair of alternating nanotube and nanowire segments and thus contribute to their utilization in future applications.

Furthermore we performed a detailed structural and magnetic study on arrays and individual Co-Pt nanowires synthesized in AAO template via electrodeposition with a diameter of 200 nm. The crystal structure study revealed that the NWs consist of an intermixture of hcp and fcc phases and have a double crystallographic texturing of both phases in $[111]_{fcc}$+$[001]_{hcp}$ directions which is attributed to similar atomic arrangements and interatomic distances (misfit of ≈2%). In addition the c-axis of the hcp and [111] of the fcc phase was found to be textured perpendicular to the NW long axis which strongly influences the effective anisotropy of Co-Pt NWs. Thus, the perpendicular easy magnetization axis found in this system via magnetometery is attributed to the strong contribution from MCA in NWs. Based on good agreement between the ADC and the analytical calculations, a transition from vortex to transverse reversal mode was identified at angle (θ=30°), and the fitting of the experiment to the analytical calculations revealed an effective anisotropy constant (K_{eff}= 2.6 x 10^4 J/m^3) for Co-Pt NWs which further explained magnetic behaviour of individual NWs. The competition between MCA and shape anisotropy is responsible for order of magnitude lower effective anisotropy constant and also responsible for the lower values of coercivity for Co-Pt NWs.

It was concluded that the preferential orientation of the hcp c-axis perpendicular to the $Co_{83\pm5}Pt_{17\pm5}$ NWs long axis is due to a large pore diameter (D_o>D≈200) which is in

accordance with the literature. Small variations in the orientation of the hcp c-axis in the perpendicular plane of the NWs' long axis are due to the "oblivious" electrodeposition, including a small deposition fluctuations, e.g., the pore diameter, pore shape etc. The sharp peak along interaction axis in FORC measurement indicates that the dipolar interactions between the Co-Pt NWs with diameter 200 nm are negligible. A complex FORC diagram observed for Co-Pt NWs in AAO membrane in perpendicular field direction is an indication of small variation in the hcp c-axis orientation which is confirmed by the large FMR linewidth. Thus, based on these observations we conclude that the perpendicular easy magnetization axis is due to the strong hcp MCA in Co-Pt NWs, which is obviously stronger than the shape anisotropy. Therefore, small fluctuations in the hcp c-axis orientations can significantly affect the magnetic properties of the Co-Pt NWs such as switching field distribution etc. In this thesis we have estimated the effective anisotropy constant for Co-Pt NWs into AAO membranes (diameter~200 nm) with three different methods (angular dependence of coercivity, hysteresis loop and FMR measurements) and we have found very close values in the range of K_{eff}=2-5 $\times 10^4$ J/m^3.

Furthermore, systematic MFM measurements on individual hcp Co-Pt NWs with diameter 200 nm revealed three distinct group of domain configurations, (1) periodic domain structure along the length of the NWs (2) stripe-like domain structure and (3) alternating domain structure across the diameter of the NWs. Combined results with microstructural study revealed that such domain configurations indeed originate from the competition between the shape anisotropy and the MCA. The results of the micromagnetic simulations compared with MFM measurements indicate that the first two types of domain structure in Co-Pt NWs can be interpreted as transverse stripe (TS) and longitudinal stripe (LS) domain structures which are the most energetically favorable states when the MCA and the shape anisotropy are at 90°, while at acute angles, the third type of domain structure interpreted as vortex-like domain structure becomes favorable. Our hypothesis is valid for smaller diameter Co-Pt NWs as well, for example in Co-Pt NWs with diameters less than 100 nm, the shape anisotropy and MCA are again in competition with each other. The magnetic domain structures in the 80 nm diameter NWs can be attributed to the combination between TS and LS domain structure whereas 50 nm diameter NW are due to the presence of a non-symmetrical z-vortex state. This is due to the fact that in 50 nm diameter we observed an acute angle (~70°-80°) between easy magnetization direction ($[111]_{fcc}$) and wire axis. Finally, we study the stability and magnetization dynamics of first type of domain structure in in-field MFM measurements and results indicating that these domain structures are energetically stable in Co-Pt NWs. Indeed, more work needs to be done in this area to fully understand the magnetic domain structures in NWs with a strong perpendicular MCA. Our results provide a deep insight in the magnetic properties of Co-Pt nanowires with strong MCA and thus make them useful for possible applications in racetrack memory devices and nanoelectronics.

The objective of the present study was to investigate the magnetic domain structure and magnetization reversal in Co-Pt NWs and we found that MCA was a driving force for magnetic properties of Co-rich Co-Pt NWs. For the proof of principle we investigated shape-anisotropy-governed fcc equiatomic Fe-Pd NW and found a single domain

structure with magnetization along the length of the NWs. We have also shown that by applying the field in the direction parallel to the NW's axis we were able to flip the magnetization ($H_{CII} \approx 3.3$ kA/m). The MFM study of the magnetostatic interactions revealed that the NWs are strongly coupled unlike Co-Pt NWs due to their strong shape anisotropy.

9.1 Future Directions

Although several ground breaking tasks were performed within this thesis but a lot of work has to be done to utilize these NWs for possible applications. First in the near future the work that can be done is the completion of work-in-progress given in Chapter (miscellaneous results). In the far future the work that should be under focus is given in the following:

- Measuring the magnetotransport properties of a single Co-Pt NW with four contact technique, such as spin Hall Effect etc.
- Study domain wall propagation in single Co-Pt NWs with different diameters and study of their domain wall velocity and domain propagation mechanism.

Appendix

List of Publications

10.1 Journal Papers Submitted and Published:

1. **Muhammad Shahid Arshad,** Sašo Šturm, Janez Zavašnik, Alvaro P. Espejo, Juan Escrig, Matej Komelj, Paul J. McGuiness, Spomenka Kobe, Kristina Žužek Rožman, "Effect of magnetocrystalline anisotropy on the magnetic properties of electrodeposited Co-Pt nanowires", *J. Nanopart. res.*, vol. 16, str. 2688-1-2688-16, 2014, doi: 10.1007/s11051-014-2688-4.
2. **Muhammad Shahid Arshad,** Janez Zavašnik, Sašo Šturm, Paul J. McGuiness, Spomenka Kobe, Kristina Žužek Rožman, "Microstructure and magnetic properties of electrodeposited Co-Pt nanowires (NWs) with diameters below 100 nm", *IEEE magn. lett.*, vol. 5, str. 6700204-1-6700204-4, 2014, doi: 10.1109/LMAG.2014.2362106.
3. Darja Pečko, **Muhammad Shahid Arshad**, Sašo Šturm, Spomenka Kobe, Kristina Žužek Rožman, "Magnetization-switching study of fcc Fe-Pd Nanowire and Nanowire Arrays studied by In-Field Magnetic Force Microscopy." *IEEE Trans Magn,* 99, pp. 1-4, 2015, doi:10.1109/TMAG.2015.2449773.
4. Nina Kostevšek, Kristina Žužek Rožman, **Muhammad Shahid Arshad**, Matjaž Spreitzer, Spomenka Kobe, Sašo Šturm, "Multimodal hybrid FePt/SiO2/Au nanoparticles for nanomedical applications : combining photothermal stimulation and manipulation with an external magnetic field", The journal of physical chemistry. C, Nanomaterials and interfaces, 9 str., 2015, doi: 10.1021/acs.jpcc.5b03725.
5. Darja Pečko, Kristina Žužek Rožman, Nina Kostevšek, **Muhammad Shahid Arshad**, Boštjan Markoli, Zoran Samardžija, Spomenka Kobe, "Electrodeposited hard-magnetic $Fe_{50}Pd_{50}$ nanowires from an ammonium-citrate-based bath", J. alloys compd., vol. 605, str. 71-79, 2014, doi: 10.1016/j.jallcom.2014.03.156.
6. Janez Zavašnik, Nadežda Stanković, **Muhammad Shahid Arshad**, Aleksander Rečnik, "Sonochemical synthesis of mackinawite and the role of Cu addition on phase transformations in the FeS system", *J. nanopart. res.*, vol.16, no. 2, str. 2223-1-2223-13, 2014, doi: 10.1007/s11051-013-2223-z.
7. **Muhammad Shahid Arshad**, Mariana P Proenca, Špela Trafela, Volker Neu, Ulrike Wolff, Sven Stienen, Manuel Vazquez, Spomenka Kobe, and K. Žužek Rožman, "Oblivious growth mechanism of high perpendicular anisotropic Co-Pt nanowire arrays: role of crystal orientation (c-axis) on Switching-Field Distribution

and Magnetic Domain configurations", Journal of Physics D: Applied Physics (Submitted)

10.2 Conference Papers/Presentations Accepted and Published:

8. **Muhammad Shahid Arshad,** Darja Pečko, Sašo Šturm, Juan Escrig, Matej Komelj, Paul J. McGuiness, Spomenka Kobe, Kristina Žužek Rožman, "Angular dependence of the coercivity in electrodeposited Co-Pt nanostructures with a tube-wire morphology", V: Proceedings of the INTERMAG 2014, IEEE International Magnetics Conference, May 4-8, 2014, Dresden, Germany, (IEEE trans. on magn., vol. 50, no. 11, 2014), , New York, Institute of Electrical and Electronics Engineers, 2014, vol. 50, no. 11, str. 2302904-1-2302904-4, 2014, doi: 10.1109/TMAG.2014.2320911.
9. **Muhammad Shahid Arshad**, Janez Zavašnik, Sašo Šturm, Juan Escrig, Volker Neu, Spomenka Kobe, Kristina Žužek Rožman, "Cobalt-platinum alloy nanostructures as potential candidates for future magnetic data storage devices", V: From 3D nanostructuring towards novel magnetic data storages: program, abstract booklet, IWMNN 2015, International Workshop on Magnetic Nanowires and Nanotubes 2015, May 17-20, 2015, Meersburg, Germany, [S. l., s. n.], 2015.
10. **Muhammad Shahid Arshad**, Darja Pečko, Janez Zavašnik, Sašo Šturm, Spomenka Kobe, Kristina Žužek Rožman, *et al.*, "Cobalt-platinum alloy nanostructures as potential candidates for racetrack magnetic data storage devices", V: Zbornik, 7. študentska konferenca Mednarodne podiplomske šole Jožefa Stefana = 7th Jožef Stefan International Postgraduate School Students' Conference, 20.-22. 5. 2015, Ljubljana, Andraž Rešetič, ur., *et al*, Ljubljana, Mednarodna podiplomska šola Jožefa Stefana, 2015, zv. 1, str. 270-277.
11. **Muhammad Shahid Arshad**, Bojan Ambrožič, Špela Trafela, Spomenka Kobe, Kristina Žužek Rožman, "Domain-wall-pinning in notched cylindrical electrodeposited Co-Pt nanowires", V: 9th Young researchers' day, April 7, 2015, Ljubljana : program and abstract book, Nežka Kavčič, ur., *et al*, Ljubljana, Institut Jožef Stefan, 2015, str. 15.
12. **Muhammad Shahid Arshad**, "Investigation of different magnetocrystalline anisotropies with FORC analysis in electrodeposited Co-Pt nanowires", V: Abstract book, 20th International Conference on Magnetism, ICM 2015, July 5-10 2015, Barcelona, Spain, [S. l., s. n.], 2015.
13. **Muhammad Shahid Arshad**, Kristina Žužek Rožman, Sašo Šturm, Janez Zavašnik, Paul J. McGuiness, Spomenka Kobe, "Periodic domain structure in electrodeposited polycrystalline Co-Pt nanowires", V: Program and abstract book, 8th Young Researchers' Day, February 18, 2014, Ljubljana, Vojka Žunič, ur., *et al*, Ljubljana, Institut Jožef Stefan, 2014, str. 34
14. **Muhammad Shahid Arshad**, Kristina Žužek Rožman, Sašo Šturm, Matej Komelj, Paul J. McGuiness, Spomenka Kobe, "Different energy contributions on magnetic domain configurations in electrodeposited CoPt nanowires", V: Program

in knjiga povzetkov, 21. Mednarodna konferenca o materialih in tehnologijah, 13.-15. november 2013, Portorož = 21st International Conference on Materials and Technology, 13-15 November 2013, Portorož, Slovenia, Matjaž Godec, ur., *et al*, Ljubljana, Inštitut za kovinske materiale in tehnologije, 2013.

15. **Muhammad Shahid Arshad**, Kristina Žužek Rožman, Zoran Samardžija, Spomenka Kobe, "Fabrication and magnetic properties of CoPt nanostructures", V: Program in knjiga povzetkov, 20. jubilejna konferenca o materialih in tehnologijah, 17.-19. oktober 2012, Portorož, Slovenija, Matjaž Godec, ur., *et al*, Ljubljana, Inštitut za kovinske materiale in tehnologije, 2012, str. 34.
16. Kristina Žužek Rožman, **Muhammad Shahid Arshad**, Fabian Rhein, Ulrike Wolff, Volker Neu, Spomenka Kobe, "Magnetization reversal behaviour in electrodeposited ferromagnetic Co-Pt-based nanotubes and nanowires", V: Abstracts, EDNANO 9, 9th International Workshop on Electrodeposited Nanostructures, 8-10th November 2012, Porto, Portugal, [S. l., s. n.], 2012, str. 13.
17. Kristina Žužek Rožman, Špela Trafela, Darja Pečko, **Muhammad Shahid Arshad**, Nina Kostevšek, Sašo Šturm, Spomenka Kobe, "Tailoring the magnetization distribution in ferromagnetic nanowires and nanotubes for (bio) applications", V: Nanotech Tunisia 2015 : International Nanotechnology Conference, 22-24 April 2015, Hannamet, Tunisia, .
18. Darja Pečko, Kristina Žužek Rožman, Sašo Šturm, **Muhammad Shahid Arshad**, Spomenka Kobe, "Electrodeposited hard and soft magnetic $Fe_{50}Pd_{50}$ nanowires and their characterization", V: Program and abstract book, 8th Young Researchers' Day, February 18, 2014, Ljubljana, Vojka Žunič, ur., *et al*, Ljubljana, Institut Jožef Stefan, 2014.
19. Kristina Žužek Rožman, Darja Pečko, **Muhammad Shahid Arshad**, Nina Kostevšek, Sašo Šturm, Paul J. McGuiness, Spomenka Kobe, Nanostructured materials : from synthesis to end use : od sinteze do končne uporabe : invited talk, Maribor, Univerza v Mariboru, Fakulteta za strojništvo, 3. jun. 2014.
20. Kristina Žužek Rožman, Darja Pečko, **Muhammad Shahid Arshad**, Ulrike Wolff, V. Neu, Spomenka Kobe, "Magnetization reversal behaviour in ferromagnetic Co-Pt-based nanotubes studied using MFM and angular dependence measurements", V: Abstracts, IEEE International Magnetics Conference, INTERMAG 2012, May 7-11, 2012, Vancouver, Canada, [S. l., s. n.], 2012.

10.3 Research Poster Presentations

21. **Muhammad Shahid Arshad**, Janez Zavašnik, Sašo Šturm, Paul J. McGuiness, Spomenka Kobe, Kristina Žužek Rožman, Microstructure, composition and magnetic properties of electrodeposited CoPt nanowires: presented at 7th IEEE Magnetics Society Summer School, 10-15 August 2014, Rio de Janeiro, Brazil, 2014.
22. **Muhammad Shahid Arshad**, Kristina Žužek Rožman, Matej Komelj, Paul J. McGuiness, Spomenka Kobe, "Static and dynamic magnetic domain configuration in electrodeposited cobalt platinum nanowires", V: Book of abstracts, 9th

International Symposium on Hysteresis and Micromagnetics, HMM 2013, 13-15 May 2013, Taormina, Italy

23. **Muhammad Shahid Arshad**, Kristina Žužek Rožman, Matej Komelj, Paul J. McGuiness, Spomenka Kobe, "Static and dynamic magnetic domain configuration in electrodeposited cobalt platinum nanowires", V: [Program and abstract book], 7th Young Researchers' Day, 19 February, 2013, Ljubljana, Slovenia, Darja Lisjak, ur., Peter Dušak, ur., Slavko Kralj, ur., Ljubljana, Institut Jožef Stefan, 2013, str. 32.
24. **Muhammad Shahid Arshad**, Kristina Žužek Rožman, Zoran Samardžija, Spomenka Kobe, "Fabrication and magnetic properties of CoPt nanostructures", V: Book of abstracts, SLONANO 2012, 24-26 October 2012, Ljubljana, Slovenia, Dragan Mihailović, ur., *et al*, Ljubljana, Institut Jožef Stefan, 2012, str. 77.
25. Kristina Žužek Rožman, **Muhammad Shahid Arshad**, Matej Komelj, Paul J. McGuiness, Spomenka Kobe, "Static and dynamic magnetic domain configuration in electrodeposited cobalt platinum nanowires", V: Final program, EUROMAT 2013, European Congress and Exhibition on Advanced Materials and Processes, September 8-13, 2013, Sevilla, [S. l.], The Federation of European Materials Society, 2013.

References

[1] Y. P. Ivanov, L. G. Vivas, A. Asenjo, A. Chuvilin, O. Chubykalo-fesenko and M. Vázquez, "Magnetic structure of a single-crystal hcp electrodeposited cobalt nanowire," *Europhys. Lett.* vol. 102, pp. 17009-17014, 2013.

[2] S. Allende, J. Escrig, D. Altbir, E. Salcedo and M. Bahiana, "Angular dependence of the transverse and vortex modesin magnetic nanotubes," *EPJ B* vol. 66, pp. 37-40, 2008.

[3] L. A. Bauer, N. S. Birenbaum and G. J. Meyer, "Biological applications of high aspect ratio nanoparticles," *J. Mater. Chem.* vol. 14, pp. 517-526, 2004.

[4] http://researcher.watson.ibm.com/researcher/view_group_subpage.php?id=3811, 04 Oct 2015.

[5] http://eng.thesaurus.rusnano.com/wiki/article1371%E2%80%9D, 17 Sept. 2015

[6] G. Kartopu, O. Yalçın, K. L. Choy, R. Topkaya, S. Kazan and B. Aktaş, "Size effects and origin of easy-axis in nickel nanowire arrays," *J. Appl. Phys.* vol. 109, pp. 033909, 2011.

[7] J. De La Torre Medina, M. Darques, L. Piraux and A. Encinas, "Application of the anisotropy field distribution method to arrays of magnetic nanowires," *J. Appl. Phys.* vol. 105, pp. 023909-023918, 2009.

[8] T. Wang, Y. Wang, Y. Fu, T. Hasegawa, F. S. Li, H. Saito and S. Ishio, "A magnetic force microscopy study of the magnetic reversal of a single Fe nanowire," *Nanotechnology* vol. 20, pp. 105707, 2009.

[9] U. Netzelmann, "Ferromagnetic resonance of particulate magnetic recording tapes," *J. Appl. Phys.* vol. 68, pp. 1800-1808, 1990.

[10] A. Encinas-Oropesa, M. Demand, L. Piraux, U. Ebels and I. Huynen, "Effect of dipolar interactions on the ferromagnetic resonance properties in arrays of magnetic nanowires," *J. Appl. Phys.* vol. 89, pp. 3, 2001.

[11] G. Kartopu, O. Yalc, K. L. Choy, R. Topkaya, S. Kazan and B. Akta, "Size effects and origin of easy-axis in nickel nanowire arrays," *J. Appl. Phys.* vol. 109, pp. 033909-033901, 2011.

[12] Y. Dahmane, L. Cagnon, J. Voiron, S. Pairis, M. Bacia, L. Ortega, N. Benbrahim and A. Kadri, "Magnetic and structural properties of electrodeposited CoPt and FePt nanowires in nanoporous alumina templates," *J. Phys. D: Appl. Phys.* vol. 39, pp. 4523-4528, 2006.

[13] I. Zana, G. Zangari, J.-W. Park and M. G. Allen, "Electrodeposited Co–Pt micron-size magnets with strong perpendicular magnetic anisotropy for MEMS applications," *J. Magn. Magn. Mater.* vol. 272-276, pp. E1775-E1776, 2004.

[14] C. Bran, Y. P. Ivanov, D. G. Trabada, J. Tomkowicz, R. P. del Real, O. Chubykalo-Fesenko and M. Vazquez, "Structural Dependence of Magnetic Properties in Co-Based Nanowires: Experiments and Micromagnetic Simulations," *IEEE Trans. Magn.* vol. 49, pp. 4491-4497, 2013.

[15] X. H. Huang, G. H. Li, G. Z. Sun, X. C. Dou, L. Li and L. X. Zheng, "Initial Growth of Single-Crystalline Nanowires: From 3D Nucleation to 2D Growth," *Nanoscale Res. Lett.* vol. 5, pp. 1057 - 1062, 2010.

[16] H. Pan, B. Liu, J. Yi, C. Poh, S. Lim, J. Ding, Y. Feng, C. H. A. Huan and J. Lin, "Growth of Single-Crystalline Ni and Co Nanowires via Electrochemical Deposition and Their Magnetic Properties," *J. Phys. Chem. B* vol. 109, pp. 3094-3098, 2005.

[17] H. Forster, T. Schrefl, R. Dittrich, D. Suess, W. Scholz, V. Tsiantos, J. Fidler, K. Nielsch, H. Hofmeister, H. Kronmuller and S. Fischer, "Magnetization reversal in granular nanowires," *IEEE Trans. Magn.* vol. 38, pp. 2580-2582, 2002.

[18] Y. P. Ivanov, M. Vázquez and O. Chubykalo-fesenko, "Magnetic reversal modes in cylindrical nanowires," *J. Phys. D: Appl. Phys.* vol. 46, pp. 485001-485012, 2013.

[19] H. Xianghua, L. Qingfang, W. Jianbo, L. Shiliang, R. Yong, L. Ronglin and L. Fashen, "Influence of crystal orientation on magnetic properties of hcp Co nanowire arrays," *J. Phys. D: Appl. Phys.* vol. 42, pp. 095005-095009, 2009.

[20] A. S. Samardak, F. Nasirpouri, M. Nadi, E. V. Sukovatitsina, A. V. Ognev, L. A. Chebotkevich and S. V. Komogortsev, "Conversion of magnetic anisotropy in electrodeposited Co–Ni alloy nanowires," *J. Magn. Magn. Mater.* vol. 383, pp. 94-99, 2015.

[21] V. Vega, T. Böhnert, S. Martens, M. Waleczek, J. M. Montero-Moreno, D. Görlitz, V. M. Prida and K. Nielsch, "Tuning the magnetic anisotropy of Co-Ni nanowires: comparison between single nanowires and nanowire arrays in hard-anodic aluminum oxide membranes," *Nanotechnology* vol. 23, pp. 465709-465709, 2012.

[22] S. S. A. Razee, J. B. Staunton and F. J. Pinski, "First-principles theory of magnetocrystalline anisotropy of disordered alloys: Application to cobalt platinum," *Phys. Rev. B* vol. 56, pp. 8082-8090, 1997.

[23] M. Getzlaff, *Fundamentals of Magnetism,* Springer Science & Business Media, 2007, pp.

[24] J. Fu, S. Cherevko and C.-H. Chung, "Electroplating of metal nanotubes and nanowires in a high aspect-ratio nanotemplate," *Electrochem. Commun.* vol. 10, pp. 514-518, 2008.

[25] U. S. Mohanty, "Electrodeposition: a versatile and inexpensive tool for the synthesis of nanoparticles, nanorods, nanowires, and nanoclusters of metals," *J. Appl. Electrochem.* vol. 41, pp. 257-270, 2011.

[26] C. R. Martin, "Nanomaterials: A Membrane-Based Synthetic Approach," *Science* vol. 266, pp. 1961-1966, 1994.

[27] C. R. Martin, "Membrane-Based Synthesis of Nanomaterials," *Chem. Mater.* vol. 8, pp. 1739-1746, 1996.

[28] S. Parkin and S.-H. Yang, "Memory on the racetrack," *Nat Nano* vol. 10, pp. 195-198, 2015.

[29] S. S. P. Parkin, M. Hayashi and L. Thomas, "Magnetic Domain-Wall Racetrack Memory," *Science* vol. 320, pp. 190-194, 2008.

[30] M. Hayashi, L. Thomas, C. Rettner, R. Moriya and S. S. P. Parkin, "Direct observation of the coherent precession of magnetic domain walls propagating along permalloy nanowires," *Nat. Phys.* vol. 3, pp. 21-25, 2007.

[31] M. Hayashi, L. Thomas, C. Rettner, R. Moriya, X. Jiang and S. S. P. Parkin, "Dependence of Current and Field Driven Depinning of Domain Walls on Their Structure and Chirality in Permalloy Nanowires," *Phys. Rev. Lett.* vol. 97, pp. 207205, 2006.

[32] R. Allenspach and P. O. Jubert, "Magnetic domain walls in nanowires," *Mrs Bull* vol. 31, pp. 395-399, 2006.
[33] M. S. Arshad, D. Pecko, S. Sturm, J. Escrig, M. Komelj, P. J. McGuiness, S. Kobe and K. Z. Rozman, "Angular Dependence of the Coercivity in Electrodeposited Co-Pt Nanostructures With a Tube-Wire Morphology," *IEEE Trans. Magn.* vol. 50, pp. 1-4, 2014.
[34] R. F. Neumann, M. Bahiana, N. M. Vargas, D. Altbir, S. Allende, D. Gorlitz and K. Nielsch, "Domain wall control in wire-tube nanoelements," *Appl. Phys. Lett.* vol. 102, pp. 202407-202412, 2013.
[35] D. Salazar-Aravena, R. M. Corona, D. Goerlitz, K. Nielsch and J. Escrig, "Magnetic properties of multisegmented cylindrical nanoparticles with alternating magnetic wire and tube segments," *J. Magn. Magn. Mater.* vol. 346, pp. 171-174, 2013.
[36] A. P. Espejo, N. Vidal-Silva, J. A. López-López, D. Goerlitz, K. Nielsch and J. Escrig, "Current-driven vortex domain wall motion in wire-tube nanostructures," *Appl. Phys. Lett.* vol. 106, pp. 132405, 2015.
[37] D. Pecko, M. S. Arshad, S. Sturm, S. Kobe and K. Z. Rozman, "Magnetization-Switching Study of fcc Fe-Pd Nanowire and Nanowire Arrays Studied by In-Field Magnetic Force Microscopy," *IEEE Trans. Magn.* vol. 51, pp. 1-1, 2015.
[38] J. U. Cho, J.-H. Wu, J. H. Min, S. P. Ko, J. Y. Soh, Q. X. Liu and Y. K. Kim, "Control of magnetic anisotropy of Co nanowires," *J. Magn. Magn. Mater.* vol. 303, pp. e281-e285, 2006.
[39] M. S. Arshad, S. Šturm, J. Zavašnik, A. Espejo, J. Escrig, M. Komelj, P. McGuiness, S. Kobe and K. Rožman, "Effect of magnetocrystalline anisotropy on the magnetic properties of electrodeposited Co–Pt nanowires," *J Nanopart Res* vol. 16, pp. 1-16, 2014.
[40] M. S. Arshad, J. Zavasnik, S. Sturm, P. McGuiness, S. Kobe and K. Z. Rozman, "Microstructures and Magnetic Properties of Electrodeposited Co-Pt Nanowires With Diameters Below 100nm," *Magnetics Letters, IEEE* vol. 5, pp. 1-4, 2014.
[41] G. S. D. Beach, M. Tsoi and J. L. Erskine, "Current-induced domain wall motion," *J. Magn. Magn. Mater.* vol. 320, pp. 1272-1281, 2008.
[42] J. Wunderlich, D. Ravelosona, C. Chappert, F. Cayssol, V. Mathet, J. Ferre, J. P. Jamet and A. Thiaville, "Influence of geometry on domain wall propagation in a mesoscopic wire," *Magnetics, IEEE Transactions on* vol. 37, pp. 2104-2107, 2001.
[43] F. Cayssol, D. Ravelosona, C. Chappert, J. Ferré and J. P. Jamet, "Domain Wall Creep in Magnetic Wires," *Phys. Rev. Lett.* vol. 92, pp. 107202, 2004.
[44] P. Landeros, S. Allende, J. Escrig, E. Salcedo, D. Altbir and E. E. Vogel, "Reversal modes in magnetic nanotubes," *Appl. Phys. Lett.* vol. 90, pp. 102501-102503, 2007.
[45] R. Lavin, J. C. Denardin, J. Escrig and D. Altbir, "Angular dependence of magnetic properties in Ni nanowire arrays," *J. Appl. Phys.* vol. 106, pp. 103903-103901-103905, 2009.
[46] R. Lavin, J. C. Denardin, A. P. Espejo, A. Cortes and H. and Gomez, "Magnetic properties of arrays of nanowires: Anisotropy, interactions, and reversal modes," *J. Appl. Phys.* vol. 107, pp. 09B504-509B507, 2010.
[47] R. Lavín, C. Gallardo, J. L. Palma, J. Escrig and J. C. Denardin, "Angular dependence of the coercivity and remanence of ordered arrays of Co nanowires," *J. Magn. Magn. Mater.* vol. 324, pp. 2360-2362, 2012.

[48] E. C. Stoner and E. P. Wohlfarth, "A Mechanism of Magnetic Hysteresis in Heterogeneous Alloys," *Philosophical Transactions of the Royal Society of London A: Mathematical, Physical and Engineering Sciences* vol. 240, pp. 599-642, 1948.

[49] M. Brands and G. Dumpich, "Experimental determination of anisotropy and demagnetizing factors of single Co nanowires by magnetoresistance measurements," *J. Appl. Phys.* vol. 98, pp. 014309, 2005.

[50] J. Escrig, P. Landeros, D. Altbir, E. E. Vogel and P. Vargas, "Phase diagrams of magnetic nanotubes," *J. Magn. Magn. Mater.* vol. 308, pp. 233-237, 2007.

[51] J. Escrig, J. Bachmann, J. Jing, M. Daub, D. Altbir and K. Nielsch, "Crossover between two different magnetization reversal modes in arrays of iron oxide nanotubes," *Phys. Rev. B* vol. 77, pp. 2008.

[52] A. Aharoni, "Angular dependence of nucleation by curling in a prolate spheroid," *J. Appl. Phys.* vol. 82, pp. 1281, 1997.

[53] O. Albrecht, R. Zierold, S. n. Allende, J. Escrig, C. Patzig, B. Rauschenbach, K. Nielsch and D. Görlitz, "Experimental evidence for an angular dependent transition of magnetization reversal modes in magnetic nanotubes," *J. Appl. Phys.* vol. 109, pp. 093910, 2011.

[54] L. G. Vivas, M. Vazquez, J. Escrig, S. Allende, D. Altbir, D. C. Leitao and J. P. Araujo, "Magnetic anisotropy in CoNi nanowire arrays: Analytical calculations and experiments," *Phys. Rev. B* vol. 85, pp. 2012.

[55] C.-R. Chang, C. M. Lee and J.-S. Yang, "Magnetization curling reversal for an infinite hollow cylinder," *Phys. Rev. B* vol. 50, pp. 6461-6464, 1994.

[56] L. G. Vivas, M. Vazquez, J. Escrig, S. Allende, D. Altbir, D. C. Leitao and J. P. Araujo, "Magnetic anisotropy in CoNi nanowire arrays: Analytical calculations and experiments," *Phys. Rev. B* vol. 85, pp. 035439-035443, 2012.

[57] L. G. Vivas, J. Escrig, D. G. Trabada, G. A. Badini-Confalonieri and M. Vázquez, "Magnetic anisotropy in ordered textured Co nanowires," *Appl. Phys. Lett.* vol. 100, pp. 252405-252409, 2012.

[58] I. D. Mayergoyz, "Hysteresis models from the mathematical and control theory points of view," *J. Appl. Phys.* vol. 57, pp. 3803-3805, 1985.

[59] J. D. Medina, L. Piraux, J. M. O. Govea and A. Encinas, "Double ferromagnetic resonance and configuration-dependent dipolar coupling in unsaturated arrays of bistable magnetic nanowires," *Phys. Rev. B* vol. 81, pp. 2010.

[60] T. Sorop, C. Untiedt, F. Luis, M. Kröll, M. Raşa and L. de Jongh, "Magnetization reversal of ferromagnetic nanowires studied by magnetic force microscopy," *Phys. Rev. B* vol. 67, pp. 1-8, 2003.

[61] Y. Henry, K. Ounadjela, L. Piraus, S. Dubois, J.-M. George and a. J.-L. Duvail, "Magnetic anisotropy and domain patterns in electrodeposited cobalt nanowires," *EPJ B* vol. 20, pp. 35-44, 2001.

[62] Zuwei Liu, Pai-Chun Chang, Chia-Chi Chang, Evgeniy Galaktionov, Gerd Bergmann and J. G. Lu, "Shape Anisotropy and Magnetization Modulation in Hexagonal Cobalt Nanowires," *Adv. Funct. Mater.* vol. 18, pp. 1573-1578, 2008.

[63] P. Grutter, H.J. Mamin and D. Rogar, *Magnetic Force Microscopy,* Springer, Berlin, Heidelberg: Springer, 1992, pp.

[64] K. R. Pirota, F. Béron, D. Zanchet, T. C. R. Rocha, D. Navas, J. Torrejón, M. Vazquez and M. Knobel, "Magnetic and structural properties of fcc/hcp bi-crystalline multilayer Co nanowire arrays prepared by controlled electroplating," *J. Appl. Phys.* vol. 109, pp. 083919, 2011.
[65] L. Clime, S.-Y. Zhao, F. Normandin and T. Veres, "Characterization of ferromagnetic nanowires by partial first order reversal curves," *J. Appl. Phys.* vol. 102, pp. 063903, 2007.
[66] C.-I. Dobrotă and A. Stancu, "Tracking the individual magnetic wires' switchings in ferromagnetic nanowire arrays using the first-order reversal curves (FORC) diagram method," *Physica B: Condensed Matter* vol. 457, pp. 280-286, 2015.
[67] F. Béron, D. Ménard and A. Yelon, "First-order reversal curve diagrams of magnetic entities with mean interaction field: A physical analysis perspective," *J. Appl. Phys.* vol. 103, pp. 07D908, 2008.
[68] E. Torre, "Effect of interaction on the magnetization of single-domain particles," *Audio and Electroacoustics, IEEE Transactions on* vol. 14, pp. 86-92, 1966.
[69] C. Kittel, "On the Theory of Ferromagnetic Resonance Absorption," *Phys. Rev.* vol. 73, pp. 155-161, 1948.
[70] S. P. a. M. S. Manish Sharma, *FMR Measurements of Magnetic Nanostructures, Ferromagnetic Resonance - Theory and Applications,* InTech, 2013, pp.
[71] H. G. B. J. Smit, "Ferromagnetic resonance absorption in BaFe12O19, a highly anisotropic crystal," *Philips Res. Rep.* vol. 10, pp. 113-130, 1955.
[72] J. B. Youssef and C. Brosseau, "Magnetization damping in two-component metal oxide micropowder and nanopowder compacts by broadband ferromagnetic resonance measurements," *Phys. Rev. B* vol. 74, pp. 214413, 2006.
[73] T. Fischbacher, M. Franchin, G. Bordignon and H. Fangohr, "A Systematic Approach to Multiphysics Extensions of Finite-Element-Based Micromagnetic Simulations: Nmag URL: http://nmag.soton.ac.uk/nmag/," *IEEE Trans. Magn.* vol. 43, pp. 2896-2898, 2007.
[74] A. Colli, A. Fasoli, S. Pisana, Y. Fu, P. Beecher, W. I. Milne and A. C. Ferrari, "Nanowire Lithography on Silicon," *Nano Lett.* vol. 8, pp. 1358-1362, 2008.
[75] M. Munoz and J. L. Prieto, "Suppression of the intrinsic stochastic pinning of domain walls in magnetic nanostripes," *Nat Commun* vol. 2, pp. 562, 2011.
[76] M. Jaafar, L. Serrano-Ramón, O. Iglesias-Freire, A. Fernández-Pacheco, M. Ibarra, J. De Teresa and A. Asenjo, "Hysteresis loops of individual Co nanostripes measured by magnetic force microscopy," *Nanoscale Res. Lett.* vol. 6, pp. 1-6, 2011.
[77] M. Kumar and Y. Ando, "Chemical Vapor Deposition of Carbon Nanotubes: A Review on Growth Mechanism and Mass Production," *J. Nanosci. Nanotechnol.* vol. 10, pp. 3739-3758, 2010.
[78] F. Chen, Y.-J. Zhu, K.-W. Wang and K.-L. Zhao, "Surfactant-free solvothermal synthesis of hydroxyapatite nanowire/nanotube ordered arrays with biomimetic structures," *CrystEngComm* vol. 13, pp. 1858-1863, 2011.
[79] C. T. Sousa, A. M. L. Lopes, M. P. Proença, D. C. Leitão, J. G. Correia and J. P. Araújo, "Rapid Synthesis of Ordered Manganite Nanotubes by Microwave Irradiation in Alumina Templates," *J. Nanosci. Nanotechnol.* vol. 9, pp. 6084-6088, 2009.

[80] S. H. Ko, D. Lee, H. W. Kang, K. H. Nam, J. Y. Yeo, S. J. Hong, C. P. Grigoropoulos and H. J. Sung, "Nanoforest of Hydrothermally Grown Hierarchical ZnO Nanowires for a High Efficiency Dye-Sensitized Solar Cell," *Nano Lett.* vol. 11, pp. 666-671, 2011.
[81] L. Cattaneo, S. Franz, F. Albertini, P. Ranzieri, A. Vicenzo, M. Bestetti and P. L. Cavallotti, "Electrodeposition of hexagonal Co nanowires with large magnetocrystalline anisotropy," *Electrochim. Acta* vol. 85, pp. 57-65, 2012.
[82] D. W. Shi, J. Y. Chen, S. Riaz, W. P. Zhou and X. F. Han, "Controlled nanostructuring of multiphase core-shell nanowires by a template-assisted electrodeposition approach," *Nanotechnology* vol. 23, pp. 2012.
[83] H. Schlörb, V. Haehnel, M. S. Khatri, A. Srivastav, A. Kumar, L. Schultz and S. Fähler, "Magnetic nanowires by electrodeposition within templates," *Phys. Status Solidi B* vol. 247, pp. 2364-2379, 2010.
[84] G. E. J. Poinern, N. Ali and D. Fawcett, "Progress in Nano-Engineered Anodic Aluminum Oxide Membrane Development," *Materials* vol. 4, pp. 487-526, 2011.
[85] S. Ono, M. Saito and H. Asoh, "Self-ordering of anodic porous alumina formed in organic acid electrolytes," *Electrochim. Acta* vol. 51, pp. 827-833, 2005.
[86] H. Schlorb, V. Haehnel, M. S. Khatri, A. Srivastav, A. Kumar, L. Schultz and S. Fahler, "Magnetic nanowires by electrodeposition within templates," *Physica Status Solidi B-Basic Solid State Physics* vol. 247, pp. 2364-2379, 2010.
[87] J. F. Rohan, D. P. Casey, B. M. Ahern, F. M. F. Rhen, S. Roy, D. Fleming and S. E. Lawrence, "Coaxial metal and magnetic alloy nanotubes in polycarbonate templates by electroless deposition," *Electrochem. Commun.* vol. 10, pp. 1419-1422, 2008.
[88] E. Mafakheri, A. Salimi, R. Hallaj, A. Ramazani and M. A. Kashi, "Synthesis of Iridium Oxide Nanotubes by Electrodeposition into Polycarbonate Template: Fabrication of Chromium(III) and Arsenic(III) Electrochemical Sensor," *Electroanalysis* vol. 23, pp. 2429-2437, 2011.
[89] J. Zhang, G. A. Jones, T. H. Shen, S. E. Donnelly and G. Li, "Monocrystalline hexagonal-close-packed and polycrystalline face-centered-cubic Co nanowire arrays fabricated by pulse dc electrodeposition," *J. Appl. Phys.* vol. 101, pp. 054310-054315, 2007.
[90] S. Yang, H. Zhu, D. Yu, Z. Jin, S. Tang and Y. Du, "Preparation and magnetic property of Fe nanowire array," *J. Magn. Magn. Mater.* vol. 222, pp. 97-100, 2000.
[91] H. Khurshid, Y. H. Huang, M. J. Bonder and G. C. Hadjipanayis, "Microstructural and magnetic properties of CoPt nanowires," *J. Magn. Magn. Mater.* vol. 321, pp. 277-280, 2009.
[92] Fashen Li, Tao Wang, L. Ren and J. Sun, "Structure and magnetic properties of Co nanowires in self-assembled arrays," *J. Phys.: Condens. Matter* vol. 16, pp. 8053-8060, 2004.
[93] A. Encinas, L. Vila, M. Darques, J. M. George and L. Piraux, "Configurable multiband microwave absorption states prepared by field cycling in arrays of magnetic nanowires," *Nanotechnology* vol. 18, pp. 2007.
[94] S. D. Bader, "Colloquium: Opportunities in nanomagnetism," *Review of Modern Physics* vol. 78, pp. 1-15, 2006.
[95] L. Sun, Y. Hao, C. L. Chien and P. C. Searson, "Tuning the properties of magnetic nanowires," *Ibm J Res Dev* vol. 49, pp. 79-102, 2005.

[96] K. M. Krishnan, "Biomedical Nanomagnetics: A Spin Through Possibilities in Imaging, Diagnostics, and Therapy," *IEEE Trans. Magn.* vol. 46, pp. 2523-2558, 2010.
[97] S. J. Hurst, E. K. Payne, L. Qin and C. A. Mirkin, "Multisegmented one-dimensional nanorods prepared by hard-template synthetic methods," *Angew Chem Int Ed Engl* vol. 45, pp. 2672-2692, 2006.
[98] P. Landeros, S. Allende, J. Escrig, E. Salcedo, D. Altbir and E. E. Vogel, "Reversal modes in magnetic nanotubes," *Appl. Phys. Lett.* vol. 90, pp. 102501, 2007.
[99] http://www2.technologyreview.com/article/412189/tr10-racetrack-memory/ , 17 Sept 2015.
[100] S. M. Ahn, K. W. Moon, C. G. Cho and S. B. Choe, "Control of domain wall pinning in ferromagnetic nanowires by magnetic stray fields," *Nanotechnology* vol. 22, pp. 2011.